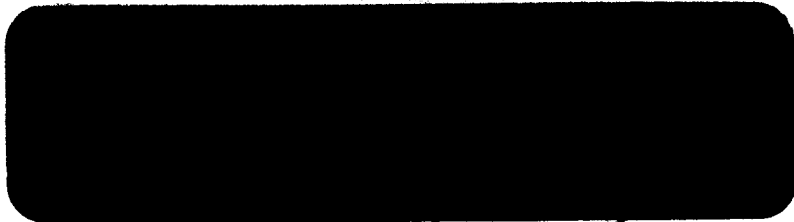


T



N66-19501

FACILITY FORM 602

(ACCESSION NUMBER)

273

(PAGES)

CR 56494

(NASA CR OR TMX OR AD NUMBER)

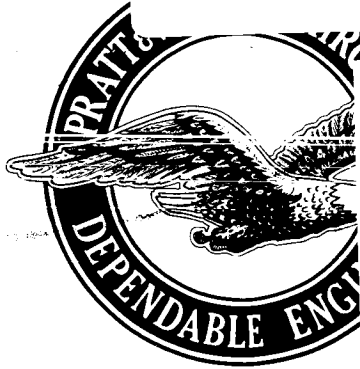
(THRU)

1

(CODE)

33

(CATEGORY)



CFR PRICE \$ _____

CFSTI PRICE(S) \$ _____

Hard copy (HC) \$4.00

Microfiche (MF) \$1.50

653 July 65



Pratt & Whitney Aircraft DIVISION OF UNITED AIRCRAFT CORPORATION

U
A

EAST HARTFORD 8, CONNECTICUT

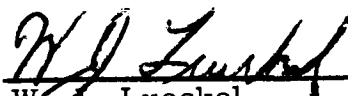
Interim Final Report
Determination of the Emissivity of Materials
Report No. PWA-2206
Volume I

Report Period: July 1, 1959 through December 31, 1962
Contract NASw-104 with 8 Amendments

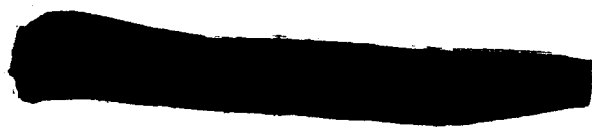
Technical Management: National Aeronautics &
Space Administration, Lewis Research Center,
Nuclear Technology Branch, Harold Nastelin



Approved by:


W. J. Lueckel
Chief, Space Power Systems


R. C. Huttinger
Program Manager


Pratt & Whitney Aircraft DIVISION OF UNITED AIRCRAFT CORPORATION

U
A

EAST HARTFORD

CONNECTICUT

COPY NO. 50

NOTICE

This report was prepared as an account of Government sponsored work. Neither the United States, nor the National Aeronautics and Space Administration (NASA), nor any person acting on behalf of NASA:

- A) Makes any warranty or representation, expressed or implied, with respect to the accuracy, completeness, or usefulness of the information contained in this report, or that the use of any information, apparatus, method, or process disclosed in this report may not infringe privately-owned right; or
- B) Assumes any liabilities with respect to the use of, or for damages resulting from the use of any information, apparatus, method or process disclosed in this report.

As used above, "person acting on behalf of NASA" includes any employee or contractor of NASA, or employee of such contractor, to the extent that such employee or contractor of NASA, or employee of such contractor prepares, disseminates, or provides access to, any information pursuant to his employment or contract with NASA, or his employment with such contractor.

Requests for copies of this report should be referred to:

National Aeronautics & Space Administration
Office of Scientific and Technical Information
Washington 25, D. C.
Attention: AFSS-A

FOREWORD

This report describes the research activity carried out in fulfillment of contract NASw-104 as modified by amendments 1 through 8, during the period July 1, 1959 through December 31, 1962. The principal investigators included W. H. Askwyth, R. J. Hayes, R. D. House, and G. Mikk. Contributors to the program were H. Schwartz of the National Aeronautics & Space Administration, and R. C. Huttinger, W. H. Atkinson, R. Curry, W. H. Podolny, F. D. Bittle, and G. J. Lyons of Pratt & Whitney Aircraft.

SUMMARY

This report is a compilation of the results of a program carried out during the period of July 1, 1959 through December 31, 1962 in which the thermal emittance of candidate materials for use in space radiators was measured in high vacuum. Measurement techniques were developed and facilities were constructed which permitted the accurate determination of spectral normal and total hemispherical emittance of materials at elevated temperatures. As a result of the experience gained during the program, the equipment has been modified and refined to permit more rapid and precise emittance data collection.

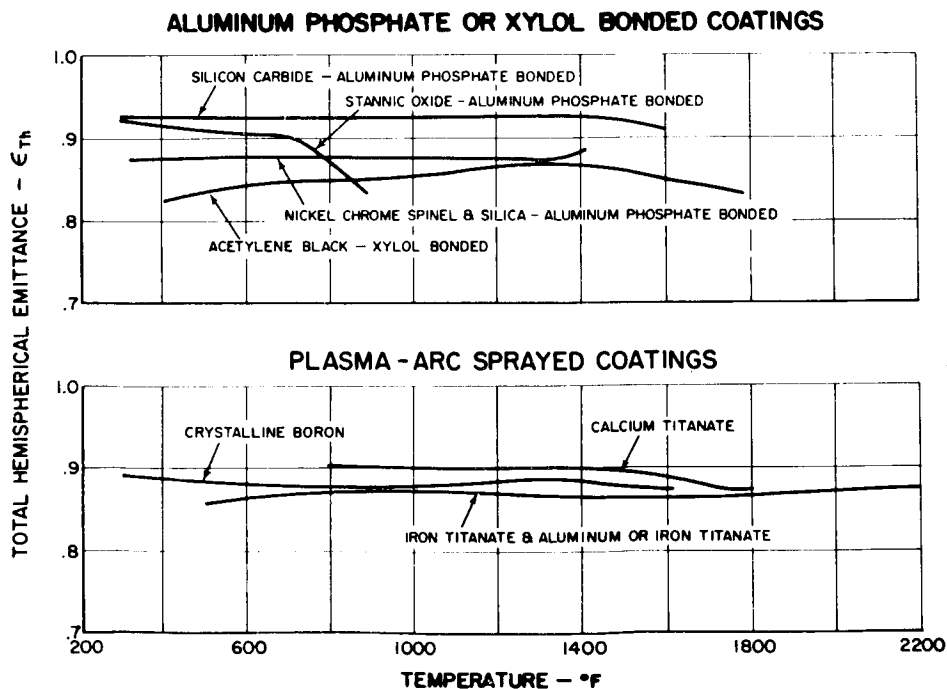
Several methods of applying high-emittance coatings have been investigated. Of these, the two most successful methods were thermal spraying and aluminum-phosphate bonding. These two methods permitted the successful application of a variety of coatings to several substrate materials including molybdenum, AISI-310 stainless steel, and columbium-1 per cent zirconium.

Both total hemispherical and spectral normal emittance measurements were made at temperatures ranging from 200°F to 3100°F, at indicated pressures as low as 4×10^{-9} mm Hg. Emittance changes resulting from exposure to elevated temperatures for periods up to 900 hours were determined for the more promising materials. In addition, the stability and adherence of three coating materials were determined for periods extending over 10,000 hours at a temperature of 700°F and a pressure of 10^{-7} mm Hg. These three materials were tested on SNAP-8 or Sunflower I tube-half fin radiator sections.

Total hemispherical emittance was determined by comparing the electrical power dissipation per unit area in a heated strip or tube with the theoretical emissive power of a black body operating at the specimen temperature. Spectral normal emittance was determined by comparing the intensity of spectral normal radiation emitted from the surface of an electrically heated tubular specimen to the intensity of spectral radiation emitted by an integral source of black-body radiation. Intensity ratios were obtained for particular temperatures and wavelengths using a dual-beam spectrophotometer viewing the tubular specimen through a sodium chloride window in the vacuum chamber wall. Measurements were made over the wavelength range of 0.45 to 13.0 microns. Platinum-platinum 10 per cent rhodium and chromel-alumel thermocouples as well as an optical pyrometer were used for specimen temperature measurement. The materials tested on tube-half fin radiator sections were evaluated by visual observation and by monitoring temperatures at selected thermocouple locations.

Thermal emittance data are included for the following types of materials: the refractory metals (tantalum, columbium, molybdenum, and tungsten); oxides of aluminum, copper, chromium, cobalt, columbium, nickel, manganese, silicon, tin, titanium, and zirconium; carbides of silicon, titanium, and vanadium; titanates of barium, calcium, iron, and strontium, and other ceramics.

Of the sixty materials tested in this program, several materials have been found which have high emittances and good high-temperature stability under high vacuum conditions. The better coating materials can be divided into three major groups: (1) single and complex oxides of titanium or binary oxide mixtures with titanium as one of the two constituents; (2) single and complex oxides of iron, nickel, and chromium; and (3) a miscellaneous group constituted primarily of carbon and its compounds and of boron. Of particular interest are calcium titanate, iron titanate and iron titanate with aluminum oxide, silicon carbide, nickel chrome spinel, crystalline boron, acetylene black, and stannic oxide. Representative total hemispherical emittance values for these materials appear in the figures below. Although variations in emittances for these materials occurred during the program, it is believed that the values shown can be consistently obtained.



Several investigations were made to permit estimation of the accuracy of the emittance measurements. Errors caused by reflection from the chamber walls, local perturbations of specimen temperature, and heat conduction from the ends of the specimen were studied with regard to both total and spectral measurements. Effects of scattered radiation and imperfections in the black-body radiation were examined with regard to spectral measurements, and the thermocouple calibration drift associated with the total hemispherical emittance measurements was also investigated. On the basis of these investigations, it is believed that spectral emittance values as reported are within +3 per cent to -5 per cent of the correct values. Total hemispherical emittance values are within ± 3 per cent when measured in the spectral rig and within ± 5 per cent when measured in the total hemispherical emittance rig.

TABLE OF CONTENTS

Volume I

	<u>Page</u>
Notice	ii
Foreword	iii
Summary	iv
Table of Contents	vii
List of Figures	xii
List of Tables	xvi
I. Introduction	1
II. Apparatus	3
A. Introduction	3
B. Spectral Normal Emittance Rig	3
C. Total Hemispherical Emittance Rig	8
D. Endurance Rigs	12
1. Short Term Endurance Rig	12
2. Long Term Endurance Rig	15
E. Aluminum Fin Thermal Cycling Rig	19
III. Procedure	21
A. Specimens	21
1. Specimens for Measurement of Emittance	21
2. Specimens for Endurance Testing	24
B. Testing Procedures	25
1. Spectral Normal Emittance Rig	25
2. Total Hemispherical Emittance Rig	26
3. Endurance Rigs	29
a. Short Term Endurance Rig	29
b. Long Term Endurance Rig	30
4. Aluminum Fin Thermal Cycling Rig	31
IV. Coating Procedures	33
A. Thermal Spraying	33
1. Plasma-Arc Spraying	33
2. Rokide Spraying	33
B. Slurry Applications	
1. Aluminum Phosphate Bonding	34
2. Synar Bonding	35
3. Graphite Varnish	35
4. Acetylene Black in Xylol	35

TABLE OF CONTENTS (cont'd)

	<u>Page</u>
C. Electroplating	35
1. Chromium Black	35
2. Platinum Black	36
D. Electrophoresis	36
E. Oxidizing Processes	37
1. Oxidized Columbium	37
2. Cupric Oxide	37
3. Oxidized Nichrome	37
4. Nickel Oxide	37
5. Oxidized Stainless Steel	37
6. Oxidized Kennametal	37
V. Analytical and Physical Test Procedures	38
A. Emission Spectrographic Analysis	38
B. X-Ray Diffraction Analysis	38
C. Physical Property Analysis	38
VI. Quality of Measurement	40
A. Quality of Measurement Before Equipment Modifications	40
1. Spectral Emittance Rig	40
2. Total Hemispherical Emittance Rigs	44
3. Long Term Endurance Rigs	46
B. Quality of Measurement After Equipment Modifications	47
1. Spectral Emittance Rig	47
2. Total Hemispherical Emittance Rig	48
VII. Test Results	49
A. Metallic and Oxidized Metallic Surfaces	49
1. Columbium and Oxidized Columbium	49
2. Columbium -1 Per Cent Zirconium Alloy	51
3. Cupric Oxide	52
4. Molybdenum	53
5. Oxidized Nichrome	55
6. Lithiated and Oxidized Nickel	56
7. Oxidized AISI-310 Stainless Steel	57
8. Tantalum	58
9. Tungsten	58
10. Chromium Black	60
11. Platinum Black	63

TABLE OF CONTENTS (cont'd)

	<u>Page</u>
B. Sprayed Coatings	64
1. Borides	64
a. Crystalline Boron	64
b. Boron and Silica	68
c. Molybdenum Diboride	68
d. Tantalum Boride	68
e. Zirconium Boride	69
2. Carbides	69
a. Acetylene Black in Xylol	69
b. Boron Carbide	70
c. Graphite Varnish	73
d. Hafnium Carbide	73
e. Molybdenum Carbide	74
f. Silicon Carbide	74
g. Silicon Carbide and Silicon Dioxide	77
h. Tantalum Carbide	79
i. Titanium Carbide	79
j. Vanadium Carbide	80
3. Fluorides - Calcium Fluoride	80
4. Nitrides - Boron Nitride in Synar	81
5. Single Oxides	81
a. Aluminum Oxide	81
b. Ceric Oxide	83
c. Chromic Oxide	84
d. Cobalt Oxide	87
e. Manganese Oxide	89
f. Nickel Oxide	90
g. Silicon Dioxide	90
h. Stannic Oxide	91
i. Titania	92
j. "Titania Base" Powder	96
k. Zirconium Oxide	98
6. Multiple Oxides	100
a. Silicates - Zirconium Silicate	100
b. Spinels	105
1. Magnesium Aluminate	105
2. 40 Per cent Nickel Chrome Spinel - 60 Per Cent Silicon Dioxide	106

TABLE OF CONTENTS (cont'd)

	<u>Page</u>
c. Titanates	111
1. Barium Titanate	111
2. Calcium Titanate	111
3. Iron - Titanium Oxide	116
4. Iron - Titanium - Aluminum Oxide	118
5. Strontium Titanate	120
d. Zirconates - Calcium Zirconate	124
7. Silicides - Molybdenum Disilicide	124
8. Miscellaneous Sprayed Coatings	125
a. Iron Oxide	125
b. Oxidized Kennametal K-151-A	125
c. Krylon Black	126
d. Palladium Black	127
e. Titanium Oxide and Aluminum Oxide	128
C. Electrophoretic Coating - Silicon Carbide	129
D. Other Coatings	129
Appendix A - Definition of Terms and Spectral Emittance Integration	A-1
Appendix B - Theoretical Evaluation of the Effect of Reflections from the Container Walls on Measurements of Emittance	B-1
Appendix C - Unity Emittance Line Characteristics and Application of Unity Emittance Line in Spectral Emittance Determi- nation	C-1
Appendix D - Elimination of Scattered White Light in Monochromator as an Appreciable Source of Error in Spectral Emittance Data	D-1
Appendix E - Scattered Light in the External Optics	E-1
Appendix F - Specimen End Cooling	F-1

TABLE OF CONTENTS (Cont'd)

	<u>Page</u>
Appendix G - Analytical Evaluation of the Quality of the Black-Body Hole and Associated Heat Generation and Temperature Perturbations	G-1
Appendix H - Experimental Evaluation of Temperature Perturbations and Black-Body Quality	H-1
Appendix I - Effect of Nonuniform Wall Thickness on Temperature Distribution	I-1
Appendix J - Temperature Difference Between Two Surfaces of a Thin Strip Radiating at Two Emittances	J-1
Appendix K - Errors in Total Hemispherical Emittance Measurements Resulting From the Use of Alternating Heating Currents	K-1
Appendix L - Thermocouple Lead Conduction Error	L-1
Appendix M - Temperature Perturbation at Scratch in Specimen Surface Coating	M-1
Appendix N - Comparison of Thermocouple and Optical Pyrometer Temperature Measurements	N-1
Appendix O - References	O-1
Appendix P - Nomenclature	P-1
<u>Volume II</u>	
Appendix Q - Tables	1
<u>Volume III</u>	
Appendix R - Figures	1

LIST OF FIGURES

<u>Number</u>	<u>Title</u>	<u>Number</u>	<u>Title</u>
1	Spectral Normal Emittance Rig	24	Sketch of the Short Term Endurance Rig Showing the Relative Location of Specimen and Rig Detail
2	Vacuum Chamber for Spectral Normal Emittance Rig	25	Short and Long Term Endurance Rigs
3	Instrumentation Flange Assembly and Specimen for Spectral Normal Emittance Rig	26	Typical Instrumentation and Accessory Equipment for Long Term Endurance Rig
4	Optical Pyrometer and Alignment Microscope Assembly on Spectral Normal Emittance Rig	27	Sectioned Drawing of Instrumentation Flange of Long Term Endurance Rigs with a SNAP-8 Fin Segment Installed
5	Schematic Wiring Diagram of Regulated Power Supply and Measuring Circuits for the Spectral Emittance Rig	28	Typical SNAP-8 Fin Segment Instrumented with Platinum-Platinum 10% Rhodium Thermocouples Installed in Long Term Endurance Rig with Vacuum Chamber Removed
6	Schematic Diagram of the Optical System of Perkin Elmer Model 13U Infrared Spectrophotometer Adapted for Measurements of Spectral Emittance	29	Typical SNAP-8 Fin Segment Showing Platinum-Platinum 10% Rhodium Thermocouple Support Assembly
7	Spectral Emittance Rig Optical System with Modified Infrared Spectrophotometer	30	Sunflower I Fin Segment Showing Platinum-Platinum 10% Rhodium Thermocouple Support Assembly on Tube Side of Specimen
8	Beam Separator on Spectral Normal Emittance Rig	31	Sunflower I Fin Segment Showing Platinum-Platinum 10% Rhodium Thermocouple Support Assembly on Flat Side of Specimen
9	Aperture Microscope Assembly on Spectral Normal Emittance Rig	32	Control and Instrumentation Console for High Vacuum Endurance Rigs
10	Alignment Lamp on Spectral Normal Emittance Rig	33	Block Diagram of Instrumentation and Accessory Equipment for Endurance Rig
11	Schematic Diagram of the Optical System of Perkin Elmer Model 13U Infrared Spectrophotometer Adapted for Measurements of Spectral Emittance	34	Instrumentation Flange Installed on Base Plate for Aluminum Fin Thermal Cycling Rig
12	Instrumentation Flange of New Total Hemispherical Emittance Rig	35	Specimen Installed In Aluminum Fin Thermal Cycling Rig Instrumentation Flange
13	Circular Tubular Emittance Test Specimen Showing Thermocouple Locations	36	Typical Test Specimen with Thermocouples for Aluminum Fin Thermal Cycling Rig
14	Rear of Control and Instrumentation Console for New Total Hemispherical Emittance Rig	37	Aluminum Fin Thermal Cycling Rig
15	Control and Instrumentation Console for New Total Hemispherical Emittance Rig	38	Jig for Drilling Specimen Black Body Holes
16	New Total Hemispherical Emittance Rig and Associated Equipment	39	Jig for Forming Triangular-Shaped Specimens
17	Block Diagram of Instrumentation for New Total Hemispherical Emittance Rig	40	Typical Segment of Coated Strip Sample with Thermocouple
18	Original Total Emittance Rig and Associated Equipment	41	Typical Spectrophotometer Beam Power Ratio Scans
19	Sectioned Drawing of Original Total Hemispherical Emittance Rig Showing the Relative Location of Specimen & Rig Detail	42	Drawing of Circular Tubular Emittance Specimen Showing Thermocouple and Potential Lead Locations when Prepared for Measurements in the Spectral Emittance Rig
20	Block Diagram of Vacuum System & Power Supplies for Original Total Hemispherical Emittance Rig	43	Total Hemispherical Emittance vs Temperature, Oxidized Columbium Tube and Grit Blasted Columbium Tube
21	Test Specimen Geometry & Instrumentation Arrangement of Original Total Hemispherical Emittance & Short Term Endurance Rigs	44	Total Hemispherical Emittance vs. Time, Grit Blasted Columbium
22	Block Diagram of Original Total Hemispherical Rig Instrumentation	45	Appearance of Grit Blasted Columbium Tube Before and After Testing
23	Short Term Endurance Rig Showing the Assembled Vacuum Chamber		

LIST OF FIGURES (Continued)

<u>Number</u>	<u>Title</u>	<u>Number</u>	<u>Title</u>
46	Spectral Normal Emittance vs. Temperature, Oxidized Columbium Tube	70	Total Hemispherical Emittance vs. Temperature, Chromium Black on AISI-310 Stainless Steel and Nickel
47	Appearance of Oxidized Columbium Tube Before and After Testing	71	Total Hemispherical Emittance vs. Time, Chromium Black on AISI-310 Stainless Steel and Nickel
48	Total Hemispherical Emittance vs. Temperature, Columbium - 1% Zirconium	72	Spectral Normal Emittance vs. Wavelength, Chromium Black on AISI-310 Stainless Steel
49	Spectral Normal Emittance vs. Wavelength, Uncoated, Polished Columbium - 1% Zirconium	73	Total Hemispherical Emittance vs. Temperature, Platinum Black on AISI-310 Stainless Steel
50	Total Hemispherical Emittance vs. Temperature, Ebonol C on AISI-310 Stainless Steel	74	Appearance of AISI-310 Stainless Steel Strip Coated with Platinum Black Before and After Testing
51	Appearance of AISI-310 Stainless Steel Strip Coated with Cupric Oxide Before and After Testing	75	Total Hemispherical Emittance vs. Time, Platinum Black on AISI-310 Stainless Steel
52	Spectral Normal Emittance vs. Wavelength, Molybdenum	76	Total Hemispherical Emittance vs. Temperature, Crystalline Boron on Molybdenum and Columbium
53	Total Hemispherical Emittance vs. Temperature, Molybdenum Wedge	77	Total Hemispherical Emittance vs. Time, Crystalline Boron on Molybdenum
54	Total Hemispherical Emittance vs. Temperature, Molybdenum	78	Bonding Failure of Boron Coating on Molybdenum Strip
55	Total Hemispherical Emittance vs. Temperature, Molybdenum, Comparison of Spectral Normal and Total Hemispherical Emittance Rigs	79	Spectral Normal Emittance vs. Wavelength, Crystalline Boron on Columbium
56	Total Hemispherical Emittance vs. Temperature, Effect of Vapor-Blast on Molybdenum Strip	80	Total Hemispherical Emittance vs. Temperature, Boron and Silica on Aluminum
57	Total Hemispherical Emittance vs. Temperature, Oxidized Nichrome	81	Total Hemispherical Emittance vs. Temperature, Molybdenum Diboride on Molybdenum
58	Total Hemispherical Emittance vs. Temperature, Oxidized and Lithiated Nickel C on AISI-310 Stainless Steel	82	Total Hemispherical Emittance vs. Temperature, Tantalum Boride on Molybdenum
59	Microstructure of Lithiated and Oxidized Nickel C Coating Sintered on Stainless Steel, Before Test	83	Total Hemispherical Emittance vs. Temperature, Zirconium Boride on Molybdenum
60	Microstructure of Lithiated and Oxidized Nickel C Coating Sintered on Stainless Steel, After Test	84	Total Hemispherical Emittance vs. Temperature, Acetylene Black in Xylo on AISI-310 Stainless Steel and Aluminum
61	Total Hemispherical Emittance vs. Time, Oxidized and Lithiated Nickel C on AISI-310 Stainless Steel	85	Total Hemispherical Emittance vs. Temperature, Boron Carbide on Columbium - 1% Zirconium and Molybdenum
62	Total Hemispherical Emittance vs. Temperature, Oxidized and Grit Blasted AISI-310 Stainless Steel	86	Total Hemispherical Emittance vs. Time, Boron Carbide on Molybdenum
63	Appearance of Oxidized AISI-310 Stainless Steel Strip Before and After Testing	87	Spectral Normal Emittance vs. Wavelength, Boron Carbide on Columbium - 1% Zirconium
64	Appearance of Oxidized and Grit Blasted AISI-310 Stainless Steel Strip Before and After Testing	88	Total Hemispherical Emittance vs. Temperature, Graphite Varnish on AISI-310 Stainless Steel
65	Total Hemispherical Emittance vs. Time, AISI-310 Stainless Steel	89	Total Hemispherical Emittance vs. Temperature, Hafnium Carbide on Molybdenum
66	Spectral Normal Emittance vs. Wavelength, Tantalum	90	Total Hemispherical Emittance vs. Temperature, Molybdenum Carbide on Molybdenum
67	Spectral Normal Emittance vs. Wavelength, Tungsten	91	Total Hemispherical Emittance vs. Temperature, Silicon Carbide on Columbium - 1% Zirconium
68	Spectral Normal Emittance vs. Wavelength, Tungsten	92	Spectral Normal Emittance vs. Wavelength, Silicon Carbide on Columbium - 1% Zirconium
69	Total Hemispherical Emittance vs. Temperature, Tungsten	93	Total Hemispherical Emittance vs. Time, Silicon Carbide on Columbium - 1% Zirconium
		94	Total Hemispherical Emittance vs. Temperature, Silicon Carbide and Silicon Dioxide on AISI-310 Stainless Steel and Aluminum

LIST OF FIGURES (Continued)

<u>Number</u>	<u>Title</u>	<u>Number</u>	<u>Title</u>
95	Silicon Carbide and Silicon Dioxide Coated SNAP-8 Test Section Prior to Testing	117	Total Hemispherical Emittance vs. Temperature, "Titania Base" on Aluminum and AISI-310 Stainless Steel
96	Silicon Carbide and Silicon Dioxide Coated SNAP-8 Test Section After 8683 Hours of Endurance Testing	118	Total Hemispherical Emittance vs. Time, "Titania Base" on AISI-310 Stainless Steel
97	Long Term Endurance Test, Silicon Carbide and Silica Coating on SNAP-8 Test Section	119	Titania Coated SNAP-8 Test Section Before Testing
98	Total Hemispherical Emittance vs. Temperature, Tantalum Carbide on Molybdenum	120	Titania Base Coated SNAP-8 Fin Segment After 2810 Hours of Endurance Testing
99	Total Hemispherical Emittance vs. Temperature, Titanium Carbide on Molybdenum	121	Titania Base Coated SNAP-8 Fin Segment After 3490 Hours of Endurance Testing
100	Total Hemispherical Emittance vs. Temperature, Vanadium Carbide on Molybdenum	122	Titania Base Coated SNAP-8 Test Section After 6840 Hours of Endurance Testing
101	Total Hemispherical Emittance vs. Temperature, Calcium Fluoride on AISI-310 Stainless Steel	123	Titania Base Coated SNAP-8 Test Section After Approximately 8300 Hours of Endurance Testing
102	Total Hemispherical Emittance vs. Temperature, Boron Nitride on Tantalum	124	Long Term Endurance Test, Titania Base Coating on SNAP-8 Test Section
103	Total Hemispherical Emittance vs. Temperature, Aluminum Oxide on AISI-310 Stainless Steel	125	Titania Base Coated Sunflower I Test Section After 9914 Hours of Endurance Testing
104	Total Hemispherical Emittance vs. Temperature, Ceria on Columbium - 1% Zirconium and AISI-310 Stainless Steel	126	Long Term Endurance Test, Titania Base Coating on Sunflower I Test Section
105	Total Hemispherical Emittance vs. Temperature, Chromic Oxide	127	Total Hemispherical Emittance vs. Temperature, Zirconium Oxide on Molybdenum and Stainless Steel
106	Total Hemispherical Emittance vs. Time, Chromic Oxide on Columbium and AISI-310 Stainless Steel	128	Total Hemispherical Emittance vs. Temperature, Zirconium Silicate on Columbium - 1% Zirconium and AISI-310 Stainless Steel
107	Spectral Normal Emittance vs. Wavelength, Chromic Oxide (Rokide) on Columbium	129	Spectral Normal Emittance vs. Wavelength, Zirconium Silicate on Columbium - 1% Zirconium
108	Total Hemispherical Emittance vs. Temperature, Cobalt Oxide on Columbium - 1% Zirconium	130	Total Hemispherical Emittance vs. Time, Zirconium Silicate (Rokide) on Columbium - 1% Zirconium
109	Total Hemispherical Emittance vs. Temperature, Manganese Oxide on Columbium - 1% Zirconium	131	Total Hemispherical Emittance vs. Temperature, Magnesium Aluminate (Rokide) on Columbium - 1% Zirconium
110	Total Hemispherical Emittance vs. Temperature, Nickel Oxide on Columbium - 1% Zirconium	132	Spectral Normal Emittance vs. Wavelength, Magnesium Aluminate (Rokide) on Columbium - 1% Zirconium
111	Total Hemispherical Emittance vs. Temperature, Silica on Columbium - 1% Zirconium	133	Total Hemispherical Emittance vs. Temperature, Nickel-Chrome Spinel and Silica on AISI-310 Stainless Steel and Aluminum
112	Total Hemispherical Emittance vs. Temperature, Stannic Oxide on Columbium - 1% Zirconium	134	Total Hemispherical Emittance vs. Time, Nickel-Chrome Spinel on AISI-310 Stainless Steel
113	Total Hemispherical Emittance vs. Temperature, Titanium Oxide on AISI-310 Stainless Steel, Columbium and Aluminum	135	Long Term Endurance Test, Nickel-Chrome Spinel and Silica on SNAP-8 Test Section
114	Total Hemispherical Emittance vs. Temperature, Titania on Columbium - 1% Zirconium	136	Nickel-Chrome Spinel and Silicon Dioxide Coated SNAP-8 Test Section After Being Overheated After Approximately 2700 Hours of Endurance Testing
115	Total Hemispherical Emittance vs. Time, Titania on AISI-310 Stainless Steel		
116	Spectral Normal Emittance vs. Wavelength, Titania on Columbium - 1% Zirconium and Columbium		

LIST OF FIGURES (Continued)

<u>Number</u>	<u>Title</u>	<u>Number</u>	<u>Title</u>
137	Nickel Chrome Spinel and Silicon Dioxide Coated SNAP-8 Test Section After 7200 Hours of Endurance Testing	149	Total Hemispherical Emittance vs. Temperature, Iron-Titanium-Aluminum Oxide on Columbium - 1% Zirconium
138	Nickel Chrome Spinel and Silicon Dioxide Coated SNAP-8 Test Section After 7200 Hours of Endurance Testing	150	Total Hemispherical Emittance vs. Time, Iron-Titanium-Aluminum Oxide on Columbium - 1% Zirconium
139	Nickel Chrome Spinel and Silicon Dioxide Coated SNAP-8 Test Section After 7200 Hours of Endurance Testing	151	Spectral Normal Emittance vs. Wavelength, Iron-Titanium-Aluminum Oxide on Columbium - 1% Zirconium
140	Nickel Chrome Spinel and Silicon Dioxide Coated SNAP-8 Test Section After Approximately 10,800 Hours of Endurance Testing	152	Total Hemispherical Emittance vs. Temperature, Strontium Titanate on Columbium - 1% Zirconium and AISI-310 Stainless Steel
141	Total Hemispherical Emittance vs. Temperature, Barium Titanate on Columbium - 1% Zirconium	153	Spectral Normal Emittance vs. Wavelength, Strontium Titanate on Columbium - 1% Zirconium
142	Spectral Normal Emittance vs. Wavelength, Barium Titanate on Columbium - 1% Zirconium	154	Total Hemispherical Emittance vs. Time, Strontium Titanate on Columbium - 1% Zirconium
143	Total Hemispherical Emittance vs. Temperature, Calcium Titanate on Columbium - 1% Zirconium and AISI-310 Stainless Steel	155	Total Hemispherical Emittance vs. Temperature, Calcium Zirconate on AISI-310 Stainless Steel
144	Total Hemispherical Emittance vs. Time, Calcium Titanate on Columbium	156	Total Hemispherical Emittance vs. Temperature, Molybdenum Disilicide on Molybdenum
145	Spectral Normal Emittance vs. Temperature, Calcium Titanate on Columbium and Columbium - 1% Zirconium	157	Total Hemispherical Emittance vs. Temperature, Iron Oxide on Nickel
146	Total Hemispherical Emittance vs. Temperature, Iron-Titanium Oxide on Columbium - 1% Zirconium	158	Total Hemispherical Emittance vs. Temperature, Oxidized Kennametal (K-151-A) on AISI-310 Stainless Steel
147	Total Hemispherical Emittance vs. Time, Iron-Titanium Oxide on Columbium - 1% Zirconium	159	Total Hemispherical Emittance vs. Temperature, Krylon Black on AISI-310 Stainless Steel
148	Spectral Normal Emittance vs. Wavelength, Iron-Titanium Oxide on Columbium - 1% Zirconium	160	Total Hemispherical Emittance vs. Temperature, Palladium Black on AISI-310 Stainless Steel
		161	Total Hemispherical Emittance vs. Temperature, 50% Titanium Oxide - 50% Aluminum Oxide on AISI-310 Stainless Steel and Aluminum
		162	Total Hemispherical Emittance vs. Temperature, Electrophoretic Silicon Carbide on Molybdenum

LIST OF TABLES

<u>Number</u>	<u>Title</u>	<u>Page</u>	<u>Number</u>	<u>Title</u>	<u>Page</u>
1	Grit Blasted Columbium	2	34	Acetylene Black in Xylol on AISI-310 Stainless Steel Tube	59
2	Oxidized Columbium	3	35	Acetylene Black in Xylol on Aluminum	63
3	Columbium-1% Zirconium, As Received	7	36	Boron Carbide with Synar Binder on Molybdenum	65
4	Columbium-1% Zirconium, Polished	8	37	Boron Carbide Plasma-Arc Sprayed on Molybdenum	67
5	Cupric Oxide on AISI-310 Stainless Steel	9	38	Boron Carbide Aluminum-Phosphate Bonded to Columbium-1% Zirconium	73
6	Molybdenum Wedge	10	39	Graphite Varnish on AISI-310 Stainless Steel	74
7	Chemically Cleaned Molybdenum Strip	11	40	Hafnium Carbide on Molybdenum	75
8	Vapor Blasted Molybdenum Strip	12	41	Molybdenum Carbide on Molybdenum	76
9	Grit Blasted Molybdenum	13	42	Silicon Carbide on Columbium-1% Zirconium - First Specimen	77
10	Grit Blasted Molybdenum Strip	14	43	Silicon Carbide on Columbium-1% Zirconium - Second Specimen	78
11	Nichrome Oxidized in Air	15	44	Silicon Carbide on Columbium-1% Zirconium - Third Specimen	79
12	Nichrome Strip Oxidized in Oxygen	16	45	Silicon Carbide on Columbium-1% Zirconium - Fifth Specimen	80
13	Lithiated and Oxidized Nickel C on AISI-310 Stainless Steel	18	46	Silicon Carbide on Columbium-1% Zirconium - Fifth Specimen	81
14	Lithiated and Oxidized Nickel C (3-Mil) on AISI-310 Stainless Steel	19	47	Silicon Carbide and Silicon Dioxide on AISI-310 Stainless Steel	82
15	AISI-310 Stainless Steel - Oxidized	21	48	Silicon Carbide and Silicon Dioxide on Aluminum	84
16	AISI-310 Stainless Steel - Grit Blasted and Oxidized Strip	23	49	Tantalum Carbide on Molybdenum	87
17	AISI-310 Stainless Steel - Grit Blasted and Oxidized Tube	24	50	Titanium Carbide on Molybdenum	89
18	Tungsten	26	51	Vanadium Carbide on Molybdenum	91
19	Chromium Black on AISI-310 Stainless Steel Strip	27	52	Calcium Fluoride on AISI-310 Stainless Steel	93
20	Chromium Black on AISI-310 Stainless Steel Tube	30	53	Boron Nitride and Synar Binder on Tantalum	94
21	Chromium Black on Nickel	31	54	Aluminum Oxide (1.3-Mil) on AISI-310 Stainless Steel	95
22	Platinum Black on AISI-310 Stainless Steel - First Specimen	34	55	Aluminum Oxide (2.0-Mil) on AISI-310 Stainless Steel	96
23	Platinum Black on AISI-310 Stainless Steel - Second Specimen	35	56	Aluminum Oxide (2.1-Mil) on AISI-310 Stainless Steel	97
24	Platinum Black on AISI-310 Stainless Steel - Third Specimen	36	57	Ceria on AISI-310 Stainless Steel	98
25	Crystalline Boron on Molybdenum - First Specimen	38	58	Ceria on Columbium - 1% Zirconium	99
26	Crystalline Boron on Molybdenum - Second Specimen	39	59	Chromic Oxide on Molybdenum	100
27	Crystalline Boron on Molybdenum - Third Specimen	48	60	Chromic Oxide on Columbium	102
28	Crystalline Boron on Columbium	50	61	Rokide C on AISI-310 Stainless Steel	105
29	Boron and Silicon Dioxide on Aluminum	51	62	Rokide C on Columbium	106
30	Molybdenum Diboride on Molybdenum	54	63	Chromia (3.0-Mil) on Columbium - 1% Zirconium	107
31	Tantalum Boride on Molybdenum	56	64	Chromia (4.0-Mil) on Columbium - 1% Zirconium	108
32	Zirconium Boride on Molybdenum	57			
33	Acetylene Black in Xylol on AISI-310 Stainless Steel Strip	58			

LIST OF TABLES (Continued)

<u>Number</u>	<u>Title</u>	<u>Page</u>	<u>Number</u>	<u>Title</u>	<u>Page</u>
65	Cobalt Oxide on Columbium - 1% Zirconium	109	95	Barium Titanate on Columbium - 1% Zirconium	148
66	Manganese Oxide on Columbium - 1% Zirconium	110	96	Calcium Titanate on AISI-310 Stainless Steel	149
67	Nickel Oxide on Columbium - 1% Zirconium	111	97	Calcium Titanate on Columbium	151
68	Silica on Columbium - 1% Zirconium	112	98	Calcium Titanate on Columbium	152
69	Stannic Oxide on Columbium - 1% Zirconium	113	99	Calcium Titanate on Columbium - 1% Zirconium First Specimen	153
70	Titanium Oxide on AISI-310 Stainless Steel - First Specimen	114	100	Calcium Titanate on Columbium - 1% Zirconium - Second Specimen	154
71	Titanium Oxide on AISI-310 Stainless Steel - Second Specimen	117	101	Calcium Titanate on Columbium - 1% Zirconium - Third Specimen	155
72	Titanium Oxide on Aluminum	119	102	Iron-Titanium Oxide on Columbium - 1% Zirconium - First Test	156
73	Titanium Oxide on Columbium	122	103	Iron-Titanium Oxide on Columbium - 1% Zirconium - Second Test	157
74	Titanium Oxide (5.0-Mil) on Columbium - 1% Zirconium	123	104	Iron-Titanium Oxide on Columbium - 1% Zirconium - Third Test	158
75	Titanium Oxide (1.0-Mil) on Columbium - 1% Zirconium	124	105	Iron-Titanium-Aluminum Oxide on Columbium - 1% Zirconium	159
76	"Titania Base" (1.6-Mil) on AISI-310 Stainless Steel	125	106	Iron-Titanium-Aluminum Oxide on Columbium - 1% Zirconium	160
77	"Titania Base" (2.7-Mil) on AISI-310 Stainless Steel	128	107	Iron-Titanium-Aluminum Oxide on Columbium - 1% Zirconium	161
78	"Titania Base" on Aluminum	129	108	Strontium Titanate on AISI-310 Stainless Steel	162
79	Zirconium Oxide on Molybdenum	131	109	Strontium Titanate (2-Mil) on Columbium - 1% Zirconium	163
80	Zirconium Oxide (1-Mil) on AISI-310 Stainless Steel	133	110	Strontium Titanate (4.0-Mil) on Columbium - 1% Zirconium	164
81	Zirconium Oxide (6-Mil) on AISI-310 Stainless Steel	134	111	Strontium Titanate (4.0-Mil) on Columbium - 1% Zirconium	165
82	Zirconium Silicate Plasma-Arc Sprayed on Columbium - 1% Zirconium	135	112	Strontium Titanate (4.0-Mil) on Columbium - 1% Zirconium	166
83	Zirconium Silicate Plasma-Arc Sprayed on AISI-310 Stainless Steel	136	113	Calcium Zirconate on AISI-310 Stainless Steel	167
84	Zirconium Silicate Aluminum-Phosphate Bonded to Columbium - 1% Zirconium	137	114	Molybdenum Disilicide on Molybdenum	168
85	Rokide ZS on AISI-310 Stainless Steel	138	115	Iron Oxide on Nickel	169
86	Rokide ZS on Columbium - 1% Zirconium	139	116	Oxidized Kennametal on AISI-310 Stainless Steel	173
87	Rokide ZS on Columbium - 1% Zirconium	140	117	Krylon Black (1.3-Mil) on AISI-310 Stainless Steel	174
88	Rokide MA on Columbium - 1% Zirconium	141	118	Krylon Black (3.0-Mil) on AISI-310 Stainless Steel	175
89	Nickel-Chrome Spinel and Silica on AISI-310 Stainless Steel	142	119	Palladium Black (1.0-Mil) on AISI-310 Stainless Steel	176
90	Nickel-Chrome Spinel and Silica on AISI-310 Stainless Steel - First Endurance Test	143	120	50% Titanium Oxide - 50% Aluminum Oxide on AISI-310 Stainless Steel Strip	177
91	Nickel-Chrome Spinel and Silica on AISI-310 Stainless Steel - Second Endurance Test	144	121	50% Titanium Oxide - 50% Aluminum Oxide on AISI-310 Stainless Steel Tube	179
92	Nickel-Chrome Spinel and Silica (2.2-Mil) on Aluminum	145	122	50% Titanium Oxide - 50% Aluminum Oxide on Aluminum	181
93	Nickel-Chrome Spinel and Silica (2.8-Mil) on Aluminum	146	123	Silicon Dioxide - Electrophoretic Process, on Molybdenum	183
94	Nickel-Chrome Spinel and Silica (3.9-Mil) on Aluminum	147			

I. INTRODUCTION

Space propulsion systems have emphasized the importance of radiant heat transfer systems. The achievement of proper design requires a knowledge of the emittance, absorptance, and reflectance of radiator component materials under conditions similar to those encountered in space.

In space systems using solar or nuclear energy for electrical propulsion machinery, the efficient rejection of waste heat is of the utmost importance. Radiators with sufficient capacity to remove this heat comprise one-third to one-half of the total weight of the powerplant. In addition to the heat rejection requirements of the propulsion power system, cooling of the electrical equipment, instruments, guidance systems, and crew all require radiation of heat to space. Since radiator weights are approximately inversely proportional to the emittances of their surfaces for a given rate of heat rejection, it is particularly important that high emittance radiator surface materials be developed and evaluated. In addition, radiators operating below 1000°F and exposed to the sun ideally should have relatively low absorptance for solar radiation in conjunction with high thermal emittance.

Prior to this program, published data on thermal radiation properties were not sufficient to design optimum space propulsion systems. It was found that information was lacking for many potential radiator materials operating at elevated temperatures and that most data had not been obtained from material in vacuum. Further, little information was found on the change of emittance of materials exposed to elevated temperatures and high vacuum for extended periods where changes can occur as a result of chemical reactions, sublimation, and other phenomena.

Contract NASw -104 was awarded to the Pratt & Whitney Aircraft Division of United Aircraft Corporation by the National Aeronautics and Space Administration to provide basic information on the radiant characteristics of materials suitable for space power and propulsion systems under high vacuum conditions. In accordance with the requirements of this contract, Pratt & Whitney Aircraft investigated the emittance of metals and coated metal surfaces at temperatures up to 3100°F in high vacuum at its East Hartford, Connecticut facility. The program, as reported herein, was conducted between July 1, 1959, and December 31, 1962.

The total hemispherical emittance and the spectral normal emittance of a large number of materials were measured. The total normal emittance of a number of materials was calculated by integrating spectral normal emittance data. In addition, endurance characteristics have been obtained for selected materials operating at elevated temperatures and vacuum for various periods, some of which have exceeded 10,000 hours. These tests are continuing.

Prior to the contract, the techniques used for similar work by other experimenters were studied. Through consultation with Dr. Wayne B. Nottingham, Professor of Physics at the Massachusetts Institute of Technology, and Dr. William L. Trousdale, Assistant Professor of Physics at Trinity College, the decision was made to use the method of Larrabee¹ and DeVos² for measuring spectral normal emittance, and the method used by Langmuir³ for measuring total hemispherical emittance.

To measure spectral normal emittance by the method of Larabee and DeVos, the intensity of radiation emitted normally from a tubular specimen surface at a particular wavelength is compared with the intensity of radiation from a small "black-body" hole drilled in the tube wall. Since both sources of radiation are at essentially the same temperature, and since radiation from the hole closely approximates that emitted by a black body, the ratio of the intensity of radiation from the surface to that from the black-body hole is a close measure of the spectral normal emittance of the specimen surface.

Total hemispherical emittance was determined by Langmuir's method for which the power input to the specimen and the specimen surface temperature are used for calculating the emittance. The test conditions are such that essentially all of the energy supplied to the specimen is rejected by radiation, and the theoretical radiation from a black body operating at the specimen surface temperature may be calculated from the Stephan - Boltzmann equation. Hence, the total hemispherical emittance is determined by calculating the ratio of the specimen power input per unit area to the theoretical intensity of black body radiation at the same temperature.

The specimens for determining the emittance of metals were in the form of strips or tubes. When nonmetallic materials were tested, they were applied as thin coatings onto metal substrates to form composite test specimens. The emittances reported are based on the temperature of the metal substrate. Using this procedure, the test specimen simulated a radiator section and the effective emittance values reported are, therefore, directly applicable to radiator design and do not require corrections for coating temperature drop or opaqueness.

II. APPARATUS

A. Introduction

In order to measure accurately the emittances of materials under simulated space conditions, eight rigs were designed and fabricated in accordance with the following basic requirements:

1. No significant amount of radiation from the surface of the specimen should be reflected back to the specimen by the vacuum chamber walls.
2. Conduction heat losses from the specimen through the power connections and instrumentation lead wires should be negligible compared to heat rejection by radiation.
3. Pressure in the test chamber must be 10^{-6} mm Hg or lower.

The test rigs used for this program included a spectral normal, a total hemispherical, and a short term endurance emittance rig. In addition, four long term endurance rigs and an aluminum fin thermal cycling rig were used.

The spectral normal emittance rig, which was usually operated at temperatures above 1400°F, permitted values of spectral normal emittance to be obtained over the wavelength range of 0.45 to 15 microns. Any of the three emittance rigs could be used for measurement of total hemispherical emittance, but the total hemispherical emittance rig was generally used when this parameter was the only one of interest. Operation was generally between 300°F and 2200°F, although measurements at higher temperatures were made when required. The short term endurance rig was usually operated at a constant temperature to allow determination of emittance changes with time. The four long term endurance rigs were used to determine the stability and adherence of coating materials when exposed to high temperatures and low pressures for extended periods. The aluminum fin thermal cycling rig was used for evaluating the coating-substrate bond strengths of various coating materials being considered for long term endurance testing.

B. Spectral Normal Emittance Rig

Modified Rig - As may be seen in Figure 1, the spectral normal emittance apparatus includes a vacuum chamber and associated evacuation equip-

ment, a power supply for specimen heating, instrumentation for power and temperature measurement, and an infrared spectrophotometer equipped with transfer optics to focus on the specimen.

The vacuum chamber, shown in Figure 2, is a thirteen-inch long flanged tube with a 3-inch inside diameter. The inside wall of the chamber is grooved and coated with Ebonol C to minimize reflection. The chamber is wrapped with 3/16-inch diameter copper tubing for water-cooling to minimize radiation from the walls. In addition, a 2.5-kilowatt heating element is wound over the cooling coil to bake out the chamber during initial evacuation. The instrumentation flange at the upper end of the chamber is sealed with a 0.020-inch thick gold O-ring compressed between polished surfaces. Incorporated into this flange is the water-cooled copper electrode assembly which both supplies power to the specimen and supports it inside the chamber. The electrodes are insulated from the flange by a commercial glass potting compound (Pyrocera) and provision is made for thermal expansion of the specimen. Details of the flange are shown in Figure 3. The bottom of the chamber is connected to a vacuum manifold. The entire assembly is mounted on a milling machine table to permit the specimen under test to be positioned at the focal point of the spectrophotometer optical system.

The evacuation equipment used for attaining the required low pressures consists of an oil-sealed mechanical pump in conjunction with a liquid-nitrogen cold trap and an ion-gettering pump. The mechanical pump, which has a limiting pressure of 10^{-4} mm Hg, was used for initial pumping and while the system was being baked out. The ion-gettering pump was then used to attain pressures in the 10^{-10} mm Hg range. The chamber pressure was measured with a Bayard-Alpert type ionization gauge and also by monitoring the current to the ion-gettering pump.

The viewing port was located in the side of the chamber and consisted of an optically plane sodium chloride window cemented with epoxy resin to a stainless steel cell. The cell assembly was bolted and sealed with a gold O-ring to a mating flange which was welded to a tubular extension from the chamber wall. The window was protected from condensate by a magnetically controlled rolling disk shutter installed in a slot between the cell and the flange.

The specimens were direct-current resistance heated using the specimen substrate material as the resistive element. Current through the specimen was measured with a shunt and a slide wire potentiometer. This potentiometer did not have sufficient range to measure the voltage across the specimen, however, and it was therefore necessary to use an auxiliary reference potentiometer with a 100:1 voltage divider. Power for the specimen was supplied by a three-phase full wave rectifier rated at 650 amperes. Voltage output was variable from 0 to 24 volts by a three-phase autotransformer. A shunt-type servo-controlled regulator maintained either the output voltage or current to within ± 0.02 per cent and provided fine control for precise power setting. The schematic wiring diagram of the power supply is shown in Figure 5.

Specimen temperatures lower than 1400°F were measured by thermocouples. A proportional buck-boost circuit was used to cancel the emf introduced into the thermocouple circuit by the specimen voltage drop. Specimen temperatures higher than 1400°F were measured with an optical pyrometer. The optical pyrometer was mounted on a hinged bracket attached to the viewing port and could be swung away from the window when not in use. The optical pyrometer assembly is shown in Figure 4.

The optical system used for measuring spectral emittance is shown in Figures 6 and 7. The system consists of a modified Perkin-Elmer Model 13-U dual beam spectrophotometer with special transfer optics. Three mirrors are used in the transfer system to direct the radiant energy from the specimen into the optical system of the spectrophotometer. The first of these, M -2 (read as "M minus two") is an eight-inch off-axis ellipsoidal mirror with a twenty-four inch radius of curvature that was specially designed to render high resolution with off-axis operation to permit precise focusing on small black-body holes. Following the ellipsoidal mirror is a diagonal mirror, M -1, and a double diagonal mirror, MO. Permanent alignment is maintained by bolting the spectrophotometer and the external optics to an optical bench.

The spectrophotometer was modified in two ways: a port was provided in the source optics cover to permit the entrance of radiant energy from the diagonal mirror, M⁻¹, and the radiation source was removed to permit installation of a beam separator (see Figure 8). The principal elements of the beam separator are the double diagonal mirror and a plate with two holes 0.0185 inch in diameter. The hole centers are separated by 0.0525 inch, which is slightly greater than the separation of the specimen black-body holes to allow for thermal growth of the specimen. The two plane diagonal mirrors which comprise MO are located directly behind the aperture plate and independently intercept all of the energy from the corresponding apertures. These mirrors are adjusted to different azimuths and reflect the two beams to separate areas of spherical mirror M1. The measuring beam (originating from the sample surface) is intercepted by a full height mirror M2 which replaces the original half height mirror. The reference beam (originating from the black-body hole) completely passes mirror M2 and is intercepted by M3. With this arrangement, the beams are separated without loss of aperture which would result if the half-height beam splitting mirror were used. Both beams pass through apertures located at the second focal points to eliminate stray radiation. The reference beam is then intercepted by mirror M5 which directs the radiation to mirror M6. The measuring beam is directed to mirror M6 by mirror M4. Mirror M5 (Figure 9) was specially designed to fully intercept the reference beam without obstructing the measuring beam. The remainder of the spectrophotometer is unchanged.

The spectrophotometer wavelength drum has been calibrated over the wavelength range of 0.45 to 15 microns by the use of the emission spectra of mercury, sodium, potassium, thorium, and cadmium, and by the use of the absorption spectra of water, ammonia, carbon dioxide, and Mylar film.

Two microscopes and an alignment lamp (see Figures 4, 9, and 10) are used as a visual aid in the positioning of the specimen at the focal point of the collecting mirror. The microscope which views the specimen is equipped with a number 47 Wratten blue filter and an infrared absorbing filter and is mounted on the optical pyrometer bracket. The instrument may be swung clear of the spectrophotometer beam when spectral emittance measurements are made. The other microscope is hinge-mounted on the spectrophotometer table and enables

observation of the aperture plate. The viewing mirrors for both microscopes are arranged to provide erect images of the specimen so that any uncertainty in the orientation of the images with respect to the specimen is eliminated. The alignment lamp assembly is mounted in a vertical slide on the monochromator cover and consists of an adjustable microscope illuminator and a diagonal mirror. Light from the illuminator is injected into the optical system which projects a high intensity image of the beam separator aperture onto the specimen. At temperatures below 2200°F, the specimen microscope is used in conjunction with the alignment lamp. At higher temperatures, contrast between the aperture images and the specimen surface is lost. However, at these temperatures, the specimen is sufficiently luminous for its image to be visible at the aperture plate and therefore the aperture microscope is used without the alignment lamp.

Comparison With Original Rig - The spectral normal emittance rig in its present form incorporates several features not included in the original design. The original design did not have the alignment microscopes and lamp and used a 6-inch spherical mirror rather than the ellipsoidal mirror. The new mirror eliminates the severe astigmatism previously encountered. Further, the present system of beam separation replaces an earlier system which used a half-height mirror (M2 in Figure 11) in conjunction with beam isolation apertures which were located at the second focal point of each beam. The new system, which uses all of the energy from each beam and which incorporates the larger ellipsoidal mirror, provides about 3 1/2 times the energy previously available.

A new vacuum chamber flange and specimen holder assembly was constructed. The new flange is held in place by a bolt ring which permits the specimen to be aligned with the viewing port by rotating the cover before the bolts are tightened. Previously, it was necessary to bend the sample holder to align the specimen. The new flange and specimen holder assembly has provisions for 8 chromel-alumel thermocouples, 8 platinum-platinum 10 per cent rhodium thermocouples, and 4 voltage leads.

Changes were also made in the specimen design. The original design included a single black-body hole measuring 0.035 x 0.076 inch and

a flattened tube wall to enhance the black-body quality. The superior resolution of the new collecting mirror permitted the use of a smaller black-body hole. Although it was thought that a narrow slot measuring 0.023 x 0.080 inch would eliminate the need for flattening the rear tube wall, this proved unsatisfactory and the two-hole design was developed.

These changes simplified the test procedure and extended the range of operating conditions at which spectral emittance measurements could be made.

C. Total Hemispherical Emittance Rig

New Rig - The total hemispherical emittance rig presently in use was built in the early part of 1962 and replaced the rig used earlier in the program. The design of the new rig incorporated several features not included in the earlier version. The new rig was provided with a window to permit observation of the specimen during testing and to permit the use of optical measuring equipment. The new rig also allowed easier access to the vacuum chamber interior and was capable of testing specimens with a variety of geometries and configurations. The radiant energy sink of the new rig was larger than that of the old, and greater flexibility in the arrangement of the instrumentation was possible.

The vacuum chamber of the new total hemispherical emittance rig is made of AISI-304 stainless steel and measures 20 inches in height by 15-1/2 inches in diameter. The inner walls were grit blasted and are coated with an aluminum-phosphate bonded mixture of silicon carbide and silicon dioxide. The high emittance (low reflectance) surface and the large diameter of the chamber result in negligible reflected radiation from the chamber walls to the specimen. Permanent bakeout heaters and cooling coils are incorporated into the chamber walls. Water has normally been used for cooling, but, with appropriate accessory systems, other coolants, including liquid nitrogen, can be used. Two windows, 5.4 and 2.0 inches in diameter, respectively, are located 180° apart. Magnetically operating shutters protect the windows from condensable materials when they are not in use. By reflecting the radiation

originating from the specimen onto nearby coated walls, the shutters also eliminate heating of the windows and subsequent radiation of energy from the windows to the specimen. An instrumentation flange (see Figure 12) provides support for the specimen and accessory systems and feedthroughs for control and instrumentation circuitry. The instrumentation flange provides terminals for seven platinum-platinum 10 per cent rhodium and five chromel-alumel thermocouples. The flange is removable so that the rig can be conveniently converted for other purposes. The chamber is usually assembled with Viton O-rings, but O-rings of other materials, including soft metals such as annealed gold, can be used.

For routine operation, the chamber is evacuated by a 400 l/sec oil diffusion pump backed by a liquid nitrogen cold trap and a mechanical roughing pump. Pressures lower than 1×10^{-7} mm Hg are attainable with this system. The chamber can also be operated with an ion-gettering pump when better vacuums are desired. A Bayard-Alpert type ionization gage is used for pressure measurement.

The specimens are generally thin-walled metal tubes 9 inches long and 1/4 inch in diameter and are resistance heated with AC power. The specimen support assembly is cooled to provide high current-carrying capacity and to minimize radiation to the specimen. The specimen supports keep the specimen in tension to prevent buckling as a result of thermal expansion. Both platinum-platinum 10 per cent rhodium and chromel-alumel thermocouples are usually used.

Radiation-type end heaters are used to minimize thermal conduction from the specimen to the cooled power connections and specimen clamps. These heaters are tantalum-wire coils which are oriented coaxially with the specimen and shielded to prevent radiation from the heaters from striking the test section of the specimen. Thermocouples numbers 1 and 7 (see Figure 13) are used to control the end heaters. When end heaters are not used, the temperature profile along the specimen may be determined from thermocouple data and the conduction losses accurately calculated.

The control and instrumentation console is shown in Figures 14, 15, and 16. Contained within the console are power supplies for specimen heating and for each of the end heaters and instruments for measuring temperature and power. Power input to the console is regulated to within 0.25 per cent.

AC power for specimen heating is supplied by a multi-tap step-down transformer with an autotransformer in the primary circuit. The maximum output voltage ranges from 2 to 20 volts in 1-volt increments with a maximum power output of 2.3 kva. The power supplies for each of the end heaters are stepdown transformers with autotransformers in the primary circuits for control. Each of these power supplies has a maximum output of 1 kva.

Power input is determined by measuring the current through and the voltage across the test section. The current is determined by measuring the voltage drop across a calibrated shunt. Four shunts, which are water cooled to ensure constancy of calibration, are used to provide a measurement range from 0 to 500 amperes. The voltage is measured directly with an AC-DC differential voltmeter. Thermocouple wires are used for voltage leads and the position of the thermocouples precisely determines the length of the test section. Switching circuitry permits any two of the thermocouple wires to be used for voltage leads.

Thermocouple outputs are measured with a slide-wire millivolt potentiometer. Temperatures at the center and at the ends of the specimen are monitored when end heaters are used to ensure a satisfactory temperature profile. A block diagram of the instrumentation arrangement is shown in Figure 17.

Original Rig - The original total hemispherical emittance rig consisted of a vacuum chamber, instrumentation flange, evacuating equipment, power supplies for sample heating, and instrumentation for measuring power and temperature. The test setup is shown in Figure 18.

The vacuum chamber was a windowless cylinder made of AISI 304 stainless steel and measuring 8 inches in length with a

3-inch inside diameter. The inner walls were grooved and blackened with cupric oxide to provide a low reflectance surface. Energy radiated directly from the chamber to the specimen was minimized by water cooling the walls.

The instrumentation flange, which formed the top cover plate of the chamber, contained the vacuum connection, power and thermocouple feedthroughs, and the specimen support assembly. The vacuum connection was a 1-inch diameter tube which led to the vacuum manifold. The power feedthroughs were water-cooled copper leads which were soldered into AISI 410 stainless steel tubes. These were installed into the flange with Pyroceram which is a form of solder glass manufactured by Corning Glass Works. Pyroceram was also used to seal the thermocouple feedthroughs. This method of installation provided a high-vacuum seal and electrical insulation between the wires and the chamber components. The specimen support assembly which included the sample holder, fastening clamps, and thermocouple wire supports, was oriented so as to position the specimen away from the centerline of the chamber and thereby minimize the radiation specularly reflected from the chamber to the specimen. A beryllium-copper leaf spring holding the lower specimen clamp was used to compensate for specimen thermal expansion. The details of the chamber construction are shown in Figure 19.

The chamber was evacuated with an oil-sealed mechanical roughing pump and a 5-liter/sec ion-gettering pump (Figure 20). The mechanical pump was used in conjunction with a cryogenic trap to remove condensable materials while the system was being baked out. Pressures on the order of 10^{-4} mm Hg were attainable with the roughing pump. After bakeout, the pressure was reduced to about 10^{-9} mm Hg with the ion-gettering pump. Pressures were measured with a Bayard-Alpert type ionization gage and by monitoring the current to the ion-gettering pump.

Specimens tested in the rig were in the form of metal strips (usually coated stainless steel, molybdenum, or aluminum) about 6 inches long, 0.40 inch wide, and 0.002 to 0.005 inch thick (see Figure 21). The specimens were generally coated on

both sides although a few tests were conducted with specimens coated on only one side. The testing of specimens coated on only one side was abandoned after a few tests because of the difficulty in determining the emittance of the uncoated side.

The specimens were resistance heated with AC power, using the substrate material as the resistive element. The use of AC power simplified power control and eliminated thermocouple error introduced by misalignment of thermocouple wires. With DC, misalignment results in a portion of the specimen voltage drop being introduced into the thermocouple circuit. Power was obtained from a 7.5 kva transformer. The input voltage to the transformer was regulated to provide a constant output and could be varied to produce a secondary voltage ranging from 0 to 32 volts. In order to obtain a uniform temperature profile across the specimen, it was necessary to use end heaters to reduce the heat lost to the cooled power leads and specimen supports. Separate AC power supplies were used for end heating and were connected across 3/4-inch long segments at either end of the specimen. The end heating power supplies were electrically phased to aid the main heating power supply and were controlled to provide equal temperatures at thermocouples numbers 1, 2, and 3. Usually the end heaters were used only at temperatures below 1000°F. A block diagram showing the vacuum and power system is shown in Figure 20. A block diagram of the instrumentation system is shown in Figure 22.

D. Endurance Rigs

1. Short Term Endurance Rig - A total hemispherical emittance endurance rig was built to provide a means of determining changes in emittance resulting from prolonged exposure to high temperatures and vacuum. A photograph and schematic diagram of this rig is shown in Figures 23 and 24 respectively. The rig includes a vacuum chamber,

an evacuation system, an instrumentation flange, a specimen heating power supply, and temperature measurement instrumentation.

The vacuum chamber, which was made from AISI-304 stainless steel, is 13 inches long and has a 3-inch inside diameter. The design is similar to that of the spectral normal emittance rig. The inside of the chamber is coated with acetylene black in xylol to provide a low reflectance radiation sink. Unlike the spectral normal emittance rig, the chamber walls are not grooved. Since it is the change in emittance with time which is of primary interest for specimens tested in this rig, the additional accuracy obtained by grooving the walls is not required. Flanges at both ends of the chamber provide for attachment to the vacuum manifold and for installation of the instrumentation flange. Vacuum sealing is accomplished by means of 0.020-inch diameter fully annealed gold O-rings compressed between polished surfaces. The chamber is equipped with a 1-inch diameter viewing port to permit temperatures to be measured by an optical pyrometer and to permit observation of the specimen during testing. The window is protected by a magnetically-operated rolling disc shutter. Bakeout heaters are provided to outgas the chamber before testing, and water-cooled coils maintain the required chamber temperature during testing.

When the chamber was initially built in 1960, a vacuum manifold was attached to the instrumentation flange and the bottom of the chamber was sealed by a blank flange. The vacuum manifold interconnected a roughing pump, a 5-liter /sec ion-gettering pump, and a Bayard-Alpert type ionization gauge. Appropriate high-vacuum valves were included. In 1962 it was decided to increase the pumping rate from the chamber to reduce the pumping time and to produce a

lower ultimate pressure. Therefore, a 40-liter /sec ion-gettering pump was connected directly to the bottom of the chamber. The pump is equipped with bakeout heaters to facilitate outgassing. Since no valves or ducts were used between the pump and the chamber, the optimum system was obtained for this particular chamber geometry.

A mechanical roughing pump with a cold trap is used during bakeout to establish the starting conditions for the ion-gettering pump. Pressure during bakeout is monitored with a thermocouple gauge. During testing, the ion-gettering pump current is measured and the associated pressure is determined from calibration curves.

The instrumentation flange provides power feedthroughs, thermocouple feedthroughs, and the specimen mounting and positioning assembly which includes provisions for thermal expansion. As in the spectral emittance rig, the specimen is positioned away from the centerline of the rig. No provision has been made for end heating since endurance testing is usually conducted at temperatures which are high enough so that end heating is not required. When endurance testing is required at lower temperatures, corrections can be applied to the data. The instrumentation flange is equipped with terminals for three platinum-platinum 10 per cent rhodium thermocouples, two chromel-alumel thermocouples, and for a set of voltage leads.

Specimen temperature is measured by thermocouples while the specimen is being heated to the endurance temperature, and by a Leeds and Northrup optical pyrometer focused on the integral black-body hole in the specimen wall during endurance testing. An infrared pyrometer is used for temperatures lower than 1450°F.

AC power is used to heat the specimen. Power measurements are made by measuring the voltage drop across the specimen

test section and across a current shunt by means of an AC-DC differential voltmeter.

2. Long Term Endurance Rigs - A test program extending over a minimum period of 10,000 hours was initiated to determine the effects of high vacuum and representative space-radiator temperatures on selected coatings. A facility containing the necessary equipment was designed and built to accomplish this program and is shown in Figures 25 and 26.

At present, four rigs, each consisting of a vacuum chamber, an instrumentation flange, evacuating equipment, a power supply for specimen heating, and instrumentation for measuring power and temperatures are in operation.

The vacuum chambers (Figure 25) are similar to that used for the new total hemispherical emittance rig. They are 20 inches high, have an inside diameter of 15 1/2 inches, and were fabricated from AISI-304 stainless steel.

A 5.4-inch diameter window is provided for viewing the uninstrumented face of the test specimen and for obtaining radiation measurements. A 2.0-inch diameter window permits inspection of a portion of the instrumented face. Magnetically-controlled polished stainless steel shutters are used to prevent heating the larger window by specimen radiation and to prevent reflection and radiation to the specimen.

The inside of each chamber is coated with a high-emittance coating. Different coatings were chosen in an attempt to acquire additional information on these coatings under long-term exposure to high vacuum. The chamber for Rig No. 1 is coated with acetylene black in xylol; the chamber for Rig No. 2 is coated with nickel-chrome spinel plus silicon dioxide bonded with aluminum phosphate; the chamber for Rig No. 3 is coated with acetylene black from a torch using an oxygen-deficient mixture; and the chamber for Rig No. 4 is coated with

silicon carbide plus silicon dioxide bonded with aluminum phosphate. The large diameter and high emittance of the chamber wall satisfy the requirement that reflection of energy from the chamber to the specimen be negligible.

The instrumentation flanges are designed to be independent from the basic vacuum chambers and contain all necessary equipment such as specimen supports, thermocouple terminal networks, power and thermocouple feedthroughs, current shunts, thermocouple reference junctions, power connectors, and thermocouple and power-measurement leads. The design of the flanges is shown schematically in Figure 27.

Each of the specimens is mounted between two sets of three ceramic knife edges located at the top and bottom ends of the specimen. The knife edges are held by support structures attached to the flange and are kept in contact with the specimen by means of the spring mechanism located on the top support assembly. This type of mounting is used to minimize heat losses from the specimen. For a typical specimen installation with these supports, see Figure 28.

In the original flange design, the thermocouple terminal network used chromel-alumel thermocouple wire which had been clad in stainless steel and swaged. Although platinum-platinum 10 per cent rhodium thermocouple material was preferred, see Appendix N, the large-diameter self-supporting thermocouple lead wire required for this design made its use uneconomical. However, for the temperature range required, (ambient to 750°F), it was felt that the use of chromel-alumel thermocouple material would be satisfactory. The flange also provided for three small-diameter platinum-platinum 10 per cent rhodium thermocouples to serve as reference thermocouples. This instrumentation flange proved impractical, however, because of the difficulty encountered in obtaining satisfactory vacuum seals at the ends of the clad thermocouple wire assemblies. The design of the flange was subsequently changed to provide:

1. High vacuum feedthroughs for passage of thermocouple lead wires through the flange,

2. A framework of thin steel rods to support a network of thermocouple terminal assemblies, and
3. Small-diameter thermocouple lead wires insulated and supported by tubular ceramic insulation.

The design retains the following features:

1. It permits the use of any desired thermocouple arrangement without requiring a change in the basic instrumentation flange.
2. It permits the removal of the specimen from the chamber for evaluation or repair without requiring the thermocouple connections between the specimen and the terminal network to be broken.
3. It facilitates the switching of specimens between rigs or the installation of new specimens as the test schedule may require.

The flanges in the present test program use 0.032-inch diameter platinum-platinum 10 per cent rhodium wire for the thermocouple terminals and 0.005-inch diameter lead wire between the terminals and the high vacuum feedthroughs. Compensating wire (0.032 inch in diameter) is used between the thermocouple feedthroughs and the reference junctions. The temperature range in the region of the lead wire-compensating wire junction is such that there is negligible difference between the thermal emf characteristics of the platinum-platinum 10 per cent rhodium lead wire and the compensating wire materials. The junction of the compensating wires is placed in an ice bath to provide a reference junction, Figure 26. Copper wire is used for the remainder of the circuit to simplify the subsequent switching and handling of the thermocouple signals. The copper wires are brought back up to the instrumentation flange connector plate where a multiple pin connector joins the instrumentation flange wiring to the measurement circuitry.

The thermocouple feedthroughs consist of 28 0.032-inch diameter wires sealed with Pyroceram inside a 1-inch diameter AISI-410 stainless steel sleeve. AISI-410 stainless steel and Pyroceram have similar thermal expansion characteristics so that there is little risk of subsequent seal failure during operation. The feedthroughs are heliarc welded into the flange to ensure a vacuum-tight assembly.

The power feedthroughs are constructed in a similar manner utilizing AISI-410 stainless steel power terminals. Copper power leads are used between the feedthroughs and the standard electrical connector on the flange connector plate. A 10-ampere 50-millivolt shunt is installed in one of the power leads to provide a means of current measurement. The thermocouple terminal network for the SNAP-8 fin is shown in Figures 28 and 29, and for the Sunflower I fin in Figures 30 and 31.

A mechanical vacuum pump, in conjunction with a liquid nitrogen cold trap, is used during bake-out and pump-down of the system to the starting pressure of the 40-liter/second ion-gettering pump. The ion-gettering pump is bolted directly to the base-plate of the rig and is used continuously during testing. The pump is capable of producing pressures below 1×10^{-9} mm Hg, and, in the rigs discussed, maintains pressures in the 10^{-8} mm Hg range with the specimen at endurance conditions. Gold O-rings, copper gaskets, and Teflon seals are used for sealing the various vacuum chamber components. Pressure is determined by measuring the ion-gettering pump current.

All instrumentation and rig controls are contained in a control console as shown in Figure 32. The console is set up to provide unified control for each rig, as indicated in block diagram form in Figure 33. One of the features of the instrumentation system is the multipoint millivolt recorder which, by means of a time-controlled

stepping relay, automatically records the thermocouple outputs hourly. A manually operated slide wire potentiometer can also be used to provide high accuracy data for reference.

E. Aluminum Fin Thermal Cycling Rig

The aluminum fin thermal cycling rig was used to determine the compatibility with aluminum of various coatings being considered for long term endurance testing. Testing in the aluminum plate thermal cycling rig also provided preliminary information on the behavior of coatings when they are subjected to thermal cycling and high vacuum conditions.

A standard glass bell jar 15 inches high and 15 inches in diameter was chosen for the vacuum chamber. This provided both simplicity and the means of observing and photographing the specimen during testing. The bell jar is seated on a special base plate equipped with a shield to absorb heat radiated by the specimen and to prevent the bell jar from heating during testing, Figure 34. Vacuum grease was used to seal the bell jar to the base plate.

The instrumentation flange, shown in Figure 35, held the specimen support and heater assembly and also provided feed-throughs for power and thermocouple leads. Terminals were provided for 10 chromel-alumel and for 10 platinum-platinum 10 per cent rhodium thermocouples.

The evacuation system consisted of a 400-liter /sec oil diffusion pump which was backed up by a 6-liter /sec mechanical roughing pump. A liquid nitrogen cold trap prevented the backstreaming of oil vapors and improved the pumping action of the system. Pressures as low as 1.8×10^{-7} mm Hg were obtained with specimens heated to the maximum fin root temperature of 750°F. Pressure measurement was made with a Bayard-Alpert type ionization gauge.

The specimen itself was in the form of a coated aluminum fin measuring 4-3/8 x 4 x 0.040 inches. The fin was clamped in a

copper heater block containing a 1000-watt cartridge heater. Normally, each fin was instrumented with three 0.005-inch diameter chromel-alumel thermocouples to permit determination of the root, center, and tip temperatures. The instrumented specimen is shown in Figure 36.

An over-all view of the rig is shown in Figure 37. Provision was made for photographing the specimen by mounting a 35 mm camera on the bell jar shield.

III. PROCEDURE

A. Specimens

Two general types of specimens have been used in this program: those intended primarily for quantitative evaluation of thermal radiative properties, that is, for measurement of emittance, and those intended primarily for evaluation of the durability and adherence of coatings as a function of time.

1. Specimens for Measurement of Emittance - The specimens for measurement of emittance were in the form of coated or uncoated thin-walled metal tubes or metal strips. When coated specimens were studied, the coatings were applied in uniform layers of suitable thickness to metal substrates.

The tubes used were approximately 9 inches long and were either circular or triangular in cross section. The circular specimens were made from drawn tubing with wall thicknesses of 0.005 or 0.010 inch and with a nominal outside diameter of 0.250 inch. The maximum peripheral wall thickness variation was held to within 4 per cent in order to hold temperature variations to an acceptable value. For the effects of wall thickness variations on temperature uniformity, see Appendix I.

The tubes were fabricated from AISI-310 stainless steel, nickel, nichrome, aluminum, titanium, tantalum, columbium and columbium-1 per cent zirconium. Two black-body holes were drilled through one wall at the midpoint of each tube. The holes were 0.0235 inch in diameter, longitudinally separated by 0.0522 inch, and displaced laterally from the tube centerline by 0.043 inch. To maintain the close tolerances required for hole spacing and positioning, the holes were drilled with the aid of the jig shown in Figure 38. This jig was equipped with an adjustable hardened steel drill guide that could be positioned so that a line joining the hole centers would be precisely parallel with the tube axis. The black-body holes were deburred after drilling.

Metals such as tungsten and molybdenum could not be obtained in circular tubes with the required wall-thickness tolerance. This problem was alleviated by the use of triangular tubes fabricated from rolled strips having a highly uniform thickness.

The triangular tubes were made by forming 9-inch long sections of strip stock, 1 inch wide and 0.002 or 0.005 inch thick, into channel sections 0.1 inch wide and 0.450 inch deep by means of a forming jig. Two 0.0235-inch diameter black-body holes, with an axial separation of 0.0522 inch, were drilled in the center of the 0.1-inch wide face at the specimen midpoint with the aid of a fixture similar to that used for the circular tubes. In materials too hard for drilling, the holes were formed by punching or by electrical discharge machining. The edges of the specimen were then clamped together and resistance spot-welded or heliarc-welded to form a light-tight joint. The forming jig and several specimens in various stages of manufacture are shown in Figure 39. The use of this configuration was limited to the study of bare metals because of the difficulty in applying a uniform coating to a surface with abrupt changes in contour.

At the beginning of the program, metal strips were used for total hemispherical emittance specimens, and are still used when tubular specimens are not available or readily fabricated. The strips were usually stainless steel, molybdenum, or aluminum. They were normally 9 inches long and 0.4 inch wide. A small precision shear was fabricated to cut parallel edges on the strips. The thicknesses tested were either 0.002 or 0.005 inch with the maximum thickness limited by the material and the power available for specimen heating.

Strip specimens were either uncoated, coated on one side, or coated on both sides. The testing of strips coated on one side was abandoned after a few tests because the emittance of the uncoated side, which had to be known for each test point, changed with time in a manner which could not be repeated.

After fabrication and before coating, all tubes and strips were cleaned in a saturated solution of concentrated sulfuric acid and potassium dichromate to remove organic contaminants, and were then rinsed with distilled water.

In preparation for emittance measurements, each specimen was instrumented and prepared for installation in the rig in a manner commensurate with the type of specimen, type of test, and the particular rig in which the measurements were to be made. Tubular specimens were flattened for 3/4 inch at each end to facilitate clamping to the power electrodes. The flattening process resulted in the removal of most of the coating in the clamping region and any remaining residue was removed by means of an abrasive to ensure good electrical contact. A few flakes of the coating removed in this operation were saved and analyzed for comparison with the analysis of the tested coating. The black-body holes were then reamed with a drill to remove any coating material that might have accumulated during the coating process. The coating material was removed from the ends of strip specimens by flexure and by the use of a scraper and abrasives.

The locations for thermocouples and voltage leads to be attached to the specimen were marked on each specimen. The coating was then removed from a rectangular area 0.010 x 0.030 inch at each location by means of a tungsten-carbide scraping tool. On most substrate materials, the thermocouple and voltage leads were attached by resistance welding with a capacitive discharge welder. On materials such as copper and aluminum, the leads could not be satisfactorily attached by welding and the wires were therefore imbedded in the substrate material by a swaging process as shown in Figure 40. Using specially designed tools, a slot was made in the substrate material which was 2 to 3 wire diameters deep, 1 diameter wide, and about 25 diameters long. The end of each wire was pressed horizontally into the slot. The wire was then covered with substrate material by forcing the metal adjacent to the slot over the wire and compacting the metal to ensure a tight junction. Where thermocouples were installed, each wire occupied one-half of the slot at the particular location.

2. Specimens for Endurance Testing - The specimens being tested in the long term endurance program include three SNAP-8 tube half-fin radiator sections (supplied by Aerojet General Corporation) and one Sunflower I fin radiator section (supplied by Thompson Ramo Wooldridge, Incorporated). The SNAP-8 assemblies are composed of #6061 aluminum tubes 8.0 inches long with inside diameters of 0.5 inch and outside diameters of 1.10 inch. The fins are made of #1100 aluminum 8.0 inches long, 3.57 inches wide and 0.040 inch thick. The Sunflower I assembly is composed of an AISI-347 stainless steel tube 8 inches long with an inside diameter of 0.446 inch and an outside diameter of 0.562 inch. The fin is made of #1100 aluminum 8.0 inches long, 3.76 inches wide, and 0.040 inch thick.

Prior to coating, a 1000-watt, 240-volt cartridge-type heater was fitted into the tube section of each specimen. The specimens were cleaned with acetone and coated with selected high emittance materials. After the coatings were applied, a black-body hole 0.18 inch deep and with a diameter of 0.059 inch was drilled into each specimen. On the SNAP-8 assemblies each hole is located at the mid-point of the tube section. However, the black-body hole on the Sunflower I assembly is located at the center of the fin.

The SNAP-8 specimen assemblies were instrumented with 18 thermocouples and the Sunflower I specimen assembly with 28 thermocouples to provide temperature profiles. The thermocouples were installed by the swaging technique described above.

The specimens which were used to study the durability and adherence of coatings to aluminum substrates in the thermal cycling rig were in the form of coated aluminum fins 4-3/8 inches long, 4 inches high, and 0.040 inch thick. The substrate material in all cases was #1100 aluminum. Each fin was prepared with 4 holes along the 4-inch edge to facilitate installation into the heater block for testing. The fin was then masked so that only a 4-inch by 4-inch area would be coated. Three specimens were prepared for each coating to provide one specimen for thermal cycling tests and two specimens for reference. One of the reference specimens was subsequently used, along with the tested specimen, for bend tests to determine changes in adherence characteristics resulting from thermal cycling in vacuum.

Prior to thermal cycling tests, each specimen was instrumented with three 0.005-inch diameter chromel-alumel thermocouples. The thermocouples were installed by swaging with the root thermocouple placed 1/8 inch, the middle thermocouple 2 inches, and the edge thermocouple 3 7/8 inches from the copper heater block.

B. Testing Procedures

1. Spectral Normal Emittance Rig - Specimens tested in the spectral normal emittance rig were prepared and instrumented in the manner described in Section III A of this report. After the water-cooled expansion takeup spring has been compressed by an amount slightly greater than the maximum amount of thermal expansion anticipated, the fully instrumented specimen was clamped to the upper and lower electrodes of the support assembly. This procedure eliminated compressive forces on the specimen which might result in buckling and subsequent misalignment of the black-body holes. The thermocouple and voltage leads were then connected to the proper terminals of the electrode and thermocouple assembly and the entire specimen and supporting assembly was inserted into the chamber. The black-body holes were aligned with the window in the chamber wall and finally the cover was bolted and sealed to the chamber.

Initial evacuation was performed with a mechanical oil-sealed pump operating with a liquid nitrogen cold trap over a period of two hours. During this period the chamber was baked out at 350°F. The ion-gettering pump was then started and the valve to the roughing pump cold trap was closed. The system was allowed to cool and within 17 hours after starting the ion-gettering pump, an ultimate pressure in the range of 10^{-10} mm Hg was attained. The specimen was then heated to the operating temperature. Temperatures below 1400°F were measured with thermocouples. Above 1400°F an optical pyrometer was also used.

Spectral normal emittance data were taken with the spectrophotometer operating in the ratio mode. With this type of

operation, the spectrophotometer produces a record of the ratio of the measuring beam power to the reference beam power as a function of wavelength. Three scans over the same range of wavelengths are required at each temperature. One scan is made with the reference beam focused on a black-body hole and with the measuring beam blocked to establish the "zero emittance line." A second scan is made with the both beams focused on black-body holes to determine the "unity emittance line" for normalizing the data. A final scan is made with the reference beam focused on a black body hole and the measuring beam focused on the specimen surface to determine the "specimen emittance line".

From these three ratios, the spectral normal emittance may be determined at selected wavelengths using the following relationship:

$$\text{spectral normal emittance} = \frac{\text{specimen emittance line} - \text{zero emittance line}}{\text{unity emittance line} - \text{zero emittance line}}$$

A typical data record is shown in Figure 41. A discussion of the variations in the unity emittance line and of its use in calculating the spectral normal emittance appears in Appendix C.

When the spectral emittance rig was used for total hemispherical emittance measurements, the procedure used was the same as that described in Section III B 2 below.

2. Total Hemispherical Emittance Rig

New Rig - Although a variety of specimen configurations could be tested in the new total hemispherical emittance rig, specimens were generally in the form of tubes with circular cross-sections. The specimens were usually instrumented as shown in Figure 13 using seven **platinum-platinum 10 per cent rhodium** thermocouples and one chromel-alumel thermocouple. The distances between the thermocouple wires were measured with a measuring microscope for calculation of the test section area.

The instrumented specimen was then clamped to the instrumentation flange and held under tension by the expansion take-up device. The thermocouple wires were attached to the standoffs by resistance welding and the chamber was assembled. The chamber was then pumped down to a pressure lower than 1×10^{-6} mm Hg. If the chamber had been contaminated by previous testing, it was baked out at 350°F during pump-down. During testing, the chamber walls were cooled to maintain a constant sink temperature.

Power input to the specimen was determined by measuring the current as a voltage drop across a calibrated shunt and by measuring the voltage drop across the test section. Both measurements were made using an AC-DC differential voltmeter. The length and location of the test section was determined by the position of the thermocouples used for voltage measurement. Although instrumentation circuitry permitted any of the thermocouple leads to be used as voltage leads, thermocouple numbers 3 and 5 were usually used.

Thermocouple output for temperature measurement was measured with a slide-wire millivolt potentiometer used in conjunction with an ice bath reference junction.

The total hemispherical emittance was determined from the data by using the following equation:

$$\epsilon_{TH} = \frac{I V_{ts}}{\sigma A_{ts} (T_{ts}^4 - T_w^4)}$$

where:

- ϵ_{TH} = total hemispherical emittance
- I = current through the test section
- V_{ts} = voltage drop across the test section
- σ = Stefan-Boltzmann constant
- A_{ts} = surface area of the test section radiating power IV_{ts}
- T_{ts} = temperature near the center of the test section
- T_w = temperature of the chamber wall

The total hemispherical emittance of each specimen was usually measured over the temperature range of 200°F to 2200°F at 100°F intervals. End heating was used at temperatures below 1000°F to compensate for end conduction losses.

After emittance testing, the specimens were removed from the rig and subjected to additional testing and evaluation. Specimens are stored in transparent plastic tubes for future reference.

Original Rig - In preparation for testing in the original total hemispherical emittance rig, each strip specimen was instrumented with four 0.001-inch diameter chromel-alumel or platinum-platinum 10 per cent rhodium surface thermocouples and with a pair of voltage leads. The positioning of the thermocouples and voltage leads is shown in Figure 21. The width and thickness of the specimen and the distance between the voltage leads were determined with a measuring microscope. The specimen was installed in the instrumentation flange by clamping it under tension to compensate for thermal expansion. The instrumentation flange assembly was then bolted and sealed in the vacuum chamber.

A mechanical roughing pump in conjunction with a liquid nitrogen cold trap was used to pump down the chamber while it was baked out for 4 hours at about 425°F. The roughing pump was then shut off and the ion-gettering pump turned on. Cooling water was not applied to the walls until they had cooled to the ambient temperature. Emittance testing began when a pressure in the range of 10^{-7} mm Hg had been attained and pumping continued throughout the test to maintain the lowest possible pressure. Emittance measurements were made only while the chamber pressure was low enough to prevent a significant amount of energy to be transferred by residual gas conduction. The procedure for determining emittance values was the same as that described in the preceding section for the new total hemispherical emittance rig.

A vacuum-tube voltmeter was used to measure both the current and voltage applied to the specimen. Voltage was measured directly and current was measured as a voltage drop across a 50-ampere, 50-millivolt shunt. A millivolt potentiometer was used to measure the thermocouple outputs.

Total hemispherical emittance data was taken over the temperature range of 200°F to 2000°F except for specimens with aluminum substrates which were limited to a maximum temperature of 900°F. End heaters were used at temperatures below 1000°F to maintain a uniform temperature along the test section. Test data were taken only after steady-state conditions had been attained. To test the stability of certain coatings, some specimens were maintained at 1450°F for approximately 17 hours (overnight) with total emittance measurements being made both before and after the 17-hour period. All data obtained at temperatures higher than 1450°F were taken after an overnight endurance test. Additional emittance measurements were made as the specimen was cooled to determine what changes had occurred as a result of exposure to elevated temperatures and vacuum. When a preliminary evaluation of the data indicated that the test results were reliable, the specimen power was shut off, the test chamber vented to the atmosphere, and the specimen removed for further inspection and evaluation.

3. Endurance Rigs

- a. Short Term Endurance Rig - Specimens tested in the short term endurance rig were generally circular tubes, although other configurations could be used. Three platinum-platinum 10 per cent rhodium thermocouples and two voltage leads were attached to the specimen. The distance between the voltage leads, which determines the test section length, was measured with a measuring microscope. The procedures for specimen installation, chamber bakeout, and system pump down were similar to those used with the original total hemispherical emittance rig. During testing, specimens were maintained at a nominally constant temperature of 1450°F.

The power applied to the specimen was measured with an AC-DC differential voltmeter. The voltage was measured directly and the current was measured as a voltage drop across a calibrated shunt. Specimen temperatures were measured by thermocouples in conjunction with a slide wire millivolt potentiometer, by an optical pyrometer, and by an infrared pyrometer.

The total hemispherical emittance was determined by the same method as that used with the new total hemispherical emittance rig. At the beginning of an endurance test, data were taken frequently to ensure that initial changes in the coating would be recorded. When the data indicated that little or no change in the coating characteristics was occurring, data were taken at longer intervals. Endurance testing was conducted for a minimum of 250 hours for each specimen tested.

b. Long Term Endurance Rigs

In preparation for long term endurance testing, each specimen was mounted on the support structure of the instrumentation flange. The specimens were supported between 2 sets of 3 ceramic knife edges located at each end of the specimen. After the specimen had been mounted, the thermocouple leads were tack welded to the thermocouple standoffs and the power leads were connected between the specimen heater terminals and the power feed-throughs. When all the connections were completed and the continuity of all circuits checked, the instrumentation flange assembly was installed in the base plate of the vacuum chamber. The chamber was then assembled to the base plate and the rig checked out.

Before testing, each rig was baked out at 400°F to remove contaminating material. During the bakeout cycle, the system was pumped down with a mechanical roughing pump operating in conjunction with a liquid nitrogen cold trap. After the system was baked out, the ion-gettering pump was started, the mechanical pump valved off, and the system allowed to cool to room temperature. The chamber walls were then water cooled to maintain a constant sink temperature.

The specimen was heated to the endurance temperature by the cartridge heater. The time required to reach test conditions varied between 200 and 900 hours and was determined by the outgassing rate of the cartridge heater and specimen. The temperature at the fin root of the SNAP-8 specimens was maintained at 700°F and at the fin root of the Sunflower I specimen at 650°F.

Throughout the endurance test the following parameters were recorded manually:

1. Temperature, measured by thermocouples,
2. Brightness temperature, measured by an infrared pyrometer,
3. Specimen heater current and voltage, and
4. Chamber pressure.

Initially, the data were taken daily; however, when the specimen temperatures indicated that little or no changes were occurring, the data were taken only once a week. In conjunction with the manual data taking, the specimens were inspected regularly for changes in appearance and photographs were taken periodically. In addition to the precise manual data taking, thermocouple outputs were recorded hourly by an automatic multipoint recorder. The fin-root to fin-tip temperature, ΔT , was determined from specimen thermocouple indications.

4. Aluminum Fin Thermal Cycling Rig

Instrumented specimens prepared for thermal cycling were clamped to the cartridge heater on the instrumentation flange by means of the two heater blocks. The thermocouple lead wires were tack welded to feed-through terminals on the instrumentation flange and the entire assembly was then installed on the bell jar base plate and sealed with a Viton O-ring. The bell jar was installed and the system was pumped down to an acceptable test pressure. Pressures during testing were generally about 10^{-7} mm Hg and were always lower than 1×10^{-5} mm Hg.

Each specimen was subjected to five heating and cooling cycles. For each of these the root of the fin was heated to 750°F over a period of one hour. This temperature was maintained for

three hours and then the fin was cooled to the ambient temperature in one-half hour. During testing, the root-to-tip temperature difference was measured and the specimen was observed for possible changes in appearance.

At the completion of the thermal cycling, the rig was vented to the atmosphere and the specimen was removed for further evaluation which included bend testing, microexamination, spectrographic analysis, x-ray diffraction, and wet chemical analysis.

IV. COATING PROCEDURES

A. Thermal Spraying

The plasma-arc and Rokide thermal spraying processes were used for applying high emittance coatings to various test specimens used in this program. Both spraying methods require specially designed spray guns which melt or soften the coating material and then propel the material through the spray nozzle by a high-velocity carrier gas. The plasma-arc process used utilizes material in powdered form while the Rokide process uses a solid rod.

1. Plasma-Arc Spraying

Plasma-arc spraying utilizes the very high temperatures of an electric arc (higher than 15,000°F) to heat and ionize a gas which passes through it. The plasma gas is then combined with a second gas carrying the coating material in powder form. The powder is melted or softened and accelerated to the specimen surface by the carrier gas. Inert gases such as argon or nitrogen are generally used for plasma-arc spraying to help prevent chemical changes in the coating material during spraying. The ability to protect the coating material from an oxidizing atmosphere is a particular advantage of plasma-arc spraying not possible with other spraying techniques.

Close control of coating thickness, finish, and density is possible while still maintaining the substrate material at a temperature below 400°F. The physical and mechanical properties of coatings applied by plasma-arc spraying are superior to the properties of similar coatings applied by other thermal spraying techniques. This is particularly true with respect to bond strength and coating density.

Initially, the plasma-arc sprayed coatings were applied by the Linde Company or by Metco, Inc. The coatings are now applied by Pratt & Whitney Aircraft using Plasmadyne equipment.

2. Rokide Spraying

Rokide spraying, like conventional flame spraying, utilizes a combustible gas or a mixture of gases which, when ignited, softens or melts the material to be sprayed. The gas jet then carries the material to the specimen.

The maximum attainable flame temperature is controlled by the gas mixture used, usually oxygen-acetylene, oxygen-hydrogen or air and hydrogen. The basic difference between conventional flame-spraying and Rokide spraying is the form of the material fed into the spray gun. The conventional flame-spray gun utilizes a powder but the Rokide gun utilizes a solid rod. In the conventional flame-spray gun, the powder is forced through the flame and the degree of material melting depends on the flame temperature and the length of time the powder is exposed to the flame. In the Rokide gun, the spraying rod is fed into the flame and the material cannot leave the gun until it has been softened sufficiently to be separated from the remainder of the rod. Because a lower gas velocity and temperature are used, a more porous coating is obtained with this process than with plasma-arc spraying.

B. Slurry Applications

For slurry applications, the coating material is suspended in a liquid binder. The mixture is usually sprayed onto the substrate although brushing or dipping may also be used. Excess moisture is removed from the coating by air drying. Finally, the specimen is heated in an oven to drive off chemically-combined water or other volatile constituents.

Many materials which cannot withstand the extreme temperatures of thermal spraying may be successfully applied by slurry techniques, several of which are described below:

1. Aluminum-Phosphate Bonding

A monoaluminum phosphate slurry was prepared as follows. A mixture of 300 grams of levigated alumina, 384 ml of 85 per cent orthophosphoric acid, and 750 ml of water was allowed to stand in an open container for four hours with five minutes of agitation each hour to facilitate reaction. The open container was used to preclude the possibility of an exothermic reaction following gas formation. The mixture was then transferred to a five-gallon plastic bottle and placed on ball mill rollers and rotated for two hours, after which it was allowed to stand for 18 hours. The clear solution, monoaluminum phosphate ($\text{Al}_2\text{O}_3 \cdot 3\text{P}_2\text{O}_5 \cdot 6\text{H}_2\text{O}$), was decanted and had a pH of 1.75. This solution vigorously attacks aluminum and its alloys and therefore 24 grams of chromium trioxide (CrO_3) per 100 ml of solution were added when required to prevent the attack. Two hundred grams of filler material were added to 150 ml of monoaluminum phosphate solution to

form a creamy slurry which was stirred for 30 minutes to ensure complete mixing. The slurry was then sprayed onto various substrates. Preparation of substrates to receive slurry-type coatings included degreasing with trichloroethylene, wet grit blasting with 325-mesh silica, followed by a water flush and an acetone rinse.

The curing procedure generally included air drying at room temperature for one hour followed by oven heating for two hours at a temperature between 500°F and 800°F. The particular curing temperature depended on the type of coating and the amount of out-gassing observed during the early stages of testing.

2. Synar Bonding

Slurries of several materials were prepared using Synar, a special mortar supplied by the Pennsalt Chemical Corporation, as a binder. These slurries were sprayed on various substrates and air-dried at room temperature. The dried specimens were cured at 500°F for 20 minutes.

3. Graphite Varnish

AISI-310 stainless steel foil samples which had been roughened, cleaned, and degreased, were sprayed with graphite varnish. The coating material used was a 2-to-1 mixture of a suspension of 20 per cent colloidal graphite in isopropanol (obtained from the Acheson Colloid Company) and AMS-3132 varnish. The coated specimens were air-dried at room temperature and oven-dried at 300°F for 30 minutes.

4. Acetylene Black in Xylol

Acetylene black in xylol was supplied by the Acheson Colloid Company under the trade number Dag EC 1652. This was sprayed on substrates prepared in the same manner as those prepared for aluminum-phosphate bonded coatings. The coating was ready for testing after it was air-dried at room temperature.

C. Electroplating

1. Chromium Black

Chromium black coatings were applied to AISI-310 stainless steel and nickel substrates. The surface to be plated was degreased with trichloroethylene, scrubbed with wet alkaline pumice, and rinsed with water. The area not to be plated was coated with wax.

Electrical contact was made along the insides of tubular specimens and at the ends of specimens in strip form. The substrate material was then immersed in alkaline cleaner and made anodic at 3 volts for 1 minute. After being rinsed with water, it was immersed in a solution containing 25 per cent H_2SO_4 and 3 to 5 per cent HF by volume and made anodic at 2 amps/in² for 15 seconds and then cathodic with the same current for 5 seconds. The specimen was then rinsed with water and rerinsed with distilled water. It was next immersed in a bath of CrO_3 (250 grams per liter) and NH_4F (0.5 gram per liter) with a voltage of 2 volts which was raised to provide a current of 2 amps/in² for 12 minutes. After plating, the tube was washed with water, rinsed with distilled water, and degreased with trichloroethylene. Both the CrO_3 and the NH_4F were of J. J. Baker - reagent quality. The formula for the plating bath was obtained from "Electrodeposition of Black Chromium Coatings" by the Allied Chemical Corporation.⁴

2. Platinum Black

A coating of platinum black was plated onto a 2-mil thick AISI-310 stainless steel strip by the following procedure. The strip was initially etched at a current density of 1 amp/in² for 45 seconds. A nickel strike was then plated onto the strip by immersing the strip in sulfonate-nickel solution and maintaining a current density of 30 amps/ft² for 15 minutes. The strip was then plated for 10 minutes with a current density of 10 amps/ft² in a platinum diamino-nitride solution with a platinum anode. Ten additional minutes of plating at the same current in a Platinex solution (supplied by the Sel-Rex Corporation) and a final 10 minutes in the platinum diamino solution were followed by rinsing in distilled water. Plating was completed by immersing the strip in a solution containing 28 grams per liter chloroplatinic acid and 0.001 gram per liter lead acetate maintained at a temperature of 120°F. The strip was cathodic at 2 volts and the anode was platinum.

D. Electrophoresis

A 6-mil thick coating of silicon carbide was applied to a molybdenum strip by an electrophoretic process at Vitro Laboratories. An acrylic resin was applied by Vitro to the coated specimen to improve the adherence properties of the silicon carbide.

E. Oxidizing Processes

1. Oxidized Columbium

The columbium specimens were oxidized by heating the uncoated tubes in air to 1200°F for 5 minutes. The outer layer of powdery white oxide, Cb_2O_5 , was removed by brushing with fine steel wool to expose the inner layer of black oxide, CbO .

2. Cupric Oxide

A cupric oxide coating was produced on AISI-310 stainless steel strips by means of the Ebonol C process. This process consists of plating a layer of copper approximately 1/2-mil thick onto the substrate and then oxidizing the copper layer by immersion in Ebonol C solution for from 5 to 10 minutes at 180° to 200°F.

3. Oxidized Nichrome

The nichrome specimens were oxidized by heating in air for two hours at 1800°F.

4. Nickel Oxide

Coatings were prepared by spraying an aqueous slurry of INCO type C nickel powder on 0.002-inch thick AISI stainless steel strips. Samples were then sintered at 1830°F for 45 minutes, impregnated with aqueous LiOH at 70°F and oxidized in air at 1290°F for 30 minutes.

5. Oxidized Stainless Steel

AISI-310 stainless steel specimens were grit blasted with 90-mesh aluminum oxide to roughen the surface and were then oxidized by heating in air at 1800°F for one hour.

6. Oxidized Kennametal

Kenametal powder grade 151-A (-170 + 230 mesh), was oxidized in air at 1600°F for 20 minutes. The oxidized powder was then plasma-arc sprayed onto the substrate.

V. ANALYTICAL AND PHYSICAL TEST PROCEDURES

Coating materials were analyzed before coating, after coating, and after emittance testing. A chemical property analysis included the determination of chemical composition and crystal structure. Physical property analysis included initial particle size, coating color, texture, thickness and bond strength. The equipment and procedures used are described below.

A. Emission Spectrographic Analysis

An automatic quartz and glass Hilger spectrograph was used to determine the chemical composition of coating materials. Although the chemical properties of most of the specimens analyzed were determined only before coating, selected materials were analyzed after coating and a few were analyzed after emittance testing when it was suspected that either the coating process or exposure to elevated temperatures and vacuum had resulted in a change in the coating. No attempt was made to determine precise quantitative material compositions and the compositions reported are therefore of a qualitative nature.

B. X-Ray Diffraction Analysis

A General Electric XRD-3 diffractometer was used to determine the crystal structure of chemical compounds in the coating materials. Materials with promising emittance properties were analyzed before coating, after coating, and after emittance testing to detect possible changes in crystal structure as a result of the coating process or exposure to emittance testing conditions.

C. Physical Property Analysis

Early in the program, physical property description was restricted to coating thickness, color, and bond strength. More recently, coating evaluation has included particle size analysis of powders used for coatings and coating surface texture.

Coating Thickness - Generally, the thickness of a coating was determined by measuring the thickness of a flake which separated from the substrate during preparation of the specimen ends for insertion into the electrodes. When a flake was available, the coating thickness was measured directly with a measuring microscope. When the coating was such that no flaking occurred, the coating thickness was determined from micrometer measurements of the specimen outside diameter before and after the coating was removed from the ends.

Bond Strength - Coating-substrate bond strength was evaluated by scratching the coating and estimating the relative pressure required to remove the coating material. The resulting indication is necessarily qualitative and bond strengths are reported as excellent, very good, good, or fair. Coatings which could be rubbed off are reported as having poor bond strengths.

The coating-substrate bond strength for the finned-tube specimens was determined by bending coated specimens through 130° around a 2-inch radius and noting the degree of cracking or spalling that resulted.

Particle Size - The more recently tested coating materials have been analyzed for particle size distribution with a Model A Coulter Counter. The Coulter Counter is able to determine the overall range of particle sizes as well as the distribution of sizes in the powder sample.

Texture - The surface texture of coated specimens has been determined by comparing the specimen surface texture with that of various grit sizes of emery cloth. Comparisons are made under a microscope.

VI. QUALITY OF MEASUREMENT

During the course of the emittance program, modifications were made to the various rigs and specimen configurations. The total hemispherical emittance rig was completely redesigned and rebuilt. Smaller modifications were made to the other rigs. The specimen black body configuration was altered to reduce the temperature perturbation in the vicinity of the black body and to improve the black body quality. These changes not only increased the speed and ease of operation of the rigs but also significantly improved the quality of the resulting measurements. This section has therefore been divided into two subsections, one of which discusses measurement quality before equipment modifications were made, and the other after modifications were made.

A. Quality of Measurement Before Equipment Modifications

1. Spectral Emittance Rig - Errors were introduced into the calculated values of spectral emittance by 1) instrumentation, 2) the difference between the temperature of the small portion of the specimen that was viewed and that of the black body, 3) the departure of the black-body emittance from unity resulting from the relatively large size of the black-body hole and from nonuniformity of temperature along the surface of the walls of the tube cavity, and 4) reflected radiant energy within the chamber such as energy emitted by the specimen that is reflected first by the chamber walls and then by the specimen surface into the spectrophotometer.

Errors introduced by the instrumentation included those originating in the optical system and in the electronic system of the spectrophotometer. The sources of error investigated were

- 1) scattered light in the monochromator, 2) scattered light at the sodium chloride window and in the optics before the beam-isolation apertures, and 3) detector and amplifier noise. As described in Appendix D, the error introduced by scattered white light in the monochromator was effectively eliminated by the use of selective wave-band filters. The error resulting from scattered light at the sodium chloride window and in the optics before the beam-isolating apertures was determined to be less than 0.12 per cent. The analysis is presented in Appendix E. The error introduced by random noise in the amplifier and detectors has been minimized and may be kept within $\pm 1/2$ per cent if the recorded data is carefully processed.

Since spectral emittance does not vary appreciably with small variations of temperature, the accuracy of specimen temperature measurements and the small fluctuations of the specimen temperature are not critical to the accuracy of the spectral emittance data. The maximum error in optical pyrometer temperature measurement is ± 0.4 per cent and this error results in negligible error in the emittance data. Temperature variations of one or two per cent may be caused by line voltage changes, but since measurements are made with the measuring and reference beams alternated in rapid succession when the spectrophotometer is operated in the ratio mode, the error introduced by these fluctuations is negligible.

Black-body imperfections for an isothermal specimen tube have been analyzed by DeVos⁵. DeVos describes a method for estimating the corrections required and this method is discussed in Appendix H of this report. The amount of this isothermal cavity correction for these tests is estimated to be less than two per cent and the application of such a correction would result in a lower emittance value.

Corrections required as a result of temperature nonuniformity of the black-body cavity were also analyzed by using the method of DeVos for estimating the effect on black-body quality for any arbitrary temperature distribution.

One cause of temperature nonuniformity is the conduction of heat from the ends of the specimen into the electrodes. Temperature profiles resulting from this effect were predicted using the results of Appendix F. The profiles are presented in Appendix H, together with an estimate of the associated loss of black-body quality. The profiles presented are for the worst cases encountered. The associated loss of black-body quality was estimated to be less than 0.5 per cent and, when applied as a correction to the emittance data, decreases the emittance value.

A second cause of temperature nonuniformity was the local altering of the otherwise uniform current density in the tube wall caused by the current having to flow around the black-body hole. In the single case where a high emittance coating was tested on a base metal of low thermal conductivity, it was observed that the surface next to each end of the black-body hole was noticeably cooler than those regions on the sides of the hole. Experimental and analytical

investigation of this effect is presented in Appendix G. In the single case mentioned above, the associated error was estimated to be no more than two per cent. Application of the correction for this effect results in a higher emittance value.

Temperature nonuniformity of the tube wall resulting from non-uniformity of the tube wall thickness was also considered. A particularly adverse case of such nonuniformity was analyzed in Appendix I and the maximum error resulting from this effect was estimated to be within ± 2 per cent.

The correction for the effect of chamber wall reflection has been estimated to be on the order of 1 per cent in the worst case (specimen emittance near zero), and on the order of 0.1 per cent for materials with emittances near unity. Correction for this type of error results in a lower emittance value and is discussed in Appendix B.

These investigations of sources of error show that corrections, if applied to the calculated values of the spectral emittance, would result in corrected values which are between 5 per cent lower than and 3 per cent greater than the uncorrected values obtained before the equipment was modified.

Errors were introduced into the calculated values of total hemispherical emittance obtained with the spectral emittance rig by 1) instrumentation, 2) reflections, 3) conduction heat losses from the specimen test section, 4) local over-heating at the black body, 5) imperfect black-body quality, and 6) variable specimen substrate thickness.

The errors introduced by the instrumentation are estimated to be within ± 2.2 per cent and are distributed as follows:

Specimen heating current	$\pm 0.2\%$
Test section voltage drop	$\pm 0.2\%$
Area of test section	$\pm 0.2\%$
Temperature determined by optical pyrometer	$\pm 0.4\%$

In addition, a systematic error resulted from ripple voltage and an erroneously calibrated shunt. To correct for these factors, all total hemispherical emittance data obtained with the spectral emittance rig appearing in this report should be multiplied by a factor of 1.0096.

Since the total power radiated by the surface is approximately proportional to the fourth power of the specimen temperature, the temperature error contributes almost all of the total error.

The correction for chamber wall reflection is discussed in Appendix B and is estimated to be less than one per cent even for materials with emittance near unity. Correction for wall reflection results in an emittance value higher than that of the uncorrected value.

The effect of heat conduction losses from the specimen test section on emittance values is analyzed in Appendix F. The results of the analysis indicate that errors resulting from end conduction effects become negligible at temperatures above 1000°F for the specimen configurations and materials used.

Local overheating around the black-body hole and imperfect black-body quality introduce errors into optical pyrometer temperature measurements. The corrections of data for these errors are discussed in Appendices G and H, respectively. Based on the analysis of Appendix G, it is estimated that the average temperature of the test section lies between 0.25 per cent above and 1 per cent below the measured temperature of the test section. These limits apply to the worst case tested which was a stainless steel tube with low thermal conductivity coated with a high emittance material. The correction to the calculated total hemispherical emittance values in this case is thus a maximum of 4 per cent and the corrected emittance values would be higher than the uncorrected values. For other tests in which substrates with higher conductivities were used, the errors associated with temperature nonuniformity resulting from the presence of the black-body were estimated to be within ± 1 per cent.

Temperature nonuniformity of the tube wall resulting from non-uniformity of the tube wall thickness is considered in Appendix I. These effects are considered to be negligible with the close tolerances which are maintained for specimen substrate wall thickness.

It is estimated that the total hemispherical emittance values presented in this report which were obtained by using optical pyrometer temperature measurements are no greater than 5 per cent more or 3 per cent less than the true values in cases where stainless steel tubes were used, and are within ± 3 per cent of true values when other substrate materials were used.

2. Total Hemispherical Emittance Rigs - In the total hemispherical emittance data taken in the various rigs using thermocouple measurement of specimen temperature, corrections have been considered for 1) the effect of instrument errors, 2) the effect of reflectivity of the chamber walls, 3) the effect of conduction heat loss from the ends of the test section, 4) the effect of conduction along the thermocouple leads, 5) the effect of temperature perturbation at a scratch in the coating for installation of a thermocouple on a tube specimen or a strip specimen having a coating on both sides, 6) the effect of temperature difference between the coated and the uncoated sides of strip specimens coated on only one side, 7) the effect of variations with time on the emittance of the uncoated surfaces of specimens coated on only one side, and 8) the effect of specimen flickering when alternating current was used for specimen heating. For the strip specimens used in the great majority of these tests, the effect of nonuniformity of specimen thickness was considered negligible.

The maximum error introduced into the calculated values of emittance by the measuring instruments alone was on the order of $\pm 4\text{-}1/4$ per cent. For the majority of the tests the estimated instrument errors were as follows:

Specimen heating current	$\pm 1\%$
Test section voltage drop	$\pm 1\%$
Test section radiating area	$\pm 1/4\%$
Thermocouple measurement of test section temperature	$\pm 1/2\%$

In two instances, however, drift in the calibration of the thermocouples was encountered. One of these instances, described in Appendix N, involved the use of a chromel-alumel thermocouple welded to a molybdenum specimen. This instance led to the use of platinum-platinum 10 per cent rhodium thermocouples in all other tests

involving molybdenum as the substrate material. The other instance occurred when a platinum-platinum 10 per cent rhodium thermocouple was welded to a stainless steel tube with a chromium-black coating. Data has not been reported where more than $\pm 1/2$ per cent thermocouple drift was detected. Although this effect has not been checked in every test, spot checks were made by re-instrumenting some of the specimens and comparing emittance values. Since the thermocouple deterioration could be caused by the presence of the coating very near to a thermocouple junction, it was decided to run some tests with only one side of the specimen coated and with thermocouples attached to the uncoated side. However, coating only one side of the specimen introduced the problem of estimating the emittance of the uncoated side, which must be done not only as a function of temperature, but also, in an endurance test, as a function of time. For these tests, it is estimated that the emittances of the uncoated side, based on measurements of the substrate metal alone in earlier tests, were within ± 3 per cent of the true values. Random instrumentation errors have been estimated by noting the standard deviation of total hemispherical emittance data. For a vapor-blasted molybdenum strip coated on one side with crystalline boron and tested in the total hemispherical emittance rig, the standard deviation (rms value) was 0.7 per cent. For a specimen coated with boron carbide and tested in the short term endurance rig, the standard deviation was 0.9 per cent.

The effect of reflections by the chamber walls is discussed in detail in Appendix B. For the worst case, that is, for materials with high emittance, the correction is estimated to be less than 1 per cent and, when applied, would give a higher emittance value.

The effect of heat conduction losses at the ends of the specimen is analyzed in Appendix F. The results of this analysis indicate that the correction for heat conduction loss is generally negligible, even without compensating end heating, at temperatures above 1000°F. A molybdenum strip coated on both sides with boron carbide was tested without end heating to experimentally determine the correction required to lower the emittance value to the true value. The required correction is plotted in Figure F-1 as a function of temperature at the center of the specimen. In tests

where end heating is used, it is difficult to avoid an error on the order of ± 5 per cent at temperatures below 350°F. The error at low temperatures results from the difficulty in precisely equalizing the end and central temperatures with the specimen length used. More accurate emittance measurements at low temperatures could be achieved by using longer specimens.

The effect of temperature perturbation at the scratch in the coating where thermocouples are installed is discussed in Appendix M. It is estimated that errors from this cause did not exceed 1 per cent and in most cases were less than 1/2 per cent.

The errors introduced by the temperature drop across a specimen coated on only one side, and by flickering resulting from the use of alternating current for specimen heating, are discussed in Appendices J and K respectively. As a result of the analyses presented in these Appendices, the errors from these causes have been estimated to be negligible.

It is therefore estimated that the overall error in the uncorrected emittance values presented in this report is not greater than 4 per cent for specimens coated on both sides and 6 per cent for specimens coated on only one side.

3. Long Term Endurance Rigs - The long term endurance rigs are used to evaluate the behavior of coatings when exposed to representative radiator temperatures and vacuum for extended periods of time. Temperature, heating power, and pressure are measured.

Temperatures are measured both by thermocouples and by an infrared pyrometer. Thermocouple temperature measurements are considered to be accurate to within ± 0.5 per cent. Temperature measurements by the infrared pyrometer are corrected for the effects of surface emittance. Since the variations of the surface emittance values as a function of time are not known, pyrometer temperature measurements are accurate only to within ± 2 per cent. The instrument is therefore used to provide relative temperature indications to confirm thermocouple measurements.

Heating power during the early portion of the tests was measured with vacuum-tube voltmeters. Heater voltage was measured with a meter accurate to within ± 2 per cent and heater current was measured as the voltage drop across a 10 ampere-50 millivolt shunt, using a meter accurate to within ± 3 per cent. A large amount of scatter appeared in the data obtained by this system and evaluation proved difficult. Therefore the vacuum-tube voltmeters were replaced by an AC-DC differential voltmeter accurate to within ± 0.2 per cent. Although initially power measurements were accurate only to within ± 5 per cent, the use of the AC-DC differential voltmeter increased the accuracy to within ± 0.4 per cent.

Vacuum measurements were made by measuring the current in the ion-gettering pump and by referring to calibration curves provided by the manufacturer.

B. Quality of Measurement After Equipment Modifications

1. Spectral Emittance Rig - The modifications made to the spectral emittance rig and discussed in Section II significantly improved the quality of the resulting data. The substitution of an 8-inch ellipsoidal mirror in place of the 6-inch mirror previously used at M-2 (see Figure 2) not only increased the energy input to the spectrophotometer but also eliminated the astigmatism of the mirror previously used. Additional changes to the beam separating and isolating optics further increased the energy input to the spectrophotometer and eliminated the effects of astigmatism and spherical aberration associated with mirror M1.

The increased resolution of the system permitted changes in the specimen black-body configuration from the previously-used rectangular hole to two 0.0235-inch diameter holes axially separated by 0.052 inch. It is estimated by the method of DeVos that the new black-body holes have an effective emittance of 0.992 or better. In the visible radiation range the emittance is estimated to be 0.998 or better. This corresponds to an optical pyrometer temperature measurement error of only 0.015 per cent at 2000°F.

The combined use of the 8-inch mirror and the new black-body hole configuration permitted modification of the beam-separating optics. The beam separator was moved to a position in front of mirror M1

which both reduced errors introduced by scattered light by reducing the number of reflectances before beam separation, and eliminated the effects of astigmatism in mirror M1. Further, full-height rather than half-height mirrors were used in the separator. The use of full-height mirrors doubled the output of the optical system to the spectrophotometer detectors.

These modifications extended the useful range of the spectrophotometer and increased the overall accuracy of spectral emittance measurements to within ± 3 per cent.

2. Total Hemispherical Emittance Rig - Although modifications to the total hemispherical emittance rig largely resulted in a considerable increase in efficiency of operation, modifications also resulted in a reduction of errors. The maximum instrumentation error for each of the measured quantities is estimated as follows:

Specimen heating current	$\pm 0.2\%$
Test section voltage drop	$\pm 0.2\%$
Test section radiating area	$\pm 0.25\%$
Thermocouple measurement of test section temperature	$\pm 0.5\%$
Optical pyrometer measurement of test section temperature	$\pm 0.4\%$

Since errors from other causes contribute negligible error to total hemispherical emittance measurements, the maximum errors in reported total hemispherical emittance values obtained with the new rig are ± 2.7 per cent when temperatures were measured by thermocouples and ± 2.3 per cent when optical pyrometer temperatures were used. This compares with a 4 per cent maximum error with the old rig. It is noted that the use of the new black-body configuration in the total hemispherical emittance rig resulted in a substantial reduction in temperature measurement errors.

VII. TEST RESULTS

A. Metallic and Oxidized Metallic Surfaces

1. Columbium and Oxidized Columbium

A drawn tube of columbium having a 1/8-inch outer diameter and a 0.005-inch wall thickness was grit blasted with No. G-25 steel grit to roughen the surface. A slot in the tube wall 0.090 inch long by 0.016 inch wide was used as the black-body reference integral with the specimen.

Total hemispherical emittance measurements were obtained from this sample at temperatures from 1500° to 2200°F in increments of 100°F. The measurements were taken first while increasing the temperature of the specimen and then repeated in approximately the same increments while decreasing the temperature. At the end of the second set of readings, one of the potential leads separated from the sample, necessitating a teardown of the rig. Repairs were made and data were again taken over the temperature range of 1500° to 2200°F in both an ascending and a descending order. Data appear in Figure 43 and in Table 1.

As an endurance test, the sample was then held for over 160 hours at a temperature of 2200°F and a pressure of approximately 1×10^{-9} mm Hg. Total hemispherical emittance measurements were made periodically during the endurance run and the results are shown in Figure 44 and in Table 1. The change in total hemispherical emittance during the endurance test is attributed to the changing of the surface condition that finally became stabilized. A visual indication of the degree of change is shown in Figure 45.

A second drawn tube of columbium having a 0.235-inch outer diameter and a wall thickness of 0.005 inch was oxidized in air in a furnace at a temperature of 1200°F for a period of five minutes. The outer layer of powdery white oxide, Cb_2O_5 , was removed by brushing with fine steel wool to expose the inner layer of black oxide, CbO .

The specimen was tested in an exploratory manner for a total of 250 hours at elevated temperatures. These 250 hours included endurance testing at several approximately constant elevated temperatures, alternated with short runs in which emittance was meas-

ured over a range of temperatures. Spectral emittance was determined twice at each of three elevated temperature levels in the wavelength range of 0.62 to 11.75 microns.

The sequence of testing was:

1. Initial cleanup period of 4 hours at about 1400°F,
2. Spectral emittance Run A at 1430°F,
3. Total emittance Run 1: temperature range from 1460° to 1600°F,
4. Total emittance Run 2: temperature range from 1450° to 1820°F,
5. Spectral emittance Run B at 1610°F,
6. Spectral emittance Run C at 1820°F,
7. Spectral emittance Run D at 1430°F,
8. Endurance for 100 hours at 1600°F,
9. Total emittance Run 3: temperature range from 1420° to 1805°F,
10. Spectral emittance Run E at 1600°F,
11. Endurance for 24 hours at about 1820°F,
12. Total emittance Run 4: temperature range from 1425° to 1800°F,
13. Spectral emittance Run F at 1800°F,
14. Endurance for 24 hours at about 1810°F,
15. Total emittance Run 5: temperature range from 1430° to 2000°F,
16. Endurance for 15 hours at about 1430°F,
17. Total emittance Run 6: temperature range from 1420° to 2000°F,
18. Spectral emittance Run G at 2000°F (4 hours' duration),
19. Endurance for 65 hours over temperature range from 1980° to 2070°F,
20. Total emittance Run 7: temperature range from 1430° to 2070°F, and
21. Shutdown.

The outstanding features pointed out in this test were a rapid initial cleanup below 1480°F followed by considerable stability during endurance testing at 1600°F and below. The deterioration rate of the coating increased rapidly, however, with increasing temperature. The deterioration history of the coating is seen in Figure 43 and in Table 2, which present data for all of the total hemispherical emittance runs.

The spectral emittance data taken before the first endurance period are compared with data taken after various endurance periods in Figure 46. During a momentary shutdown before endurance testing it was found that small patches of the coating a few thousandths of an inch in diameter had cracked and had become slightly scaled. The condition of the specimen before and after the test is shown in Figure 47.

2. Columbium - 1 Per Cent Zirconium Alloy

Two uncoated specimens of columbium - 1 per cent zirconium were tested. The first was an "as-received" specimen which was tested only in the total hemispherical emittance rig. The second, a polished specimen, was tested in both the spectral normal and total hemispherical emittance rigs. The total hemispherical emittance data for both specimens are shown in Figure 48 and Tables 3 and 4.

As may be seen in the figure, above 1000°F the emittance of the as-received specimen was greater than that of the polished specimen with a maximum difference of 40 per cent being recorded at 2000°F. The total emittance of the polished specimen increased slightly with each successive test run. During this test a leak existed in the rig which resulted in the test being performed in a vacuum of only 2 to 3×10^{-6} mm Hg. Although the leak was not serious enough to preclude testing, most of the other tests were conducted with vacuum levels in the 10^{-7} mm Hg range. The fact that a good vacuum could not be maintained even though a large pump was used (400 liters/sec) shows that a significant amount of air was being pumped through the chamber during testing. It is suspected that during spectral emittance testing in a vacuum of about 10^{-8} mm Hg the specimen was cleaned up and that subsequently during total emittance testing, oxide layers formed on the surface and caused the emittance increases.

Spectral normal emittance of the polished specimen is shown in Figure 49 for test temperatures of 900°, 1450°, and 2000°F.

3. Cupric Oxide

A cupric oxide coating was produced on an AISI - 310 stainless steel strip by means of the Ebonol C process. This process consists of plating a layer of copper approximately 0.5 mil thick onto the substrate and then oxidizing the copper by immersion in Ebonol C solution for 5 to 10 minutes at 180° to 200°F.

Total hemispherical emittance was measured over the temperature range of 200° to 1500°F. Emittance values are presented in Figure 50 and Table 5.

A relatively constant total hemispherical emittance value of 0.85 was measured for temperatures up to 800°F. A drop in emittance to a value of approximately 0.5 was noted at 800°F, apparently due to the conversion of the coating to a different oxide of copper. This new level of total hemispherical emittance, 0.5, was recorded over the temperature range of 500° to 1500°F. A second change in the emittance value to approximately 0.25 occurred at 1500°F; this resulted from a second conversion of the coating, in this case to copper.

After testing, a visual inspection of the specimen showed that the central area in which the measurements were taken had a metallic copper appearance whereas areas farther from the center had the dark red color that is characteristic of cuprous oxide, Cu_2O . Figure 51 shows the specimen before and after testing.

An additional coating of cupric oxide was produced by the Ebonol C process on an aluminum strip for thermal cycling and bend testing. This coating was between 1 and 2 mils thick. The color of the coating changed during initial heating from black to green along the root of the specimen and to copper adjacent to the green-colored area. No spalling occurred during bend testing.

4. Molybdenum

Five molybdenum specimens were tested. All were tested in the total hemispherical emittance rig except for one wedge-shaped specimen which was tested in the spectral normal emittance rig. Of the remaining four strips, one was chemically cleaned, another was vapor blasted, and two were grit blasted.

Spectral normal emittance data for the wedge-shaped specimen were recorded over the wavelength range from 0.5 to 11.75 microns at 1800°, 2000° and 2200°F. The values of spectral normal emittance are shown in Figure 52. Inasmuch as there appears to be no significant trend in the variation of spectral normal emittance with temperature over the range investigated, a single smooth curve has been drawn to represent all of the points at the three different temperatures. Total hemispherical emittance data were also recorded and calculated using both optical pyrometer and platinum-platinum 10 per cent rhodium thermocouple readings. As may be seen in Figure 53 and in Table 6, the specimen cleaned up during testing so that emittance values after exposure to test conditions were lower than initially.

The chemically cleaned molybdenum strip was instrumented with three chromel-alumel thermocouples and one platinum-platinum 10 per cent rhodium thermocouple and tested in the total hemispherical emittance rig. Several runs were made over the temperature range of 300° to 2000°F. The total hemispherical emittance was measured at approximately 200°F increments as the specimen temperature was increased and as it was decreased. The emittance values calculated on the basis of the platinum-platinum 10 per cent rhodium thermocouple readings are shown in Figure 54 and in Table 7. As was the case with all of the metallic specimens, a certain amount of cleaning up of the surface was noted. This cleanup is presumed to result from the departure of oxides from the surface. Figure 55 shows the total hemispherical emittance values obtained in the total hemispherical emittance rig using a strip specimen, together with those obtained in the spectral normal emittance rig using a wedge-shaped specimen. On the basis of this testing it was established that there is good agreement between the measurements made in the two rigs.

To determine the effect of a roughened surface on the emissive properties of molybdenum, a strip was vapor-blasted with Tech-line Liguabrasive, PMC-3067, Grit No. 325. The total hemispherical emittance was measured over the temperature range of 300° to 2000°F using the technique of the first tests on the smooth specimen. The emittance values derived from the platinum-platinum 10 per cent rhodium thermocouple measurements are shown in Figure 56 and in Table 8. Figure 56 indicates that the emittance level of a vapor-blasted molybdenum surface is slightly higher than that of a smooth surface.

One side of a grit blasted molybdenum strip had previously been coated with zirconium oxide and tested. In order to reduce the data obtained, however, it was necessary to know how much the uncoated side cleaned up when exposed to elevated temperatures and what the total hemispherical emittance was after cleanup. A specimen was therefore prepared by grit blasting a 4-mil thick molybdenum strip with aluminum oxide No. 90 (PMC-3043A). Up to a temperature of 2000°F, the behavior of the specimen was erratic and data are not reported. When a temperature of 2000°F was reached, a short endurance test was conducted during which the specimen appeared to clean up completely. Therefore, during the final cooling cycle, the data reported were reliable, and accurate emittance values were obtained in the range from 1350°F to 2000°F. These values are plotted in Figure 54 and tabulated in Table 9.

A second molybdenum strip 4 mils thick was blasted with No. 90 (PMC 3043A) aluminum oxide and instrumented for testing in the total hemispherical emittance rig. Total hemispherical emittance data was measured between 250°F and 1800°F. At the latter point an endurance run was started in order to clean up the surface of the molybdenum. After about seven hours all of the thermocouples had separated from the specimen and the test was terminated. The total emittance data is listed in Table 10 and plotted in Figure 54.

The emittance of the grit blasted samples was significantly higher than that of the other samples tested. The difference between the two grit blasted samples was probably caused by differences in the surface condition resulting from preparing the samples at different times.

5. Oxidized Nichrome

Nichrome Oxidized in Air - A nichrome strip 2 mils thick was oxidized by heating it in air in a furnace for two hours at 1800°F. The specimen was then tested in the total hemispherical emittance rig.

During the initial heating cycle (Run 1), the total hemispherical emittance varied from 0.62 at 400°F to 0.66 at 870°F, as shown in Table 11 and Figure 57. After a seventeen-hour endurance run at about 900°F, the emittance varied from 0.64 at 1025°F to 0.77 at 1650°F (Run 2A). Very good agreement in the values of emittance was obtained as the temperature was reduced to 1560°F (Run 2B). As the specimen was cooled below 1560°F, the emittance was higher than the previously measured values, the difference being about five per cent at 1450°F.

Nichrome Oxidized in Oxygen - In an attempt to acquire a coating with a higher emittance, a nichrome strip was oxidized for 15 minutes in an oxygen atmosphere at 1800°F. The resulting oxide coating appeared darker, thicker, and more dense than that of the specimen oxidized in air.

The total hemispherical emittance of this sample varied from 0.72 at 300°F to 0.82 at 1450°F. The specimen was maintained at 1450°F for about 170 hours during which time the emittance increased to 0.83. At that time the last remaining thermocouple failed and the specimen had to be reinstrumented. During the second run the total hemispherical emittance at 800° and 1200°F agreed with the values measured in the initial cycle but at 1450°F the values were slightly lower (about 0.80). The temperature was maintained at 1450°F for an additional 280 hours during which time the emittance varied between 0.797 and 0.814. The data is tabulated in Table 12 and plotted in Figure 57.

The emittance of the specimen oxidized in oxygen was approximately 15 per cent higher than that of the specimen oxidized in air.

6. Lithiated and Oxidized Nickel

Total Hemispherical Emittance - A sodium alginate slurry of nickel C powder was sprayed onto an AISI - 310 stainless steel strip. The strip was sintered in a hydrogen atmosphere at 1830°F for 45 minutes. It was then impregnated with lithium hydroxide and oxidized in air at 1290°F for 30 minutes. The resultant coating was 3 mils thick. It was tested in the total hemispherical emittance rig over the temperature range from 300° to 1450°F.

As shown in Figure 58 and in Table 13, the total emittance was relatively constant at about 0.83 during the initial heating cycle until 1100°F was reached. After remaining at this temperature for 18 hours, the emittance increased, and a peak value of 0.90 was achieved at 1300°F. The emittance then dropped to 0.84 at 1450°F and remained at this value while the temperature was maintained at 1450°F for 21 hours. During cooling to 300°F the emittance values were considerably lower than those obtained previously. The specimen was heated again and results were in close agreement with those of the immediately previous run.

The tested specimen and one which was prepared at the same time but not tested were analyzed by the use of a flame spectrophotometer. The results of the analysis showed that the test reduced the lithium content of the coating from 0.20 to 0.12 per cent. Since the electrical conductivity of nickel oxide is drastically affected by the lithium content⁶, the change in emittance characteristics of this coating may possibly be attributed to the loss of lithium.

Photomicrographs were taken of sections of the specimens before and after testing. Figures 59 and 60 are 100 x magnifications of these specimens etched with Marble's reagent. Comparison of the "before" and "after" micrographs indicates a loss in the density and thickness of the coating. It cannot be determined at present whether this loss was caused by the test or by handling of the specimens. Visual examination of the specimens immediately after testing showed the untested specimen to be darker than the tested one. This is consistent with the loss of coating material observed in Figures 59 and 60. A spectro-

graphic analysis of the two specimens showed no change in the elements present in the coatings, i. e., the coatings were mostly nickel but had traces of magnesium, iron and silicon. Lithium (atomic number 7) was not detected since spectrographic analysis cannot reveal the presence of gases or of elements of atomic number less than 12.

Endurance Testing - A coating of lithium-impregnated and oxidized sintered nickel C powder was applied to a stainless steel tube by the method outlined above. The spectral emittance rig was used as an endurance rig for the purpose of measuring changes in total emittance of this coating as a function of time at an endurance temperature of 1450°F.

The total hemispherical emittance data obtained as the specimen was heated to the endurance temperature of 1450°F was consistent with the data from the coated AISI-310 stainless steel strip up to 1100°F. During the first 70 hours of the endurance run the total emittance of the specimen dropped from 0.86 to 0.84 and then remained at 0.84 for 100 hours.

During the next 90 hours the total emittance increased to 0.86 and stayed at this level for the remainder of the test (an additional 215 hours). The data are shown in Table 14 and in Figures 58 and 61.

7. Oxidized AISI-310 Stainless Steel

The total hemispherical emittance of three oxidized AISI-310 stainless steel samples was measured. One flat strip and one tubular sample were grit blasted with aluminum oxide No. 90 (PMC 304A), and then oxidized in air for one hour at 1800°F prior to testing. The third sample, a flat strip, was oxidized for one hour at 1800°F prior to testing but received no grit blasting.

Oxidized Strip - Measurements of total hemispherical emittance were made over the temperature range of 300° to 2000°F in 100° increments.

The total hemispherical emittance values are shown in Table 15 and in Figure 62. The condition of the specimen before and after testing is shown in Figure 63. After testing, the specimen was observed to have a slightly greenish tint.

Grit Blasted and Oxidized Strip - Measurements of total hemispherical emittance were taken at 100°F increments over the range of 300° to 2000°F. The total hemispherical emittance data are presented in Figure 62 and in Table 16.

The condition of the specimen before and after testing is indicated in Figure 64. After testing, the specimen had a more noticeable green tint than the oxidized stainless steel specimen that was not grit blasted.

Grit Blasted and Oxidized Tube - Total hemispherical emittance of this sample was measured from 300°F to 1450°F and the sample was then maintained at 1450°F for approximately 330 hours. The total hemispherical emittance varied from 0.74 at 300°F to 0.83 at 1450°F. No change in emittance took place as a result of keeping the sample at 1450°F for 330 hours.

The total hemispherical emittance data is shown in Table 17 and in Figures 62 and 65.

8. Tantalum

A wedge-shaped tantalum specimen was tested in the spectral emittance rig. Spectral emittance was measured at 2200°F over the wavelength range of 0.45 to 11.75 microns. Data is presented in Figure 66. No total emittance measurements were made.

An investigation into the scattering of light in the monochromator was also conducted using this specimen (see Appendix D).

9. Tungsten

Initially, tungsten was tested in order to check the operation of the rigs since reliable emittance data were available for this material for comparison purposes. Exact agreement between the published values and those obtained during this test was not anticipated since emittance is a property of the specimen surface as well as of the material from which the specimen is made. The results obtained did agree reasonably well with those of other experimenters.

Spectral Normal Emittance - A wedged-shaped tungsten specimen was used for checking the accuracy of measurements made in the spectral emittance rig.

As shown in Figure 67, measurements of spectral normal emittance were taken at temperatures of 1700°, 2110°, and 3090°F in the wavelength region between 0.5 and 12.0 microns. In comparing the results of this test with the values published by DeVos² and Larrabee¹, it was noted that all of the data showed the spectral emittance to decrease with increasing temperature in the visible wavelength range and to increase with increasing temperature in the infrared wavelength range. The node at which the constant-temperature lines of spectral emittance cross was noted at approximately the same wavelength as shown by DeVos. Figure 68 shows the results obtained by Larrabee and DeVos for comparison with those obtained in this experiment in the visible wavelength.

Total hemispherical emittance values were also measured on the wedge-shaped specimen for comparison with those obtained on a strip specimen in the total hemispherical emittance rig.

Total Hemispherical Emittance - A tungsten strip was prepared for testing in the total hemispherical emittance rig. The specimen was instrumented with three chromel-alumel thermocouples and also with an additional platinum-platinum 10 per cent rhodium thermocouple at the center of the strip. On the basis of a study made in connection with the accuracy of the thermocouple measurements (see Appendix N), the platinum-platinum 10 per cent rhodium thermocouple readings were used to calculate the total hemispherical emittance.

The total hemispherical emittance data obtained for this specimen are plotted in Figure 69 and tabulated in Table 18. Figure 69 also shows the total normal emittance data obtained on the tungsten wedge in the spectral emittance rig, along with results obtained by Forsythe and Watson⁷, Jones and Langmuir³, and Roesser and Wensel⁸.

The total emittance values obtained on the two rigs show good agreement, and the differences between the data obtained in this experiment and the data obtained in the other investigations is of the same order as the differences between the data obtained in the other investigations.

10. Chromium Black

Chromium black was applied by an electroplating process onto an AISI-310 stainless steel strip, a stainless steel tube, and a nickel tube.

The coating on the stainless steel strip was not as uniform nor as dark as the coatings on the tubular specimens. It was decided to conduct a preliminary test on the strip specimen prior to conducting more extensive tests on the tubular specimens.

Coated Stainless Steel Strip - During the first run the total emittance values ranged from 0.7 at 300°F to 0.865 at 1000°F (Figure 70 and Table 19). When the temperature was reduced to 700°F, the emittance increased from the previous value of 0.76 to 0.825. No further changes were noted as a result of temperature cycling until a temperature of approximately 2000°F was reached, at which point the emittance dropped by 7 per cent. The values of emittance ranged from 0.69 to 0.88 over the entire temperature range of 200°F to 2000°F.

When the specimen was removed from the rig, the surface was observed to have the green color characteristic of chromic oxide, Cr_2O_3 , indicating that one of the changes in emittance level might have been caused by a conversion of the coating.

Coated Stainless Steel Tube - The stainless steel tubular specimen coated with chromium black was instrumented with platinum potential leads and with a platinum-platinum 10 per cent rhodium thermocouple. The thermocouple was used to measure temperatures up to 1450°F. Above 1450°F, an optical pyrometer was used for temperature measurement. Spectral emittance data were obtained twice at 1450°F and twice at 1550°F over the wavelength range of 1 to 13 microns. Two endurance runs were made, one at 1450°F for 274 hours and one at 1550°F for 312 hours.

The total hemispherical emittance values recorded during heating are shown in Figure 70 and in Table 20. During the endurance test conducted at 1450°F, the values of total hemispherical

emittance remained relatively constant at approximately 0.92. These data are shown in Figure 71. Two spectral emittance runs were made during the time that the temperature was maintained at 1450°F. Very little change in emittance was noted, as indicated in Figure 72. The specimen was heated from 1450° to 1550°F and maintained at the higher temperature for 312 hours. During the first 50 hours, no change in total hemispherical emittance occurred; however, during the last 262 hours, the total hemispherical emittance dropped to 0.848. Two spectral emittance runs were made during this higher temperature endurance test, the results of which reflect the change that had been noted in the total hemispherical emittance values. The spectral data at 1550°F are shown in Figure 72.

The four spectral emittance runs were integrated in the manner described in Appendix A to obtain total normal emittance. The values obtained by integration agree reasonably well with the measured total hemispherical emittance values. Appendix A discusses the integrated and measured values of total emittance.

A temperature perturbation in the vicinity of the black-body hole was observed visually for the first time during this test. The cause of this perturbation and its effects on emittance are discussed in Appendix H.

Coated Nickel Tube - The tubular nickel specimen was instrumented in the same manner as the strip specimen. In addition, a small black-body hole 0.015 inch in diameter was formed at the midpoint of the axial length of the tube, in order to measure the temperature of the specimen by an optical pyrometer through a window in the endurance rig. The small size of the black-body hole and the higher thermal conductivity of the nickel tube virtually eliminated the temperature perturbation noticed in the testing of the coated stainless steel tube.

The specimen was tested for 865 hours of which about 800 hours were at a nominal endurance temperature of 1440°F. For the first 380 hours of the endurance run the total emittance remained constant at about 0.905. During the next 70 hours the total

emittance dropped about two per cent, after which it remained relatively constant at about 0.89 for the rest of the test. The drop in total emittance was accompanied by a change in color of the coating from black to green. Data for this test appear in Table 21. Total hemispherical emittance vs temperature is plotted in Figure 70 and total hemispherical emittance vs time is plotted in Figure 71.

A comparison of the data from this test with that for the coated tubular stainless steel specimen indicates that the total hemispherical emittance values of the present test are lower by about one per cent. There were two sources of error, however, in the previous test (discussed in Appendix F) which tended qualitatively to compensate for each other. These were 1) the temperature perturbation caused by the large black-body hole in the low-conductivity stainless steel tube which raised the local wall temperature above the average temperature of the specimen test section, and 2) radiation loss from the inside of the tube through the black-body hole which caused the hole to emit non-black radiation. These effects are opposite in sign so that the temperature detected by the pyrometer could have been either higher or lower than the average specimen temperature. The errors in spectral emittance due to these effects are discussed in detail in Appendix H of this report. It is not known which of the two errors has the greater effect on total emittance, but since the largest possible error has been estimated to be not more than two per cent, it can be assumed that the earlier data were reasonably accurate.

Thermal Cycling and Bend Testing - Two aluminum fins were coated with chromium black for thermal cycling and bend testing. These coatings were approximately 2 and 6 mils thick, respectively. During thermal cycling the thinner coating bubbled, but no spalling resulted from bend testing. The thicker coating flaked during thermal cycling but did not spall during bend testing. It was noticed that neither of these coatings was as dark as those used for emittance measurements.

11. Platinum Black

Three strips of AISI-310 stainless steel were coated with platinum black by the method discussed in Section IV C.

First Specimen - The first specimen was instrumented and installed in the total hemispherical emittance rig. Four runs were made over a range of temperatures to measure the total hemispherical emittance, the final temperature of each run being successively higher. The data are shown in Figure 73 and in Table 22.

A sharp drop in emittance, from 0.75 at 1267°F to 0.292 at 1716°F was obtained during the fourth run. As an attempt was made to obtain a datum point at about 1500°F, the temperature continued to increase while the heating current was held constant until the temperature finally stabilized at approximately 1700°F, at which time the drop in emittance from the previous point at 1267°F was observed. A visual inspection of the specimen upon removal from the rig indicated that the coating had been converted to shiny platinum (see Figure 74). The sharp change in emittance during the fourth run was attributed to this conversion.

Second and Third Specimens - To study the effects of surface density on the total hemispherical emittance, two strips of AISI-310 stainless steel were coated with platinum black by the process described in Section IV C. The average surface densities of these two coatings were 300×10^{-6} and 1200×10^{-6} gm/cm².

The specimen with the surface density of 300×10^{-6} gm/cm² was the first to be tested in the total hemispherical emittance rig. The total hemispherical emittance data obtained for this specimen are shown in Figure 73 and Table 23.

The data indicate that an increase in the emittance occurred after the temperature was maintained at 900°F for 16 hours. To determine the cause of this phenomenon, the testing was halted and the sample removed from the rig for inspection. There was no evidence of instrumentation failure. The appearance of the sample, however, had changed from black to gray, indicating that a change in the coating had occurred. After reinstalling the specimen in the rig without making any changes, the temperature was brought to 700°F (Run 3). The emittance values from this run agree with the higher values obtained after the 16 hour period at 900°F (Run 2).

The specimen having the higher surface density, (1200×10^{-6} gms/cm²), was tested in the total hemispherical emittance rig and data are shown in Figure 73 and Table 24.

An endurance test of this specimen was then conducted at a nominal temperature of 900°F. An increase in total hemispherical emittance of about 14 per cent was noted during the first twenty hours. A similar effect had been found with the earlier platinum-black coated specimen where the increase in total hemispherical emittance was 12 per cent. The percentage increase was the same with both chromel-alumel and with platinum-platinum 10 per cent rhodium thermocouples. As the test run continued, the emittance of the specimen dropped until it reached the same level as that recorded at the start of endurance testing. The changes in emittance during the period are shown in Figure 75.

An additional short endurance run of seventeen hours at 1200°F caused a drop in emittance of about eleven per cent. This lowering of the emittance of the coating appeared to be permanent. The data is plotted on Figure 73.

Although the greater surface density of the third specimen produced a considerable increase in total hemispherical emittance over that of the the second specimen, the data is insufficient to establish the effect of surface density. Since the emittance of the specimens tested has not been particularly high, no attempt has been made to investigate the nature of the changes which developed during the endurance runs. It is believed that these changes are probably associated with spheroidization and coalescence phenomena occurring in the coating.

B. Sprayed Coatings

1. Borides

a. Crystalline Boron

Crystalline boron was plasma-arc sprayed by the Linde Plasmarc process onto three molybdenum strips and onto a columbium tube. All of the coatings were 3 mils thick.

First Coated Molybdenum Strip - The specimen, which was coated on both sides, was tested in the total hemispherical emittance rig and data appear in Figure 76 and Table 25.

For this test, the end heaters were attached directly to the coating. However, the nonconductive nature of boron resulted in the end heaters being ineffectual and therefore the data in the lower temperature range had to be corrected for the error introduced by the nonuniformity of temperature over the section of the sample in which the thermocouples were located. This correction, as discussed in Appendix F, depends upon the temperature level at the center of the strip and the thermal conductivity of the materials involved.

Inspection of the sample at the end of the test showed that the coating had separated from the substrate but had remained intact. Since the data of the two runs were consistent, it is assumed that the separation of the coating did not occur during the cooling and reheating of the specimen between the runs. Separation occurred, therefore, either during the initial heating cycle or during the final cooling.

It was observed during the test that the thermocouple located at the top of the specimen was recording temperatures higher than those indicated by the thermocouple at the middle of the specimen. This is inconsistent with the test setup, since the end-loss effect, discussed in Appendix F, would cause both ends of the specimen to be cooler than the middle. In addition, the location of the top plate, which acts as a heat sink, normally causes the top of the strip to be cooler than the bottom. In all other tests in this rig, the thermocouple readings were in the proper order; highest at the middle, lower at the bottom, and lowest at the top. It is believed that the coating-substrate separation caused this abnormal temperature profile.

Second Coated Molybdenum Strip - This specimen, which was coated on only one side, was tested in the total hemispherical emittance rig. To establish better contact for the end heaters than was obtained for the first strip, a small amount of coating was scraped away and the end heaters were attached directly to the substrate.

The specimen was heated slowly to 1350°F in the course of which short endurance tests were run at 500°F and at 900°F for one hour each. The specimen was then maintained at a nominal temperature of 1350°F for 137 hours. Over the entire period of this test, the total emittance values dropped from 0.960 to 0.935. However, when the end heaters were turned off after 54 hours at 1350°F, no appreciable change in total hemispherical emittance was noted

immediately. Thus the size of the correction discussed in Appendix F, which is to be applied when end heaters are not used, was shown to be small for this specimen at this temperature. This is consistent with the calculations based on Appendix F. The temperature of the specimen was then brought up to 1450°F and maintained at that level for 380 hours. The total hemispherical emittance data for the endurance tests appear in Figure 77 and in Table 26. Each point on the curves represents the average of all the emittance data taken during one day. During this period the emittance decreased from 0.93 to 0.76. The bulk of the decrease occurred gradually during the first 150 hours of testing at 1450°F.

While the temperature was being reduced, a power supply failure occurred, causing a sudden large temperature change. Removal of the specimen indicated that the entire coating had separated from the substrate material.

In calculating the total hemispherical emittance values of the coating, the emittance values used for the uncoated side were the final emittance values of the vapor-blasted molybdenum strip reported in Section VII A 4. However, a cleanup of the original molybdenum specimen had taken place, and it is to be presumed that a cleanup also occurred on the molybdenum side of this specimen. Therefore, approximately 3.5 per cent of the change in the total emittance of boron shown on the endurance curves can be attributed to the cleanup of the molybdenum.

Third Coated Molybdenum Strip - This specimen, which was coated on both sides, was tested in the endurance rig. The endurance rig allows observation of the specimen and it was desired to determine when the coating separated from the substrate.

During the first 65 hours of testing, the total hemispherical emittance values dropped from 0.86 at 200°F to 0.75 at 1350°F. The emittance remained relatively constant at 0.75 during a subsequent 190 hours at 1350°F. At this point, the separation of the coating was just noticeable. An additional 75 hours at 1450°F produced a decrease in the total hemispherical emittance of approximately 3 per cent.

Since most of the decrease in the total hemispherical emittance occurred during the first 17-hour endurance at 600° to 800°F (0.86 to 0.77) and since all of the other boron-coated specimens tested had a higher total hemispherical emittance level at the start of the

endurance, it is assumed that the largest amount of separation took place during the low temperature endurance.

The total hemispherical emittance data appear in Table 27. Data obtained during heating appear in Figure 76 and data obtained during endurance testing appear in Figure 77. Each point on the figure represents the average value of the emittance recorded during an eight-hour period. The separation of the coating from the substrate is shown in Figure 78.

Coated Columbium Tube - The columbium tube used as a substrate for this coated specimen had an outside diameter of 0.25 inch and a wall thickness of 0.005 inch. Total hemispherical emittance measurements were obtained while the specimen temperature was slowly raised to 1340°F. After 120 hours, the test was halted to replace the potential leads which had become separated. These leads also separated from the specimen during the subsequent test and therefore no further total emittance measurements were attempted. The total hemispherical values which were recorded are shown in Figure 76 and in Table 28.

Spectral emittance measurements were taken in the wavelength range of 1 to 12 microns at the end of 93, 120, and 128 hours. The last measurements were recorded after the potential leads were replaced. A slight drop in the total emittance values was noted from the first to the second run, but no significant drop was noted from the second to the third run. Figure 79 presents the spectral data at 1450°F.

General Remarks - All of the crystalline boron coatings separated from their substrates except for the coating on the columbium tube. It is believed that the nonrepeatability of the data is a result of coating failures and substrate surface preparation.

Thermal Cycling and Bend Testing - Four aluminum strips were coated with crystalline boron for thermal cycling and bend testing. Two of these coatings were plasma-arc sprayed by the Linde Company and two were aluminum-phosphate bonded by Pratt & Whitney Aircraft. Two thicknesses of each type of coating were produced. The thinner coatings were between 1 and 2 mils thick and the thicker coatings were between 5 and 6 mils thick. Bend testing of the plasma-arc sprayed coatings resulted in no spalling of the thin coating and in moderate spalling of the thick coating. Heavy spalling resulted from the bend testing of both of the specimens with aluminum-phosphate bonded coatings.

b. Boron and Silica

Coatings of an aluminum-phosphate bonded mixture of 40 per cent amorphous boron and 60 per cent silicon dioxide were applied in various thicknesses to aluminum strips. Four coatings were tested, with thicknesses of 4, 5, 5, and 6 mils respectively.

The total hemispherical emittance is shown in Figure 80 and in Table 29. The total hemispherical emittance level of this coating is slightly lower than had been anticipated. This is believed to be due to the large amount of silica present.

c. Molybdenum Diboride

A molybdenum diboride coating 2 mils thick was applied to each side of a molybdenum strip by the Linde Plasmarc process. The coating had a surface density of 0.041 gm / cm^2 .

The specimen was tested in the total hemispherical emittance rig. The total hemispherical emittance data is listed in Table 30 and plotted in Figure 81. During Run 1 the emittance varied from 0.52 at 300°F to 0.605 at 1450°F . After seventeen hours at 1450°F the emittance dropped to 0.59. During Runs 2A and 2B the emittance ranged from 0.50 at 650°F to 0.64 at 1950°F . During the final cooling cycle, Runs 2C and 3, the emittance dropped slightly, varying from 0.62 at 1850°F to 0.42 at 350°F . The seventeen-hour endurance run between Runs 2C and 3 had no appreciable effect on the emittance.

d. Tantalum Boride

A coating of tantalum boride 6 mils thick was applied to both sides of a molybdenum strip by the Linde Plasmarc process. The average surface density of the coating was 0.106 gm / cm^2 . The specimen was tested in the total hemispherical emittance rig over the temperature range 300°F to 1900°F .

The total hemispherical emittance data are shown in Figure 82 and Table 31. During the first heating cycle, the emittance increased from 0.48 at 500°F to 0.57 at 1450°F . After 15 minutes of exposure to 1450°F , the specimen was cooled and reheated to 1900°F and the emittance values obtained were in agreement with those obtained during initial heating. During final cooling, emittance values were obtained down to 1000°F and these were essentially the same as obtained previously.

e. Zirconium Boride

A zirconium boride (ZrB_2) coating 3 mils thick was applied by the Linde Plasmarc process to a molybdenum strip. Testing was conducted on the specimen in the total hemispherical emittance rig.

The total hemispherical emittance values are presented in Figure 83 and in Table 32.

2. Carbidesa. Acetylene Black in Xylol

Coated Stainless Steel - An AISI-310 stainless steel strip and tube were spray-painted with acetylene black suspended in xylol, supplied by Acheson Colloid Co. under the trade name of DAG EC1652. Over the temperature range of 200° to 1850°F the total hemispherical emittance of the strip varied from a minimum of 0.82 at 200°F to a maximum of 0.87 at 1300°F and decreased to a minimum of 0.85 at 1850°F. This variation was repeatable during the 23 hours of the test. The values are shown in Figure 84 and in Table 33.

The total hemispherical emittance of the tube specimen was measured over the temperature range from 300° to 1450°F. It was then maintained at 1450°F for 760 hours. The values of emittance obtained were slightly higher than those given by the coated stainless steel strip. The data is listed in Table 34 and plotted in Figure 84.

The total hemispherical emittance dropped gradually during the endurance test from 0.90 to 0.86 over a period of about 525 hours. A power failure at that time caused a slight flaking of the coating and the emittance at 1450°F dropped to 0.76. The emittance continued to drop during the next 120 hours, finally stabilizing at a value of 0.71.

Coated Aluminum - Aluminum strips were spray-painted with a suspension of acetylene black in xylol supplied by the Acheson Colloid Company under the trade designation DAG EC1652.

It was difficult to obtain a very thick coating and only two thicknesses of this material were tested: 1.2 and 2.6 mils. As may be seen in Figure 84 and in Table 35, there was not much

difference in the total emittance levels of the two samples, based on the initial heating cycles. When the samples were removed it was observed that a significant amount of flaking had taken place in both tests and that in both cases the flaking had been from one side of the aluminum strips with approximately 10 per cent of the light coating and approximately two-thirds of the medium coating being lost. Since there has been some difficulty in obtaining adherent coatings of this material, it is not being seriously considered as a radiator coating material.

Two additional coatings of acetylene black in xylol and one of carbon black were applied to aluminum fins at Pratt & Whitney Aircraft for thermal cycling and bend testing. The acetylene black coatings were approximately 2 and 6 mils thick and the carbon black coating was about 2 mils thick. No spalling resulted from bend testing any of the specimens.

b. Boron Carbide

Boron Carbide and Synar Binder - A mixture of 325-mesh boron carbide and a Synar binder was painted on both sides of a molybdenum strip, producing a coating 2.8 mils thick. Testing was conducted in the endurance rig. The specimen was heated to 1350°F and a 90-hour endurance test was conducted. Thermocouple failure terminated the test. After repairing the thermocouples the specimen was again heated to 1350°F and a 17-hour endurance test was conducted. The temperature was then increased to 1700°F.

The total hemispherical emittance data obtained before and after the endurance testing are shown in Figure 85 and in Table 36. The data taken below 800°F was corrected for the lack of end heaters, using Figure F-1.

As indicated in Figure 85, the total hemispherical emittance varied between 0.76 and 0.79 over the entire temperature range, and was repeatable within approximately three per cent. There was no appreciable change in the emittance during the 90 hours of endurance testing at 1350°F.

Another similarly prepared specimen was subjected to a thermal cycling test in the bell jar rig. The temperature of the specimen was cycled 500 times from 400°F to 1900°F by turning the heating current on for 15 seconds and off for 15 seconds. No deterioration of the coating was observed.

Plasma-Arc Sprayed Coating - A boron carbide (B_4C) coating 2 mils thick was applied to both sides of a molybdenum strip by the Linde Plasmarc process. This specimen had become creased in shipping. Since the area of the crease was suspected to be more susceptible to failure than the rest of the specimen, the specimen was mounted in the endurance rig in such a manner that the fold mark could be seen through the window of the vacuum chamber. Thus, it was possible to check the condition of the coating in the area of the crease during the test.

Total hemispherical emittance measurements were made up to 1350°F. The data in this temperature range were corrected for the error introduced by not using end heaters. The resulting emittance values, as shown in Figure 85, were relatively constant at about 0.77.

Endurance runs were made at 1350°F for 325 hours, at 1450°F for 120 hours, and at 1550°F for 53 hours. No significant change in the total hemispherical emittance was noted during this period. The specimen was then heated to 1650°F; however, because of failure of the thermocouples at the center location, an optical pyrometer was used to measure temperatures for the remainder of the test program. Since the spectral emittance of boron carbide was not known, it was not possible to accurately measure the temperatures with the optical pyrometer. The temperature of the specimen was raised to 2000°F in several steps. An approximation of total emittance at the higher temperatures (1650° to 2000°F) was made by assuming for all temperature conditions a constant spectral emittance value of 0.77 at 0.665 microns. The data for all of the runs appear in Table 37 and Figure 86. Inspection of the specimen upon removal from the rig after testing showed it to be very brittle.

Phosphate Bonded Coatings - Powder for these specimens was obtained from the Carborundum Company. Particle size analysis

of the boron carbide (B_4C) indicated that 79 per cent of the particle diameters were between 24 and 37 microns, and that 94 per cent were between 15 and 37 microns. The remaining 6 per cent were smaller than 15 microns. The coating was aluminum phosphate bonded onto columbium-1 per cent zirconium tubes. One of these specimens was tested in the total hemispherical emittance rig and another in the spectral normal emittance rig.

The coating of the first specimen was 6 mils thick, black with a glassy appearance, hard, and had a texture similar to that of 80-grit emery cloth. The coating-substrate bond strength was fair. Total hemispherical emittance was measured over the temperature range of 300°F to 1400°F. Results of testing appear in Table 38 and in Figure 85. The emittance level remained at about 0.85 from 300°F to 700°F, then increased to about 0.94 at 1200°F where it remained until the test was terminated at 1400°F. At 1200°F cracks were visible at each end of the test specimen but not in the center section where the emittance data are obtained. At 1400°F thermocouples numbers 2, 3 and 5 (shown in Figure 13) fell off. Before 1500°F was reached, thermocouple number 4 and the voltage leads fell off, requiring the test to be terminated. The emittance values based on Run 2 show an increase in emittance and throughout this run the temperature profile was not flat along the test section, thus introducing possible errors in the results. No change in the coating was observed when the specimen was removed from the rig.

X-ray diffraction analysis indicated B_4C to be the only phase present before testing, but Cb and B_4C were both present after testing. Spectrographic analysis showed B to be the only major element present both before coating and after testing.

It is noted that the coatings bonded to molybdenum had lower emittance levels than the coatings bonded to columbium -1 per cent zirconium over the same temperature range. The coated molybdenum specimens exhibited emittances lower than 0.80.

The second columbium - 1 per cent zirconium tube had a blue-black, 5-mil thick coating which was soft and poorly bonded to the substrate. The coating texture was similar to that of 80-grit emery cloth. The results of spectral emittance testing from 1.57 to 12.4 microns at 900°F are shown in Figure 87. When the tem-

perature was increased to 1200°F it was found that the power setting had to be continually changed to maintain the required temperature. The coating had a mottled appearance and seemed to be failing so the test was terminated. The only observable change in the coating upon completion of the test was that its color had changed to black.

c. Graphite Varnish

A wedge-shaped specimen of 2-mil thick AISI-310 stainless steel foil was spray-coated with a Pratt & Whitney Aircraft varnish mixture consisting of one part AMS 3132 varnish and two parts Dag 154, which is a 20 per cent colloidal graphite dispersion in isopropanol. A platinum-platinum 10 per cent rhodium thermocouple was spot-welded to the substrate in a short scratch 2 mils wide in the coating near the black-body hole. The specimen was tested in the spectral normal emittance rig.

Since the coating flaked off the substrate at approximately 1500°F, spectral emittance measurements, which are normally taken only in the region above this temperature, were not made. However, during this initial heating of the specimen, total hemispherical emittance measurements were made using the platinum-platinum 10 per cent rhodium thermocouple. These data are shown in Figure 88 and are tabulated in Table 39. A sharp drop in emittance at 1425°F occurred when deterioration of the coating was first observed.

d. Hafnium Carbide

A hafnium carbide (HfC) coating 3 mils thick was applied to both sides of a molybdenum strip by the Linde Plasmarc process and was tested in the total hemispherical emittance rig.

The total hemispherical emittance data are presented in Figure 89 and in Table 40. During the initial heating phase the total hemispherical emittance values ranged from 0.52 at 300°F to 0.63 at 1150°F. The emittance remained relatively constant at 0.63 in the temperature range from 1150°F to 1850°F; it then dropped in the range from 1850° to 2000°F until a value of 0.61 was reached. The temperature was maintained at 2000°F for several minutes and then lowered to 300°F. The emittance values during this cooling phase were consistently lower than

those during the heating phase at temperatures in the range from 2000° to 700°F, with the greatest discrepancy (about 10 per cent) occurring in the range of 1600° to 1300°F. Below 700°F there was no appreciable difference between the emittance values obtained during heating and those obtained during cooling.

e. Molybdenum Carbide

A specimen was prepared by applying a coating of molybdenum carbide (MoC) 2 mils thick onto two sides of a molybdenum strip by the Linde Plasmarc process. Total hemispherical emittance data were obtained in the total hemispherical emittance rig. These values are shown in Figure 90 and in Table 41.

In the temperature range from 200° to 1100°F, the emittance level increased from 0.42 to 0.51. Above 1100°F the emittance decreased until a value of 0.47 was attained at a temperature of 1450°F. The emittance increased again above 1450°F until a maximum value of 0.51 was reached at 1950°F. After a few minutes of operation above 2000°F, the emittance dropped to 0.49. When the specimen was cooled from 2050° to 1600°F, the emittance values were consistently lower than those previously recorded at the corresponding temperature. The maximum deviation was 8 per cent at 1600°F.

f. Silicon Carbide

Silicon carbide (SiC) obtained from the Buehler Corporation was aluminum-phosphate bonded to columbium - 1 per cent zirconium tubes. The resulting coatings were 4 to 5 mils thick, greyish, and soft. The coating-substrate bond strengths ranged from poor to fair. In all, five specimens were tested. Two were tested in the total hemispherical emittance rig, two in the spectral normal emittance rig, and one in the short term endurance rig. Since it is possible to measure both total hemispherical and spectral normal emittance in the spectral normal emittance rig, both of the measurements were made simultaneously for one of the specimens.

The silicon carbide powder used for the first specimen was classified by Buehler as 400 mesh. Particle size analysis indicated that 53 per cent of the particles were between 15 and 24 microns in diameter and 80 per cent were between 12 and 30

microns in diameter. Another 11 per cent of the particles were about 9 or 10 microns in diameter.

The 4-mil thick coating was light grey and had a matte texture similar to that of 320-grit emery cloth. The coating-substrate bond strength was poor. The total hemispherical emittance was measured between 300°F and 1400°F, and results are shown in Table 42 and in Figure 91. The total emittance increased from about 0.80 at 300°F to about 0.88 at 1400°F, with most of the increase occurring below 900°F. Between 1400°F and 1500°F the voltage leads fell off and testing was terminated. After testing, the coating had a blue-grey color, was brittle, and was separating from the substrate.

The powder used for coating the second specimen was classified by Buehler as 600 mesh. Particle size analysis indicated that 61 per cent of the particles were between 7 and 10 microns in diameter, and 85 per cent were between 5 and 12 microns in diameter. Another 11 per cent were divided between 4 microns and 15 microns in diameter.

The coating was 4 mils thick, blue-grey, and had a matte texture similar to that of 80-grit emery cloth. The coating-substrate bond strength was fair. Total hemispherical emittance was measured from 300°F to 1700°F and, as shown in Table 43 and in Figure 91, it remained fairly constant over the entire testing temperature range. At 300°F the emittance was about 0.91 and at 1700°F it was about 0.93. At 1800°F the voltage leads failed and the test was terminated. The scatter in data between 1500°F and 1700°F is about 3.5 per cent and this is within the accuracy of the apparatus. When removed from the rig, the coating was light grey, but no other changes were observed.

The third coating was bonded with aluminum phosphate obtained from the Monsanto Chemical Company under the trade name of Alkophos C. (The aluminum phosphate used for all other coatings was prepared at Pratt & Whitney Aircraft from aluminum oxide and phosphoric acid.) The coating was 5 mils thick, grey, and had a matte texture similar to that of 40-grit emery cloth. The coating-substrate bond strength was fair. Both total hemispherical and spectral normal emittances were measured in the spectral normal emittance rig.

Total hemispherical emittance was measured over the temperature range of 700°F to 1450°F. Emittance based on thermocouple temperatures was between 0.93 and 0.94, while that based on optical pyrometer temperatures was about 0.90. (See Table 44 and Figure 91).

Spectral normal emittance was measured over the wavelength range of 1.57 to 12.4 microns at 800°F and at 900°F. The specimen was held at 900°F for 17.6 hours and another set of data over the same wavelength range was taken at 900°F at the end of this interval. Finally, the temperature was increased and the spectral normal emittance was measured over the wavelength range of 1.21 to 13.6 microns at 1300°F and at 1450°F.

Figure 92 shows results from these tests along with those determined by H. Blau, et al, Arthur D. Little, Inc., in "Infrared Spectral Emittance Properties of Solid Materials, Final Report under Contract AF19(604)-2433," October 1960. Blau's data was obtained from specimens heated in air.

He describes his method as follows:

Radiation from the heated specimen was directly compared to radiation from a black body at the same temperature. Specimens were embedded in an accurately machined cavity in the surface of a hollow silicon carbide heater element and heated by conduction. A hole in the heater wall provided the source of black body radiation.

It may be seen from Figure 92 that agreement is good. The only change in the coating observed after testing was a separation from the substrate.

The coating for the fourth specimen was made from the same silicon carbide powder used for specimen number three and was made at the same time as specimens numbers two and five.

The resulting coating was 4 mils thick, grey, and had a matte texture similar to that of 80-grit emery cloth. The coating-substrate bond strength was poor. The spectral emittance of the coating was measured between 1.57 and 12.4 microns at 900°F and between 1.01 and 13.0 microns at 1450°F. The results from

this test are in very good agreement with those of the preceding spectral normal emittance test (Figure 92). No visible changes of the coating were observed after testing.

The fifth specimen was prepared at the same time as the third and fourth specimens. The 5-mil thick coating was light grey and had a matte texture similar to that of 320-grit emery cloth. The coating-substrate bond strength was poor. Table 45 and Figure 91 show the total emittance of the coating as the temperature was increased from 300°F to 1450°F. Over this temperature range the total hemispherical emittance of the specimen decreased from about 0.94 to about 0.91 where it remained throughout the 300-hour endurance test (see Table 46 and Figure 93). The visual characteristics of the coating were unchanged by testing.

All of the data presented in this section indicate that the repeatability of the emittance values from one coating to the next, using the same silicon carbide, falls within the accuracy of the apparatus. In general, it appears that the emittance of the aluminum-phosphate bonded Buehler 600-mesh silicon carbide tested lies between 0.90 and 0.93 over the temperature range of 300°F to 1600°F.

X-ray diffraction analysis of specimens numbers one and five before and after testing showed SiC to be the only detectable phase present. Spectrographic analysis of the powders used in both of these specimens indicated that Si was the only major constituent present although Fe and Al were present as semi-major constituents. After testing, both Si and Al were present as the major constituents, but Fe was a minor constituent.

g. Silicon Carbide and Silicon Dioxide

Coatings containing 40 per cent silicon carbide and 60 per cent silicon dioxide were aluminum-phosphate bonded onto AISI-310 stainless steel tubes, aluminum strips, and onto a SNAP-8 test section.

Total hemispherical emittance measurements for the first coated stainless steel tube were made in the spectral normal emittance rig over the temperature range of 500°F to 1300°F. The data appear in Figure 94 and in Table 47. During the initial heating of the specimen from 500° to 900°F (Run 1), the total hemispherical emittance was relatively constant at 0.88. Close agreement was

obtained during the second run and the temperature was increased to 1300°F. The emittance level dropped slightly at the higher temperatures. After the second run, the specimen was cooled to room temperature and maintained in vacuum over night. When the specimen was subsequently reheated to 1450°F for endurance testing, the coating flaked off the substrate.

A second AISI-310 stainless steel tube was coated in an attempt to endurance-test a coated stainless steel sample, but results were similar to those of the first specimen. The total hemispherical emittance was relatively constant at 0.88, but the coating again flaked off as a result of thermal cycling.

Coatings were applied to three aluminum strips. There were variations in the appearance of the coatings although the variations in thickness were not found to be excessive. The coatings were so hygroscopic, however, that when they were left in a fairly dry room (relative humidity lower than 50 per cent) the coatings became muddy. This problem has not been encountered at any other time in the program. It is believed that the difficulty resulted from an improper pH of the phosphate solution. A second set of coated aluminum strips was prepared.

The coatings on the first set of aluminum strips had thicknesses of 3.5, 4, and 4.5 mils. Total hemispherical emittance data for the first two of these were similar to those for the coated stainless steel samples. The total hemispherical emittance of the third sample was somewhat lower. The lower emittance may have been a consequence of excess moisture in the coating. Heating would drive off the excess moisture and the resulting porous coating would provide a poor heat path between the substrate and the surface.

The coatings on the second set of aluminum strips were 2.5, 5.5, and 9 mils thick. The total hemispherical emittance data are shown in Figure 94 and in Table 48.

The coated SNAP-8 tube-half fin radiator segment was instrumented and installed in the long term endurance rig for testing. The specimen fin root temperature was slowly brought up to 700°F, at which point the 10,000 hour endurance test was begun. The appearance of the speci-

men before testing is shown in Figure 95. At the end of the report period the test section had accumulated 8600 hours of endurance testing. No changes in the coating have been observed. The appearance of the test section after 8683 hours is shown in Figure 96. The thermal history across the center of the test section is shown in Figure 97.

Investigation to date indicates that this material has a total hemispherical emittance of 0.8 or higher up to 1200°F. The total hemispherical emittance of most of the samples tested was higher than 0.86.

Although no difficulty was encountered in coating aluminum, considerable difficulty was encountered in maintaining a good bond to stainless steel. The results of coating aluminum and stainless steel with a mixture of 40 per cent nickel-chrome spinel and 60 per cent silicon dioxide were similar. It is believed that the difficulties encountered may be attributed to the fact that the coefficient of expansion of silicon dioxide is much closer to that of aluminum than it is to that of stainless steel.

h. Tantalum Carbide

A 3-mil thick coating of tantalum carbide (TaC) was applied to a molybdenum strip by the Linde Plasmarc process. The results of measuring the total hemispherical emittance of this specimen are shown in Figure 98 and in Table 49.

The emittance varied from 0.45 at 250°F to 0.59 at 2000°F during the first heating and cooling cycle and during the second heating cycle. While cooling the specimen after reaching the maximum temperature of 2050°F, the emittance remained unchanged down to a temperature of 1200°F. Slightly lower emittance values were noted as the specimen was cooled below 1200°F. This change varied from one per cent at 1100°F to five per cent at 500°F.

i. Titanium Carbide

A coating of titanium carbide 2.5 mils thick was applied to both sides of a molybdenum strip by the Linde Plasmarc process. The surface density of the coating was 0.032 gm /cm². The specimen was tested in the total hemispherical emittance rig over the temperature range of 250°F to 1950°F.

The total emittance data is shown in Figure 99 and in Table 50. Run 1 from 400°F to 1450°F was followed by a seventeen-hour endurance run at 1450°F. Run 2, which ran from 1450°F to 650°F and then back up to 1600°F, was followed by an eighteen-hour endurance run at 950°F. Run 3 ran from 1300°F to 1950°F and then back down to 200°F, and was followed by sixty-four hours at room temperature. Run 4 ran from 250°F to 450°F. The total emittance of this specimen varied from 0.43 at 250°F to 0.62 at 1800°F.

j. Vanadium Carbide

A coating of vanadium carbide 3 mils thick was applied to both sides of a molybdenum strip by the Linde Plasmarc process. The average surface density of the specimen was 0.026 gm /cm². The specimen was tested in the total hemispherical emittance rig over the temperature range 250°F to 2000°F.

The total hemispherical emittance data is shown in Figure 100 and Table 51. The total hemispherical emittance during the initial heating cycle (Run 1) varied from 0.51 at 250°F to 0.57 at 1450°F. Subsequent running showed agreement with Run 1 between 800°F and 1450°F, but a drop in emittance at temperatures below 800°F. Above 1450°F the emittance increased with temperature up to a maximum of 0.61 at 2000°F.

3. Fluorides - Calcium Fluoride

An AISI-310 stainless steel strip 5 mils thick was coated with a dispersion of calcium fluoride supplied by the Acheson Colloid Company under the trade designation DAG EC 1789. The specimen was tested in the total hemispherical emittance rig.

The total hemispherical emittance decreased approximately linearly during the initial heating cycle from 0.68 at 300° F to 0.47 at 1000° F. Heating the specimen above 1000° F apparently caused some change in the coating which resulted in a sharp reversal in the slope of the emittance curve (see Table 52 and Figure 101). The emittance increased to 0.59 at 1450° F. Maintaining the temperature at 1450° F for 20 hours brought the emittance up to 0.60. The data taken during the final cooling cycle indicated that the change which took place in the coating was a permanent one. Visual inspection of the specimen after the vacuum chamber was opened showed that the color of the coating had changed from white to dark grey.

4. Nitrides - Boron Nitride in Synar

Boron nitride powder (BN) in a Synar binder, colloidal silica (SiO_2), was spray-painted on both sides of a tantalum strip producing a coating with an average thickness of 3 mils.

The specimen was tested in the total hemispherical emittance rig over the temperature range of 300°F to 1200°F . The total hemispherical emittance, as shown in Table 53 and in Figure 102, varied from 0.82 at 300°F to 0.682 at 1200°F . During an attempt to maintain the specimen at 1200°F , the specimen pulled out of the lower end clamp. However, it was possible to obtain one data point at a lower temperature (600°F) by passing current through the bottom end-heater connection and the top main power supply connection. Since there was no appreciable change in the emittance and since the level of emittance was relatively low, the test was terminated.

5. Single Oxides

a. Aluminum Oxide

Three different aluminum oxide coatings were applied to AISI-310 stainless steel strips to determine the effects of variations in the coating process as well as minor variations in the coating material.

First Specimen - The first strip was plasma-arc sprayed with aluminum oxide powder supplied by the Plasmadyne Corporation. Plasmadyne spraying equipment was used. The coating had an average thickness of 1.3 mils.

During the initial heating cycle, Run 1, the total hemispherical emittance varied from 0.69 at 300°F to 0.60 at 1000°F . The specimen was maintained at 1100°F for 17 hours with no resulting change in the total hemispherical emittance. The temperature was increased to 1450°F , Run 2, and the total hemispherical emittance varied between 0.61 and 0.63 over the temperature range 1100°F to 1450°F . Maintaining the specimen at 1450°F for 48 hours produced no change in the total hemispherical emittance. The specimen was then cooled, Run 3, and the total hemispherical emittance values obtained were slightly higher than those obtained during Run 1.

The data is shown in Table 54 and in Figure 103.

Second Specimen - The second strip was plasma-arc sprayed with a 2-mil thick coating of Metco 101 aluminum oxide powder. Plasmadyne equipment was used.

The total hemispherical emittance values for this specimen are shown in Table 55 and Figure 103. During the initial heating cycle Run 1, the total hemispherical emittance varied from 0.73 at 300°F to 0.67 at 1450°F, with no significant change in the emittance values resulting from maintaining the specimen at 900°F for 17 hours. However, maintaining the specimen at 1450°F for 26 hours caused an 11 per cent increase in the total hemispherical emittance. This increase was noted over the entire temperature range as the specimen was cooled, Run 3.

Third Specimen - The third strip was flame-sprayed with a 2.1-mil thick coating of Metco 101 aluminum oxide powder. A Metco oxyacetylene flame-spraying gun was used. The total hemispherical emittance data are shown in Table 56 and in Figure 103.

This specimen had emittance characteristics similar to those of the second specimen as it was heated to 1450°F, maintained at this temperature, and then cooled to 650°F. The specimen was then heated to 1800°F, Run 2B, and the emittance values up to 1450°F agreed with those of Run 2A. Cooling the specimen to 350°F showed very little change.

General Remarks - Figure 103 shows the data obtained from the three aluminum oxide coatings. The second and third specimens which were coated with material from the same source had similar total hemispherical emittance values. Since the coatings were of approximately the same thickness, it appears that the difference in the two methods of applying the coating material does not affect the radiation characteristics of the resultant coatings. Considerably different results might occur with coating materials other than oxides, or if an oxygen-deficient oxyacetylene flame were used and carbides were formed.

Comparing the first and second specimens (i. e., the two specimens which used the same method of coating but which used material from different sources), indicates differences in emittance characteristics. The difference in total hemispherical emittance levels could probably be attributed to the differing coating

thicknesses. However, comparing the data from the three specimens shows that no change in the total hemispherical emittance of the first specimen occurred as a result of a 48-hour endurance run at 1450°F, but a considerable change in the total hemispherical emittance (about 10 per cent) of both of the other specimens occurred as a result of enduring for approximately half that time.

Thermal Cycling and Bend Testing - Two additional coatings of aluminum oxide were plasma-arc sprayed onto aluminum substrates for thermal cycling and bend testing. One of these coatings was between 1 and 2 mils thick and the other was between 5 and 6 mils thick. Although no spalling resulted from bend testing the specimen with the thin coating, bending the specimen with the heavy coating resulted in considerable spalling.

b. Ceric Oxide

Ceric oxide was plasma-arc sprayed onto an AISI-310 stainless steel strip by Metco, Inc., and aluminum-phosphate bonded to columbium - 1 per cent zirconium by Pratt & Whitney Aircraft.

The coating on the stainless steel strip was 3.3 mils thick. Total hemispherical emittance was measured over the temperature range of 300°F to 1800°F.

Data appear in Figure 104 and in Table 57. When the sample was removed from the rig it was noted that the color of the coating had changed from light brown to purple-grey.

The ceric oxide used for coating the columbium - 1 per cent zirconium substrate was supplied by the Varlacoid Chemical Company. The coating was 2 mils thick.

Total hemispherical emittance was measured from 300°F to 1700°F. As shown in Table 58, the total hemispherical emittance varied from 0.75 at 300°F to 0.65 at 1300°F and then increased. Beyond 1300°F, visual observations indicated fluctuations in the brightness of the surface. When the specimen was removed from the test rig it was noted that the color had changed from white to blue mottled with white. The low emittance level of this coating at all temperatures did not warrant further testing or material analysis.

Two additional coatings of ceric oxide were aluminum-phosphate bonded to aluminum fins for thermal cycling and bend testing. These coatings were approximately 2 and 6 mils thick respectively. Bend testing resulted in heavy spalling of both coatings.

c. Chromic Oxide

Coatings of chromic oxide were plasma-arc sprayed onto substrates of molybdenum, columbium, and columbium - 1 per cent zirconium. Additional coatings were applied by the Rokide process onto AISI-310 stainless steel and onto columbium. One coating was aluminum-phosphate bonded onto columbium - 1 per cent zirconium.

Plasma-Arc Sprayed Coating on Molybdenum - A coating of chromic oxide 2 mils thick was applied to both sides of a molybdenum strip by the Linde Plasmarc process. The specimen was tested in the total hemispherical emittance rig over the temperature range of 300° to 1800°F.

The total hemispherical emittance data are shown in Figure 105a and in Table 5). The emittance ranged from 0.71 at 300°F to 0.81 at 1400°F during Run 1, the initial heating cycle. A seventeen-hour endurance run at the latter temperature produced a drop in total hemispherical emittance to 0.79. Testing over the temperature range 1100°F to 1400°F indicated lower values than obtained previously. As the temperature was raised above 1400°F, the emittance increased rapidly to a value of 0.865 at 1660°F. The temperature was then lowered to 1360°F where the emittance was considerably higher than the previous reading at this temperature. A seventeen-hour endurance run at this temperature increased the emittance slightly. Raising the temperature back to 1670°F gave emittance values essentially the same as before. The emittance continued to increase with temperature, reaching 0.9 at about 1800°F. Lowering the temperature again to about 1350°F gave an emittance value consistent with those after the last previous endurance run. The emittance during the remainder of the final cooling cycle, Run 3B, approximated that obtained in Run 1.

The specimen was then compared with one which had not been tested. Examination by x-ray diffraction indicated that the coatings in both cases were chromic oxide. For lack of other evidence at this time it is concluded that the erratic behavior of the test specimen was caused by a series of temporary changes in the composition of the coating. Because of this erratic behavior, no attempt has been made to fit a curve to the data points in Figure 105a.

Plasma-Arc Sprayed Coating on Columbium - A coating of chromic oxide 3 mils thick was applied to a columbium tube by the Linde Plasmarc process and then tested in the endurance rig at 1450°F.

The initial heating and final cooling cycles are shown in Figure 105a and the endurance test results in Figure 106. All of the data appears in Table 60. Emittance was measured from 800°F to 1450°F and then an endurance run of about 900 hours was made at the latter temperature. Emittance was measured as the specimen was cooled from 1450°F to 700°F.

Variations in emittance at a constant temperature occurred during the endurance run, similar to those observed in the earlier test of a chromic oxide coating on a molybdenum strip. The emittance at the beginning of the endurance run was 0.84, but decreased to 0.79 during the next fifty hours. It then rose slowly to a reading of 0.83 two hundred hours later. For the remaining 640 hours of the test the emittance stayed relatively constant at 0.83 to 0.84. The emittance values obtained during the heating and cooling cycles were in close agreement with those from the earlier test.

The data obtained in this test support the theory that the erratic behavior in the early part of both chromic oxide tests was caused by temporary changes in the composition of the coating.

Rokide C Coatings - A typical analysis of Rokide C is as follows: 82.94 per cent Cr_2O_3 , 8.39 per cent SiO_2 , 3.16 per cent Al_2O_3 , 2.96 per cent MgO , 1.28 per cent CaO , and 1.22 per cent ($\text{Fe}_2\text{O}_3 + \text{NaO}_2 + \text{TiO}_2$). Coatings were applied to an AISI-310 stainless steel tube and to columbium substrates.

Total hemispherical emittance of the coated stainless steel specimen was measured over the temperature range of 300°F to 1450°F. During the initial heating cycle (Run 1), the total hemispherical emittance varied from 0.82 at 300°F to 0.84 at 1300°F as shown in Figure 105a and in Table 61. Subsequent testing (Runs 2A and 2B) resulted in a slight upward shift (about 1 per cent) in the total emittance. Although this increase is small and may be attributable to changes in indicated thermocouple output, it is consistent with the emittance calculated using optical pyrometer temperature measurements. After

establishing the level of emittance for this coating, the sample was heated to 1450°F and maintained at this temperature for 330 hours. The emittance increased from 0.85 to 0.86 during the first 110 hours and remained at 0.86 for the remainder of the test, as shown in Figure 106.

The coatings on columbium substrates were 3 mils thick, blue-grey, extremely hard, and had a fine grit texture. They were very well bonded to the substrate. Visual inspection of the specimens after testing showed that the coatings had changed from blue-grey to green.

Total hemispherical emittance was measured over the temperature range of 400°F to 2200°F. During the heating cycle, the total emittance increased from 0.72 at 400°F to 0.8 at 1000°F, remained constant to about 1600°F, and then decreased to about 0.7 at 2200°F. As the specimen was cooled, the emittance remained low, varying from 0.70 at 2200°F to 0.65 at 1500°F, indicating that a change in the coating had taken place. As shown in Figure 105a and in Table 62, the temperature indicated by the optical pyrometer and by the platinum-platinum 10 per cent rhodium thermocouple agreed very well at 1600°F and at 1800°F, and then diverged. From this point on, it is assumed that the thermocouple data are unreliable. The emittance data, however, for the cooling portion of Run 1 and for Run 2, based on temperatures obtained with the thermocouple, are included in Figure 106 to show that the emittance dropped over the entire temperature range. Any changes in the coating that may have taken place during this test were not found by x-ray diffraction. The x-ray patterns showed the principal phase present to be Cr_2O_3 before and after the test.

Spectral normal emittance was measured from 1.5 to 13.5 microns at 900°F, from 1 to 14 microns at 1450°F and from 1 to 14 microns at 2000°F. The data are shown in Figure 107. The emittances indicated are higher than had been anticipated from the total hemispherical emittance values discussed above. It is suspected that this difference is due to the quality of the black body being significantly less than unity. Subsequently, the black-body hole configuration was changed from a rectangular slot (0.028 in x 0.085 in) to two 0.023-inch diameter holes, thus reducing the size of the black body to one-third of its original size.

Aluminum-Phosphate Bonded Coating - Chromic oxide supplied by the Ceramic Color and Chemical Manufacturing Company was aluminum-phosphate bonded to columbium - 1 per cent zirconium. The 3-mil thick coating was green and had a smooth texture similar to that of 320 grit emery cloth. It was moderately hard and well bonded to the substrate. Total hemispherical emittance varied from 0.80 at 500°F to 0.73 at 1400°F. Beyond this point the behavior of the specimen was erratic and the data shown in Table 63 for this specimen is questionable at temperatures above 1400°F.

Plasma-Arc Sprayed Coating on Columbium - 1 Per Cent Zirconium - Chromic oxide (Cr_2O_3) obtained from the Plasma-dyne Corporation was plasma-arc sprayed onto a columbium - 1 per cent zirconium substrate. The resulting coating was dark grey-green, 4 mils thick, extremely hard, and had a good coating-substrate bond strength. The coating had a matte texture similar to that of 80 grit emery cloth and was tested in the total hemispherical emittance rig over the temperature range of 300°F to 2100°F. As may be seen in Table 64 and in Figure 105b, during heating the total emittance of the coating slowly decreased from about 0.82 at 500°F to 0.70 at 2100°F. Up to 1200°F, emittance values closely approximated those of the aluminum-phosphate bonded chromic oxide. At higher temperatures these two curves diverge slightly with the plasma-arc sprayed coating having the higher emittance. During the test, the color of the coating changed to a dark greenish-blue except around the thermocouple wires where it was a bright green. The coating had become brittle, but the bond strength remained good. The texture of the coating after testing was about equivalent to that of 320-grit emery cloth. Analysis by x-ray diffraction before and after testing indicated Cr_2O_3 to be the only detectable phase present.

The data indicate that the emittance of chromic oxide coatings is affected by the method of application, purity of the raw material, and possibly by the substrate to which it is applied.

d. Cobalt Oxide

The Fisher Scientific Company supplied the cobalt oxide (CoO) which was plasma-arc sprayed onto a columbium - 1 per cent zirconium substrate to produce a 4-mil thick coating. The observable characteristics of this coating before testing were recorded as matte blue-black, hard, and with a texture similar to that of 320-grit emery cloth. The coating-substrate bond strength was good. The results of total hemispherical emittance

testing from 300°F to 2200°F are shown in Table 65 and in Figure 108. The total emittance of this coating during heating was about 0.88 from 300°F to 1100°F and then decreased to about 0.79 at 1500°F. Above 1500°F the total emittance increased until a value of 0.90 was achieved at 2200°F. During cooling, the emittance data substantiated the heating values from 2150° to 1550°F, but then continued decreasing. From this data it appears that the coating underwent two changes during the test, one at about 1100°F, and a second at about 1500°F. When the specimen was removed from the rig, it could be seen that the coating had separated from the substrate at the ends of the specimen, although it remained well bonded in the center portion where data are taken.

It is not believed that the last change in the slope of the emittance curve resulted from the separation of the coating from the substrate. A separation of the coating from the substrate always causes the substrate temperature to increase. If the coating separates from the substrate but remains intact, the decreased thermal conductivity across the coating-substrate gap results in a substrate temperature increase; if the coating does not remain intact but leaves a portion of the substrate exposed, the markedly lower emittance of the substrate will also result in a substrate temperature increase. Emittance is calculated by the use of the equation found on Page 27. It follows that the increase in substrate temperature which results from coating-substrate separation is reflected as a decrease in the calculated emittance value instead of an increase such as was recorded.

After testing, the only observable changes in the characteristics of the coating were the coating-substrate separation and a change in color to a brownish grey. X-ray diffraction analysis before and after testing detected CoO as the only phase present.

e. Manganese Oxide

The manganese oxide (Mn_2O_3) used for this coating was obtained from A. D. McKay, Incorporated. A 3-mil thick coating was plasma-arc sprayed onto a columbium - 1 per cent zirconium substrate. The coating was black, hard, and had a matte texture similar to that of 80-grit emery cloth. The coating-substrate bond strength was good. Total hemispherical emittance was measured over the temperature range of 300°F to 2150°F. Table 66 and Figure 109 show that the total emittance increased from about 0.75 at less than 700°F to about 0.88 at 1900°F, and then decreased to about 0.85 at 2000°F. At 2000°F the temperature was increasing rapidly at a constant power setting, indicating a rapid reduction in emittance. At 2100°F and at 2150°F, the temperature was decreasing rapidly with a constant power setting, requiring a steadily increasing power setting to maintain the temperature long enough to obtain emittance data. At these temperatures the emittance values were increasing. As the specimen was cooled the emittance values remained close to 1.0.

When the chamber was opened it was discovered that the coating had volatilized and that a metallic coating had been deposited on the instrument flange and on other parts of the rig. The observed rapid decrease in temperature at 2100°F can probably be attributed to the progressively increasing electrical leakage between thermocouple wires resulting from deposition of metallic material. The heat of sublimation of the coating may have been an additional contributing factor.

When the specimen was removed from the rig, the remaining coating was glossy black, extremely hard, and had a texture similar to that of 320-grit emery cloth. The coating-substrate bond strength was extremely good.

The coating inside the chamber had shorted the thermocouple and voltage terminals to ground, and values of emittance recorded during cooling are not valid. These values therefore are not reported.

f. Nickel Oxide

The nickel oxide (NiO) used for this coating was the black type supplied by the Varlacoid Chemical Company. A 3-mil thick coating was plasma-arc sprayed onto a columbium - 1 per cent zirconium substrate. The coating was dark grey, hard, had a good coating-substrate bond strength, and had a matte texture similar to that of 320-grit emery cloth. The total hemispherical emittance values between 300°F and 2100°F are shown in Table 67 and in Figure 110. The total emittance slowly increased from about 0.45 at 300°F to about 0.85 at 1500°F. It remained at this level up to 1800°F and then decreased to about 0.82 at 2100°F. During cooling, the total emittance remained at about 0.80 down to 1550°F, indicating that a change in the coating had occurred. When the specimen was cooled below 1550°F, it could be seen that the coating had separated from the substrate, and no further emittance data were taken. The optical pyrometer temperatures appear to be erratic, but the platinum-platinum 10 per cent rhodium and the chromel-alumel thermocouples were in good agreement. Emittance values based on platinum-platinum 10 per cent rhodium thermocouple temperatures are therefore the only ones reported. The erratic optical pyrometer readings are believed to have been caused by a partial blocking of the pyrometer lens by one of the window shutters.

After testing, the only changes in the coating observed were an increased brittleness and the separation of the coating from the substrate.

g. Silicon Dioxide

A 5-mil thick coating of silicon dioxide (SiO₂) supplied by the Ottawa Silica Company was aluminum-phosphate bonded to a columbium - 1 per cent zirconium substrate. Analysis of the powder supplied indicated a particle size distribution with 40 per cent between 15 and 24 microns in diameter and with 79 per cent between 9 and 37 microns in diameter. The coating was white, soft, and had a matte texture similar to 320-grit emery cloth.

The coating-substrate bond strength was poor. Because the emittance at high temperature drops below values useful in space applications, measurements were made only over the temperature range of 300°F to 1000°F. Test results are shown in Table 68 and Figure 111. The emittance decreased from about 0.87 at 300°F to about 0.70 at 1000°F. Emittances during cooling were several per cent lower than during heating, indicating that a change in the coating had occurred.

Although the coating was still white after testing, it was noticed that the color was slightly darker than originally. No other changes were visible. X-ray diffraction analysis before and after testing indicated α SiO₂ to be the only detectable phase present. Spectrographic analysis indicated Si and Al to be the major constituents present before and after testing.

h. Stannic Oxide

A 4-mil thick coating of stannic oxide (SnO₂) supplied by A. D. MacKay, Incorporated, was aluminum-phosphate bonded to a columbium - 1 per cent zirconium substrate. Analysis of the stannic oxide supplied indicated a particle size distribution with 83 per cent less than 10 microns in diameter and 53 per cent less than 3 microns in diameter. The coating was white, soft, and had a matte texture similar to that of 320-grit emery cloth. The coating-substrate bond strength was fair. Because the emittance at high temperature drops below values useful in space applications, measurements were made only over the temperature range of 300°F to 1000°F. Results from these measurements appear in Table 69 and in Figure 112. The emittance values recorded during cooling were lower than those recorded during heating, indicating that a change in the coating had occurred. Visual inspection of the specimen after testing did not reveal the change and x-ray diffraction analysis indicated both before and after testing that SnO₂ was the only detectable phase. Spectrographic analysis indicated that Sn and Al were the major constituents present before and after testing.

i. Titania

Titanium oxide coatings were applied to AISI-310 stainless steel, columbium, and aluminum samples by plasma-arc spraying and to columbium - 1 per cent zirconium by aluminum-phosphate bonding. The powders used for these coatings were Metco XP-1114 and Dupont pure rutile R-510-P.

Particle size analysis of the Metco powder indicated that 16 per cent of the particles had diameters of 59 microns or larger. An additional 29 per cent had diameters about 47 microns in diameter. Seventy-nine per cent had diameters of 19 microns or larger, and 12 per cent had diameters between 12 and 19 microns.

Coated AISI-310 Stainless Steel - An AISI-310 stainless steel strip and an AISI-310 stainless steel tube were plasma-arc sprayed by the Metco process with Metco XP-1114 titanium oxide. The strip specimen was tested in the total hemispherical emittance rig and the tubular specimen was tested in the endurance rig.

The strip specimen had a coating 2.5 mils thick on both sides of the sample. Figure 113a and Table 70 show the total hemispherical emittance values. After maintaining the specimen temperature in the 900°F range over one weekend, a decrease in emittance was observed. Investigation revealed that the sample had failed at the top power connection. After repairing this connection it was heated to 1350°F and the emittance values were found to be consistent with the earlier values over the entire temperature range. Failure of the thermocouple and voltage leads necessitated another shutdown of the rig. The data obtained after repairing the instrumentation were again consistent with the previous data. At 1350°F, a second failure of the voltage leads occurred; however, the testing was continued to 1866°F. To determine the emittance above 1350°F, an estimated value of specimen resistivity that was obtained from an extrapolation of the temperature-versus-resistivity curve was used.

The coating on the tubular specimen had a surface density of 0.014 gm/cm². The specimen was tested in the endurance rig at a nominal temperature of 1450°F for more than 350 hours. The emittance data obtained during the initial heating and final

cooling cycles are shown in Figure 113a. As shown in Table 71 and Figure 115, the total hemispherical emittance dropped from 0.87 to 0.84 during the first twenty-four hours and then dropped gradually to 0.82 during the remainder of the test.

After the specimen had cooled but before the rig was disassembled, a cracking sound was heard from within the chamber. When the chamber was opened it was found that the coating had flaked off the specimen.

Coated Aluminum - Three aluminum strips were coated with Metco XP-1114 titanium oxide powder. The coatings were 1.0, 3.5, and 4.5 mils thick. All of the coatings were applied by plasma-arc spraying, the first two by Metco, Inc., and the last by Pratt & Whitney Aircraft.

Testing of the specimen with the 1.0-mil thick coating showed the total hemispherical emittance to vary from 0.75 at 300°F to 0.83 at 1450°F. In two successive runs no difference in emittance level was noted. The data are tabulated in Table 72 and presented graphically in Figure 113b.

On the first two runs, the total hemispherical emittance of the 3.5-mil thick coating was somewhat higher than that of the 1.0-mil thick coating and was relatively constant at approximately 0.84 from 400°F to 900°F. On the third run, the emittance decreased to the same level as that of the thinner coating. These data are contained in Table 72 and Figure 113b.

The third coated aluminum strip had a slightly higher emittance level than the other two. Values are shown in Figure 113b and in Table 72. Since the powder was from a different batch, and since different equipment was used for applying the coating, it is not known whether the slightly higher emittance level was the result of the increased coating thickness or a result of the different coating process.

Coated Columbium - Two columbium tubes were plasma-arc sprayed with Metco, Inc. titanium dioxide (XP-1114) by Pratt & Whitney Aircraft. The coatings were blue-black, hard, and were fairly well bonded to the substrates. One coating was 3 mils thick and was tested in the total hemispherical emittance rig, and the other was 2.5 mils thick and was tested in the spectral normal emittance rig.

The 3-mil thick coating was tested at temperatures ranging from 400°F to 2250°F. The emittance values (see Figure 113a and Table 73) varied from 0.75 at 400°F to 0.83 at 1400°F during the first two test runs. At higher temperatures the emittance decreased and continued to decrease with each successive run. A low value of 0.68 was recorded at 2250°F during the final run. Visible characteristics of the coating did not change during testing.

Spectral normal emittance of the 2.5-mil thick coating was measured from 1.5 to 13.5 microns at 900°F, from 1 to 13.5 microns at 1450°F, and from 0.9 to 13.5 microns at a nominal temperature of 2000°F. The temperature increased from 1980°F to 2125°F while power was held constant during the final test, which indicates a decrease in total emittance. The spectral normal emittance data presented in Figure 116 show evidence of this change. The 2000°F test was re-run with little change in temperature, indicating that no further large changes in emittance were taking place. Spectral emittances were determined to be essentially the same at 900°F and 1450°F but were found to decrease drastically as the specimen was heated to 2000°F. This decrease in emittance is consistent with the similar decrease observed for the total hemispherical emittance specimen. The visible characteristics of the coating did not change as a result of testing.

Analysis of the coatings before and after testing by x-ray diffraction showed Ti_2O_3 to be the principal phase present. Spectrographic analysis showed no change in the elements present.

Coated Columbium - 1 Per Cent Zirconium - Columbium-1 per cent zirconium tubes were coated with Metco XP-1114 titanium oxide powder and with Dupont rutile powder by aluminum-phosphate bonding.

The Metco coating was 5 mils thick, white, soft, and had a matte texture similar to that of 80-grit emery cloth. The coating-substrate bond strength was fair. It was also observed that the area around the black-body holes was a shade lighter than the rest of the specimen, which may be attributed to a greater coating thickness in that region. This white specimen was also tested between 300°F and 1000°F.

As shown in Table 74 and in Figure 114, the total hemispherical emittance curve is typical for a white coating. Total hemispherical emittance decreased with increasing temperature. The total

emittance decreased from about 0.77 at 300°F to about 0.64 at 1000°F during heating, and essentially the same values were obtained during cooling. When the specimen was removed from the rig it was noticed that an area about one-half inch in diameter around the black-body holes had changed to a light grey color while the rest of the coating was still white. The coating was slightly harder after testing and still had a fair coating-substrate bond strength. The texture was unchanged. X-ray diffraction analysis before and after testing indicated rutile TiO_2 to be the only detectable phase present. Ti was found to be the only element present in large quantities both before coating and after testing.

The Dupont coatings were 1 mil thick, white, fairly hard, and brittle with a matte texture similar to that of 320-grit emery cloth, although there were small lumps distributed throughout. The coating-substrate bond strengths were fair.

One specimen was tested in the total hemispherical emittance rig and another in the spectral normal emittance rig. Since this was a white coating and its anticipated usefulness as a spacecraft radiator coating would be at temperatures less than 1000°F, thermal emittance values were obtained only between 300°F and 1000°F. Table 75 and Figure 114 show the emittance level of this coated tube. The emittance was about 0.82 over the temperature range. The electric current values obtained for the 700°F point appear to be in error and cast doubt on the validity of the corresponding emittance value.

It is believed that the 1-mil thick coating was thick enough so as not to be transparent to the longer wavelengths which constitute the major part of low temperature black-body energy. The emittance values were found to be similar to those of previously tested plasma-arc sprayed titania although the plasma-arc sprayed coating was dark rather than white. Had the coating been partially transparent, emittance from the substrate would have occurred and, unless the substrate had oxidized, would have resulted in somewhat lower emittance values. X-ray diffraction, however, confirmed that TiO_2 was the only oxide present and it may therefore be concluded that the coating had adequate thickness. After testing, the coating was greyish and there were dark areas around the thermocouples, which possibly resulted from a loss of the coating in this region when the

thermocouples were tack welded. X-ray diffraction analysis before and after testing indicated that rutile TiO_2 was the only detectable phase present. Spectrographic analysis indicated that Ti was the principal element present after testing.

Spectral normal emittance of the second specimen was measured over the wavelength range of 1.45 to 12.4 microns at 900°F , and from 1.01 to 13.6 microns at 1450°F . The specimen was held at 1450°F for 17.5 hours. After this interval the spectral normal emittances were measured a second time at 1450°F and at 900°F . As can be seen in Figure 116, the first emittance curve for 900°F was lower than that for 1450° at wavelengths shorter than 7.5 microns. The second curve for 900°F , however, matches the higher temperature curves. This can probably be accounted for by the change in color of the coating, since it was white before testing and grey after testing. Note that at all temperatures there is a dip in the curve between 8.5 and 11.5 microns. There was no change in the coating-substrate bond strength, coating hardness, or texture as a result of testing.

Thermal Cycling and Bend Testing - Two aluminum fins were coated with titanium oxide for thermal cycling and bend testing. The coatings were approximately 2 and 6 mils thick respectively. Neither of the coatings spalled during bend testing.

j. "Titania-Base" Powder

A material designated by Plasmadyne Corporation as "Titania-Base" was plasma-arc sprayed onto substrates of AISI-310 stainless steel and aluminum. Also coated were a SNAP-8 and a Sunflower I test section for long term endurance testing. "Titania-Base" powder is a mixture of titanium dioxide and other oxides.

The total hemispherical emittance of a coated stainless steel tube was measured in the spectral normal emittance rig over the temperature range of 500°F to 1400°F . The coating was 1.6 mils thick. As shown in Figure 117 and in Table 76, the total hemispherical emittance increased approximately linearly from 0.83 at 500°F to 0.85 at 1450°F . The specimen was then endurance tested at 1450°F . As may be seen in Figure 118, the total hemispherical emittance gradually increased to 0.88 during the first 450 hours.

After 450 hours the emittance dropped sharply. The decrease continued for 30 hours until a value of 0.84 was reached. The emittance remained constant at that value for the last 65 hours of endurance testing. The specimen was cooled slowly to room temperature. While the specimen was being removed from the chamber a crackling sound was heard for about five minutes. This was caused by cracking of the coating which occurred over about 95 per cent of the specimen surface. Ten per cent actually dropped off the substrate.

The total hemispherical emittance of a coated stainless steel strip was measured and data appear in Table 77 and in Figure 117. The coating was 2.7 mils thick. This coating also separated from the substrate.

Four aluminum strips were coated with "Titania-Base" and the total hemispherical emittances of the specimens were measured. The coating thicknesses were 2.5, 3.5, 5.1, and 5.4 mils. Data appear in Table 78 and in Figure 117.

It may be noted from Figure 117 that there is no appreciable difference between the emittance level of the 2.5 and the 3.5-mil thick coatings. The emittance levels of the 5.1 and the 5.4-mil thick coatings were also consistent with each other but were slightly lower than those of the thinner coatings. Coated aluminum fins were subjected to thermal cycling and bend testing. Light spalling occurred as a result of bending.

"Titania-Base" coatings were selected for long term endurance testing for the following reasons:

1. The emittance level is high (above 0.8),
2. Results of short term endurance testing indicated that the coating is stable,
3. None of the coatings separated from the aluminum fins during thermal cycling or from the aluminum strips during emittance testing, and
4. Bend testing resulted in only light spalling.

As a result, a SNAP-8 and a Sunflower I test section were plasma-arc sprayed with "Titania-Base" powder and endurance tested in the long term endurance rigs with fin root temperatures of 700°F and 650°F respectively.

The appearance of the SNAP-8 tube-half fin radiator segment before and during early testing is shown in Figures 119, 120, and 121. During the first 2810 hours of testing, no changes in the coating were observed. After 2810 hours, however, faint cracks in the coating were observed on the top of the tube. After 3490 hours, these cracks were plainly visible. At 6840 hours, loss of the coating on the tube portion of the specimen was observed (Figure 122). The coating loss continued to progress as shown in Figure 123. No deterioration of the coating on the fin portion of the specimen has been observed. At the end of the report period, the test section had accumulated approximately 9870 hours of endurance testing. The thermal history across the center of the test section is shown in Figure 124.

The appearance of the Sunflower I tube-fin radiator segment before testing is shown in Figure 31. The specimen fin root temperature was slowly raised to 650°F and endurance testing began. At the end of the report period a total of 9830 hours of endurance testing had been accumulated. The appearance of the test section after 9914 hours of testing is shown in Figure 125. No change in the appearance of the coating has been observed during this period. The thermal history across the center of the test section is shown in Figure 126.

k. Zirconium Oxide

First Specimen - A zirconium oxide (ZrO_2) coating 3 mils thick was applied to a molybdenum strip by the Linde Plasmarc process. The resulting surface was grey. The specimen was tested in the total hemispherical emittance rig. The total hemispherical emittance data are presented in Figure 127 and in Table 79.

During the first run, the temperature of the specimen was increased and then decreased several times, with each cycle reaching a higher temperature, until a maximum of approximately 2000°F was attained. The total hemispherical emittance values on the final run were 0.88 in the temperature range from 400°F

to 1100°F and 0.86 in the range from 1100°F to 2000°F. On the second run, these emittance values closely agreed with those of the first run until a temperature of 1800°F was reached. At this temperature, an unstable condition occurred. The emittance values finally stabilized at a temperature of 1900°F at the lower value of 0.80. Throughout the remainder of the second run, during which the temperature was decreased from 2000°F to 400°F, the emittance values continued to be lower than those obtained earlier.

Second Specimen - A zirconium oxide (ZrO_2) coating 1 mil thick was applied to an AISI -310 stainless steel strip by the Metco plasma-flame spraying process. This specimen was white rather than grey. The specimen was tested in the endurance rig.

Since end heaters are not used in the endurance rig and since at the time this test was conducted no correction was being applied to the data to compensate for the lack of end heaters, the lower temperature range (below 1500°F) was not covered. Data were obtained in the range from 1500°F to 1800°F. The total hemispherical emittance values ranged from 0.70 at 1500°F to 0.82 at 1800°F. The failure of the specimen at one of the power leads terminated the testing at 1800°F. Data appear in Figure 127 and in Table 80.

Third Specimen - A 6-mil thick coating of zirconium oxide was applied to an AISI -310 stainless steel tube by the Metco plasma flame-spraying process. Total hemispherical emittance was measured over the temperature range of 500°F to 1450°F.

The total emittance varied from 0.75 at 500°F to 0.67 at 1400°F during the initial heating cycle, as shown in Figure 127 and in Table 81. After 24 hours at 1450°F, the emittance had risen to 0.70. Cooling the specimen to room temperature and repeating the heating cycle showed that the increase in emittance was probably a result of a change in the coating since the increase was noted over the whole range of temperatures.

General Remarks - The emittance values of the coating on the molybdenum strip were higher than those of the coatings applied to stainless steel substrates. It is noted that the coating on the molybdenum strip was grey and the coatings on the stainless steel substrates were white.

6. Multiple Oxides

a. Silicates - Zirconium Silicate

Six zirconium silicate coatings ($ZrO_2 \cdot SiO_2$) were applied by plasma-arc spraying and by aluminum-phosphate bonding. The zirconium silicate powder used all came from a single container and was supplied by the Continental Coatings Corporation (FCZ-11). One specimen was prepared by Metco, Inc. by plasma-arc spraying zirconium silicate onto AISI-310 stainless steel. Three additional specimens were prepared by the Rokide process utilizing Rokide ZS rods which are primarily zirconium silicate. Two of these used a substrate material of columbium - 1 per cent zirconium and the third used a substrate of AISI-310 stainless steel. Two aluminum-phosphate bonded coatings were applied to columbium - 1 per cent zirconium substrates.

Plasma-Arc Sprayed Coating on Columbium-1 Per Cent Zirconium-

These coatings were white, 4 mils thick, moderately hard, rough in texture, and were well bonded to the substrate.

The total hemispherical emittance was measured from 300°F to 2200°F (Figure 128 and Table 82). The total emittance decreased from 0.83 at 300°F to 0.51 at 2200°F. The data obtained during the final cooling cycle indicated that a change in the coating had taken place. When the specimen was removed from the rig, small dark spots were noticed which further indicated a change in the coating.

It may be noted that the emittance data calculated using temperatures obtained with an optical pyrometer are somewhat lower than those obtained with the use of a platinum-platinum 10 per cent rhodium thermocouple. It is believed that the optical pyrometer temperatures (obtained by sighting into the black-body hole) are the more reliable. The data based on thermocouples during the final portion of the cooling cycle is presented to give some indication of the shape of the emittance curve after the change, although the emittances reported are higher than the true values.

Spectral emittance was measured from 1.5 micron to 13.5 microns at 900°F, from 1 micron to 13.5 microns at 1450°F,

and from 1 micron to 14 microns at 2000°F. The data are shown in Figure 129 and are typical of that for a white coating, i. e., the spectral emittance is low at short wavelengths, rapidly increases with increasing wavelengths in the 2- to 6-micron range, and then remains high. The dip at 9.5 microns is in the wavelength range where silica emittance data typically shows a minimum.

Plasma-Arc Sprayed Coating on AISI-310 Stainless Steel - The coating, which was applied by Metco, Inc., was 4.1 mils thick. Total hemispherical emittance was measured over the temperature range of 300°F to 1000°F. The data are shown in Figure 128 and in Table 83. As may be seen, the total hemispherical emittance varied between 0.78 at 500°F and 0.51 at 1800°F. When the sample was removed from the rig it was noted that some of the coating had started to peel from the substrate in areas outside of the test section.

Aluminum-Phosphate Bonded Coating on Columbium-1 Per Cent Zirconium - Zirconium silicate powder was aluminum phosphate bonded onto two columbium-1 per cent zirconium substrates. One specimen was tested in the total hemispherical emittance rig and the other in the spectral normal emittance rig. The coatings were 4 mils thick, white, very soft, and were poorly bonded to the substrates.

Total hemispherical emittance was measured from 300°F to 1850°F. As may be seen in Table 84, the emittance decreased from 0.75 at 300°F to about 0.39 at 1850°F. It was noticed that the specimen was whiter after the test than before.

Comparison of the curves in Figure 128 shows that for temperatures ranging up to approximately 1400°F the emittance values of the aluminum-phosphate bonded coating are about 10 per cent lower than those of the plasma arc-sprayed coatings. Above 1400°F the differences increase.

As in the tests discussed previously, at elevated temperatures there existed considerable discrepancy between temperature measurements obtained with an optical pyrometer and those obtained with a platinum-platinum 10 per cent rhodium thermocouple. The size of this discrepancy indicated that the platinum-platinum 10 per cent rhodium thermocouple was completely unreliable for the high-temperature portion of this test. A chromel-alumel thermocouple used as a reliability check provided temperature data in reasonably

good agreement with those of the optical pyrometer. Data based on the chromel-alumel thermocouple are therefore reported rather than data based on the platinum-platinum 10 per cent rhodium thermocouple.

The spectral normal emittance of the second specimen was measured from 1.5 to 12.5 microns at 900°F, from 1 to 13.5 microns at 1400°F, and from 0.5 to 13.5 microns at 2000°F. The coating was whiter after testing than before. The spectral emittance data are shown in Figure 129.

It is to be noted that at short wavelengths the spectral emittance was higher at 900°F and 1450°F than would have been expected for a white coating, but that when the test temperature was raised to 2000°F the emittance dropped to a more reasonable level. The emittance drop is consistent with the increased whiteness of the specimen after testing.

Comparison of the curves in Figure 129 reveals that the curve for the aluminum-phosphate bonded specimen is similar to that of the plasma arc-sprayed specimen but is shifted 1 to 2 microns to the right. The shift appears most noticeably at the dip, which has a minimum at 9.5 microns for the plasma arc-sprayed specimen, and at about 11 microns for the aluminum-phosphate bonded specimen. It is further noticed that the curve for the aluminum-phosphate bonded specimen shows a dip at about 6 microns which does not appear on the curve for the plasma arc-sprayed specimen.

Rokide ZS Coatings - Rokide rods obtained from the Norton Company were used to apply coatings to both AISI-310 stainless steel and to columbium - 1 per cent zirconium substrates. A typical analysis of these rods as determined by the Norton Company is as follows: 64.12 per cent Zr O₂, 33.22 per cent SiO₂, 1.42 per cent Al₂O₃, and 0.97 per cent (CaO + TiO₂ + Fe₂O₃ + NaO₂). The coatings were white and had a rough but glassy appearance.

The coating applied to AISI-310 stainless steel was 4 mils thick, very hard, and had a fair coating-substrate bond strength. As shown in Table 85, the total hemispherical emittance decreased from 0.65 at 1000°F to approximately 0.53 at 2150°F, then increased to approximately 0.56 at 2200°F. When the specimen was removed from the rig it was noted that the color had changed from white to grey, indicating that the emittance increase at 2200°F probably resulted from a change in the coating. It was

also observed that a considerable amount of the coating had spalled off the tube, which probably resulted from the large difference in coefficients of thermal expansion between the coating and the substrate.

The coating applied to columbium - 1 per cent zirconium was 5 mils thick, hard, and was well bonded to the substrate. As shown in Table 86, the total hemispherical emittance decreased from 0.75 at 500°F to 0.6 at 1500°F and then increased to approximately 0.68 at 2200°F. The data agreed fairly well with those for Rokide ZS on AISI-310 stainless steel between 1000°F and 1500°F. At this temperature the emittance started to increase, apparently the result of a change in the coating. The color of this specimen also changed to grey. This is consistent with the similar changes in emittance of the two specimens. No spalling of the coating occurred. None was expected since the difference in coefficients of thermal expansion between the coating and this substrate is small compared to that of the previous specimen.

The physical characteristics of the specimen to be endurance tested were identical to those of the specimen discussed previously. The specimen was maintained at a nominally constant temperature of 1450°F for 280 hours. During the early portion of the test, the optical pyrometer readings obtained were found to be in error and a platinum-platinum 10 per cent rhodium thermocouple was used for temperature measurement until the source of the error was found. The optical pyrometer and the thermocouple were both used for the remainder of the test, but by this time a discrepancy of about 25° to 30°F existed between the two instruments. This results in a corresponding discrepancy in computed emittance of about 5 to 6 per cent. During the portion of the test in which the pyrometer was not used (95 hours) the emittance increased from 0.65 to 0.75, using thermocouple temperature indications and to 0.79, using optical pyrometer temperature indications. A gradual increase to an emittance of 0.83, (based on optical pyrometer temperature measurements) occurred during the next 170 hours. The difference between the emittance values calculated using the thermocouple and the pyrometer remained about 5 to 6 per cent throughout the test. During the remaining 50 hours of testing, no further changes took place.

Since an increase in emittance had occurred and since previous tests with Rokide ZS on columbium - 1 per cent zirconium substrates have indicated difficulty in obtaining reliable temperature data with platinum-platinum 10 per cent rhodium thermocouples, it was not possible to determine whether the indicated emittance values at the start of the test were reliable. For this reason, another specimen from the same batch was tested for about 75 hours at the same temperature. The emittance at the start of the second test based on optical pyrometer temperature measurements was 0.65 and increased to about 0.80 during the 75 hours of testing. These results, which were almost identical to those of the first endurance test, confirmed the reliability of the optical pyrometer in the first test, and also indicated that the thermocouple was reliable at the beginning of the endurance test.

The data for these two endurance tests are shown in Figure 130. (During the portion of the first test in which emittance was not changing rapidly, average daily values are shown for days when more than one point was taken.) Emittance data obtained as the specimen was heated to the endurance test temperature are shown in Figure 128. Also see Table 87.

In each case, when the specimen was removed from the test rig, it was noted that the coating color had changed from white to grey.

General Remarks - X-ray diffraction analyses of the Rokide and plasma-arc sprayed specimens before testing showed cubic zirconia (ZrO_2) to be the principal phase present. Apparently the zirconium silicate decomposed at the very high spraying temperatures and the silica thus formed was in a glassy state^{9, 10}. Spectrographic analysis confirmed the presence of large amounts of silicon in addition to the zirconium. The plasma-arc sprayed specimen used for total hemispherical emittance testing and the Rokide ZS coating on AISI-310 stainless steel were examined after testing and the spectrographic analysis showed no significant change in the elements present. X-ray diffraction showed the

presence of both monoclinic and cubic zirconia. The change in crystal structure of the Rokide coatings may be attributed to the presence of magnesium in the coating which, when present as an oxide, can cause zirconia to have either of these structures at room temperature. Spectrographic analysis of the powder used for plasma-arc spraying did not show the presence of magnesium, however. Once the powder has been stabilized and converted to the cubic structure, it would not be expected that it would change back to the monoclinic form. No explanation can therefore be given at this time as to why the plasma-arc sprayed powder changed from cubic to monoclinic zirconia.

It has been noted that all of the specimens with coatings applied by thermal spraying showed changes in emittance as well as a change in color from white to grey. Whether or not these changes are related to the indicated changes in the structure of zirconia cannot be determined at the present time. Inspection of Figure 128 reveals that, with the exceptions of the Rokide ZS endurance and the aluminum phosphate bonded specimens, all of the curves are in good agreement between 1000°F and 1400°F.

X-ray diffraction analysis of the aluminum-phosphate bonded coatings before and after testing showed zirconium silicate ($ZrO_2 \cdot SiO_2$) to be the only crystalline phase present.

b. Spinels

1. Magnesium Aluminate

Coatings of magnesium aluminate ($MgO \cdot Al_2O_3$) were applied to columbium - 1 per cent zirconium tubes by the Rokide process using Rokide MA rods. The composition of typical Rokide MA rods is described by the supplier, The Norton Co., as follows: 66.8 per cent Al_2O_3 , 29.5 per cent MgO , 2.9 per cent SiO_2 , 0.69 per cent Cr_2O_3 and 0.08 per cent ($Fe_2O_3 + TiO_2 + Na_2O$). The well bonded coatings were 5 mils thick, white, very hard, and had a rough, glossy appearance. Two specimens were tested, one in the total hemispherical emittance rig and the other in the spectral emittance rig. Both were prepared at the same time using rods from the same batch.

Total hemispherical emittance was measured from 300° F to 2200° F and the data are shown in Figure 131 and in Table 88. During the heating cycle, the emittance varied from approximately 0.8 at 300° F to 0.48 at 1800° F and then slowly increased to 0.55 at 2200° F. Maintaining the specimen at this temperature for 30 minutes produced a further increase in emittance of 0.60. Emittances measured as the specimen was cooled indicated that the emittance had increased at all temperatures so it was suspected that the increase resulted from a change in the coating. When the specimen was removed from the rig, it was noted that the color of the specimen had changed from white to grey and that the surface had a matte appearance as contrasted to its glossy appearance before testing. Although a change in the coating was indicated by the increase in emittance level and further substantiated by the change in color of the coating, x-ray diffraction analysis showed magnesium-aluminate ($MgO \cdot Al_2O_3$) to be the only crystalline phase present, both before and after testing.

Spectral emittance was measured from 1.5 to 12.4 microns at 900° F, from 1.1 to 12.5 microns at 1450° F, and from 0.45 to 13.5 microns at 2000° F. The spectral emittance data appears in Figure 132. An interesting phenomenon is the local maximum at approximately 3 microns which is very pronounced at 900°, still exists at 1450° F, but does not appear at all at 2000° F (see inset - Figure 132).

During testing, the coating color changed to a grey-white and the hardness was reduced but brittleness increased. The coating remained well bonded to the substrate.

2. 40 Per Cent Nickel-Chrome Spinel - 60 Per Cent Silicon Dioxide

Nickel-chrome spinel ($NiO \cdot Cr_2O_3$) was formed by heating a mixture of NiO and Cr_2O_3 in a one-to-one mole ratio for two hours at 2300° F in air. X-ray diffraction analysis of the resulting mixture indicated the composition to be 50 per cent $NiO \cdot Cr_2O_3$, 40 per cent Cr_2O_3 , and 10 per cent NiO. Forty grams of the mixture were added to 60 grams of SiO_2 and about 70 ml of Pratt & Whitney Aircraft aluminum phosphate solution. The slurry was then mixed and sprayed onto substrates of AISI-310 stainless steel, aluminum, and onto a finned tube for a 10,000-hour endurance test. Spraying and curing were in accordance with the usual procedures used for aluminum-phosphate bonded coatings outlined in Section IV . B. 1.

Initially, two thicknesses of coatings were applied to aluminum plates for thermal cycling and bend testing. The root-to-tip temperature, ΔT , remained unchanged during thermal cycling, but heavy spalling occurred on both specimens as a result of subsequent bend testing.

A coating 3.5 mils thick was applied to both sides of an AISI-310 stainless steel strip. Total hemispherical emittance was measured in the total hemispherical emittance rig over the temperature range of 300°F to 1450°F.

Total hemispherical emittance was measured from 400°F to 800°F at 100°F intervals during the initial heating, Run 1. The specimen was then maintained at 800°F for 63 hours, during which time the total hemispherical emittance dropped from 0.88 to 0.86. As the temperature of the specimen was being increased, Run 2, failure of the voltage and thermocouple leads interrupted the test. Failure occurred at 1000°F. The specimen was reinstrumented and testing was resumed. The total hemispherical emittance was then measured from 300°F to 1450°F, Run 3, and was found to vary between 0.87 and 0.89 over the entire temperature range. The values of the total hemispherical emittance obtained during Run 3 were in close agreement with those of previous runs, although they were slightly lower than those obtained during Run 1 at 500°F and 700°F, as shown in Table 89 and Figure 133. An attempt to maintain the specimen at 1450°F failed due to parting of the specimen at the top end clamp. The resulting thermal shock caused severe spalling and the test was terminated.

A coating 2.5 mils thick of the same material was applied to an AISI-310 stainless steel tube. The spectral normal emittance rig was used for making total hemispherical emittance measurements over the temperature range of 500°F to 1300°F at 100°F intervals. The emittance values obtained over this range were consistent with those obtained with the strip specimen discussed above. The emittance of the coated tube was slightly lower than that of the coated strip at all temperatures, probably due to the difference in thicknesses or surface textures. The specimen was left overnight at 1300°F, during which time the thermocouple readings became erratic. The temperature was then raised to 1450°F and an endurance test was started at this temperature using an optical pyrometer to measure the temperature of a small black-body hole in the specimen. At the start of the endurance test the total hemispherical emittance at 1450°F was 0.83. After 170 hours it dropped to 0.78 and no further change occurred in the next 160 hours.

An analysis of the tested specimen and a similar specimen that had not been tested detected no significant change in the coating of the tested specimen. Initial attempts to section the tested specimen produced a large amount of flaking of the coating, indicating possible deterioration of the bond between the coating and the substrate during testing. Poor thermal contact between the substrate and the coating would result in a pronounced temperature drop between the substrate and the coating. A temperature change of 30°F would result in the observed drop in effective emittance. Since the data for the two coated stainless steel specimens are generally consistent, one might assume that the true value of total hemispherical emittance was in fact somewhat higher than was recorded. Extrapolation of the endurance curve to the point where the last temperature reading was made with a thermocouple results in a value of 0.864 which is consistent with previous data. The drop in effective emittance from 0.864 to 0.78 corresponds to a theoretical temperature drop of 50°F. Data are shown in Figures 133 and 134 and in Table 90.

A second coated AISI-310 stainless steel tube was tested to further evaluate the endurance characteristics of the coating material. Although the second coating appeared to be slightly thinner than the first and would therefore have a slightly lower emittance, the specimen was nevertheless acceptable for determining changes in emittance with time. Endurance testing was conducted in the spectral normal emittance rig with temperature measurements being made with an optical pyrometer. No data was taken until the specimen reached the 1450°F endurance temperature.

At the start of the test, the total hemispherical emittance was 0.81. After approximately 40 hours, the total hemispherical emittance dropped to 0.80. This one per cent change contrasts with the much larger decrease in total hemispherical emittance observed during the endurance testing of the first specimen. The emittance remained constant during the next 200 hours. A gradual increase in emittance was recorded after 200 hours until at the end of the test, at approximately 550 hours, the total hemispherical emittance was 0.82. The data are presented in Table 91 and in Figure 134.

The same material was used to coat several aluminum strips. The coatings were produced in three thicknesses, 2.2, 2.8, and 3.9 mils.

The total hemispherical emittance of the 2.2-mil thick coating was measured from 300°F to 900°F in Run 1A. From 300°F to 700°F the emittance varied between 0.84 and 0.85. The point taken at 900°F indicated a drop in total hemispherical emittance to 0.83. Points taken as the specimen was cooled to lower temperatures confirmed this drop (Run 1B). The test was then repeated, Run 2, and the data obtained was in close agreement with that of Run 1B. The total hemispherical emittance data is shown in Figure 133 and in Table 92.

The total hemispherical emittance of the 2.8-mil thick coating was measured from 300°F to 600°F in 100°F increments in Run 1. An instrument limitation which was subsequently corrected confined temperatures to this range. Total hemispherical emittance was then measured from 300°F to 900°F in Run 2. The emittance values obtained in Run 2 were slightly lower than those of Run 1 (Table 93).

The total hemispherical emittance of the 3.9-mil thick coating was measured during four runs over the temperature range of 300°F to 900°F. See Table 94. As shown in Table 94 and in Figure 133, the total hemispherical emittance level was approximately 0.8 over the entire temperature range. No inconsistencies were noted between the data of the various runs. The emittance level was lower than was anticipated on the basis of the tests conducted on the other two coatings. During their initial heating cycles, the emittance of the light coating was approximately 0.84 and that of the medium coating 0.88. Since the heavy coating was darker in color than the others, there is a possibility that the compositions of the coatings were different; e.g., incomplete reaction of the nickel and chrome oxides to form the spinel, $\text{NiO} \cdot \text{Cr}_2\text{O}_3$.

The SNAP-8 tube-half fin radiator segment was coated with a mixture of nickel-chrome spinel and silicon-dioxide, and installed in the long term endurance rig for testing. The appearance of this specimen before testing is shown in Figure 28. The fin root temperature was slowly increased to 700°F and endurance testing began. The temperature profile across the center of the section is shown in Figure 135.

The endurance test was continued for 2703 hours, at which time the specimen heater control was inadvertently increased to supply about 800 to 900 watts to the heater. The normal power dissipation of the specimen at the endurance temperature is 270 watts. When the overpower condi-

tion was discovered, the heater power was immediately cut off and the specimen allowed to cool to the ambient temperature.

A visual examination of the specimen revealed a slight loss of coating near the fin root and the coating on portions of the tube was wrinkled. However, the coating remained bound to the substrate even where wrinkles appeared on the surface. The appearance of the coating at this time is shown in Figure 136.

The specimen heater power was then restored to a level of 270 watts to enable determination of other possible damage to either the coating or the thermocouples.

Comparison of thermocouple indications obtained before and after the overheating condition occurred showed that the thermocouple output characteristics had changed with the greatest change occurring for thermocouples located on the tube and at the fin root. The characteristics of thermocouples at the edge of the fin were unchanged.

Since the damage resulting from overheating did not appear to be serious enough to warrant termination of the test, testing was continued. With the indications from the fin root thermocouples no longer reliable, the endurance conditions were maintained by keeping the specimen heater power constant and by monitoring the fin edge thermocouples for evidence of coating deterioration.

Endurance testing was continued until a total of 7200 hours had been accumulated. At this time the rig was shut down for inspection and re-instrumentation. No coating deterioration occurred between 2700 hours and 7200 hours. See Figures 137 through 139.

After inspection and re-instrumentation were completed, the specimen was installed in the rig and endurance conditions were re-established. Comparison of data from the new thermocouples with data obtained before the overheating occurred revealed that no appreciable change in temperature level or temperature distribution occurred, indicating that the coating emittance characteristics were stable over the period.

The endurance test was continued and at the end of the contract period, the section had been exposed to test conditions for 10,720 hours. The appearance of the specimen after 10,800 hours of endurance testing is shown in Figure 140.

c. Titanates

1. Barium Titanate

Barium titanate was plasma-arc sprayed onto columbium-1 per cent zirconium tubes. The barium titanate powder was obtained from Continental Coatings Corporation (FCE-11). Two specimens were prepared at the same time, one for testing in the total hemispherical emittance rig, and the other for testing in the spectral normal emittance rig.

The 5-mil thick coating on the total hemispherical emittance sample was grey-black, had a fine grit texture, and was well bonded to the substrate. Emittance values varied from 0.75 at 300°F to about 0.84 at 1600°F, as shown in Figure 141 and Table 95. At higher temperatures the emittance dropped to a low value of 0.64 at 2250°F. As the specimen was cooled, it was observed that the emittance had dropped over the entire temperature range, indicating that a change in the coating had occurred. The color of the coating had changed to black mottled with violet.

Spectral emittance measurements were made at 900°F, 1450°F and 2000°F on the second sample.

Since the shapes of the spectral emittance curves are quite different (see Figure 142), it is assumed that a change in the coating took place. This is consistent with the results of the total emittance test described above. A change in color was also observed but the final color was brown rather than the violet and black of the total emittance specimen.

X-ray diffraction and spectrographic analysis showed no change in the coating as a result of testing. Both before and after testing, the primary phase present was BaTiO₃.

2. Calcium Titanate

Eight specimens coated with calcium titanate (CaO · TiO₂) were tested in the total hemispherical emittance, the spectral normal emittance, and in the short term endurance rigs. Coatings were applied to AISI-310 stainless steel, to columbium, and to columbium - 1 per cent zirconium substrates by either plasma-arc spraying or by aluminum-phosphate bonding.

Coated AISI-310 Stainless Steel - The specimen was prepared by plasma-arc spraying a 1.2-mil thick coating of calcium titanate supplied by Metco, Inc. onto a stainless steel strip. The total hemispherical emittance was measured over a range of temperatures from 300°F to 1450°F.

During the initial heating cycle (Run 1), the total hemispherical emittance increased from 0.81 at 300°F to 0.88 at 1450°F. Maintaining the specimen at 1450°F for 17 hours resulted in a further increase in emittance up to 0.90. While cooling the specimen to 650°F (Run 2), it was observed that the overall level of the emittance curve was higher. A consistency in the data was obtained between Run 2 and Run 3 during which the specimen temperature was raised to 1600°F. After the 1600°F temperature was maintained for 22 hours, the emittance increased sharply from the 0.90 level to 0.95 at 1700°F. Decreasing the temperature to 850°F (Run 4) showed that this increase marked another shift upward in the emittance over the entire temperature range, the increase being greater at the higher temperatures. The specimen was maintained at 850°F for 16 hours and then cooled to room temperature. The data from all runs are presented in Figure 143a and in Table 96.

A new thermocouple was installed on the specimen and measurements of emittance were taken a second time to determine whether or not thermocouple deterioration had caused the apparent increases in total hemispherical emittance. The emittance recorded during the heating of the specimen to 1450°F agreed closely with that of the second and third runs, indicating that the first increase in emittance had been an actual change. After maintaining the specimen at 1450°F for 18 hours, the emittance level rose to that obtained during Run 4, thus indicating that the second increase in emittance had resulted from thermocouple deterioration or contamination.

Coated Columbium - Three columbium tubes were plasma-arc sprayed with calcium titanate supplied by Metco, Inc. The first was tested in the short term endurance rig, the second in the total hemispherical emittance rig, and the third in the spectral normal emittance rig.

The total hemispherical emittance of the first coated columbium tube was measured as the specimen temperature was brought up

to 1450°F. As shown in Table 97, the emittance was relatively constant at approximately 0.92. The specimen was then maintained at a nominal temperature of 1450°F for approximately 320 hours. No significant change in the emittance was noted during this time. Figure 144 shows the emittance at 1450°F as a function of time, each point representing the average daily value of emittance. During this test, temperature measurements were made with an optical pyrometer viewing a black-body hole in the specimen wall.

After 75 hours of endurance testing the test section voltage readings became erratic. Since there was no noticeable change in resistance during the first 75 hours at 1450°F, it was assumed that the resistance of the sample substrate did not change from this point on, and voltage was taken as equal to the current times the last value of resistance.

The second specimen, which was tested in the total hemispherical emittance rig, had a coating 5 mils thick which was grey-black and extremely hard. The texture was rough and the coating was extremely well bonded to the substrate. As shown in Table 98, the total emittance of the plasma-arc sprayed coating varied from 0.74 at 400°F to 0.85 at 1500°F during the initial heating, and then dropped to 0.74 at 2200°F. The drop in emittance at the high temperature appears to be the result of a permanent change, since the level of emittance was lower during cooling over the entire temperature range. The increase in emittance during the first portion of the test may be a result of a change in the coating. Similar increases were noted in other tests with plasma-arc sprayed coatings of calcium titanate, strontium titanate and barium titanate. However, the emittance of this specimen was lower than has previously been reported for the same plasma-arc sprayed coating. No visible changes in the coating were observed as a result of testing.

The third coated columbium tube was tested in the spectral normal emittance rig. The 3.5-mil thick coating was grey-black, extremely hard, had a rough texture, and was very well bonded to the substrate. Spectral normal emittance was measured at 900°F, 1450°F and 2000°F. The spectral normal emittance data is presented in Figure 145. It may be noted that the general level of the spectral normal emittance curve is highest at 1450°F. This is consistent with the changes noted above in the discussion of the total hemispherical emittance test of the same coating. That is, an increase in emittance took place at some temperature below 1500°F and

when the specimen was heated to 2000°F a decrease in emittance took place. As noted in the discussion of the coated stainless steel specimen, the rise in emittance that occurred below 1500°F was a permanent change for temperatures up to about 1675°F. However, as shown in Figure 143b, heating the specimen to temperatures above 1700°F causes the emittance to decrease. This decrease appears to be a result of a second permanent change. This second change is consistent with the decrease in the level of the spectral normal emittance curve at 2000°F. The specimen showed no visible change in characteristics as a result of testing.

Coated Columbium - 1 Per Cent Zirconium - Four columbium - 1 per cent zirconium tubes were coated with calcium titanate. Two of these tubes were coated with material supplied by Metco, Inc. by aluminum-phosphate bonding. The other two were plasma-arc sprayed with material supplied by the Titanium Division of the National Lead Company.

The first aluminum phosphate-bonded coating was 5 mils thick and hard on the surface but soft underneath, probably due to insufficient drying time. The coating was cream colored with a texture similar to that of 80 grit emery cloth and was well bonded to the substrate. Total hemispherical emittance was measured from 300° to 1400°F. As shown in Table 99, the total hemispherical emittance decreased from 0.88 at 300°F to 0.61 at 1100°F and then remained relatively constant up to 1400°F. The coating failed when heated above 1400°F and had changed to a white color during testing.

The second aluminum phosphate-bonded coating was tested in the spectral normal emittance rig. The 5-mil thick coating was hard, cream colored, and had a texture similar to that of 80 grit emery cloth. Before testing, the coating was well bonded to the substrate, but, when the specimen was heated above 900°F, cracks developed in the coating and the data subsequently taken was unreliable. After testing, the coating was white with blue blotches. The data which was obtained (see Figure 145) shows a higher emittance at longer wavelengths which is typical of a white coating.

The third columbium - 1 per cent zirconium coated specimen was tested originally in the total hemispherical emittance rig. These measurements may be in error, however, as a result of difficulties arising from the volatilization of the Mn_2O_3 specimen described in Section VII B 5 e of this report. Results from this test will not be reported until corrective measures have been completed.

The plasma-arc sprayed coating, before the first test, was 5 mils thick with white crystals on a blue background. It was hard and the coating-substrate bond strength was good. The matte texture was about the same as that of 40-grit emery cloth. After the first test, white crystals were still present, but the background was now grey. No other changes in the characteristics of the coating were observed.

Since the test was originally conducted only to compare the total hemispherical emittance rig with the short term endurance rig, and since changes in the coating had already taken place during initial testing, measurements were taken only during heating to 1500°F and only above 800°F. As shown in Table 100 and in Figure 143c, the emittance level remained constant at about 0.90 during heating. This test run was terminated at 1500°F and the specimen was cooled to room temperature with the vacuum maintained. The next day the specimen was reheated to 1500°F and then cooled to 1050°F. The emittance values obtained duplicated those taken the previous day. After testing, the coating was uniformly grey.

The final coated columbium - 1 per cent zirconium specimen was tested in the spectral normal emittance rig although only total hemispherical emittance data were taken. The plasma-arc sprayed coating was 5 mils thick and had both white and blue crystals present on a light grey background. It was hard and had a matte texture similar to that of 80-grit emery cloth. The coating-substrate bond strength was good. Table 101 and Figure 143c show the total hemispherical emittance values of this coating on two test runs between 800°F and 1800°F. The emittance increased from about 0.82 at 800°F to about 0.90 at 1200°F, where it remained on subsequent thermal cycling. However, when heated above 1600°F, the emittance decreased and then during cooling remained at the lower level. This same phenomenon also occurred with specimens coated with powder supplied by Metco, Inc. After the specimen was removed from the rig, the only change in the coating was that the color was all dark grey.

The curves for the plasma-arc sprayed calcium titanate powders indicate that the emittance reaches a maximum at about 1400°F during the first heating cycle. The level attained at 1400°F is

then maintained during subsequent thermal cycling between 800°F and 1600°F, but heating above 1600°F causes the emittance to decrease. Testing has not been conducted below 800°F after the emittance increased at 1400°F.

Further testing of this coating is required to determine (1) what change in the coating causes the emittance increase, (2) whether or not the change can be induced at temperatures below 1400°F, and (3) the endurance characteristics of the coating.

X-Ray Diffraction Analysis - X-ray diffraction patterns were obtained for each of the specimens coated with powder supplied by Metco, Inc., and these showed no change in the structure of any of the specimens as a result of testing. The principal phase present in each case was CaTiO_3 . Spectrographic analysis was performed on the aluminum phosphate bonded coating tested in the spectral normal emittance rig and this showed no change in the elements present as a result of testing.

3. Iron-Titanium Oxide

Powder obtained from Continental Coatings Corporation (FCT-11) was plasma-arc sprayed onto four columbium-1 per cent zirconium tubes. The specimens were tested in the total hemispherical emittance rig, in the short term endurance rig, and in the spectral normal emittance rig.

Particle size analysis indicated a diameter size distribution with 50 per cent 28 microns or larger. Thirty-two per cent fell between 28 and 35 microns and the remainder of the particles had diameter sizes evenly distributed between 3 and 28 microns.

The first 4-mil thick coating was grey-black, hard, and had a texture similar to that of 80 grit emery cloth. The coating-to-substrate bond was good. Total hemispherical emittance was measured over the temperature range of 300°F to 2100°F and was relatively constant at approximately 0.85 over the entire temperature range. Several test runs were made with no appreciable changes in emittance resulting from repeated heating. (See Figure 146 and Table 102).

The second coating was tested in the short term endurance rig. The coating was 4 mils thick, grey-black, hard, and had a texture similar to that of 80 grit emery cloth. The coating-to-substrate bond was good. Figure 145 shows the total hemispherical emittance of the specimen as it was heated from 300°F to 1450°F. The specimen was subjected to 300 hours of endurance testing at 1450°F. The results of the endurance testing are shown in Figure 147 and Table 103.

These two samples show that the emittance of this material was relatively constant at 0.87 from 800 to 1450°F and that no significant change occurred during the 300 hours at 1450°F.

No change in the coating was observed as a result of testing. X-ray diffraction analysis of the second specimen indicated that Fe_2TiO_5 was present both before and after testing. By spectrographic analysis it was found that Fe and Ti were two major constituents present both before coating and after testing. Also, Mn was detected as a minor element before coating and after testing.

One of the plasma-arc sprayed specimens had different visible coating characteristics than the other three and therefore this specimen was tested in the total hemispherical emittance rig to determine how its total emittance was affected. The coating was 4 mils thick and had a dark grey background with metallic yellow specks on its surface. This was a very hard coating that was very well bonded to the substrate and had a matte texture similar to that of 40-grit emery cloth. Total hemispherical emittance was measured between 300°F and 1900°F. Table 104 and Figure 146 show that the total hemispherical emittance of the coating increased from about 0.45 at 300°F to about 0.64 at 1500°F. The emittance remained at this level up to 1800°F and then rapidly decreased to about 0.45 at 1900°F where it remained during cooling. After removing the specimen from the rig it was observed that the coating was light grey but otherwise unchanged in appearance.

The final specimen was tested in the spectral normal emittance rig. Before testing, the coating was 4 mils thick, grey-black, hard, and had a matte texture similar to that of 80-grit emery cloth. The coating-substrate bond strength was fair. Spectral normal emittance was measured from 1.5 to 12.4 microns at 900°F, from 1.1 to 13.5 microns at 1450°F, and from 0.45

to 13.5 microns at 2000°F. As can be seen in Figure 148, the curve is relatively flat from about 1 to 12.5 microns. The data obtained at 900 and 1400°F were slightly higher than that obtained at 2000°F, but the changes in emittance with wavelength are similar and only one curve is drawn in Figure 148. After testing, no changes in the appearance of the coating were found.

The third specimen which was tested for total hemispherical emittance appears to be an exception for plasma-arc sprayed iron-titanium oxide coatings. While data for this specimen show no emittance values higher than 0.65, data for the other three specimens show no values lower than 0.80. Further, the change in emittance at temperatures around 1900°F was not observed for the other specimens tested. These emittance differences are attributable to the different external characteristics of the coatings.

4. Iron-Titanium-Aluminum Oxide

Powder obtained from the Continental Coatings Corporation (FCT-12) was plasma-arc sprayed onto three columbium-1 per cent zirconium tubes for testing in the total hemispherical emittance, spectral normal emittance, and short term endurance rigs. Particle size analysis of the powder indicated that 7 per cent of the particles were 69 microns in diameter or greater, and 8 per cent were 3 microns in diameter or less. Twenty-six per cent were between 4 and 10 microns in diameter. The remainder had diameters with fairly uniform size distribution over the range of 10 to 69 microns.

The first specimen had a coating 5 mils thick which was grey-black, fairly hard, had a medium grit texture, and a poor substrate bond. The total hemispherical emittance of the coating varied from about 0.83 at 300°F to about 0.88 at 900°F and then remained relatively constant up to 2150°F. The emittance values obtained during cooling were about the same as those obtained during heating. The data are shown in Figure 149 and in Table 105.

When the specimen was removed from the rig the only noticeable change was that the color had slightly darkened. The sample was then retested, primarily to determine the repeatability of the data and to measure changes in emittance at temperatures above 1000°F. Measurements were made only between 1000°F and 2200°F. Test results appear in

Table 106 and in Figure 149. Comparison of the results from the two tests reveals that below 1500°F the emittance during the first test was about 0.87 but during the second test about 0.82. Between 1500°F and 2200°F the data coincide at a value of about 0.87. During the final cooling, however, the emittance dropped below 0.87 to return to the same level as that measured at the start of the second test.

After testing, the coating was black and hard with a good coating-substrate bond strength. No change in the texture occurred.

Spectrographic analysis of the powder before coating indicated that Fe, Ti and Al were the major constituents, while Mn was one of the minor constituents. After testing, Fe, Ti, Al and Mn were found to be the major constituents present. No analysis of this type was run on the specimen after coating but before testing and therefore it is not known when the Mn changed from a minor to a major constituent. X-ray diffraction analysis indicates that before testing, the coating consisted of Fe_2TiO_5 . There is a possibility that $\eta\text{Al}_2\text{O}_3$ was also present, since lines for this phase coincide with those of Fe_2TiO_5 . After testing, two phases were definitely present, namely Fe_2TiO_5 and $\alpha\text{Al}_2\text{O}_3$. Since Al was found by spectrographic analysis before as well as after testing, and since Al_2O_3 was found by x-ray diffraction after testing, it appears probable that $\eta\text{Al}_2\text{O}_3$ was present before testing but could not be detected because of the Fe_2TiO_5 .

The specimen tested in the short term emittance rig had a coating 4 mils thick which was medium black, fairly hard, and had a matte texture similar to that of 80-grit emery cloth. The coating-substrate bond strength was fair. Table 107 and Figure 149 show the emittance vs temperature curve as the specimen was heated from 300°F to 1450°F. The curve indicates that the emittance of this coating was about 0.86 and it varied little with temperature. The results of the endurance test are shown in Table 107 and in Figure 150. The emittance remained at about 0.87 throughout the 300 hours. The coating did not change as a result of testing.

Figure 149 indicates that the emittance of iron-titanium-aluminum oxide is reasonably constant over the temperature range 300°F to 2200°F. The most probable values between these temperatures were 0.85 and 0.88. Exposure to high temperatures results in little change, aside from the darkening of the coating at temperatures above 1450°F. This corresponds closely with the data obtained with iron-titanate.

The specimen tested in the spectral normal emittance rig had a coating 4 mils thick which was dark grey, fairly hard, had a medium grit texture, and was poorly bonded to the substrate. Spectral normal emittance was measured from 1.5 to 12.5 microns at 900°F and from 1.0 to 13.5 microns at 1450°F. The specimen was then maintained overnight at 1450°F and spectral emittance was measured again at these temperatures. Finally, the test temperature was raised to 2000°F and spectral emittance was measured from 0.45 to 13.5 microns. The results (Figure 151) produce curves which are similar to those for iron titanate. There was no change in the appearance of the specimen as a result of testing.

5. Strontium Titanate

Strontium titanate was plasma-arc sprayed onto an AISI-310 stainless steel strip and onto columbium - 1 per cent zirconium tubes. The coated stainless steel strip was tested in the total hemispherical emittance rig and the coated columbium - 1 per cent zirconium tubes were tested in the total hemispherical and in the spectral normal emittance rigs.

Coated AISI-310 Stainless Steel Strip - This specimen was prepared by Metco, Inc. and the resulting coating was 2.2 mils thick. Total emittance of the specimen was measured over the temperature range of 300°F to 1800°F.

During the initial heating cycles (Runs 1, 2 and 3), the total hemispherical emittance varied from 0.82 at 500°F to 0.88 at 1700°F, as shown in Figure 152a and in Table 108. As the sample was cooled after being brought to 1800°F, it was noted that the entire emittance curve had been raised to approximately 0.89. To eliminate the possibility of error due to thermocouple contamination, a new thermocouple was installed on the sample and emittance measurements were made over the entire temperature range. The total hemispherical emittance obtained using the new thermocouple was in close agreement with the previous set of data, indicating that a permanent change in the coating had taken place, causing the emittance to rise.

Coated Columbium - 1 Per Cent Zirconium Tubes - Several coatings were prepared by plasma-arc spraying strontium titanate powder, obtained from the Plasmadyne Corporation, onto columbium - 1 per cent zirconium tubes. A particle size analysis

of this powder indicated that 87 per cent of the particles had diameters fairly evenly distributed between 10 and 22 microns. Half of the remaining material was larger than 22 microns, and half smaller than 10 microns in diameter. Two separate sets of specimens were prepared using powder from the same container for both sets.

One specimen from each of the two sets was tested in the total hemispherical emittance rig because the quality of the coating in the first set was not as good as was desired.

The first coating tested was 2 mils thick, light gray, and moderately hard. The texture was similar to that of 320 grit emery cloth, and the coating was well bonded to the substrate. This specimen was tested over the temperature range of 200 to 2100°F. As may be seen in Table 109 and Figure 152b, the total hemispherical emittance remained relatively constant at about 0.68 from 200 to 700°F and then increased to about 0.88 at 1400°F where it remained constant up to 1600°F. A similar increase was observed for the coated stainless steel specimen. As the specimen was heated above 1600°F, the emittance decreased to about 0.5 at 2125°F. During cooling, the emittance remained at this low level, indicating that the drop was due to an additional change in the coating.

Figure 152b indicates that between 1700°F and 2000°F the total emittance data based on optical pyrometer temperature measurements do not agree very well with those based on thermocouple measurements. This is somewhat misleading because the temperature was steadily increasing during this period, although the electrical power input to the specimen remained constant. The temperature was changing rapidly enough so that during the time required for obtaining current and voltage readings, the temperature changed by several degrees. Thus, some of the discrepancies in the emittance data based on these two types of temperature readings are due to transient conditions.

At temperatures of 2000°F and higher, the platinum-platinum 10 per cent rhodium thermocouple no longer gave reliable data. Therefore, only total hemispherical emittance based on optical pyrometer temperatures are shown for the cooling portion of the test. This data indicates that the decrease in emittance is permanent and exists over the entire temperature range.

The second coating tested was 4 mils thick, white, and hard. The texture was similar to that of 80 grit emery cloth and the coating was well bonded to the substrate. The specimen was tested over the temperature range of 300 to 2250°F.

Except for a change in color (from light grey to golden brown) no differences in the appearance of the coating before and after testing were noted.

The shape of the total hemispherical emittance curve of this specimen was very similar to that of the first specimen, although the level at certain temperatures was different. This coating had a relatively constant emittance level of 0.74 from 300° to 700°F. The emittance then increased to a maximum of about 0.9 at 1400°F and remained relatively constant to 1700°F. As the specimen temperature was increased above 1700°F, the emittance decreased until a value of about 0.64 was reached at 2250°F. This specimen, like the other specimens, had a much lower emittance as the specimen was cooled. The results of this test are shown in Figure 152b and Table 110.

When the specimen was heated above 2000°F, the same problem of unreliable temperature measurement with platinum-platinum 10 per cent rhodium thermocouples was encountered. The emittance data based on thermocouple temperatures is included for the final portion of the test. However, the emittance values obtained after the data point taken at 2000°F should be considered to be qualitative only, and are included for the purpose of indicating the approximate emittance level of the coating after exposure to higher temperatures. When the specimen was removed from the test rig, it was noted that the color of the coating had changed from white to yellow-brown. No other visible characteristics had changed.

Comparing the data for these two specimens shows that the emittance of the second specimen was about 5 per cent higher than that of the first over the temperature range of 300° to 1000°F. From 1100° to 1800°F, the two sets of data agree very well. Above 1800°F the curves start to diverge, which is probably a result of the nonrepeatability of the rates of deterioration of the two coatings.

The specimen tested in the spectral emittance rig was from the same set as the second strontium titanate specimen tested in the total hemispherical emittance rig. This coating was 4 mils thick, light gray, and hard. The texture was similar to that of 320 grit emery cloth and the coating was well bonded to the substrate. A different test sequence was used for this specimen than was used for most specimens tested in the spectral emittance rig. The spectral normal emittance was measured at 900°F from 1.5 to 12.5 microns and at 1450°F from 1 to 13.5 microns. The specimen was then maintained overnight at 1450°F and the spectral emittance was measured again at this temperature over the same wavelength range. The spectral test at 900°F was repeated and the temperature was then raised to 2000°F and spectral emittance was measured from 0.45 to 13.5 microns. As may be seen from Figure 153, there is very little difference in the shapes of the curves. The only difference is that the curves for the second 900°F and 1450°F tests are flatter than for the first tests, thus indicating a possible change in the coating during the overnight endurance period. When the specimen was removed from the rig, the only noticeable change was that the color had changed from light gray to light brown.

A spectrographic analysis of the second specimen tested in the total emittance rig and an untested specimen from the same set showed no change in the elements present as a result of testing. X-ray diffraction patterns on these same specimens and the other specimens tested in the total hemispherical emittance rig show Sr TiO₃ to be the principal phase present in all of the coatings.

The remaining specimen had a coating 4 mils thick, grey-white, hard, and had a matte texture similar to that of 320-grit emery cloth. The coating-substrate bond strength was good. Short term endurance testing, measuring total hemispherical emittance, was conducted in the spectral normal emittance rig. Total hemispherical emittance values obtained during the heating of the specimen from 300°F to 1450°F appear in Table 111 and in Figure 152b. The curve based on thermocouple temperatures in Figure 152b agrees very well with that of the first two coated tubes.

As shown in Table 112 and in Figure 154, the total hemispherical emittance remained at about 0.87 throughout the endurance test. Since the optical pyrometer and window are periodically checked

using an optical pyrometer calibrated by the National Bureau of Standards, the emittance values based on optical pyrometer readings are considered the more accurate and therefore these values are the only ones plotted in Figure 154. After testing, the specimen was grey-black, but no other change was observed.

General Remarks - All the data obtained from plasma-arc sprayed strontium titanate have resulted in curves which have a shape similar to those for calcium titanate specimens. The emittance of strontium titanate, similar to that of calcium titanate, decreases when the specimen is heated above 1600°F. The data is relatively reproducible between 1300°F and 1600°F. It remains to determine whether or not the high emittance value achieved at 1400°F will remain while the specimen is cooled, whether the increased emittance can be obtained without heating the specimen to 1400°F, and to determine the effects of endurance testing at temperatures under 1400°F.

d. Zirconates - Calcium Zirconate

A 3.2-mil thick coating of calcium zirconate ($\text{CaO} \cdot \text{ZrO}_2$) was plasma-arc sprayed onto an AISI-310 stainless steel strip by Metco, Inc.

Total hemispherical emittance measurements were made over the temperature range of 300°F to 1450°F. The emittance values, as shown in Figure 155 and Table 113, varied from 0.74 at 300°F to 0.62 at 900°F during initial heating. A 17-hour endurance test was conducted at 900°F and no change in the emittance occurred. When the specimen was heated to 1450°F the emittance dropped to 0.56. During cooling the emittance was about 6 per cent lower than that measured during heating.

7. Silicides - Molybdenum Disilicide

A 2-mil thick coating of molybdenum disilicide (MoSi_2) was plasma-arc sprayed onto both sides of a molybdenum strip by the Linde Plasmarc process.

The specimen was tested in the total hemispherical emittance rig and data are shown in Figure 156 and in Table 114. The total hemispherical emittance values increased from 0.50 at 200° to 0.66 at 1500°F.

8. Miscellaneous Sprayed Coatings

a. Iron Oxide

A 1.8-mil thick coating of iron oxide was aluminum-phosphate bonded onto a nickel strip. The iron oxide used was derived from Ferro Black Label clay.

The specimen was endurance tested for 210 hours at a nominal temperature of 1350°F in the total hemispherical emittance rig. Total hemispherical emittance values are shown in Figure 157 and Table 115. During the first 120 hours of endurance testing the emittance increased from 0.65 to 0.75. No change occurred during the remaining 90 hours of exposure to 1350°F, but an additional rise in emittance to 0.78 occurred during cooling. To confirm that the increase in values resulted from a change in the specimen, the specimen was cooled to room temperature and new thermocouples were installed. The data obtained with the new thermocouples confirmed the emittance increase.

b. Oxidized Kennametal K-151-A

The powder used in this coating was obtained from Kennametal, Inc. and supplied as having particles between 53 and 88 microns in diameter. The powder was oxidized by the supplier for 20 minutes at 1600°F so data could be obtained to compare with work conducted by Wade and Casey¹¹ on oxidized sheets of this material. A 4-mil thick coating was plasma-arc sprayed on an AISI-310 stainless steel tube. The coating was dark grey, fairly hard, and had a fair coating-substrate bond strength. Its matte texture was similar to that of 40-grit emery cloth. The total hemispherical emittance of the coating was measured from 700°F to 1600°F in the spectral normal emittance rig. On each successive run the emittance of the coating decreased, as may be seen in Table 116 and in Figure 158. Between heating Run 1 and cooling Run 3 the emittance at 700°F decreased from 0.85 to 0.82, but the differences were less at higher temperatures. To determine if any further changes will occur, an endurance test should be conducted. The visual characteristics of the coating did not change during testing.

Comparison of the data reported by Wade and Casey with that reported here shows fair agreement when the different methods of specimen preparation and test conditions are considered. Wade and Casey prepared their specimen by oxidizing flat sheets of Kennametal rather than by plasma-arc spraying oxidized powder onto a substrate. Further, Wade and Casey measured emittance in air while Pratt & Whitney Aircraft measurements have been in vacuum.

c. Krylon Black

Krylon Coating 1.3 Mils Thick - A coating of Krylon Black 1.3 mils thick was applied to each side of an AISI-310 stainless steel strip. Krylon Black is a commercial blackening compound produced by the Krylon Company of Morristown, Pennsylvania. It is a mixture of carbon black and silicates in a lacquer carrier. The coating applied to the specimen had an average surface density of 0.0229 gm/cm^2 .

The specimen was tested in the total hemispherical emittance rig between 300° F and 1700° F . The total hemispherical emittance data is shown in Figure 159 and in Table 117. Between 300° F and 600° F the emittance was relatively constant at about 0.89. Between 600° F and 700° F a sharp drop in emittance to a level of 0.80 occurred, together with severe outgassing. For the remainder of the test the emittance varied from 0.77 to 0.82.

Visual observation of a similar specimen in a glass chamber indicated a change in the appearance of the coating which is attributed to sublimation of the lacquer binder. After this change has taken place the coating can be easily rubbed off, although in its original condition it cannot. Inspection of the specimen tested in the emittance rig indicated minute spots of metal shining through the coating. It is presumed that the drop in emittance between 600° F and 700° F was caused either by the loss of the binder with the possible loss of some of the coating material, or by the reduced surface density of the coating after loss of the binder.

Krylon Coating 3 Mils Thick - A coating of Krylon Black 3 mils thick was applied to each side of an AISI-310 stainless steel strip,

The emittance data is listed in Table 118 and is plotted in Figure 159. No explanation for the seemingly erratic emittance data can be offered at this time. Since this coating does not appear to be a practical one for space radiator applications, no further testing was conducted.

d. Palladium Black

Palladium black was prepared at Pratt & Whitney Aircraft by dissolving Engelhard alloy sheet stock containing 75 per cent palladium and 25 per cent silver with aqua regia. The solution was then diluted with distilled water to precipitate out all of the silver as silver chloride. The precipitate was removed by filtration and sodium hypophosphite was added to reduce the palladium ions to palladium black. A second filtering removed the palladium black which was given a final rinse with distilled water.

The palladium black was aluminum-phosphate bonded to AISI-310 stainless steel and tested in the total hemispherical emittance rig. Before testing, the olive drab coating was 1 mil thick, hard, and had a good coating-substrate bond strength. The texture of the coating was similar to that of 320-grit emery cloth and had a glassy appearance. The total hemispherical emittance of the specimen was measured between 300° and 1500°F. The data presented in Table 119 and in Figure 160 indicate that this 1-mil thick coating was partially transparent at temperatures lower than 700°F, since the total emittance increased from about 0.66 at 300°F to approximately 0.86 at 700°F and then leveled off. The emittance remained at about this level up to a temperature of 1300°F, and then began decreasing as the temperature was increased to 1500°F. At 1500°F the total emittance was about 0.80. Between 1400°F and 1500°F the temperature was continuously drifting upwards at a given power setting, indicating that the coating properties were changing. As a result of these changes, no measurements were made at higher temperatures. When the temperature was decreased, the emittance values obtained were found to be much lower than those recorded during heating. This further confirmed that a change in the coating properties had occurred. After removal of the specimen from the rig, it was apparent that the coating had separated from the substrate, but no other visible characteristics were found to have changed. Both before and after testing, Pd was the only phase detected by x-ray diffraction analysis.

e. Titanium Oxide and Aluminum Oxide

A blend of 50 per cent titanium oxide, TiO_2 , and 50 per cent aluminum oxide, Al_2O_3 , was plasma-arc sprayed onto a molybdenum strip, an AISI-310 stainless steel tube, and onto aluminum strips. The blend was Metco, Inc. XP-1121 and the Metco spraying process was used. All of the specimens were tested in the total hemispherical emittance rig.

Coated Stainless Steel - The stainless steel strip was plasma-arc sprayed on both sides with a 2.4-mil thick coating. The specimen was instrumented for testing in the total hemispherical emittance rig. The test data are shown in Figure 161 and in Table 120. The specimen was heated initially to 1350°F (Run 1). Over this temperature range, the total hemispherical emittance varied between 0.84 and 0.87. During the following 95 hours of endurance testing at a nominal temperature of 1340°F, a slight increase in the emittance level occurred. The specimen was then subjected to a cooling-heating cycle, that is, it was cooled to 300°F and reheated to 1700°F. As shown in Table 120, the data obtained during this cycle were consistent in that the emittance values obtained while the temperature was being raised to 1340°F agreed with those obtained while the temperature was being lowered from the previous maximum of 1340°F. However, the emittance level during this cycle was approximately two per cent higher than that during the initial heating phase. During the heating phase above 1400°F, the data indicated a continuous increase in emittance until, at 1718°F, an emittance of 0.95 was recorded.

Since an emittance value greater than 1.0 was obtained after an overnight period at 1700°F, the test was stopped to determine the reliability of the thermocouple indication. This investigation revealed that thermocouple poisoning occurred at a temperature above 1200°F and was aggravated by running at temperatures higher than this, but no significant amount of poisoning was noted up to 1350°F. From this check, it was concluded that the data obtained up to 1350°F during Run 1 and the endurance data presented in Table 120 were reasonably accurate.

Coated AISI-310 Stainless Steel - The coated stainless steel specimen was heated to 1450°F and maintained at this temperature for 310 hours. The total hemispherical emittance at this temperature was approximately 0.83 for the entire duration of the test.

Total hemispherical emittance was measured from 300°F to 1450°F before endurance testing began. The total hemispherical emittance

of the specimen is shown in Figure 161 and Table 121. As may be seen in Figure 161, the total hemispherical emittance increased slightly with increasing temperature.

Coated Aluminum - Specimens were prepared with coating thicknesses of 0.8, 1.9, and 3.7 mils. The emittance data are presented in Figure 161 and in Table 122.

Comparison of these results with results from the coated stainless steel and coated molybdenum specimens, reveals a considerable difference in emittance levels. The emittance level for the aluminum strip with the 3.7-mil thick coating was about 0.8 whereas the level was about 0.85 for the 2.4-mil thick coating on molybdenum. The emittance of the coated stainless steel specimen is in good agreement with that of the 3.7-mil thick coated aluminum specimen up to about 800°F.

Two additional aluminum fins were coated for thermal cycling and bend testing. Coating thicknesses were approximately 2 and 6 mils respectively. Bend testing of the specimen with the thinner coating resulted in no spalling. The thick coating, however, spalled heavily on both sides and the aluminum substrate was found to be very brittle after testing.

C. Electrophoretic Coating - Silicon Carbide

A coating of silicon carbide 6 mils thick was applied to a molybdenum strip by an electrophoretic process at Vitro Laboratories. To increase the green handling strength, Vitro coated the specimen with an acrylic resin.

Total hemispherical emittance was measured and values varied from 0.80 at 400°F to 0.64 at 2000°F, as shown in Figure 162 and in Table 123. After the initial heating cycle, the emittance tended to decrease with increasing temperature, but the emittance values obtained during cooling cycles were higher than those obtained during heating.

D. Other Coatings

Three coating materials which were not tested for emittance were subjected to thermal cycling and bend testing. A mixture of rare earth oxides was plasma-arc sprayed onto two aluminum fins in thicknesses of about 2 and 6 mils respectively.

Bend testing of the specimens resulted in no spalling of the thinner coating but in heavy spalling from the thicker coating.

Two specimens were prepared with coatings of Parson's optical black lacquer. Heating of the first specimen in vacuum resulted in considerable outgassing which formed a deposit on the glass bell jar and which resulted in a pressure rise of 5×10^{-4} mm Hg. The second specimen was baked in air at 800°F for four hours. The coating became powdery and the color changed from black to green. Since it has been found that this material is not suitable for use in a vacuum, further investigations were not conducted.

Two additional aluminum fins were plasma-arc sprayed with calcium-zirconium-magnesium spinel and subjected to thermal cycling and bend testing. Coating thicknesses were approximately 2 and 6 mils respectively. Although no spalling resulted from bend testing the specimen with the thick coating, moderate spalling occurred during bend testing of the thinner coating.

APPENDIX A

Definition of Terms and Spectral
Emittance Integration

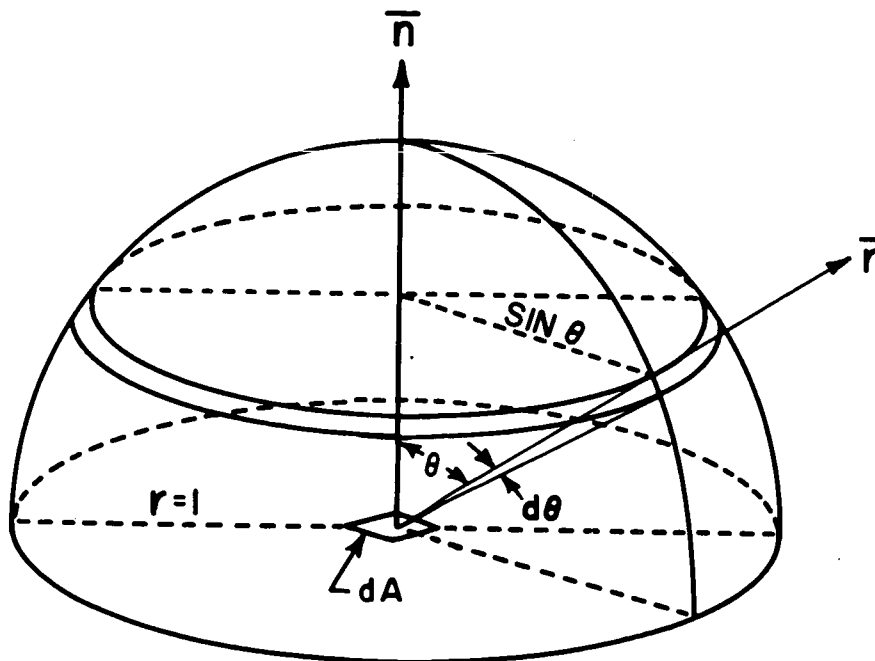
APPENDIX A

DEFINITION OF TERMS AND SPECTRAL
EMITTANCE INTEGRATIONA. Intensity and Emissive Power

The rate of emission of thermal radiation from a surface of area dA in the wavelength range $d\lambda$ about λ , and in the solid angle $d\omega$ about a direction \bar{r} making an angle θ with \bar{n} , the normal to the surface, is a function of the temperature of the surface, T , the material of the surface, and the surface texture, as well as of wavelength λ and θ . This quantity may be expressed

$$d^3E_{\lambda\theta}(T) = I_{\lambda\theta}(T) d\lambda d\omega dA \cos \theta \quad (A-1)$$

where $I_{\lambda\theta}(T)$ is the spectral (or monochromatic) directional intensity of radiation emitted from a surface at temperature T in a direction making angle θ with the surface normal and at wavelength λ . It may be deduced from equation (A-1) that $I_{\lambda\theta}(T)$ is the rate at which the area dA radiates energy in a given direction \bar{r} per unit wavelength, per unit solid angle, and per unit of its own area, as projected on a plane perpendicular to the given direction.



A black surface is defined as a surface which absorbs all radiant energy incident upon it. For a black surface, the monochromatic directional intensity of emitted radiation, $I_{\lambda\theta}(T)$, is independent of θ and is given by the Planck radiation law

$$I_{\lambda\theta b}(T) = I_{\lambda b}(T) = \frac{2c^2 h \lambda^{-5}}{e^{hc/\lambda kT} - 1} = \frac{C_1 \pi^{-1} \lambda^{-5}}{e^{C_2/\lambda T} - 1} \quad (A-2)$$

where $I_{\lambda b}(T)$ is the monochromatic intensity of radiation of a black surface in power per unit area of projected surface area, per unit wavelength, and where

λ is the wavelength

c is the speed of light

h is Planck's constant

k is the Boltzmann constant,

C_1 is the first radiation constant and equals $2\pi hc^2$

C_2 is the second radiation constant which equals ch/k

b indicates "for a black surface"

The total directional intensity of radiation is the rate at which the area dA radiates energy in the direction \bar{r} over all wavelengths per unit solid angle and per unit of its own area as projected on a plane perpendicular to the given direction. This quantity, $I_{\theta}(T)$, is obtained by integrating $I_{\lambda\theta}(T)$ with respect to wavelength over all wavelengths

$$I_{\theta}(T) = \int_{\lambda=0}^{\infty} I_{\lambda\theta}(T) d\lambda \quad (A-3)$$

For a black surface, $I_{\lambda\theta}(T)$ is independent of θ and equals $I_{\lambda b}(T)$, and the integration of equation (A-3) for this case may be carried out after substituting equation (A-2). This yields the total directional intensity of radiation for a black surface (which is independent of θ)

$$I_b(T) = \int_{\lambda=0}^{\infty} I_{\lambda b}(T) d\lambda = \frac{2\pi^4 k^4 T^4}{15c^2 h^3} = \sigma T^4 / \pi \quad (A-4)$$

where σ is the Stefan-Boltzmann constant, and equals

$$(2\pi^5 k^4) / (15c^2 h^3)$$

Consider a black surface at a particular temperature viewed by a spectrophotometer with fixed optics. Provided that this isothermal black surface fills the field of view of the spectrophotometer, the output of the spectrophotometer will be independent of its distance away from the surface and of the angle at which it views the surface. This situation is true whether the spectro-

photometer accepts monochromatic radiation in a particular wavelength band or radiation over the entire spectrum emitted. These results may be derived directly from the fact that the intensity of radiation emitted from a black surface (either monochromatic or total) is independent of θ . It is thus apparent that in this case, the spectrophotometer output gives a measure of radiant intensity of the surface viewed. For a dual-beam spectrophotometer operated in the ratio mode, the recorded ratio is a measure of the ratio of intensities of the two surfaces viewed, provided that the optical paths from surface to detector are completely identical.

The monochromatic emissive power at wavelength λ of a surface is the rate of emission of thermal radiation into the entire space above the surface per unit area of the surface and per unit of wavelength. This may be obtained for isotropic surfaces by integrating $I_{\lambda\theta}(T)\cos\theta$ over the 2π steradians of solid angle above the surface. The monochromatic emissive power is thus

$$E_{\lambda}(T) = \int_{\theta=0}^{\pi/2} [I_{\lambda\theta}(T)\cos\theta][2\pi\sin\theta d\theta] \quad (A-5)$$

where $I_{\lambda\theta}(T)\cos\theta$ is the rate of emission of thermal radiation per unit of surface area, per unit of wavelength, and per unit of solid angle in the direction θ , and $2\pi\sin\theta d\theta$ is the differential solid angle in the direction θ . For a black surface $I_{\lambda\theta}(T)$ is replaced by $I_{\lambda b}(T)$, which is not a function of θ , and equation (A-5) may be integrated directly, giving

$$E_{\lambda b}(T) = \pi I_{\lambda b}(T) \quad (A-6)$$

where $E_{\lambda b}(T)$ is the monochromatic emissive power of a black surface at temperature T and wavelength λ , i.e., the rate of emission of thermal radiation from a black surface into the entire space above the surface per unit area of the surface and per unit of wavelength.

The total emissive power of a surface is the rate of emission of thermal radiation per unit area of the surface and over all wavelengths. It may be obtained by integrating $E_{\lambda}(T)$ over all wavelengths. Thus, the total emissive power of a surface at temperature T is

$$E(T) = \int_{\lambda=0}^{\infty} E_{\lambda}(T) d\lambda \quad (A-7)$$

For a black surface, $E_{\lambda}(T)$ may be replaced in equation (A-7) with $\pi I_{\lambda b}(T)$, by virtue of equation (A-6). The resulting integral is π times the integral of equation (A-4). The total emissive power of a black surface at temperature T may thus be written

$$E_b(T) = \pi \int_{\lambda=0}^{\infty} I_{\lambda b}(T) d\lambda = I_b(T) = \sigma T^4 \quad (A-8)$$

Alternately, the total emissive power of a surface may be obtained by integrating $I_{\theta}(T) \cos \theta$ over the 2π steradians of solid angle above the surface. Thus

$$E(T) = \int_{\theta=0}^{\pi/2} [I_{\theta}(T) \cos \theta] [2\pi \sin \theta d\theta] \quad (A-9)$$

where $I_{\theta}(T) \cos \theta$ is the rate of emission of thermal radiation per unit of surface area, and per unit of solid angle in the direction θ , and $2\pi \sin \theta d\theta$ is the differential solid angle in the direction θ . For a black surface, $I_b(T)$ as given by equation (A-4) may be substituted for $I_{\theta}(T)$ in equation (A-9) and the integration over θ performed directly. This procedure, of course, simply yields the final form of equation (A-8) for the total emissive power of a black surface.

From equation (A-6) and the second form of equation (A-8), the useful ratio equality may be formed

$$\frac{E_{\lambda b}(T)}{E_b(T)} = \frac{I_{\lambda b}(T)}{I_b(T)} \quad (A-10)$$

B. Emittance - Definitions

All real surfaces depart from the Planck and Stefan-Boltzman radiation laws by varying degrees. In order to describe the radiation emitted from real surfaces, various emittances (emissivities, for optically smooth surfaces), may be defined. In the subject tests, two of these have been measured, namely, total hemispherical emittance and spectral normal emittance. A third, total normal emittance, was calculated from spectral normal emittance data. The difference between total hemispherical and total normal emittance is discussed in the next section.

Total hemispherical emittance of a surface at temperature T is defined as the ratio of the total emissive power of the surface at T , $E(T)$, to emissive power of a black surface at the same temperature, $E_b(T)$. Total hemispherical emittance is thus

$$\epsilon_{th}(T) = \frac{E(T)}{E_b(T)} \quad (A-11)$$

Spectral directional emittance of a surface at temperature T , at wavelength λ , and for a direction making an angle θ with the surface normal, is defined as the ratio of monochromatic directional intensity at T and λ in direction θ for the surface, to the monochromatic intensity of radiation at wavelength λ from a black surface at temperature T . Thus, spectral directional emittance is defined as

$$\epsilon_{\lambda\theta}(T) = \frac{I_{\lambda\theta}(T)}{I_{\lambda b}(T)} \quad (A-12)$$

Spectral normal emittance is the value of spectral directional emittance for the case where θ equals zero. Denoting normal quantities with the subscript n , spectral normal emittance is defined as

$$\epsilon_{\lambda n}(T) = \frac{I_{\lambda n}(T)}{I_{\lambda b}(T)} \quad (A-13)$$

Total directional emittance of a surface at temperature T and in a direction making an angle θ with the surface normal is defined as the ratio of total directional intensity at T in direction θ for the surface, to the total intensity of radiation from a black surface at temperature T . Thus, total directional emittance is defined as

$$\epsilon_{\theta} = \frac{I_{\theta}(T)}{I_b(T)} \quad (A-14)$$

Similarly, the total normal emittance is

$$\epsilon_{tn} = \frac{I_n(T)}{I_b(T)} \quad (A-15)$$

C. Interrelations Between Emittances

The total directional emittance may be related to the spectral directional emittance as follows*: solve equation (A-12) for $I_{\lambda\theta}$ and substitute the value obtained for it in equation (A-3), divide both sides of the resulting equation by I_b and substitute the result into equation (A-14), thus obtaining for the total directional emittance

$$\epsilon_{\theta} = \int_{\lambda=0}^{\infty} \epsilon_{\lambda\theta} \left(\frac{I_{\lambda b}}{I_b} \right) d\lambda \quad (\text{A-16})$$

where the ratio of $I_{\lambda b}$ to I_b can be obtained directly from equations (A-2) and (A-4).

The total hemispherical emittance may be related to the total directional emittance as follows: solve equation (A-14) for I_{θ} and substitute the value obtained into equation (A-9), divide the resulting equation by the second form of equation (A-8), thus obtaining for the total hemispherical emittance

$$\epsilon_{th} = \int_{\theta=0}^{\pi/2} 2\epsilon_{\theta} \sin\theta \cos\theta d\theta \quad (\text{A-17})$$

It is seen that total normal emittance, i.e. the value of ϵ_{θ} for $\theta = 0$, is the value obtained from equation (A-16) if spectral normal emittance is used in obtaining the value of the integral. From equation (A-17) it is readily seen that if ϵ_{θ} is independent of θ , the spectral normal emittance and the total hemispherical emittance are equal. This special case is the situation of a diffusely emitting surface. While an infinite number of possible variations of ϵ_{θ} with θ can yield equality of the spectral normal and the total hemispherical emittances of a surface, the probability of such a case being found is essentially zero.

* In the presentation following this point the temperature dependence of emittances, emissive powers, and intensities is not written, e.g., $I_b = I_b(T)$

In the spectral emittance testing conducted under the present contract, only spectral normal emittances have been measured. However, with some modifications of the spectral rig, it would be possible to measure directional spectral emittances as a function of θ in excess of 45 degrees.

D. Calculation of Total Emittance From Spectral Normal Emittance Data

Using equations (A-4) and (A-6) and letting $\theta = 0$, equation (A-16) may be written as

$$\epsilon_{\tau h} = \int_{\lambda=0}^{\infty} \epsilon_{\lambda n} \left(\frac{E_{\lambda b}}{\sigma T^4} \right) d\lambda = \int_{\lambda=0}^{\infty} \epsilon_{\lambda n} \left(\frac{E_{\lambda b}}{\sigma T^5} \right) T d\lambda \quad (A-18)$$

Since T is constant for each integration, equation (A-18) may be written

$$\epsilon_{\tau h} = \int_{\eta=0}^{\infty} \epsilon_{\lambda n}(\eta) F(\eta) d\eta \quad (A-19)$$

where $\eta = \lambda T$

$$F(\eta) = \frac{E_{\lambda b}}{\sigma T^5} = \frac{(C_1/\sigma)(\eta)^{-5}}{e^{C_2/\eta} - 1}$$

$\epsilon_{\lambda n}(\eta) = \epsilon_{\lambda n}$ expressed as a function of η .

The expression $\int_{\eta_1}^{\eta_2} \epsilon_{\lambda n}(\eta) F(\eta) d\eta$ is integrated graphically over the range of η corresponding to the wavelength range in which data is obtained, λ_1 to λ_2 . The error incurred from the lack of data over the entire wavelength range from zero to infinity is usually very small, and it may be reduced even further by estimating a correction. For this purpose, it is assumed 1) that the spectral emittance is constant from the longest wavelength measured λ_2 , to infinity, and is equal to the spectral emittance at the longest wavelength measured, and 2) that the spectral emittance is constant from zero wavelength to the shortest wavelength measured λ_1 , and

is equal to the spectral emittance at the shortest wavelength measured. The final equation for total normal emittance is then

$$\epsilon_{tn} = \epsilon_{\lambda n}(\eta_1) \int_0^{\eta_1} F(\eta) d\eta + \int_{\eta_1}^{\eta_2} \epsilon_{\lambda n}(\eta) F(\eta) d\eta + \epsilon_{\lambda n}(\eta_2) \int_{\eta_2}^{\infty} F(\eta) d\eta \quad (A-20)$$

The evaluation of the first and last terms can be simplified by using the tables contained in Reference 12, where $\int_0^{\eta_1} F(\eta) d\eta$ is written as $\frac{E_b(0-\lambda T)}{\sigma T^4}$ and is tabulated as a function of λT .

APPENDIX B

Theoretical Evaluation of the Effect of Reflections
from the Container Walls on Measurements of Emittance

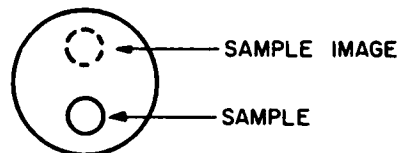
APPENDIX B

THEORETICAL EVALUATION OF THE EFFECT OF
REFLECTIONS FROM THE CONTAINER WALLS ON
MEASUREMENTS OF EMITTANCEA. Determination of Reflected Energy Incident on the Specimen

The accurate determination of the total and spectral emittance of a test specimen requires that the energy radiated by the specimen be absorbed by the walls of the chamber in which it is tested. The effectiveness of the chamber walls in minimizing reflected energy, therefore, depends not only on the absorptance of the walls, but also on the geometry of the system, including the size of the specimen compared to the size of the chamber.

Both diffuse and specular reflectance are considered in evaluating the container, even though specular reflection effects from the rough walls of the container are believed to be small compared to diffuse reflection effects.

1. Specular Reflection - Assume that a cylindrical specimen is located in a cylindrical chamber parallel to, but off the axis of the chamber as shown. Let the chamber wall have a reflectivity r_w , and let the specimen emit radiant energy



at a rate P_0 . The portion of P_0 that is reflected from the chamber wall P_1 is then equal to $P_0 r_w$. This once-reflected radiation forms an image of the specimen at the conjugate focal point. The power P_1 emanating from this image is reflected a second time from the chamber wall. The twice-reflected radiation then forms an image at the specimen location with power P_2 where $P_2 = P_1 r_w = P_0 r_w^2$. Neglecting further wall reflections, P_2 is the maximum power that could be reflected back to the specimen surface. However, due to aberration, the image formed at the specimen is larger than the actual specimen, and F_r , the maximum fraction of P_0 representing the twice-reflected power incident on the specimen, is less than r_w^2 . Thus, for r_w equal to 0.1, F_r is less than 0.01.

2. Diffuse Reflection - In this case, the calculation of the portion of the energy emitted by the specimen that reflects back onto the specimen surface depends on the following assumptions:

- a) The reflectivity of the walls is so low that multiple specimen-to-wall reflections need not be considered.
- b) The radiant flux density of the wall-reflected radiation inside the container is uniform and isotropic. This is a valid assumption if the walls reflect diffusely.

Let the specimen emit radiation at a rate P_0 . If A_s is the surface area of the specimen, then the radiant flux density resulting from P_0 just outside the specimen is P_0/A_s . The radiant flux density of this outbound radiation at the container wall φ_w , is P_0/A_w , where A_w is the inside surface area of the container wall. At the wall, the radiant flux density of the portion of P_0 surviving a first reflection is $\varphi_w r_w = P_0 r_w / A_w$. By assumption b), this quantity equals the radiant flux density at the specimen surface of the once-reflected portion of P_0 . Thus the once-reflected energy incident on the specimen surface is $\varphi_w r_w A_s$, or $P_0 r_w A_s / A_w$. F_r , the fraction of P_0 representing this once-reflected energy, is thus $r_w A_s / A_w$. For a 1/4-inch diameter specimen tube in a 3-inch diameter chamber, with r_w equal to 0.1, F_r equals 0.008.

B. Correction of Spectral Emittance Measurements for Effect of Container Wall Reflectance

The part of the power radiated by the specimen that returns to the specimen is $P_0 F_r$. If the reflectivity of the specimen surface is r_s , then part of this reflected energy, $r_s P_0 F_r$, is reflected by the specimen and joins the radiation directly emitted from the specimen. Therefore, the power of the measuring beam entering the spectrophotometer includes not only directly emitted power from the specimen surface, but an additional increment of reflected power equal to $r_s F_r$ times the directly emitted power. As a result, the value of the spectral emittance determined by the procedure outlined in Section VI of this report should be corrected by multiplying by the factor $\frac{1}{1+r_s F_r}$. For F_r equal to 0.01 and r_s equal to 0.9, the corrected value is lower than the uncorrected value by less than 1 per cent.

C. Correction of Total Hemispherical Emittance Measurements for Effect of Container Wall Reflectance

A complete power balance on the specimen must include the following:

1. Power input
 - a) Heat generation in the specimen due to joule heating
 - b) Radiant power absorbed by the specimen
 - 1) originally emitted by the container wall and falling on the specimen
 - 2) originally emitted by the specimen, reflected by the container wall, and finally incident upon the specimen
2. Power output
 - a) Radiant power emitted by the specimen
 - b) Conduction of heat away from the specimen into the end electrodes, and into the thermocouple and potential leads

Neglecting items 1. b) 2) and 2. b), assuming that the container wall is black, and assuming that the absorptance of the specimen for directly emitted wall radiation is the same as the specimen total hemispherical emittance at the specimen temperature, then the equating of the remaining terms, 1.a), 1.b) 1), and 2.a), gives

$$P_e + A_s \epsilon_{th} \sigma T_w^4 = A_s \epsilon_{th} \sigma T_s^4$$

where P_e is the electrical heat generation rate in the specimen

T_w is chamber wall temperature

T_s is specimen temperature

This may be shown to be the equation presented in Section III B 2 applied over a test section length equal to the specimen length.

A simple expression for the correction to ϵ_{th} due to the effects of chamber wall reflection is derived by considering the case where the wall temperature term in the equation for ϵ_{th} is negligible. In this case $P_e = A_s \epsilon_{th} \sigma T_s^4$. Now let ϵ be the emittance calculated for the same specimen operating under the same conditions of power and temperature, but with wall reflection effects included. In this case the power balance from 1.a), 1.b) 1), and 2.a), becomes

$$P_e + A_s \epsilon \sigma T_s^4 F_r = A_s \epsilon \sigma T_s^4$$

Eliminating P_e between the expressions for ϵ_{th} and ϵ , and solving for ϵ_{th}

$$\epsilon_{th} = \epsilon(1 - \epsilon F_r) = \epsilon(1 - \epsilon r_w A_s / A_w)$$

for a diffuse reflecting chamber wall. For r_w of 0.1 and ϵ of 0.9, the above relation gives ϵ_{th}/ϵ equal to 0.993.

The uncorrected total hemispherical emittance value should therefore be increased by 0.7 per cent. For a lower specimen emittance than selected in the above example or for a lower wall reflectance, the correction is less than 0.7 per cent. The magnitude of the correction obtained by this simple analysis compares favorably with that obtained using the Christiansen equation (Reference 13, Equation 31-10).

APPENDIX C

Unity Emittance Line Characteristics and
Application of Unity Emittance Line in
Spectral Emittance Determination

APPENDIX C

UNITY EMITTANCE LINE CHARACTERISTICS AND
APPLICATION OF UNITY EMITTANCE LINE IN
SPECTRAL EMITTANCE DETERMINATION

This appendix discusses the reasons for the nonflatness of the unity emittance line obtained from the Model 13 U Perkin-Elmer spectrophotometer adapted for measurements of spectral emittance and operated in the ratio mode, and explains and justifies the method of calculating spectral emittance from the data obtained.

A. Nonflatness of the Unity Emittance Line

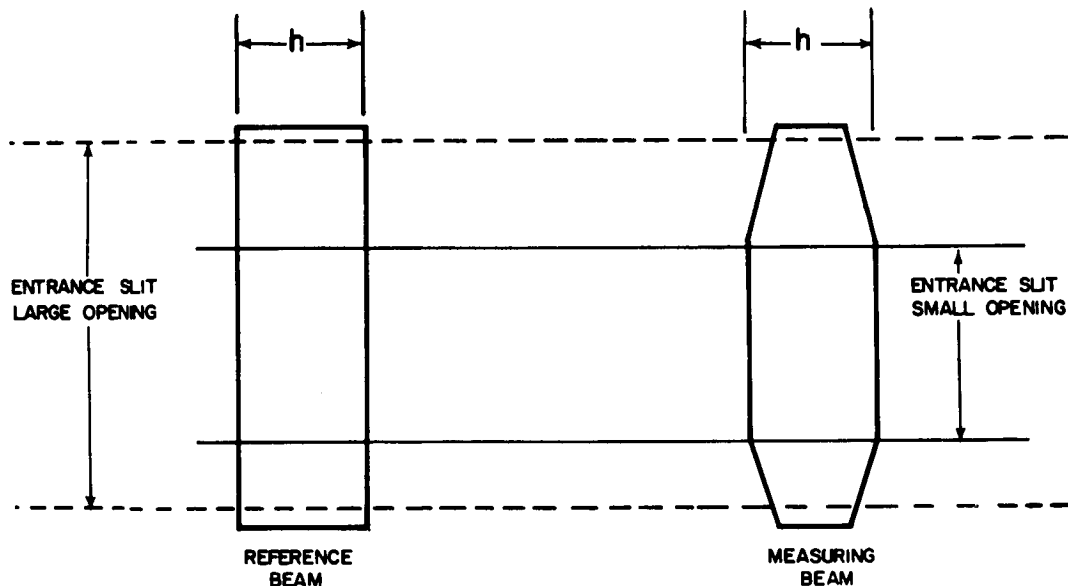
It would be expected that a double-beam spectrophotometer operated in the ratio mode would indicate a beam power ratio of 1.0 at all wavelengths if the reference beam and the measuring beam emanated from adjacent portions of a single black body or from two identical black bodies at the same temperature. It has been found, however, that the plot of beam power ratio vs wavelength (the unity emittance line) varies from unity. The flatness of the unity emittance line may be improved by careful adjustment of the optical system of the spectrophotometer. Initial experiments were conducted to determine whether or not the unity emittance lines obtained with each of the three detectors were within normal limits and it was found necessary to obtain the services of a specialist from the Perkin-Elmer Company to make the necessary adjustments to yield unity emittance lines within the specified tolerances of the instrument.

However, because the two beams travel different optical paths, and because they strike different areas of the detector, their ratio will still vary with wavelength after all possible adjustments have been made.

It may be seen from Figure 6 that the optical paths of the two beams differ. The beams pass through slightly different parts of the window and prism, they are reflected from slightly different portions of certain mirrors, they pass through entirely different slits and are reflected in some cases by entirely different mirrors. Since the transmittances and reflectances of the components of the optical paths are functions of wavelength and since, for different components, or even for different areas of the same component, these functions differ from each other, the result is a variation in the intensity ratio of the two beams and subsequent nonflatness of the unity emittance line.

The combined effects of slight nonuniformities in the motion of the monochromator slit jaws and slight differences in the characteristics of the two beams at the slits, result in additional variations in the intensity ratio of the beams with changes in wavelength.

In normal operation, a servo mechanism varies the width of the entrance and exit slits in unison as the spectrum is scanned so that the detector output corresponding to the reference beam remains constant. If both beams had the same shape and had identical energy distributions across their respective cross-sections, then the change in slit openings would result in the same proportional change for each beam. However, if the beam shapes or energy distributions differ, changes in the slit openings will result in a change in the intensity ratio. As an example, suppose that the reference and measuring beams have the shapes shown in the sketch below, but have equal and uniform intensity. It may be seen that with a large slit opening, more power will pass through



the slit from the reference beam than from the measuring beam. Variations in the characteristics of the beams result from unequal aberrations, slight differences in their respective focus locations relative to the slits, and imperfections in the fabrication or placement of the apertures.

Nonflatness of the unity emittance line is also contributed by the detector. The response characteristic of the detector is a function of wavelength and this function differs for different areas of the detector target and for different incident beam impingement directions. Since the two beams strike the detector at different areas and at different angles, the indicated intensity ratio will vary with wavelength.

B. Emittance Measurement with Nonflat Unity Emittance Lines

A method of correcting the spectral emittance data for nonflatness of the unity emittance line is outlined below. It is noted that at each wavelength the same slit widths must be used when obtaining the specimen and unity emittance lines for the results of the correction to be valid.

Let $\tau_{\lambda 1}$ and $\tau_{\lambda 2}$ represent the combined transmission and detector coefficients for the measuring and the reference beam respectively at wavelength λ . The detector output voltages for the two beams when both originate from adjacent areas in the black-body hole are

$$V_{\lambda 1b} = \tau_{\lambda 1} I_{\lambda b} \Delta \lambda$$

and

$$V_{\lambda 2b} = \tau_{\lambda 2} I_{\lambda b} \Delta \lambda$$

where $I_{\lambda b}$ represents the monochromatic intensity of the black-body radiation at wavelength λ and is expressed in units of power per unit projected surface area per unit solid angle per unit wavelength.

In plotting $V_{\lambda 1b} / V_{\lambda 2b}$, the spectrophotometer plots $\tau_{\lambda 1} / \tau_{\lambda 2}$ as the unity emittance line. If $\tau_{\lambda 1}$ and $\tau_{\lambda 2}$ were independent of wavelength, or if their variations with wavelength were identical, then the unity emittance line would be flat. It has been shown, however, that for several reasons this is not the case.

When emittance data is taken with the measuring beam originating from the surface of the specimen and with the reference beam originating from the black-body hole, the detector output voltages for the two beams are

$$V_{\lambda 1sa} = \tau_{\lambda 1} I_{\lambda sa} \Delta \lambda$$

and

$$V_{\lambda 2b} = \tau_{\lambda 2} I_{\lambda b} \Delta \lambda$$

where $I_{\lambda sa}$ represents the monochromatic intensity of the specimen tube surface. The instrument then plots the specimen emittance line as the ratio

$$\frac{V_{\lambda 1sa}}{V_{\lambda 2b}} = \frac{\tau_{\lambda 1} I_{\lambda sa} \Delta \lambda}{\tau_{\lambda 2} I_{\lambda b} \Delta \lambda}$$

It may now be seen that by dividing the ratio $V_{\lambda 1sa} / V_{\lambda 2b}$ by the ratio obtained for the unity emittance line $V_{\lambda 1b} / V_{\lambda 2b}$, the beam intensity ratio $I_{\lambda sa} / I_{\lambda b}$ will be obtained, thus

$$\frac{V_{\lambda 1sa} / V_{\lambda 2b}}{V_{\lambda 1b} / V_{\lambda 2b}} = \left[\frac{\tau_{\lambda 1} I_{\lambda sa} \Delta \lambda}{\tau_{\lambda 2} I_{\lambda b} \Delta \lambda} \right] \left[\frac{\tau_{\lambda 2} I_{\lambda b} \Delta \lambda}{\tau_{\lambda 1} I_{\lambda b} \Delta \lambda} \right] = \frac{I_{\lambda sa}}{I_{\lambda b}}$$

In connection with this analysis it should be noted that $\Delta \lambda$ has been taken as being the same for all measurements, and that the zero line correction discussed in Section III of this report must also be made, but, for the sake of simplicity, has not been discussed a second time in this appendix.

APPENDIX D

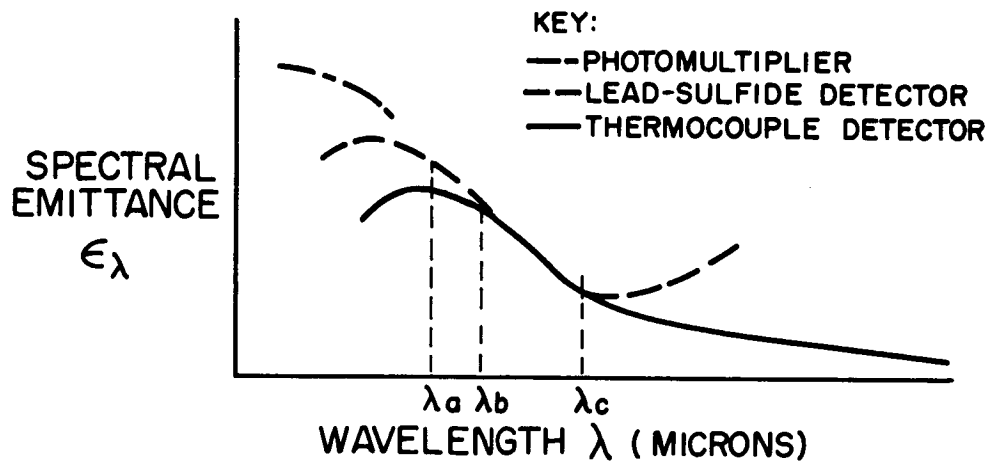
Elimination of Scattered White Light
in the Monochromator as an Appreciable
Source of Error in Spectral Emittance
Data

APPENDIX D

ELIMINATION OF SCATTERED WHITE LIGHT IN THE
MONOCHROMATOR AS AN APPRECIABLE SOURCE OF ERROR
IN SPECTRAL EMITTANCE DATA

1. Determination of the Source of Error

Early in this program it was observed that the data obtained from the spectral emittance rig when using the lead-sulfide detector was erroneous in the wavelength region between 0.67 and 1.15 micron and at wavelengths of 2.7 microns and longer. These regions overlapped those covered by the photomultiplier tube detector and those covered by the thermocouple detector. The curves, as shown in the sketch below, are based upon the results of several tests of a tungsten tube with a triangular cross-section at a temperature of 2000°F. These curves are similar to those obtained with other metals.



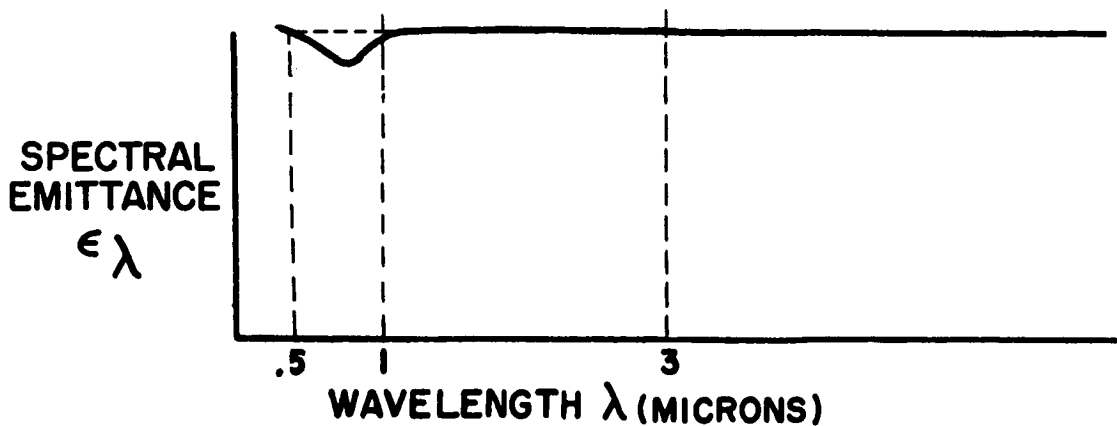
In the shorter wavelength region, the values obtained with the lead-sulfide detector start becoming less than those extrapolated from the values obtained with the photomultiplier tube detector at λ_a (approximately 1.1 micron at 2000°F). The difference between the values increases as the wavelength decreases. A similar phenomenon was observed in the data obtained with the thermocouple detector in the short wavelength region. In this case, the spectral emittance values obtained with the thermocouple detector as compared to those extrapolated from the values obtained with the other two detectors start to fall off at λ_b (approximately 1.15 micron at 2000°F). Again, the discrepancy increases at the

shorter wavelengths. In the longer wavelength region the values obtained with the lead-sulfide detector show a discrepancy in the opposite direction from those obtained with the thermocouple detector, that is, the values obtained with the lead-sulfide detector start becoming larger than those obtained with the thermocouple detector at λ_c (approximately 2.7 microns at 2000°F) and the difference between the two values increases as the wavelength increases.

Initially, it was believed that these discrepancies resulted from nonlinearity of the detectors. If the responses of the detectors were nonlinear, and if the degree of nonlinearity varied with wavelength, data such as that plotted above could be achieved. Such nonlinearity might result from the two beams traveling slightly different optical paths. Tests were therefore conducted using the spectrophotometer in the single-beam mode of operation. The results, however, were substantially identical to those obtained with dual-beam ratio mode of operation.

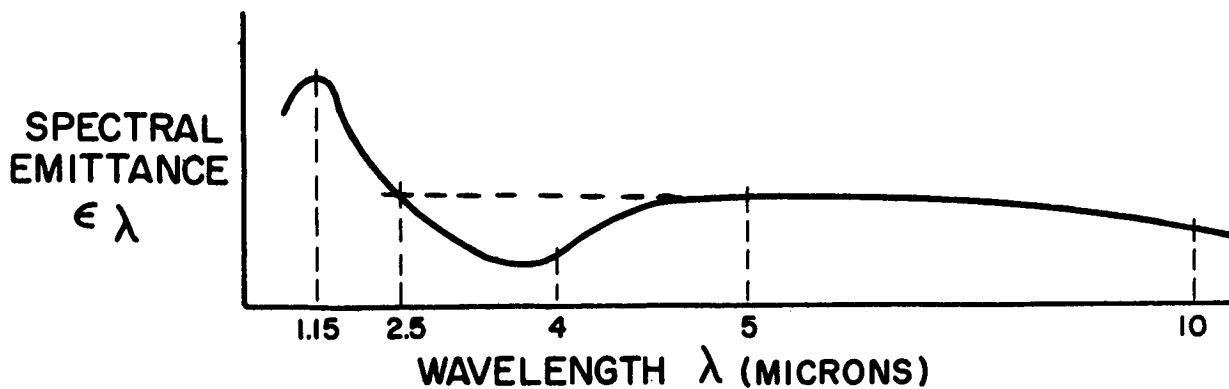
Since the initial work did not indicate the source of error, a program was instituted to gain a better insight into the operation of the spectrophotometer and of the three detectors used for the intensity measurements. To extend the range of spectral data obtained with each of the detectors, tests were conducted using a tungsten sample heated to a higher temperature (3100°F) than that used in previous tests. Spectral emittance data were recorded using both the double-beam and the single-beam modes of operation of the spectrophotometer.

The first tests were conducted using the photomultiplier detector. Data could be recorded at wavelength settings up to 7 microns even though the quartz lens in front of the detector was not capable of transmitting above 4.0 microns and the detector itself was not sensitive above 0.8 micron. Analysis of this data revealed that the emittance value was constant at wavelengths longer than 1 micron and was about 300 per cent higher than the value obtained when using the thermocouple detector. Furthermore, it was noted that this constant value of emittance obtained at the long wavelength settings was exactly equal to the value of emittance that is obtained at the wavelength setting corresponding to the peak response of the photomultiplier at a sample temperature of 3100°F. The data are shown in the sketch below.



It was concluded as a result of this test that the detector had received radiation other than the monochromatic radiation corresponding to the particular wavelength setting of the instrument.

Similar tests were then conducted using the lead-sulfide detector and a similar phenomenon occurred. Data could be recorded at wavelength settings in the 5- to 10-micron range even though the detector itself is not sensitive to radiation at wavelengths longer than 3.5 microns. The emittance values obtained at the longer wavelengths were constant and were equal to the values of emittance obtained at the wavelength setting corresponding to the peak response of the lead-sulfide detector, 2.5 microns. It was also noted that the emittance values started to decrease at a wavelength of approximately 1.15 micron. The data for the lead-sulfide detector is shown below. This data would indicate that radiation other than monochromatic radiation was reaching the lead-sulfide detector.



The unintended radiation which caused the error in the measurements was considered to be white light scattered by the optical components of the monochromator. Further proof that scattered white light was the cause of the error was obtained by running spectrograms of polystyrene in the 7-micron wavelength region when using both the lead-sulfide and the thermocouple detectors. The spectrogram obtained with the thermocouple detector indicated strong absorption lines at wavelengths of 6.925 and 6.71 microns. However, with the lead-sulfide detector, the absorption lines were completely absent (see Figure D-1). Since the lead-sulfide detector was receiving enough energy to operate the slit servo, it was concluded that the detector was being activated by the component of scattered white light that was in the wavelength region of the peak detector response and that the scattering originated in the monochromator.

2. Analysis of the Cause of the Erroneous Data

The value of spectral emittance determined by the spectrophotometer is the ratio of the beam power from the surface of the specimen to that from the black-body hole. The radiant energy of each beam is comprised of the spectral and scattered white light components that pass through the exit slits and are incident on the detector. This ratio may be represented as:

$$\epsilon_{\lambda} = \frac{P_{s\lambda}^* + P_{ss}^*}{P_{b\lambda}^* + P_{bs}^*}$$

where

- ϵ_{λ} is the apparent spectral emittance at wavelength λ
- $P_{s\lambda}^*$ is the surface spectral beam power at wavelength λ
- $P_{b\lambda}^*$ is the black-body spectral beam power at wavelength λ
- P_{ss}^* is the surface scattered beam power in the region of the maximum overall detector response
- P_{bs}^* is the black-body scattered beam power in the region of the maximum overall detector response

If P_{bs}^* and $P_{b\lambda}^*$ are very small compared to $P_{s\lambda}^*$ and P_{ss}^* , then ϵ_{λ} will be very close to the true spectral emittance ϵ_{λ} . On the other hand, if P_{ss}^* and P_{bs}^* are significant compared to $P_{s\lambda}^*$ and $P_{b\lambda}^*$, then ϵ_{λ} will depend on the relative magnitudes of $P_{s\lambda}^*$ and $P_{b\lambda}^*$ as well as the absolute magnitudes of P_{ss}^* and P_{bs}^* . Thus, if the ratio of P_{ss}^* to P_{bs}^* is equal to the ratio of $P_{s\lambda}^*$ to $P_{b\lambda}^*$, then ϵ_{λ} will be equal to the true

value, regardless of the absolute values of P_{ss}^* and P_{bs}^* . However, if the ratio of P_{ss}^* to P_{bs}^* is not equal to the ratio of $P_{s\lambda}^*$ to $P_{b\lambda}^*$, and P_{ss}^* and P_{bs}^* are large compared to $P_{s\lambda}^*$ and $P_{b\lambda}^*$, then the value $\epsilon_{\Delta\lambda}$ will approach the ratio of P_{ss}^* to P_{bs}^* .

When the spectrophotometer is operated at wavelengths where $P_{b\lambda}^*$ is low, the slits open wider to maintain a constant detector output. As a consequence, more power is admitted in the region of the peak detector response, resulting in the value of P_{ss}^* and P_{bs}^* becoming large in comparison with $P_{s\lambda}^*$ and $P_{b\lambda}^*$. When this occurs, the slit servo becomes controlled by P_{bs}^* rather than by $P_{b\lambda}^*$, and $\epsilon_{\Delta\lambda}$ approaches the ratio of P_{ss}^* to P_{bs}^* rather than the ratio of $P_{s\lambda}^*$ to $P_{b\lambda}^*$.

3. Elimination of the Source of Error

To minimize the effect of scattered light components, various optical filters were obtained that would prevent light in the wavebands of peak detector response from entering the monochromator. Any scattering of light at other wavelengths would have little, if any, effect on the values of spectral emittance.

A Corning #4303 blue-green glass filter was obtained for the photomultiplier tube detector, a Schott KG 3 glass was obtained for the lead-sulfide detector, and a water filter, one-half inch thick, was obtained for both the lead-sulfide and thermocouple detectors.

Using a tantalum tube with a triangular cross-section, spectral emittance measurements were obtained both with and without the filters. The data indicated that the filters eliminated the discrepancies in emittance values that had been caused by scattered white light in the monochromator.

SPECTROGRAMS OF POLYSTYRENE FILTER TRANSMISSIVITY VS. WAVE LENGTH

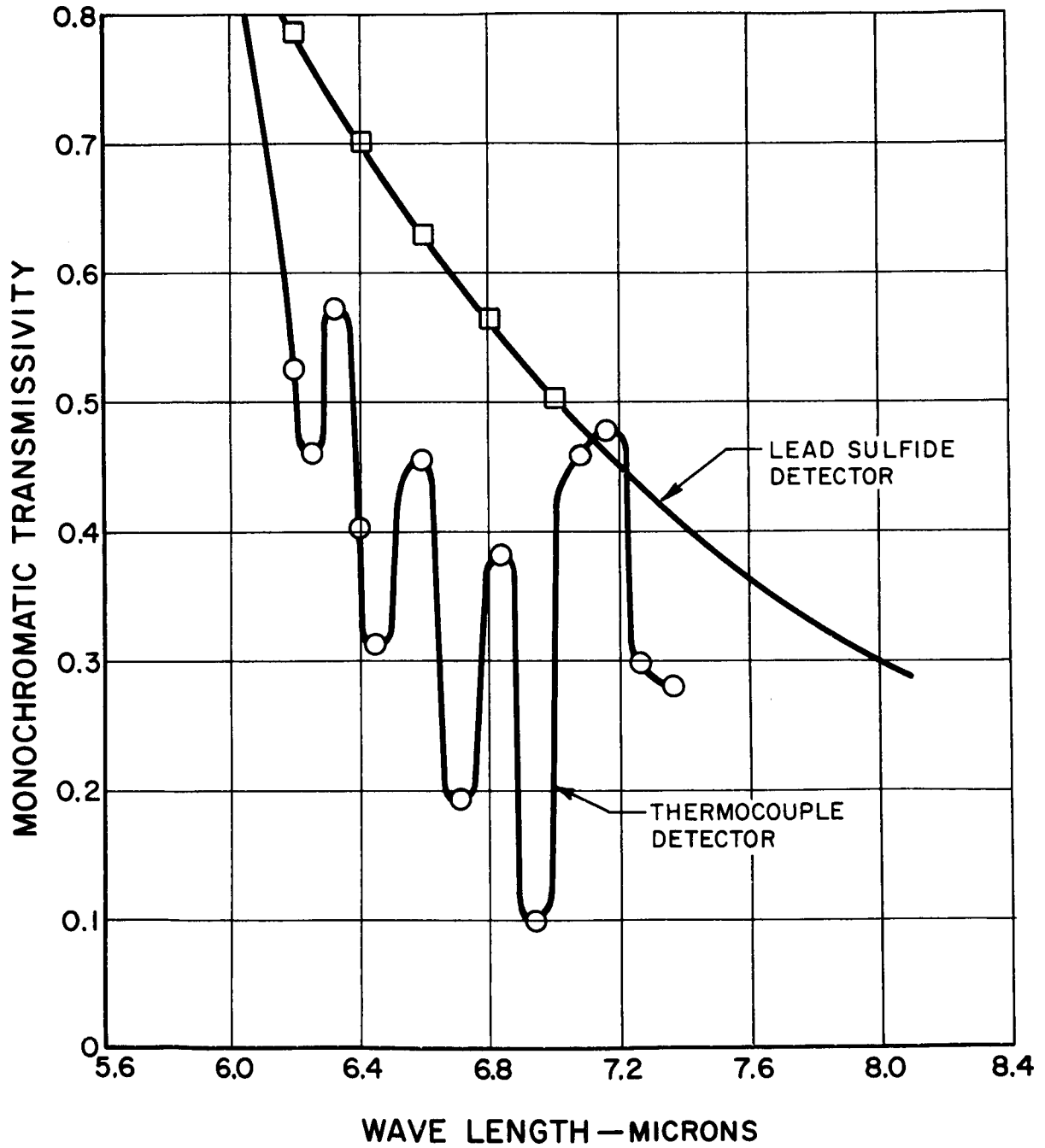


Figure D-1

APPENDIX E

Scattered Light in the External Optics

APPENDIX E

SCATTERED LIGHT IN THE EXTERNAL OPTICS

During the early portion of the program, considerable effort was devoted to determining the magnitude of errors introduced by beam intermixing and scattered light. An early estimate of this error was 1.5 per cent. Beam intermixing can cause large errors since spectral emittance is determined from the ratio of the intensities of the two beams.

There are three possible causes of beam intermixing:

1. Improper positioning of the specimen with respect to the optical system results in the beams emanating from other than the desired areas.
2. Accumulated aberrations in the reflecting elements before the beam isolation apertures result in intermixing. The more serious aberrations were astigmatism associated with the six-inch spherical mirror (M -2 in Figure 11), and combined astigmatism and spherical aberration of the spherical mirror M1. A certain amount of spherical aberration also is introduced by the thick viewing window in the vacuum chamber although this is insignificant compared with that introduced by mirror M1.
3. Light scattered by surface imperfections and foreign material on any of the optical surfaces before the beam isolation apertures.

The first cause may be eliminated by carefully aligning the specimen before each run. The second cause, astigmatism and spherical aberration, may be overcome by providing a black-body hole of sufficient size so that the sampling area within the black body will be well removed from the specimen surface, and, in addition, by selecting the location of the sampling area on the surface so that it will be sufficiently removed from the black-body hole. Scattered light, however, cannot be completely eliminated, although it may be reduced by ensuring superior optical surface conditions. Since the error resulting from scattered light cannot be eliminated, it must either be shown to be insignificant or evaluated so that the data may be corrected.

In a system free from scattered light, the focal regions on the specimen are the only sources of the radiation passing through the beam-

isolating apertures. However, in a system with scattered light, the sources of the scattered light are small areas on the specimen surrounding each individual sampling region as shown in Figure E-1.

The intensity ratio γ of the two beams, as indicated by the spectrophotometer, would be

$$\gamma = \frac{(A_s^* I_{s\lambda} + A_s^+ S_{s\lambda}) \Delta\lambda}{(A_b^* I_{b\lambda} + A_b^+ S_{b\lambda}) \Delta\lambda}$$

Where:

$I_{s\lambda}$ = the monochromatic brightness of the surface sampling region at wavelength λ

$I_{b\lambda}$ = the monochromatic brightness of the black-body sampling region at wavelength λ

$S_{s\lambda}$ = the effective monochromatic brightness of the auxiliary area surrounding the surface sampling region at wavelength λ

$S_{b\lambda}$ = the effective monochromatic brightness of the auxiliary area surrounding the black-body sampling region at wavelength λ

A_s^* = the area of the sampling region on the surface

A_b^* = the area of the sampling region on the black body

A_s^+ = the area of the small auxiliary region which surrounds the surface sampling region and from which originates the major portion of the scattered light component of the surface beam

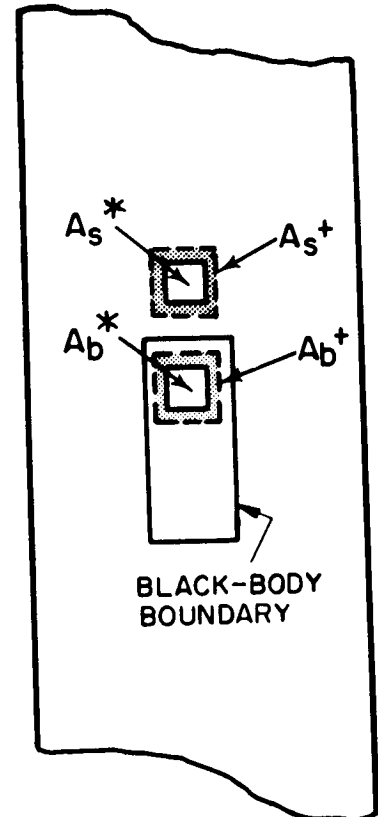


Figure E-1

A_b^+ = the area of the small auxiliary area which surrounds the black-body sampling region and from which originates the major portion of the scattered light component of the black-body beam

Since $A_s^+ S_{s\lambda}$ and $A_b^+ S_{b\lambda}$ are in the same ratio as $A_s^* I_{s\lambda}$ and $A_b^* I_{s\lambda}$, and if the area of A_s and A_b are assumed to be equal for optically similar beams, the ratio γ reduces to the desired emittance ratio, that is

$$\gamma = \epsilon_\lambda = \frac{I_{s\lambda} \Delta\lambda}{I_{b\lambda} \Delta\lambda}$$

In the case shown in Figure E-2, however, the sources of the scattered light are small overlapping areas surrounding the surface and black-body sampling areas. The area A_s^+ surrounding the surface region A_s^* consists of subareas e, f, and g. The area A_b^+ surrounding the sampling region A_b^* , consists of subareas f, g, j, k, and l. The ratio γ indicated by the instrument would be

$$\gamma = \frac{[A_s^* I_{s\lambda} + (e+f) S_{s\lambda} + g S_{b\lambda}] \Delta\lambda}{[A_b^* I_{b\lambda} + (k+g) S_{b\lambda} + (f+k+j) S_{s\lambda}] \Delta\lambda}$$

Because of the presence of a black-body term in the numerator and a surface term in the denominator, this expression cannot be reduced to that for the ideal case, and consequently, the expression would not be valid for use in determining spectral emittance.

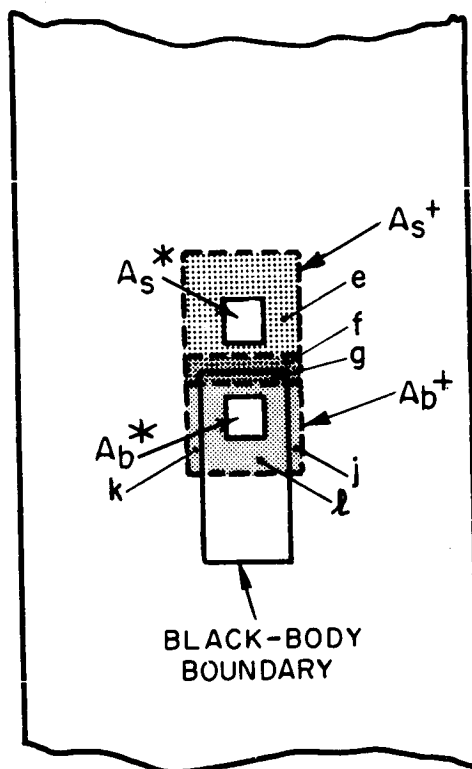


Figure E-2

In the case shown in Figure E-3, the sources of the scattered light in the surface and black-body beams are large areas from which the light in each beam originates more or less uniformly. The area A_s^+ surrounding the sampling region A_s^* consists of the subareas $e, f, g,$ and A_b^* . The area A_b^+ surrounding the sampling region A_b^* consists of the subareas $A_s^*, g, f,$ and h . The ratio γ indicated by the instrument would become

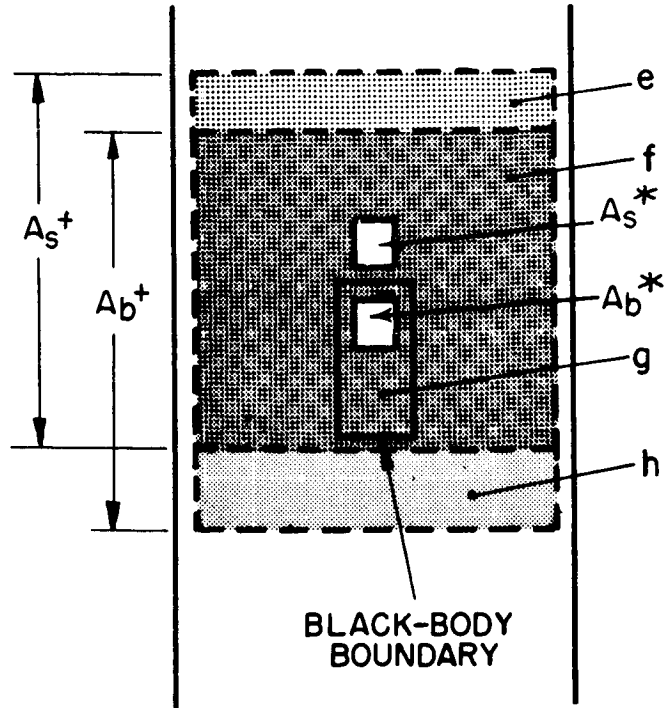


Figure E-3

$$\gamma = \frac{[A_s^* I_{s\lambda} + (e+f) S_{s\lambda} + (A_b + g) S_{b\lambda}] \Delta\lambda}{[A_b^* I_{s\lambda} + g S_{b\lambda} + (A_s^* + f+h) S_{s\lambda}] \Delta\lambda}$$

This expression would also be invalid for spectral emittance because of the intermixing of the beams.

These analyses of the effect of scattered light on the measurement of spectral emittance are oversimplified but serve to illustrate the basic concepts. Under actual test conditions, equal auxiliary areas will not as a rule contribute equal effects. To ascertain the exact nature and magnitude of error introduced by scattered light, tests were conducted to measure the relative contribution to scattered light of each elemental area ΔA of the specimen.

The first test was conducted to determine which portions of the specimen contribute most to scattered light. For this program, the vacuum chamber and specimen were replaced with a 0.005-inch diameter pinhole light source. While operating the spectrophotometer in the single-beam mode, the aperture image was systematically scanned in the fourth quadrant with the source in the stations shown in Figure E-4, and the response of the photomultiplier detector noted at 5640 angstroms as a function of position. For these tests, the salt window was omitted for convenience as it was felt that the amount of scattered light resulting from such a window in good optical condition would be small. The data, as shown in Figure E-4, indicate that when the source was approximately 0.030 inch from the center of the aperture image, the response was 1/8000 of the maximum response. Using the sulfide cell at a wavelength of 2.2 microns, this response at the same position was 1/12500 of the maximum response as shown in Figure E-5. From this test, it was demonstrated that the source of the scattered light is localized around the aperture image.

Tests were then conducted to ascertain the percentage of surface energy which would be scattered into the black-body beam during actual emittance measurements. For these tests, the entire optical system, including the normal 0.100 x 0.100-inch apertures, was arranged and adjusted as it would be for actual measurements, except that a special specimen operated outside of the chamber was employed. This specimen had a triangular cross-section and had both a black-body hole measuring 0.076 inch by 0.035 inch and a second hole of the same size which went entirely through the specimen. (See Figure E-6). The fully oxidized specimen was heated in air to approximately 1800°F. Since the test was conducted in total darkness, room-temperature black-body conditions were obtained with the second hole. The spectrophotometer was operated in the single-beam mode with a salt window in front of the specimen. Two readings were taken, with the monochromator slits wide open, one from each hole. The ratio of the two readings indicated that 0.115 per cent of the black-body radiation resulted from scattered light. With narrower slit openings the percentage was slightly lower. When the salt window was removed, the percentage dropped to 0.037 per cent, which indicates that the salt window is responsible for the major portion of the scattered light.

As a result of these tests, it is evident that the errors caused by aberrant and scattered light may be neglected if a sufficiently large black-body hole is used and if the salt window is in good optical condition.

RESPONSE OF PHOTOMULTIPLIER
 VS
 PINHOLE LIGHT SOURCE POSITION Y, RELATIVE TO
 APERTURE IMAGE WITH X AS A PARAMETER
 IN THE FOURTH QUADRANT

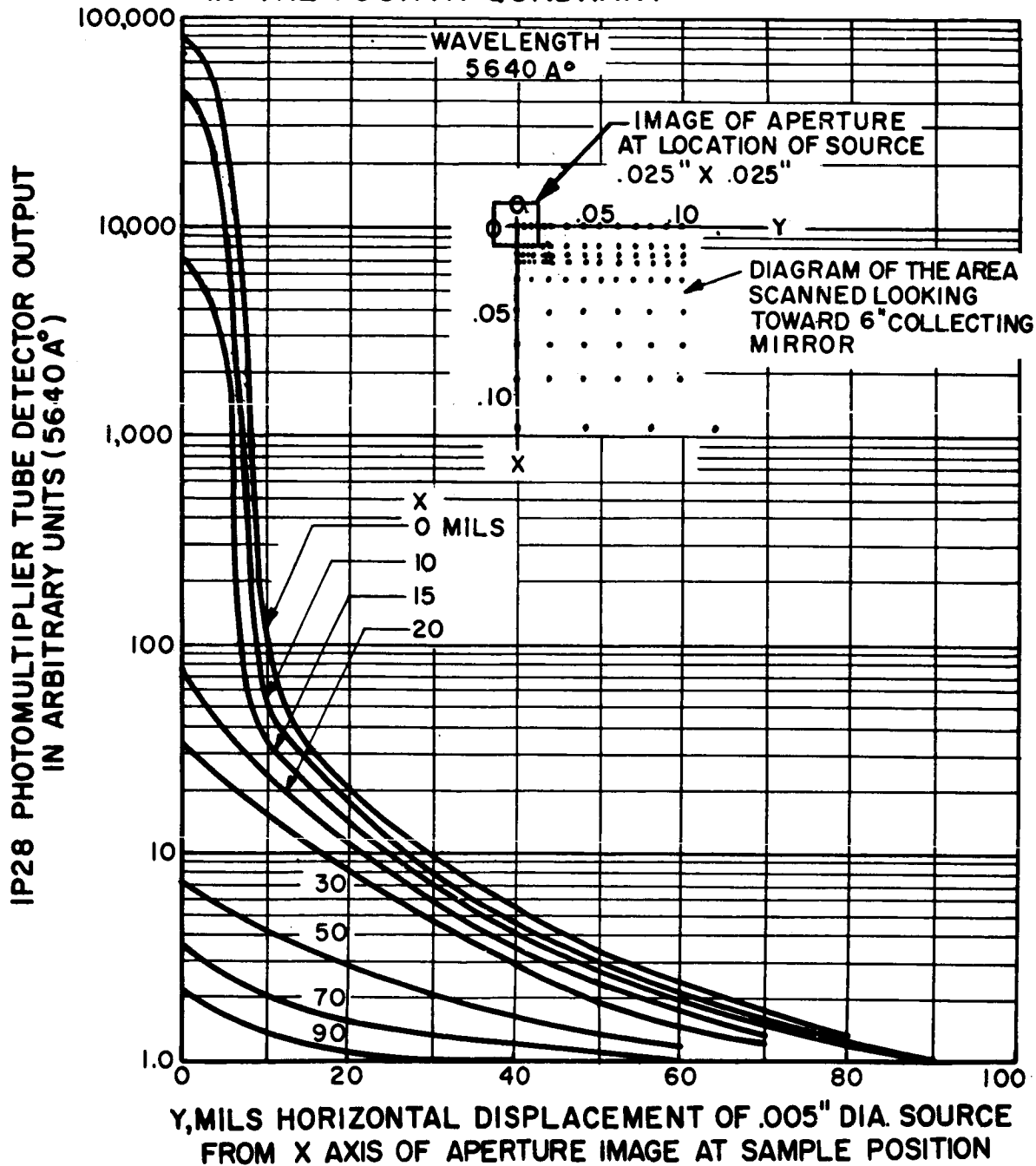


Figure E-4

RESPONSE OF LEAD SULFIDE DETECTOR
VS
PINHOLE LIGHT SOURCE POSITION Y, RELATIVE TO
APERTURE IMAGE

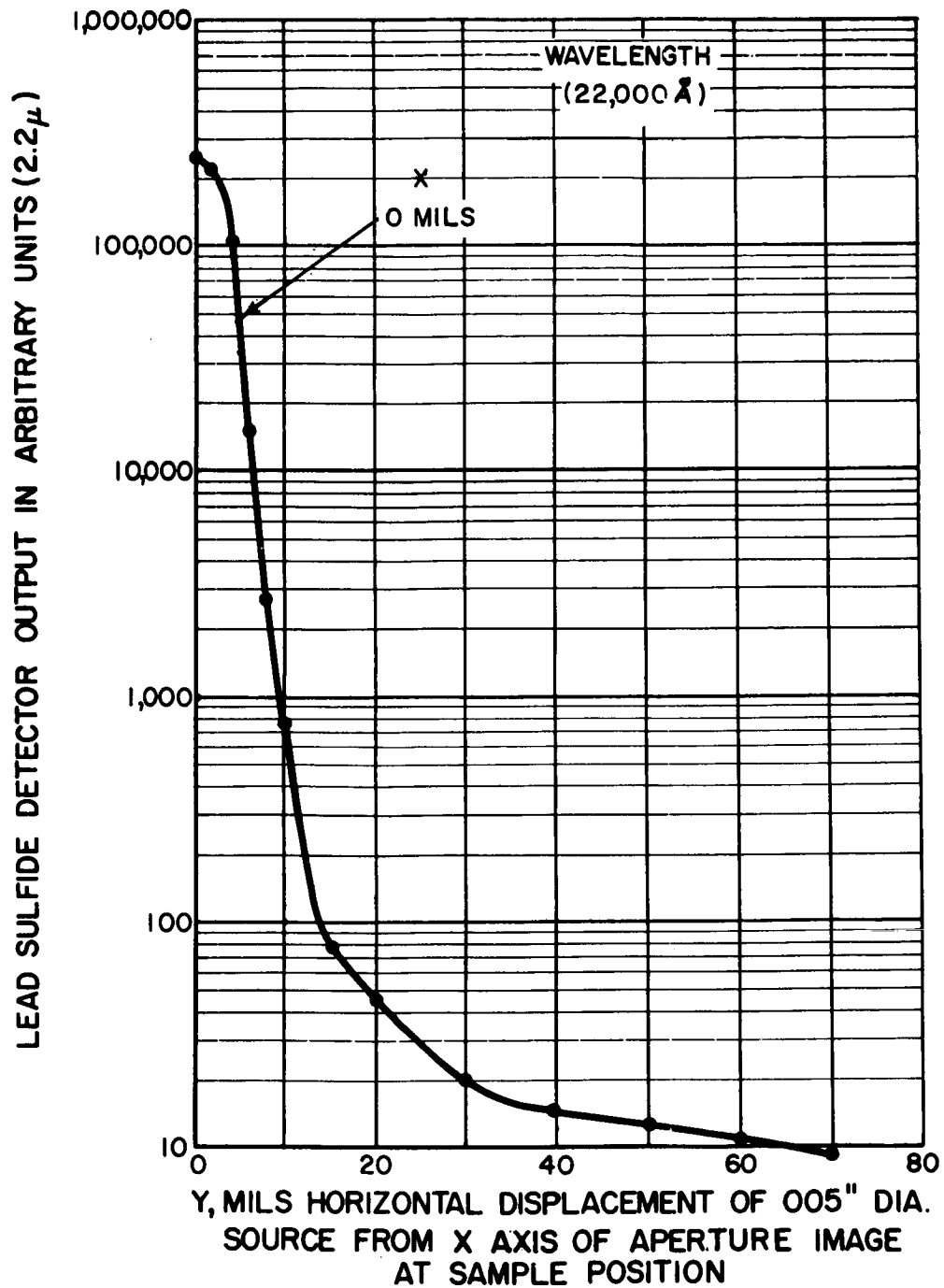
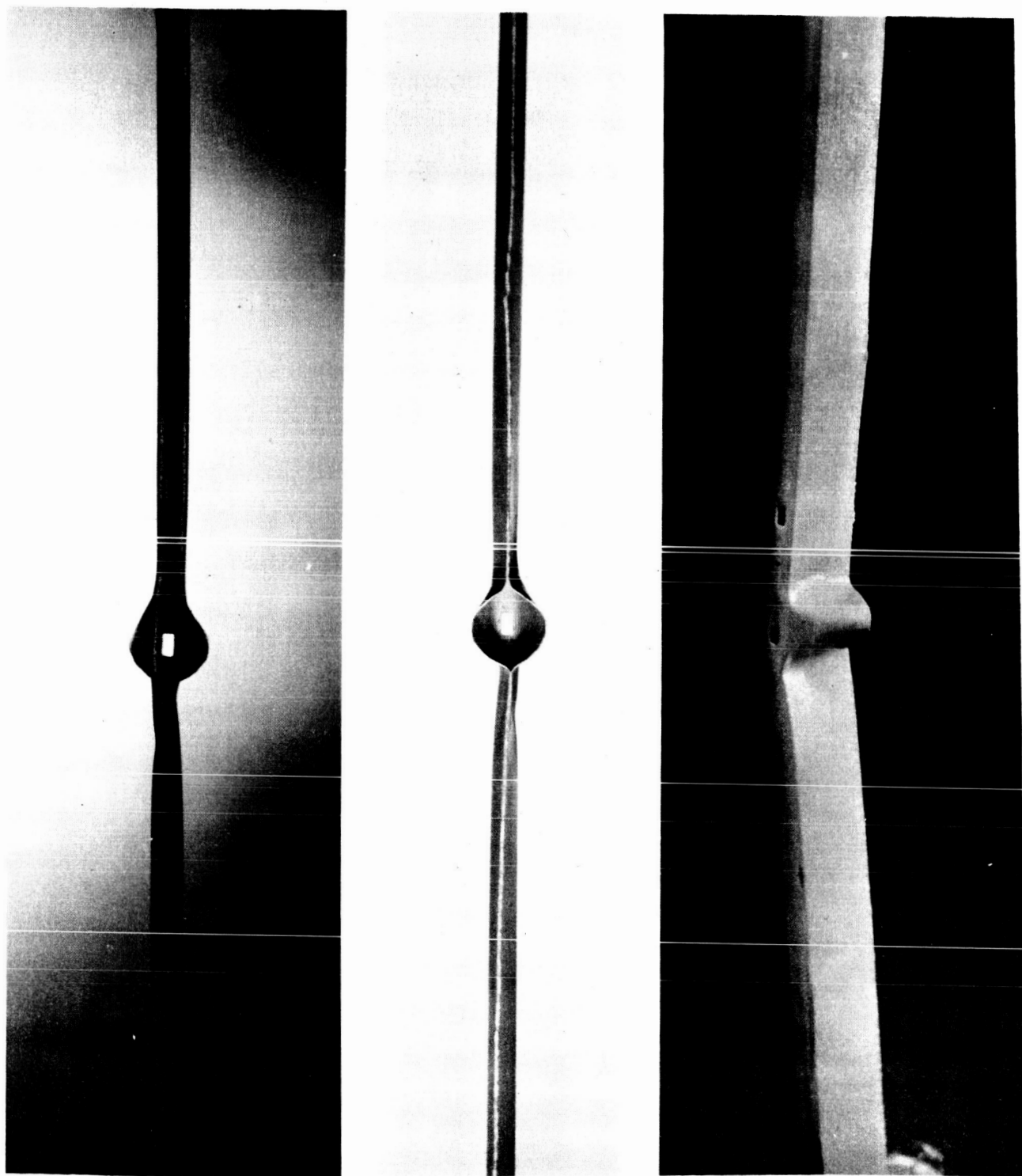


Figure E-5



AISI-310 STAINLESS STEEL SPECIMEN WITH TRIANGULAR CROSS-SECTION USED FOR EVALUATION OF SCATTERED LIGHT IN THE SPECTRAL EMITTANCE RIG

Figure E-6

APPENDIX F
Specimen End Cooling

APPENDIX F

SPECIMEN END COOLING

Conduction of heat away from the test section by the cold electrodes at the ends of a total hemispherical emittance specimen alters the temperature profile within the test section. When the rate of heat conduction becomes appreciable compared to the rate of heat radiation, the equation for total hemispherical emittance expressed in terms of power generation rate, specimen temperature, and sink temperature no longer produces accurate results. End heaters improve the temperature profile, but as the specimen temperature is lowered, the degree of precision required in setting the end-heater and specimen power inputs increases until it is no longer possible to adequately equalize the end- and center-section specimen temperatures.

End-cooling effects may also produce problems in the measurement of spectral normal emittance. Since end cooling alters the temperature profile, the temperature of the black-body and the temperature of the surface may not be equal. This affects the accuracy of spectral data. Black-body defects are discussed in Appendix H.

It is therefore necessary to determine how much temperature profile deviation is permissible and what temperature distribution occurs for given center and off-center temperatures.

A solution to both problems may be obtained by considering a one-dimensional heat balance on an element of length along the specimen axis. Heat is generated in the element of length dx by direct resistance heating at the rate per unit volume g . Heat is radiated from the free surface of the element at a rate per unit area of $\epsilon\sigma [T(x)^4 - T_w^4]$ where $T(x)$ is the specimen temperature at location x and T_w is the sink temperature. In addition, heat is conducted away from the element at a rate per unit volume of $[d/dx][kT(x)]$. Equating the heat generation rate in the element to the outflow from the element by radiation and conduction

$$gA_{cs}dx = \epsilon\sigma [T(x)^4 - T_w^4]pdx - kT(x)''A_{cs}dx$$

or

$$T(x)'' = [\epsilon\sigma p/kA_{cs}][T(x)^4 - T_w^4] - g/k \quad (F-1)$$

where A_{CS} is the specimen cross-sectional area, and p is the specimen outside perimeter.

Now, the calculated emittance ϵ_c is determined experimentally by the relation

$$\epsilon_c = \frac{g A_{CS}}{\sigma p (T_o^4 - T_w^4)} \quad (F-2)$$

where T_o is the maximum temperature along the specimen. Solving equation (F-2) for g and substituting into equation (F-1) yields

$$T(x)'' = (\epsilon \sigma p / k A_{CS}) |T(x)^4 - T_w^4| - (\epsilon_c \sigma p / k A_{CS}) (T_o^4 - T_w^4) \quad (F-3)$$

$$\phi(x) = \frac{T(x) - T_o}{T_o}, \quad a = \left[1 - \left(\frac{T_w}{T_o} \right)^4 \right] \left[\frac{\epsilon_c - \epsilon}{\epsilon} \right], \quad b = \frac{\epsilon \sigma T_o^3 p}{k A_{CS}} \quad (F-4)$$

Equation (F-3) may be written:

$$\phi(x)'' = b \{ [1 + \phi(x)]^4 - 1 - a \} \quad (F-5)$$

By taking $x = 0$ at the point of symmetry of the temperature profile, and by assuming that T_o is the temperature at this point, the boundary conditions are

$$\phi(x=0) = 0, \quad \phi'(x=0) = 0 \quad (F-6)$$

Two solutions are presented. For the first, $\phi(x)$ is restricted to the range of -0.1 to $+0.1$ and the solution is adequate for determining the range of permissible temperature profile deviation. The second is an exact solution for determining the temperature distribution.

Approximate Solution for $-0.1 < \phi(x) < +0.1$

With $\phi(x)$ restricted so that $-0.1 < \phi(x) < +0.1$

$$[1 + \phi(x)]^4 \approx 1 + 4\phi(x) \quad (\text{F-7})$$

and the differential equation becomes

$$\phi(x)'' - 4b\phi(x) \cong -ab \quad (\text{F-8})$$

Assuming constant g , ϵ , and k (i.e., constant a and b), the general solution of equation (F-8) is

$$\phi(x) = C_1 \cosh(2b^{1/2}x) + C_2 \sinh(2b^{1/2}x) + a/4 \quad (\text{F-9})$$

where C_1 and C_2 are constants dependent on the boundary conditions. Symmetry of the temperature profile about $x=0$ requires that $C_2=0$. Since

$$0 = \phi(x=0) = C_1(1) + a/4, \quad C_1 = -a/4$$

Thus, equation (F-9) becomes

$$\phi(x) = - (a/4) [\cosh(2b^{1/2}x) - 1]$$

$$\phi(x) = - (a/2) \sinh^2(b^{1/2}x) \quad (\text{F-10})$$

$$\frac{T(x) - T_0}{T_0} = - \left(\frac{1}{2} \right) \left[\frac{\epsilon_c - \epsilon}{\epsilon} \right] \left[1 - \left(\frac{T_w}{T_0} \right)^4 \right] \sinh^2(b^{1/2}x) \quad (\text{F-11})$$

By letting $\Delta T = T_0 - T(x)$ and $\Delta \epsilon = \epsilon_c - \epsilon$, the ratio of the fractional error in emittance $\Delta \epsilon / \epsilon$, to the fractional error in setting end and center temperatures equal $\Delta T / T_0$, is

$$\left(\frac{\Delta \epsilon}{\epsilon} \right) / \left(\frac{\Delta T}{T_0} \right) = \frac{2}{\left[1 - (T_w/T_0)^4 \right] \sinh^2(b^{1/2}x)} \quad (\text{F-12})$$

This result is plotted in Figure F-1. As an example of its use, consider an attempt to measure emittance of a specimen with end heating employed to set $T(x)$ equal to T_0 , and so that the distance between central and end thermocouples is 1.63 inch. Let

the specimen width be 0.5 inch, thickness be 0.002 inch, temperature level be 500°R, total hemispherical emittance be 0.1, and thermal conductivity be that of nickel, 40 B/hr-ft-°R. Then

$$bx^2 = \frac{\epsilon \sigma T_o^3 px^2}{k A_{cs}} = 0.120$$

and with sink temperature T_w much less than T_o , $\left(\frac{\Delta \epsilon}{\epsilon}\right) / \left(\frac{\Delta T}{T_o}\right) = 16$.
Thence, a 1 per cent error in obtaining equality between the central and the end temperatures results in a 16 per cent difference between true emittance ϵ and emittance calculated from $g A_{cs} / \sigma p (T_o^4 - T_w^4)$.

Exact Solution for the Temperature Profile

Returning to equation (F-5) with boundary conditions (F-6), let

$$\xi = b^{1/2} x \quad \text{whence equations (F-5) and (F-6) yield}$$

$$\phi''(\xi) = [1 + \phi(\xi)]^4 - 1 - a, \quad \phi(\xi=0) = 0, \quad \phi'(\xi=0) = 0 \quad (\text{F-13})$$

Now, let $\zeta = \phi'(\xi)$, whence $\phi''(\xi) = d\zeta/d\xi = (d\zeta/d\phi)(d\phi/d\xi) = \zeta(d\zeta/d\phi)$.

Substituting this in the differential equation of (F-13), and separating variables, yields

$$\zeta d\zeta = [(1 + \phi)^4 - 1 - a] d\phi \quad (\text{F-14})$$

with $\zeta = 0$ at $\phi = 0$. Integrating equation (F-14) with this limit yields

$$\frac{d\phi}{d\xi} = \zeta = [-2a\phi + 4\phi^2 + 4\phi^3 + 2\phi^4 + (2/5)\phi^5]^{1/2} \quad (\text{F-15})$$

Since $\phi(\xi=0) = 0$, integration of (F-15) takes the form

$$\int_{\xi=0}^{\xi} d\xi = \int_{\phi=0}^{\phi} [-2a\bar{\phi} + 4\bar{\phi}^2 + 4\bar{\phi}^3 + 2\bar{\phi}^4 + 2/5\bar{\phi}^5]^{-1/2} d\bar{\phi} \quad (\text{F-16})$$

To facilitate numerical integration, since the integrand is infinite at $\phi = 0$, let $\mu = (-\phi)^{1/2}$, whence $-2\mu d\mu = d\phi$, so equation (F-16) becomes

$$\xi = \int_{\mu=0}^{\mu} \left[a/2 + \bar{\mu}^2 - \bar{\mu}^4 + \frac{\bar{\mu}^6}{2} - \frac{\bar{\mu}^8}{10} \right]^{-1/2} d\bar{\mu} \quad (\text{F-17})$$

The integral was evaluated using a Bendix G15 computer by employing Simpson's rule, and the results are presented in Figures F-2 and F-3. For any given pair of corresponding values of $[\tau_0 - \tau(x)]/\tau_0$ and $b^{1/2}x$, the value of a may be found from Figure F-2. Figure F-3 may then be used to construct the complete plot of $\tau(x)$ vs x .

APPROXIMATE SOLUTION FOR EMITTANCE ERROR DUE TO SPECIMEN END COOLING EFFECT

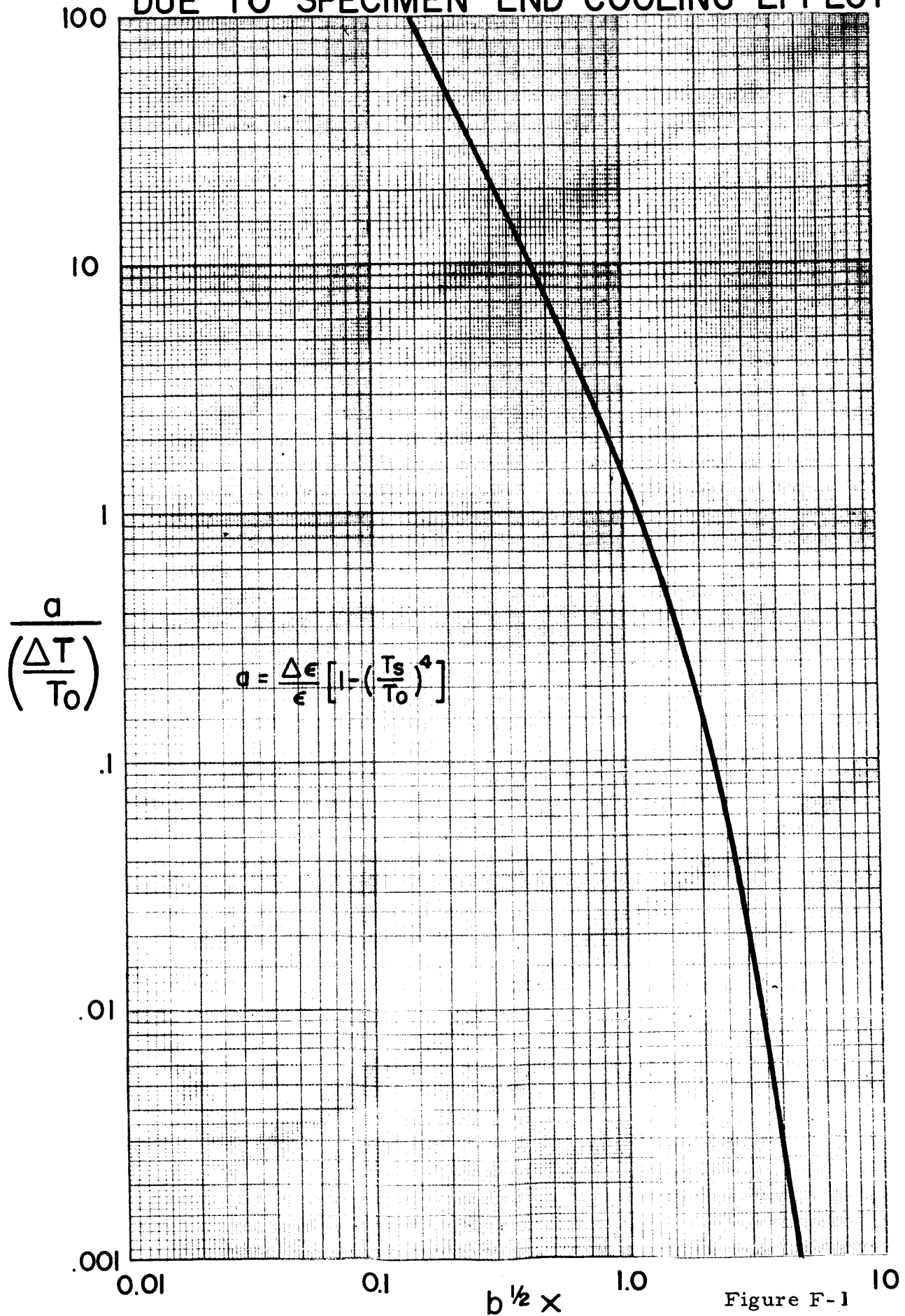


Figure F-1

EXACT SOLUTION FOR EMITTANCE ERROR DUE TO SPECIMEN
END COOLING EFFECT

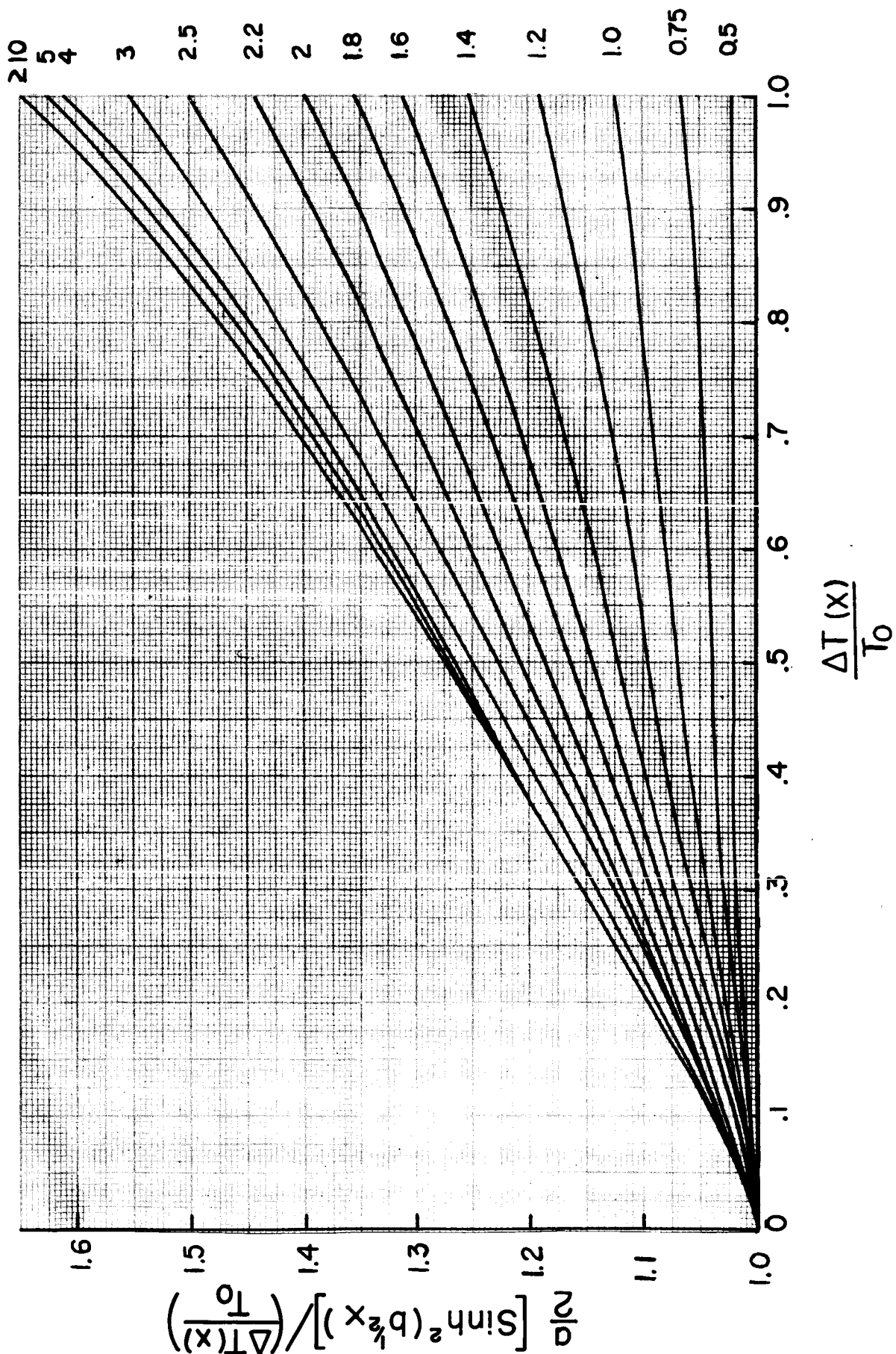


Figure F-2

EXACT SOLUTION FOR EMITTANCE ERROR DUE TO SPECIMEN
END COOLING EFFECT

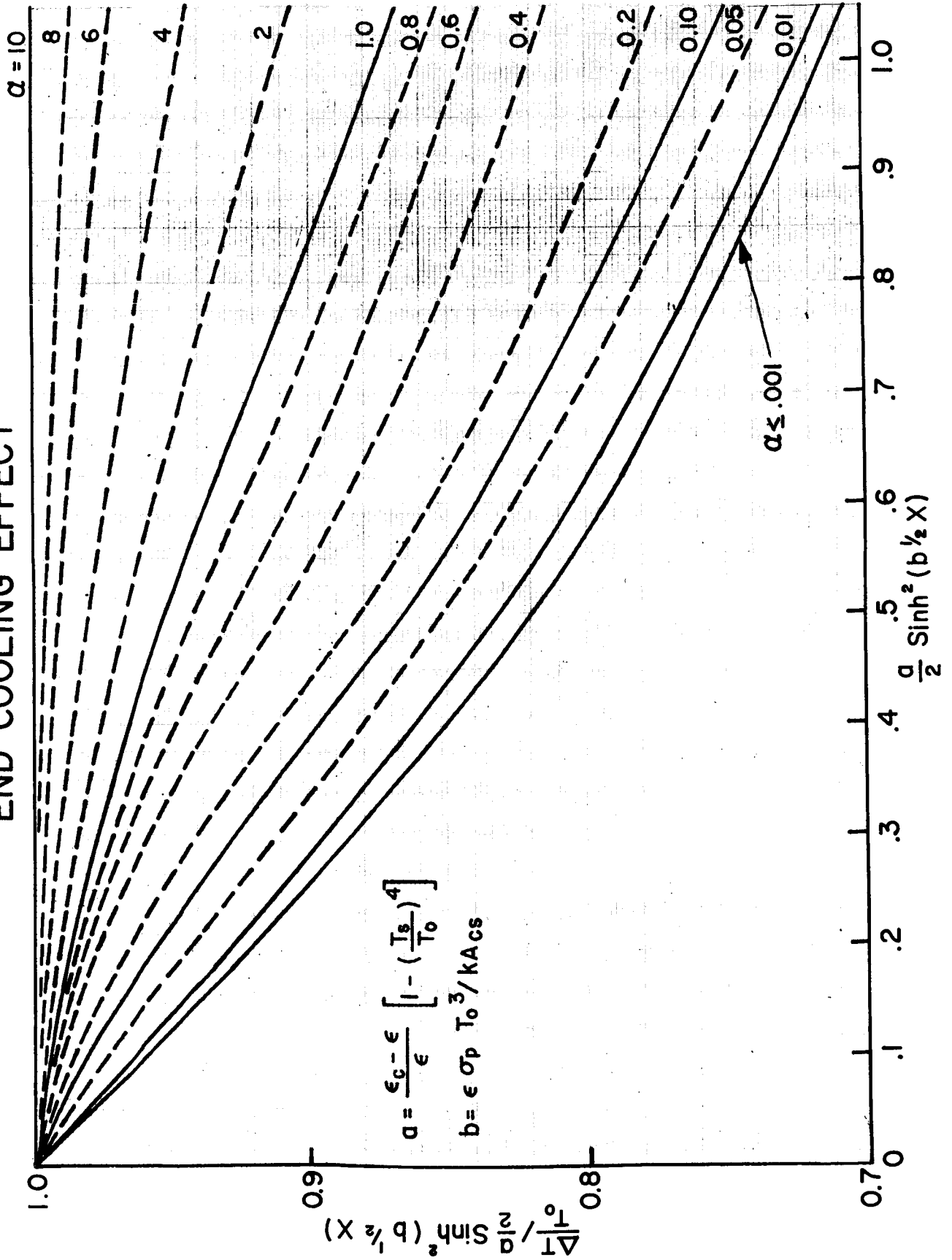


Figure F-3

APPENDIX G

Analytical Evaluation of the Quality
of the Black-Body Hole and Associated
Heat Generation and Temperature Perturbations

APPENDIX G

ANALYTICAL EVALUATION OF THE QUALITY OF THE BLACK-BODY HOLE AND ASSOCIATED HEAT GENERATION AND TEMPERATURE PERTURBATIONS

A. Introduction

Spectral emittance measurements and temperature measurements made using an optical pyrometer are made using radiation from a small hole in the specimen wall. The accuracy of these measurements depends on how closely the radiation from the black-body hole simulates that from an ideal black body operating at the specimen surface temperature.

Two effects produce deviation of the black-body hole radiation from that of an ideal black body.

1. The finite size of the black-body hole allows radiation to leak from the enclosure. The magnitude of this effect depends on the geometry of the tubular specimen and hole, the portion of the inner wall viewed, and the nature (diffuse or specular) and value of the reflectance of the tube inner wall.
2. Temperature nonuniformities over the tube wall cause the black-body hole to produce radiation with an intensity and spectral distribution that is characteristic of radiation from a black body operating at a temperature other than that of the specimen surface. Wall temperature nonuniformities result from:
 - a) end conduction heat losses,
 - b) variations in wall thickness, and
 - c) the presence of the black-body hole in the tube wall.

The first two of these causes is discussed and shown to be negligible in Appendices F and I, respectively. The last will be discussed below.

B. Analysis of Radiation Leakage from Black-Body Hole

The method of DeVos⁵ was used for estimating the loss of black-body quality resulting from radiation leakage. The first analysis was based on the specimen geometry used for the spectral emittance rig before modifications were made. The black-body hole measured 0.035 inch by 0.076 inch. The inside diameter of the tube was 0.25 inch and the inside cavity length was 7 inches between the pinched ends. A reflectance of 0.85 that was primarily specular was assumed for the tube inner wall. The analysis indicates that radiation losses through the black-body hole would not reduce the black-body quality by more than 2 per cent.

If the tube were isothermal but the ends of the tube were open to cold surroundings, it is estimated that radiation losses through the tube ends would result in an additional quality loss of 1 per cent. However, since the ends are closed and the ends of the cavity are at a temperature considerably higher than that of the electrodes, it is estimated that radiation losses to the end of the cavity do not result in a reduction of black-body quality greater than 1/2 per cent. Figure G-1 shows the calculated temperature profile for the worst cases.

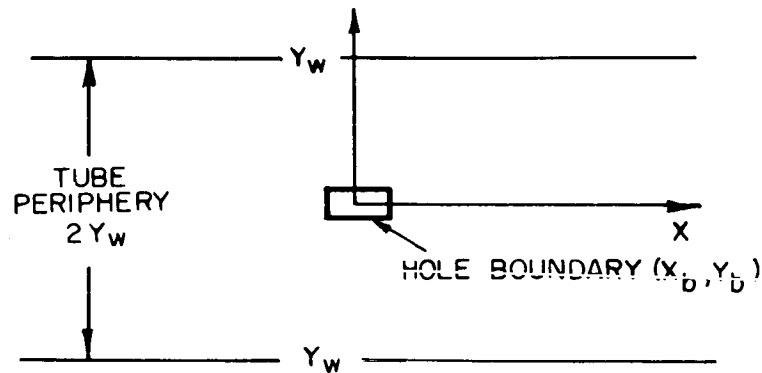
Solely on the basis of radiation losses it is estimated that the rectangular black body has a quality better than 97.5 per cent.

C. Perturbations Caused by the Black-Body Hole

Perturbation of heat generation rate and temperature result from the change in the paths of current flow caused by the presence of the black-body hole coupled with insufficient thermal conduction to level out the temperature variations. The black-body hole causes the current lines to separate at either end of the hole and to crowd together along the sides of the hole. The result is

cooler-than-average areas at the ends and hotter-than-average areas on either side of the hole. In this section the rate of heat generation will be analyzed and then the resulting temperature distribution will be determined.

1. Distribution of Heat Generation - Consider the situation shown in the sketch below. The tube has been split opposite the black-body hole and opened out flat.



It is assumed that the wall thickness is uniform and that the current flow may be approximated by two-dimensional flow since the wall thickness is small compared to the tube diameter. With these assumptions, the governing differential equation for the electrical potential $V(x, y)$ is the two-dimensional Laplace equation

$$\frac{\partial^2 V}{\partial x^2} + \frac{\partial^2 V}{\partial y^2} = 0$$

For the boundary conditions it is noted that $\overline{\text{grad } V}$ approaches a constant at large positive and negative x and assumes a direction parallel to the negative x axis. Further, if \bar{n} is a unit vector normal to the boundary surfaces, then $\bar{n} \cdot \overline{\text{grad } V} = 0$ at $y = y_w, -y_w$ and at the hole boundary.

The ohmic heat generation rate per unit volume $q(x, y)$ equals $\rho [\bar{j}(x, y)]^2$, where ρ is the resistivity and $\bar{j}(x, y)$ is the current density. The current density

$\bar{j}(x,y)$ equals $\bar{E}(x,y)/\rho$, where $\bar{E}(x,y)$ is the electric field strength. Since $\bar{E}(x,y)$ equals $-\text{grad } V$

$$g(x,y) = (\text{grad } V)^2 / \rho$$

To simplify the analysis, the rectangular black-body hole is closely approximated by an oval hole. A solution is then found by adding potentials for 1) a uniform flow parallel to the x axis from x to $-x$, 2) an infinite set of identical line sources which are perpendicular to the $x-y$ plane at $(x=x_0, y=0 \pm 2y_w, \pm 4y_w \dots)$, and 3) an infinite set of identical line sinks which are also perpendicular to the $x-y$ plane at $(x=-x_0, y=0, \pm 2y_w, \pm 4y_w \dots)$, where each sink is the same strength as each source.

The two-dimensional flow model described above was evaluated using the component potentials as derived in references dealing with hydrodynamics, taking advantage of the use of complex numbers to supplant the vector algebra. Using the methods and nomenclature of Milne-Thompson in "Theoretical Hydrodynamics" ¹⁴, the problem was reduced to one of constructing and manipulating the two-dimensional complex potential $w(x,y)$ for inviscid and irrotational fluid flow by adding the complex potentials for the uniform flow, the multiple source flow, and the multiple sink flow. The fluid flow complex velocity v was then formed by the relation $v = -dw/dz$, where $z = x + iy$.

Setting v equal to zero gave the relationship of the stagnation point coordinates to U , the uniform velocity at $x = +\infty$ and $x = -\infty$ and to the magnitude associated with each individual source and sink strength m . The stream function ψ was determined from the complex potential by the defining equation $w = \phi + i\psi$. Setting $\psi = 0$ gave the relationship of hole boundary coordinates (x_b, y_b) , except for the stagnation point coordinates. The oval-shaped obstruction to the flow (the $\psi = 0$ streamline) was fitted to the black-body hole boundary by appropriate selection of the parameters $y_w U/m$ and x_0/y_w appearing in the $\psi = 0$ equation. This equation has the form

$$y_w U/m = f_n \left(\frac{x_b}{y_w}, \frac{y_b}{y_w}, \frac{x_0}{y_w} \right)$$

where x_b and y_b are coordinates of the general point on the oval boundary.

The ratio of the magnitude of the complex velocity $|\psi(x, y)|$ to the uniform velocity in the region far from the obstruction U , is identical to the ratio of current density magnitudes in the corresponding electrical problem. This ratio was found directly upon constructing the magnitude of $\psi(x, y) = u - iv$. Thus

$$|\psi(x, y)|^2 = u^2 + v^2 = f_n(U, \gamma_w U/m, x_0/\gamma_w, x, y)$$

yielded $\frac{|\psi(x, y)|^2}{|\psi(\infty, y)|^2} = \frac{u^2 + v^2}{U^2} = f_n(\gamma_w U/m, x_0/\gamma_w, x, y)$

where $(u^2 + v^2)/U^2$ was identical to $q(x, y)/q(\infty, y)$ required in the corresponding electrical problem.

Equations used in this analysis are outlined, and values of relative power generation and the approximation to black-body hole geometry used are presented below.

The complex potential for a uniform stream parallel to the x axis and for flow direction from $+x$ to $-x$ is, by Milne-Thompson

$$w_1 = Uz \quad (G-1)$$

where $z = x + iy$

U = magnitude of the uniform velocity far from the flow obstruction

The complex potential for the flow out from an infinite set of equal line sources located at $(x=x_0, y=0, \pm 2\gamma_w, \pm 4\gamma_w, \dots)$ is, by Milne-Thompson

$$w_2 = -m \log \sinh \left[\frac{\pi(z - x_0)}{2\gamma_w} \right] \quad (G-2)$$

where γ_w = half the periphery of the tube specimen, or distance from the center of a centrally-located flow obstruction to the channel wall

m = source strength of each line source

Similarly, the complex potential for the flow into an infinite set of equal line sinks located at $(x=x_0, y=0, \pm 2\gamma_w, \pm 4\gamma_w, \dots)$

$$w_3 = +m \log \sinh \left[\frac{\pi(z + x_0)}{2\gamma_w} \right] \quad (G-3)$$

Addition of the complex potentials w_1 , w_2 , and w_3 gives the complex potential for two-dimensional flow in a channel (from plus x to minus x) with parallel walls $2y_w$ apart, having an oval-shaped obstruction located at the origin whose axes are parallel to the coordinate axes. This complex potential is

$$w = w_1 + w_2 + w_3 \quad (G-4)$$

$$= Uz - m \log \sinh \left[\frac{\pi(z-x_0)}{2y_w} \right] + m \log \sinh \left[\frac{\pi(z+x_0)}{2y_w} \right]$$

The complex velocity is thus

$$v = -dw/dz \quad (G-5)$$

$$= -U - (\pi m/2y_w) \coth \left[\frac{\pi(z+x_0)}{2y_w} \right] + (\pi m/2y_w) \coth \left[\frac{\pi(z-x_0)}{2y_w} \right]$$

The two stagnation points are determined by setting $v = 0$, yielding

$$Y_s = 0 = \pm \frac{1}{2} \cosh^{-1} \left[\cosh(2X_0) + \left(\frac{m\pi}{y_w U} \right) \sinh(2X_0) \right] \quad (G-6)$$

where subscript s denotes "at stagnation point"

subscript 0 denotes "at x -coordinate of source"

X = dimensionless x coordinate = $\pi x / 2y_w$

Y = dimensionless y coordinate = $\pi y / 2y_w$

All points on the oval obstruction except the stagnation points correspond to the condition $\psi = 0$. Since $w = \Phi \pm i\psi$, the stream function ψ is the imaginary part of the complex potential w and is found from equation (G-4) to be

$$\psi = Uy + m \tan^{-1} \left[\frac{\sin(2Y) \sinh(2X_0)}{\cos(2Y) \cosh(2X_0) - \cosh(2X)} \right] \quad (G-7)$$

The coordinates of each point on the oval obstruction boundary satisfy the condition $\psi = 0$, whence

$$[\cosh(2X_b) - \cos(2Y_b) \cosh(2X_0)] \left[\tan \left(\frac{2Y_b U y_w}{\pi m} \right) \right]$$

$$= \sin(2Y_b) \sinh(2X_0) \quad (G-8)$$

where subscript b denotes "on the boundary of the oval obstruction." The ratio of the square of the magnitude of the local velocity ($u^2 + v^2$), to the square of the magnitude

of the uniform velocity at $X=+\infty$ and $X=-\infty$, U^2 , was found from equation (G-5) by identifying the real and pure imaginary parts of v as u and $-v$ respectively. Thus

$$\frac{u^2 + v^2}{U^2} = \left(\frac{u}{U}\right)^2 + \left(\frac{v}{U}\right)^2 \quad (G-9)$$

where

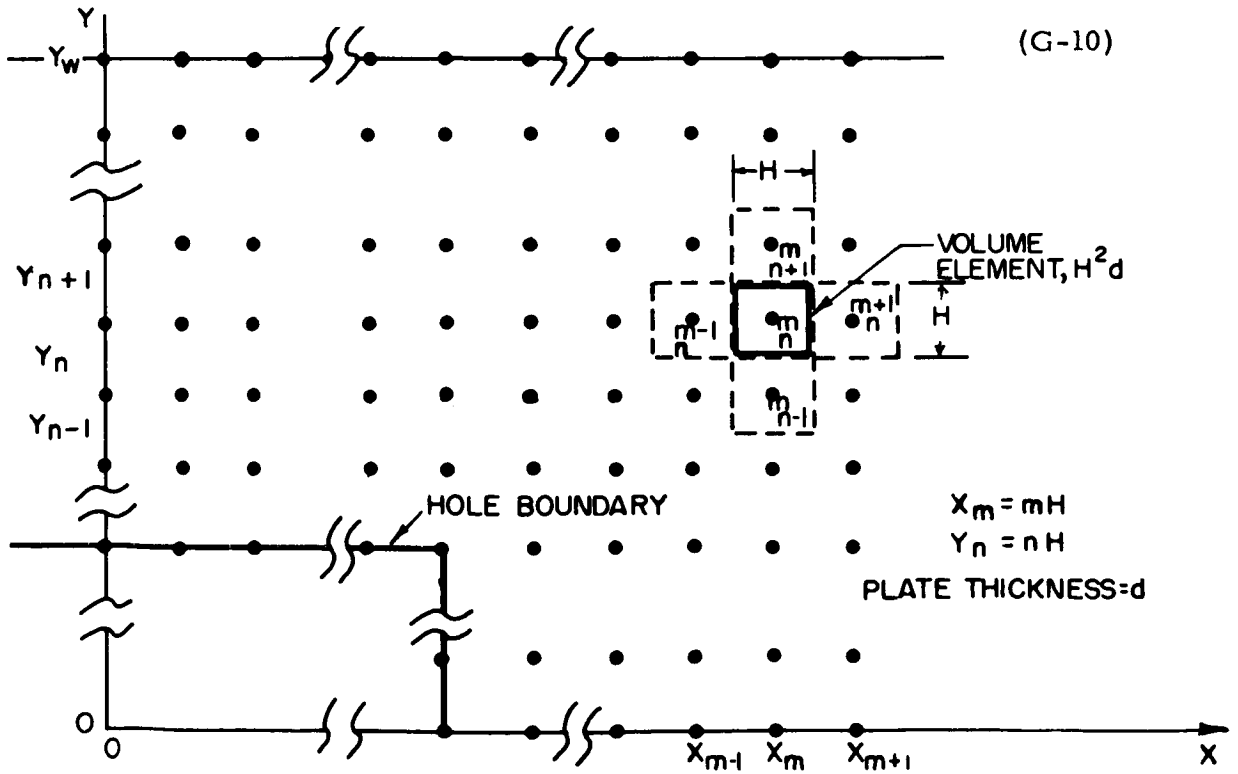
$$\begin{aligned} \frac{u(X,Y)}{U} &= -1 - \left[\frac{\pi m}{4\gamma_w U} \right] \left[\frac{\sinh(2X+2X_0)}{\cos^2(Y) \sinh^2(X+X_0) + \sin^2(Y) \cosh^2(X+X_0)} \right. \\ &\quad \left. - \frac{\sinh(2X-2X_0)}{\cos^2(Y) \sinh^2(X-X_0) + \sin^2(Y) \cosh^2(X-X_0)} \right] \\ \frac{v(X,Y)}{U} &= - \left[\frac{\pi m}{4\gamma_w U} \right] \left[\sin(2Y) \left[\frac{1}{\cos^2(Y) \sinh^2(X+X_0) + \sin^2(Y) \cosh^2(X+X_0)} \right. \right. \\ &\quad \left. \left. - \frac{1}{\cos^2(Y) \sinh^2(X-X_0) + \sin^2(Y) \cosh^2(X-X_0)} \right] \right] \end{aligned}$$

The current density distribution problem in a uniform thin-walled tube with a black-body hole, corresponds to the fluid flow problem described above. First, the values of $m/\gamma_w U$ and X_0/γ_w were found such that the oval obstruction size and shape closely approximated the rectangular black-body hole size and shape. Second, the map of relative power generation rate $(u^2+v^2)/U^2$ was constructed on X, Y coordinates. The results are shown in Figure G-2 for a rectangular black body hole measuring 0.035 by 0.070 inch in a tube with a 0.25 inch diameter. The parameters used to fit the oval obstruction to the black-body hole were $(m/\gamma_w U) = 0.104$, $X_0/\gamma_w = 0.359$. The oval boundary for these parameter values was found from equations (G-6) and (G-8), and the contour map of relative heat generation rate per unit volume, $(u^2+v^2)/U^2$, calculated from equation (G-9).

2. Temperature Distribution - The relative heat generation rate per unit volume determined above may be used analytically to estimate the temperature field in the tube wall in the vicinity of the black-body hole. A finite difference steady-state heat balance on an element of volume $d(\delta y)/(\delta x)$ is written below, neglecting the

temperature variation through the thickness d , and radiant heat exchange inside the tube. For these assumptions and with $\delta y = \delta x = H$, the heat balance on the element is:

$$\begin{aligned}
 &\text{heat generation rate in the element, } q_{m,n} H^2 d \\
 &\quad \text{plus} \\
 &\text{heat conducted into the left face, } -k(Hd)(T_{m,n} - T_{m-1,n})/H \\
 &\quad \text{plus} \\
 &\text{heat conducted into bottom face, } -k(Hd)(T_{m,n} - T_{m,n-1})/H \\
 &\quad \text{equals} \\
 &\text{heat radiated to surroundings from front face of element,} \\
 &\quad H^2 \epsilon \sigma (T_{m,n}^4 - T_w^4) \\
 &\quad \text{plus} \\
 &\text{heat conducted out from the right face, } -k(Hd)(T_{m,n} - T_{m+1,n})/H \\
 &\quad \text{plus} \\
 &\text{heat conducted out from top face, } -k(Hd)(T_{m,n} - T_{m,n+1})/H
 \end{aligned}$$



MATRIX FOR FINITE DIFFERENCE HEAT BALANCES

The adiabatic boundary condition for symmetry of the temperature field applies along the surfaces $x = 0$, $y = 0$, $y = y_w$, and along the hole boundary surface. At large x , conduction terms approach zero, and the heat balance equation (G-10) applied at these boundaries yields

$$g_{\infty, n} d = \epsilon \sigma (T_{\infty}^4 - T_w^4) \quad (G-11)$$

Letting

$$\phi_{m, n} = \frac{T_{m, n} - T_{\infty}}{T_{\infty}}, \quad \alpha = \frac{\epsilon \sigma T_{\infty}^3 H^2}{k d}, \quad (1 + \phi_{m, n})^4 \approx 1 + 4 \phi_{m, n}$$

equations (G-10) and (G-11) yield

$$\phi_{m-1, n} + \phi_{m+1, n} + \phi_{m, n-1} + \phi_{m, n+1} - 4 \phi_{m, n} (1 + \alpha) + \alpha \left[\left(\frac{g_{m, n}}{g_{\infty, n}} \right) - 1 \right] \left[1 - \left(\frac{T_w}{T_{\infty}} \right)^4 \right] = 0 \quad (G-12)$$

where $g_{m, n} / g_{\infty, n} = g(x_m, y_n) / g(\infty, y)$, as obtained in the preceding section. Application of equation (G-12) to equally spaced points on and within the boundaries in the upper right hand quadrant of the x - y plane yields a set of equations whose simultaneous solution for the temperatures $T_{m, n}$ yields the temperature map desired. The method of relaxation of Dusenberre, described in "Conduction Heat Transfer" by P. J. Schneider¹⁵ could be used to calculate the temperature field for the cases of interest in these tests.

D. Effect of Temperature Nonuniformity on Black-Body Radiation

From the temperature field, the error in spectral emittance due to not having uniform surface temperature throughout the central portion of the tube may be estimated using the method of DeVos⁵. For example, if the surface spot is operating at temperature T_1 , and the black-body hole yields perfect black-body radiation at temperature T_2 , the ratio measured by the spectrophotometer may be expressed as

$$\epsilon_{\lambda AP} = \frac{I_{\lambda \text{surf}}(T_1)}{I_{\lambda b}(T_2)} = \left[\frac{I_{\lambda \text{surf}}(T_1)}{I_{\lambda b}(T_1)} \right] \left[\frac{I_{\lambda b}(T_1)}{I_{\lambda b}(T_2)} \right] = \epsilon_{\lambda} \frac{I_{\lambda b}(T_1)}{I_{\lambda b}(T_2)} \quad (G-13)$$

Thus, the ratio of the true spectral emittance ϵ_λ to the apparent spectral emittance $\epsilon_{\lambda Ap}$ sensed by the spectrophotometer is merely the ratio of the monochromatic intensity of a black body operating at temperature T_2 to that of another black body operating at temperature T_1 . From equation (A-2), Appendix A, this ratio is

$$\frac{I_{\lambda b}(T_2)}{I_{\lambda b}(T_1)} = \frac{e^{c_2/\lambda T_1} - 1}{e^{c_2/\lambda T_2} - 1} \quad (G-14)$$

and

$$\frac{\epsilon_\lambda}{\epsilon_{\lambda Ap}} = \frac{e^{c_2/\lambda T_1} - 1}{e^{c_2/\lambda T_2} - 1} \quad (G-15)$$

Figure G-3 illustrates the effect of black-body overheating on spectral emittance for a specimen which is at a temperature level of 1900 °R (1440 °F). The hyperbolic lines represent constant black-body overheating. The vertical lines indicate the per cent of black-body energy radiated at wavelengths shorter than the indicated wavelength. Since less than 0.1 percent of the black-body energy is at wavelengths shorter than one micron, the curves were not extended into the visible wavelength region.

TEMPERATURE PROFILE ALONG TUBE WITH WORST CAVITY- END LOSS TEMPERATURE EFFECTS

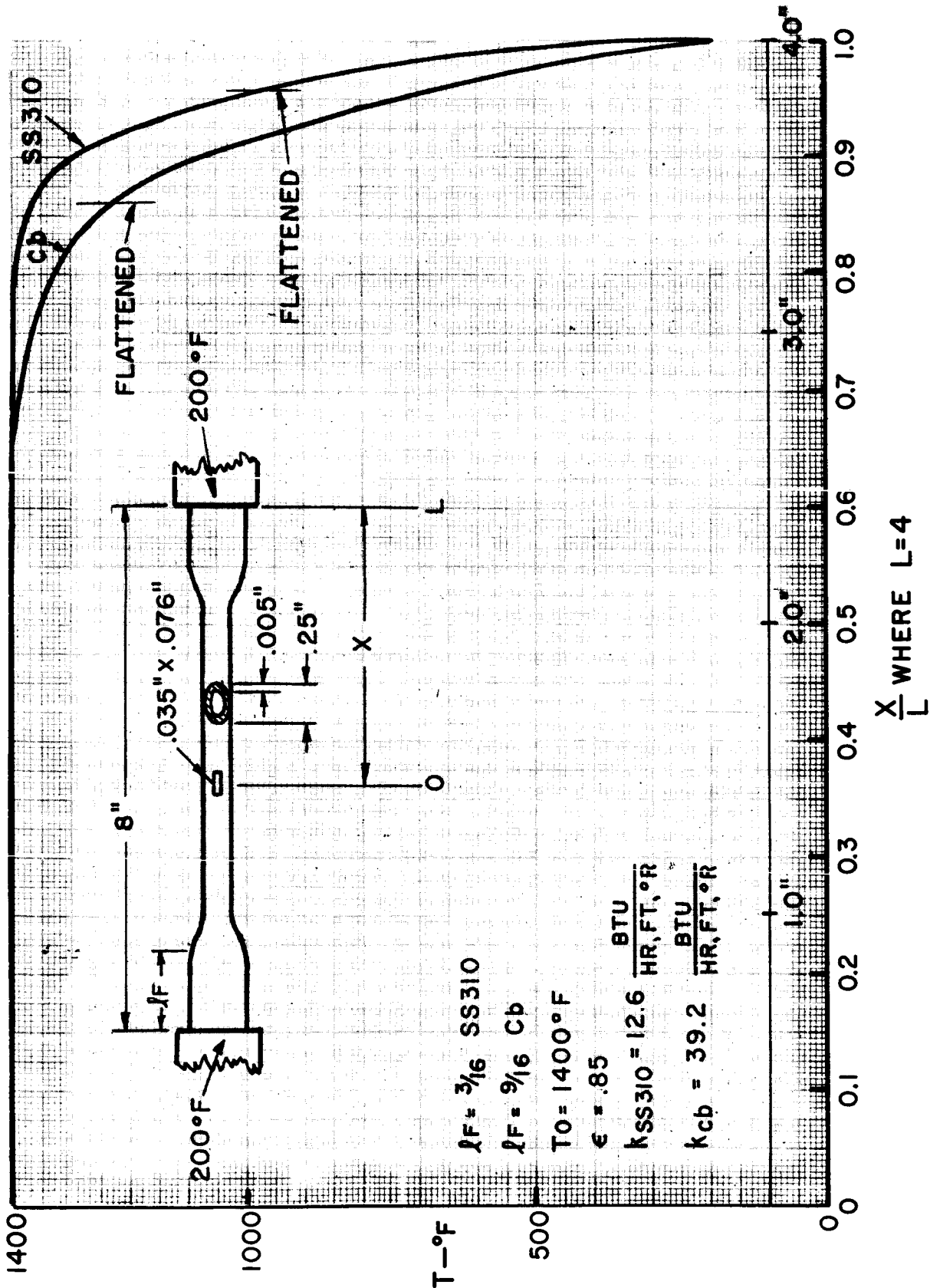


Figure G-1

MAP OF RELATIVE POWER GENERATION RATE PER UNIT AREA IN TUBE WALL

Y = DIMENSIONLESS Y - COORDINATE, $\pi Y/2 Y_w$
 X = DIMENSIONLESS X - COORDINATE, $\pi X/2 Y_w$

NOTE: RELATIVE POWER GENERATION = 1.0 AT X = ∞

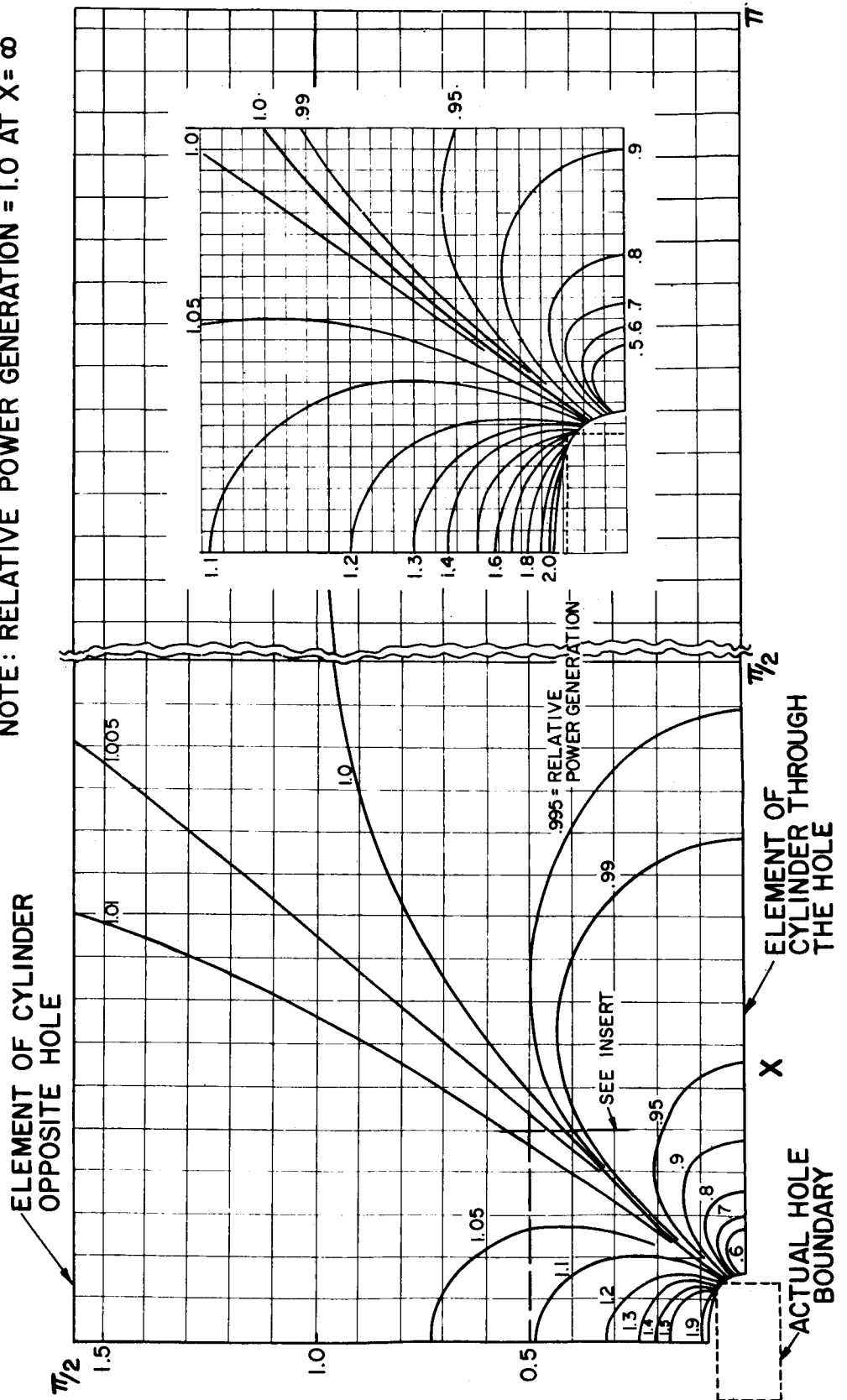


Figure G-2

EFFECT OF BLACK BODY OVERHEATING ON SPECTRAL EMITTANCE

T_1 = SURFACE TEMP. = 1900°R
 T_2 = BLACK BODY TEMP.

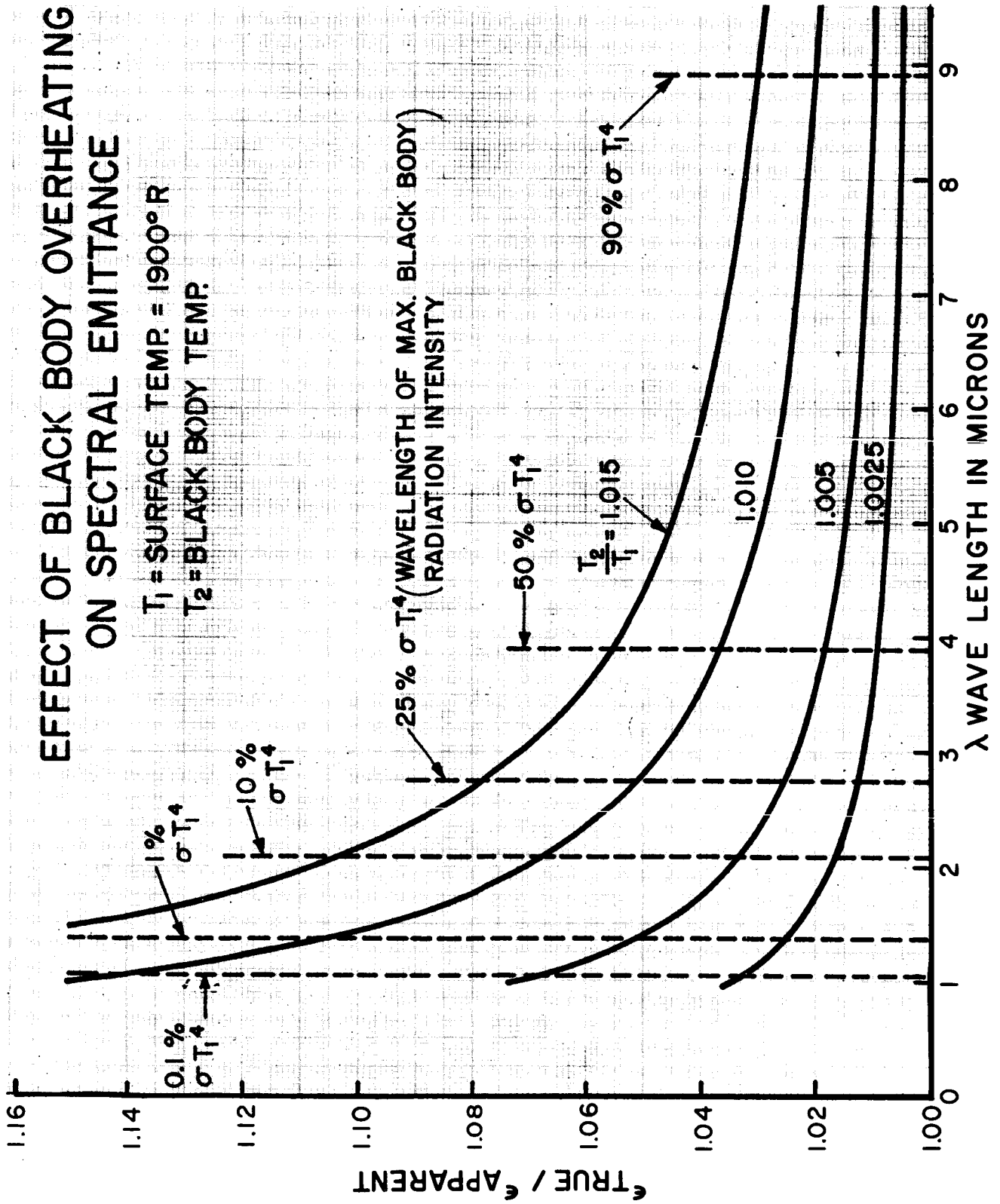


Figure G-3

APPENDIX H

Experimental Evaluation of Temperature
Perturbations and Black-Body Quality

APPENDIX H

EXPERIMENTAL EVALUATION OF TEMPERATURE
PERTURBATIONS AND BLACK-BODY QUALITY

In conjunction with the analyses described in Appendices F, G, and I, experimental measurements of temperature variations and black-body quality were made on two tubular specimens, one of columbium and the other of AISI-310 stainless steel. Both of these specimens were 0.25 inch in diameter and had wall thicknesses of 0.005 inch. Testing included the measurement of axial radiant intensity profiles for the specimens and evaluation of the quality of the rectangular black-body hole.

The measurements of the profiles of the specimen wall intensity were made to:

- 1) Indicate in a nondestructive manner any variations in the tube wall thickness (in the case of the columbium tube, tests were made with and without a coating on the specimen to distinguish between the effects caused by the variations of the tube wall thickness and the effects from nonuniformity of coating),
- 2) Demonstrate the effect of thermal conduction losses through the specimen terminals on the intensity profile as a function of surface emittance at a particular temperature, and
- 3) Determine the pattern of the axial intensity in the vicinity of the 0.035 by 0.076-inch black-body hole.

The quality or, more correctly, effective emittance of the rectangular black-body hole was evaluated by a method involving the comparison of the apparent surface emittance adjacent to this hole with the surface emittance at two 0.018-inch diameter black-body holes located approximately 0.75 inch above and below the rectangular hole. In making the comparisons, these circular black-body holes were assumed to have an effective emittance of 1.000, and the specimen wall surface emittance was assumed to be invariant along the length of the specimen.

A. Apparatus

The water-cooled metal vacuum chamber normally used in the spectral emittance rig was replaced with a Pyrex glass tube of the same dimensions, as shown in Figure H-1. This arrangement made it possible to scan the

specimens over their entire lengths by moving the chamber-specimen assembly vertically past the first focal point of the collecting mirror M -2, of the spectrophotometer, shown in Figure 11. The use of the glass-walled chamber excluded measurements at wavelengths longer than two microns.

The Perkin-Elmer Model 13U spectrophotometer was operated in the single-beam direct mode using detectors suitable for the wavelengths considered; that is, a thermocouple was used in conjunction with the sodium chloride prism for measurements at two microns, and 1P28 and 1P21 photomultiplier tubes without the prism for measurements in the visible range. To direct polychromatic radiation into the photomultiplier tube, a plane mirror was placed just before the prism in the monochromator. The resulting response was a composite of the spectral response of the photomultiplier tube and the spectral intensity of the surface spot viewed. For the surfaces and at the surface temperature tested, this response was a band whose ten per cent response points were approximately at 0.51 and 0.75 micron, and whose peak response was at 0.60 micron. (This band is referred to as a wavelength of 0.6 micron in the remainder of this report.) The spectral responses of the 1P28 and 1P21 photomultiplier tubes were practically identical. The 1P21 tube was used in place of the 1P28 tube for the more recent testing because of its somewhat higher sensitivity and lower noise level.

The intensity measurements used in determining the quality of the rectangular black-body hole were taken with the 6-inch collecting mirror, M -2, stopped down to 1.1 inch, and with a 0.0126-inch diameter aperture at its second focal point. The 1.1-inch stop improved the resolution of the optical system by reducing the astigmatism caused by operating M -2 off axis. This arrangement made it possible to take intensity readings on a 0.018-inch diameter hole with a 0.002-inch radial clearance.

The surface intensity profiles were determined with M -2 at full aperture. The 0.0126-inch diameter aperture was used for all intensity profile measurements except those on the polished AISI-310 stainless steel specimen. These were made with one of the standard 0.1-inch square beam-separating apertures.

B. Procedure

To eliminate the error caused by long-period instrument drift, all intensity profile measurements were made relative to a reference spot located within an inch of the center of each specimen. Alternate readings

were taken between selected stations on the specimen and the reference spot by traversing the specimen chamber assembly so that the first focal point of M -2 coincided with the specimen surface. The relative intensity at each station was determined by recording the intensity for several seconds at the surface station and then at the reference spot.

In the black-body evaluation study, intensity readings were taken at each of the 0.018-inch diameter black-body holes and at 0.050 inch above and below each hole. These data were used to determine an emittance value of the surface near each hole, using the associated black-body hole radiation as a standard. The same procedure was repeated for the rectangular black-body hole, that is, emittance measurements were made of the surface 0.080 inch above and below the center of the hole. The emittance of the rectangular black-body hole was determined as the ratio of the true to the indicated surface emittance, where the true emittance of the surface was taken as that measured at the 0.018-inch circular holes.

Initially, an intensity scan was made on an AISI-310 stainless steel tube without black-body holes. A second AISI-310 stainless steel tube with three black body holes was then tested to determine the quality of the black body radiation. An intensity scan of the columbium tube with black-body holes and coated with acetylene black was made followed by black-body quality measurements. The columbium tube was then vapor-blasted to remove the coating and both an intensity scan and measurement of the black-body radiation quality were made.

C. Calculation of the Effective Emittance of the Rectangular Black-Body Hole

The spectral normal emittance of the specimen surface $\epsilon_{\lambda s}(T)$ is defined as the ratio of the intensity of the surface at wavelength λ to the intensity of a black body at λ , where both the surface and black body are at temperature T . Assuming that the small black-body holes have 1) an emittance (or quality) of 1.0, and 2) the same effective temperature as the surface adjacent to the holes, spectral normal emittance of the surface near each circular hole was determined by computing the ratio of measured surface intensity near the hole to that of the hole itself. The average of the values of $\epsilon_{\lambda s}(T)$ thus obtained at the two circular holes was assumed to be the true spectral normal emittance of the surface near the rectangular black-body hole.

The apparent surface emittance obtained by taking the ratio of the surface intensity of a spot near the rectangular black-body hole to that from the rectangular hole itself is, in general, a different value than $\epsilon_{\lambda_s}(T)$, because:

- 1) Radiation loss from the relatively large rectangular hole would result in a hole emittance less than 1.0 if no temperature perturbation were present, and
- 2) When temperature perturbation is present, the radiation emanating from the rectangular black-body hole is not necessarily characteristic of the temperature T_s of the nearby surface spot, because the radiation may actually originate from surface elements which are at temperatures both higher and lower than T_s .

The radiation from the rectangular hole could be characterized by assigning an effective temperature which would account for the combined effects of both of these defects, or it could be characterized by another effective temperature which would account only for the temperature perturbation effect. For the purpose of defining an effective emittance of the rectangular hole, it is unnecessary to define an effective temperature of the hole. The effective emittance is simply

$$\epsilon_{\lambda_{he}} = I_{\lambda_h} / I_{\lambda_b}(T_s) \quad (H-1)$$

where $I_{\lambda_b}(T_s)$ is the intensity of an ideal black body at temperature T_s , the temperature of the nearby surface spot, and I_{λ_h} is the actual intensity of the rectangular hole.

Now, for the nearby surface spot the spectral normal emittance is

$$\epsilon_{\lambda_s}(T_s) = I_{\lambda_s}(T_s) / I_{\lambda_b}(T_s) \quad (H-2)$$

Substituting $I_{\lambda_b}(T_s)$ from equation (H-2) yields

$$\epsilon_{\lambda_{he}} = \epsilon_{\lambda_s}(T_s) I_{\lambda_h} / I_{\lambda_s}(T_s) \quad (H-3)$$

As defined by equation (H-1), the effective emittance of the rectangular black-body hole may assume values greater than 1.0 because of the temperature perturbation effect. An indication of the nature of this effect may be seen from the following discussion.

Consider a hypothetical specimen of the same geometry and surface emittance as the real specimen but made of a hypothetical material with such a large thermal conductivity that the temperature perturbation would be negligible, that is, its temperature would be uniform throughout. Let T_{he} be the temperature to which this hypothetical specimen must be brought to yield the same standard hole intensity for a given temperature of the nearby surface spot T_s , as that obtained with the real specimen, that is, $I_{\lambda h}$. For the hypothetical specimen, this intensity will be designated $I_{\lambda h}(T_{he})$. (T_{he} may be considered to be the effective temperature of the rectangular hole which accounts for temperature perturbation of the real specimen, but not for radiation loss.) Let the true emittance of the standard black-body hole $\epsilon_{\lambda ht}$ be defined by the relation

$$I_{\lambda h}(T_{he}) = \epsilon_{\lambda ht} I_{\lambda b}(T_{he}) \quad (H-4)$$

where $I_{\lambda b}(T_{he})$ is the radiant intensity of an ideal black body at temperature T_{he} . By combining equations (H-1) and (H-4) and eliminating $I_{\lambda h}$ the effective emittance of the rectangular hole becomes

$$\epsilon_{\lambda he} = \epsilon_{\lambda ht} [I_{\lambda b}(T_{he})/I_{\lambda b}(T_s)] \quad (H-5)$$

Applying the Planck equation for the spectral intensity at wavelength λ of an ideal black body of temperature T

$$I_{\lambda b}(T) = 2 c^2 h \lambda^{-5} (e^{hc/\lambda k T} - 1)^{-1} \quad (H-6)$$

where c is the speed of light
 h is Planck's constant
 k is the Boltzman constant

To express the ratio of ideal black-body intensities in equation (H-5), one obtains

$$\epsilon_{\lambda he} = \epsilon_{\lambda ht} \left(e^{hc/\lambda k T_s} - 1 \right) / \left(e^{hc/\lambda k T_{he}} - 1 \right) \quad (H-7)$$

While the true emittance of the rectangular black-body hole $\epsilon_{\lambda ht}$ accounts for the loss of radiant energy from the internal cavity of the tube and is thus in general less than 1.0, the ratio of the temperature-containing terms is greater than 1.0 if T_{he} is greater than T_s . Thus $\epsilon_{\lambda he}$ may be greater than 1.0 when T_{he} is sufficiently greater than T_s .

D. Discussion of Results

The variation of intensity at 0.6 micron along the length of the polished AISI-310 stainless steel (low thermal conductivity) specimen is represented in Figure H-2. This tube had no black body holes, although a nick was made in the tube to establish a reference position. Figure H-2 shows that the specimen had a smooth and symmetrical intensity profile, which was displaced approximately 0.160 inch from the physical midpoint of the specimen. The noncoincidence of the intensity profile suggests that the specimen wall had a slight taper. The absence of irregularities in the curve indicates that the tube wall was free from significant random variations in thickness along the length of the tube.

A high-contrast photograph was taken of a stainless steel tube with three black-body holes and coated with chromium black. It is apparent from the photograph (Figure H-3) that temperature perturbation is severe in the vicinity of the rectangular hole, but insignificant around the circular holes. The variation in intensity of the AISI-310 stainless steel tube coated with chromium black in the vicinity of the black-body hole is presented as a map in Figure H-4, and as an intensity profile in Figure H-5.

The variations in intensity at 0.6 and 2 microns along the columbium tube coated with acetylene black are represented by curves (1) and (2) in Figure H-6. It can be seen that at 2 microns the profile is irregular and also nonsymmetrical with respect to the specimen midpoint. The scan at 0.6 micron gave similar results, but the irregularities were even more pronounced because intensity is more affected by a change in temperature at the shorter wavelengths. The gross intensity variations were detected photographically and are shown in Figure H-7. It can be seen that the temperature perturbation in the vicinity of the rectangular black-body hole is considerably less than that observed on the stainless steel sample as a result of the greater thermal conductivity of the columbium. It is also apparent that there was either a variation in surface emittance or circumferential variations in wall thickness at the location of the circular black-body holes, indicating that the radiation from the holes was not necessarily representative of the temperature of the surface near the holes. The sudden drop in the measured surface intensity just below the rectangular black-body hole corresponds to the striations in the coating below the hole that are visible in the photograph.

Results of the intensity scan made on the uncoated, vapor-blasted columbium tube at 0.6 micron are presented by curve (3), Figure H-6. The intensity profile obtained is approximately the same as that for the coated specimen. Part of the difference that is shown by curves (2) and (3) in the region at a considerable distance above the upper black-body hole is believed caused by the nonuniformity of the coating, inasmuch as the coating, when heated, was visibly irregular in this region. Figure H-8 shows that temperature perturbation around the rectangular hole is not visually detectable on the vapor-blasted columbium tube. It can also be seen that the lower portion of the tube is not as luminous as the upper portion. This uneven distribution is substantiated by the data shown by curve (3) in Figure H-6.

The quality of the rectangular hole was determined on the basis of surface emittance values obtained at each of the circular holes. The results are shown in Table H-1.

In the case of the stainless steel tube coated with chromium black, the surface emittances measured at the circular holes were within 0.1 per cent of each other. Therefore the computed values of the quality of the rectangular black body are believed to be realistic. The fact that the values for the rectangular black-body hole are greater than 1.00 is undoubtedly a result of the significant temperature perturbation in the region of that hole.

The nonuniformity in the temperature of the columbium tube used in these experiments, as indicated both by the radiant intensity measurements and by examination of the photographs of the heated tube, presumably was the cause of the considerable difference in the surface emittance values measured at the two circular holes. It is presumed that the gross variations in temperature along the length of the tube were caused by a taper in the tube wall thickness. Of perhaps greater significance, however, is the likelihood of circumferential variations in wall thickness. Since circumferential intensity scans were not made, the only evidence that circumferential variations in thickness existed is contained in the photographs of the coated tube and the vapor-blasted tube, particularly the former, which show clearly that the small black-body hole on the cold end of the specimen (bottom) is actually brighter than the similar hole on the hot end of the specimen (top). This implies strongly that there is either a thin spot in back of the bottom hole or a thick spot in back of the top hole, or both. As would be expected, the

TABLE H-1
Rectangular Black-Body Hole Effective Emittance

	T °F	λ Microns	$\epsilon_{\lambda S U}$	$I_{\lambda S} / I_{\lambda h}$	$\epsilon_{\lambda S I}$	$\epsilon_{\lambda S, \Delta V}$	$\epsilon_{\lambda h e}$
Chromium black on AISI 310 stainless steel tube having a 0.005-inch wall	1600	0.6	0.868	0.8375	0.8745	0.871	1.04
	1600	2.0	0.7755	0.7642	0.7715	0.7735	1.012
Acetylene black in xylol on columbium tube having 0.005-in. wall and 1/4-in. diameter	1605	0.6	0.9622	0.9205	0.8696	0.9159	
	1605	2.0	0.9648	0.9511	0.9522	0.9585	
The above columbium tube with acetylene black removed and then vapor-blasted	1605	0.6	0.6505	0.6553	0.6226	0.6365	

Where:

T = specimen temperature level, °F

λ = wavelength of spectral intensity measurements, microns

$\epsilon_{\lambda S U}$ = spectral normal emittance of the specimen surface determined at the upper circular black-body hole

$\epsilon_{\lambda S I}$ = surface emittance determined at the lower circular hole

$\epsilon_{\lambda S, \Delta V}$ = average of the surface emittances obtained at the two circular holes

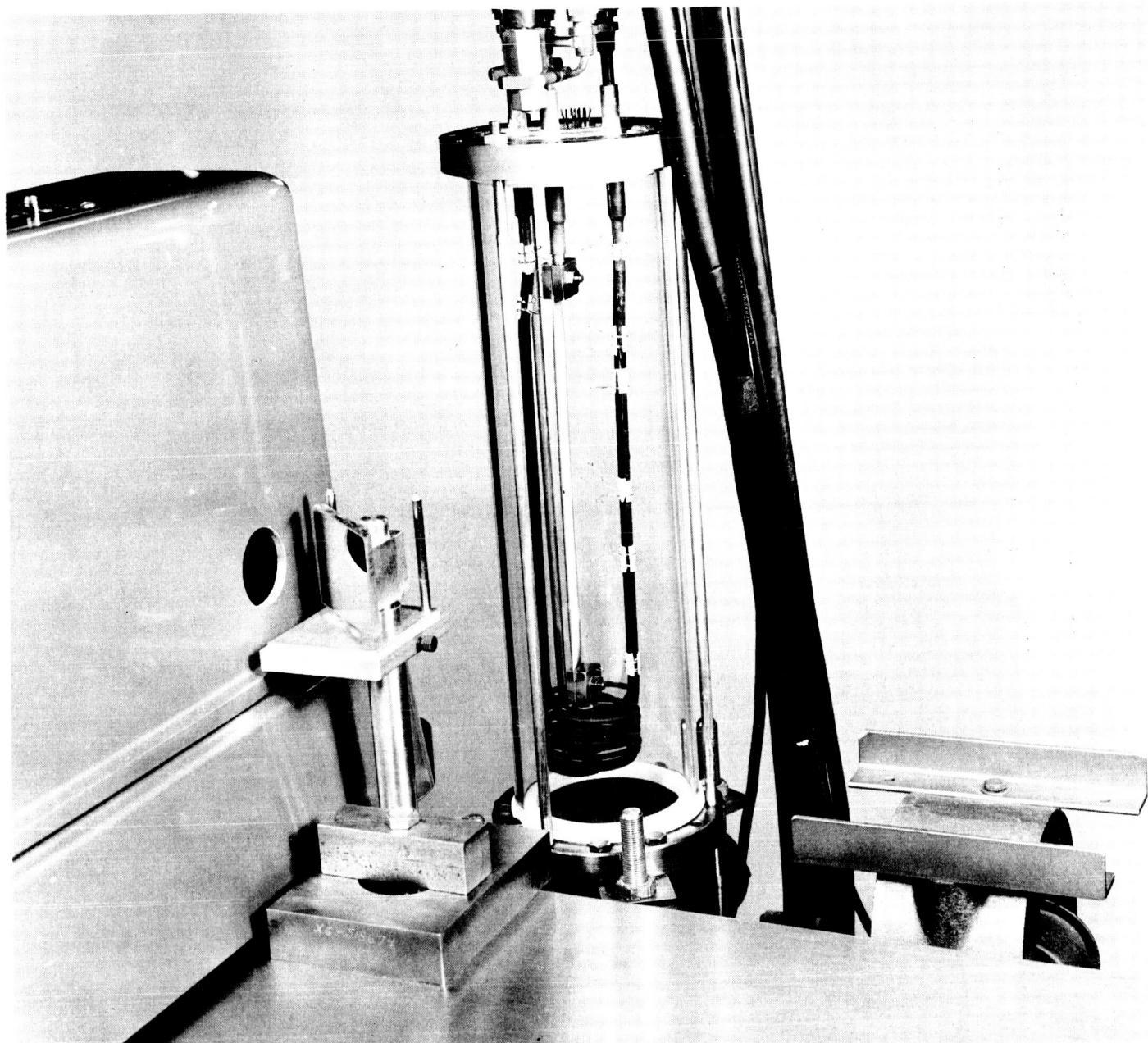
$I_{\lambda S} / I_{\lambda h}$ = surface-to-hole intensity ratio at the rectangular black-body hole

$\epsilon_{\lambda h e}$ = effective emittance of rectangular black-body hole calculated by equation (H-3), using $\epsilon_{\lambda S, \Delta V}$ as the surface emittance at the rectangular hole together with the intensity ratio measured at the rectangular hole

effect of the nonuniform tube wall thickness was accentuated when a coating of high emittance material was applied to the base metal. Since this particular tube was finish-ground on the outside after drawing, it is considered likely that the grinding operation contributed to the suspected nonuniformity of wall thickness.

Since, as shown in the photographs, the surface emittances near the two circular holes disagree considerably, a computation of the quality of the rectangular black-body hole in the columbium tube was not justified. This was particularly true of the data obtained on the blackened specimen at 0.6 micron. If, as already postulated, the discrepancies are due to local variations in wall thickness and consequently to local variations in temperature, one would expect from a consideration of Planck's law that the difference would be subsequently larger at 0.6 micron than at 2 microns.

Even though it was not possible to compute the effective emittance (black-body quality) of the rectangular black-body hole for the columbium specimen, it was demonstrated that the temperature perturbation around the rectangular black-body hole was considerably less with columbium than with stainless steel. Consequently, it may be concluded that the effective emittances for the columbium rectangular black-body hole are less than those measured for the stainless steel specimen, namely: less than 1.04 at 0.6 micron and 1.012 at 2 microns. This investigation demonstrated the desirability of using specimen tubes with high thermal conductance and the necessity of having tubes of uniform wall thickness.



PYREX CHAMBER USED FOR BLACK-BODY QUALITY EVALUATION TESTS AND FOR MEASUREMENTS OF RADIANT INTENSITY VARIATIONS

Figure H-1

VARIATION OF RELATIVE RADIATION INTENSITY ALONG AXIS OF POLISHED AISI-310 STAINLESS STEEL TUBE

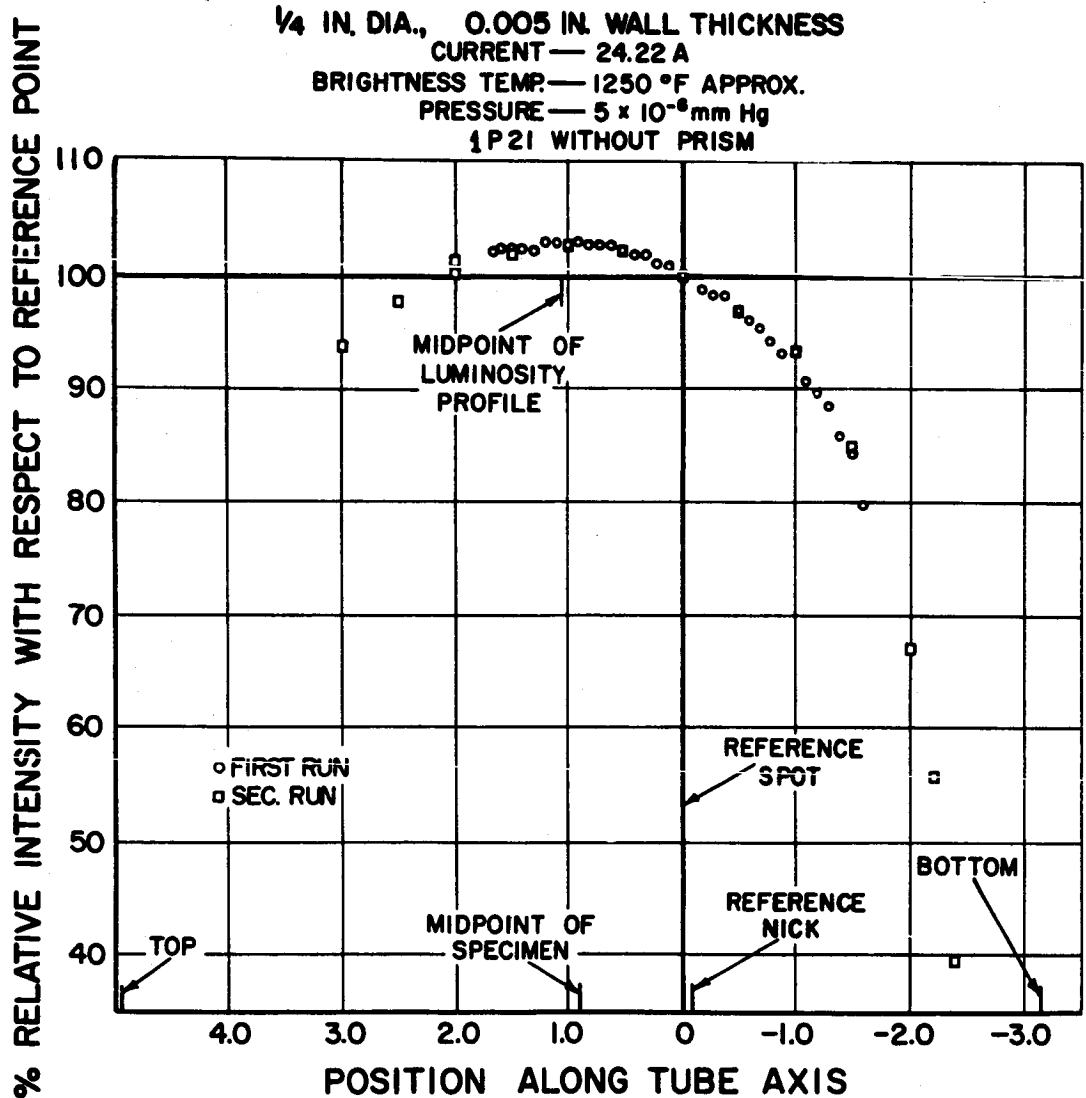
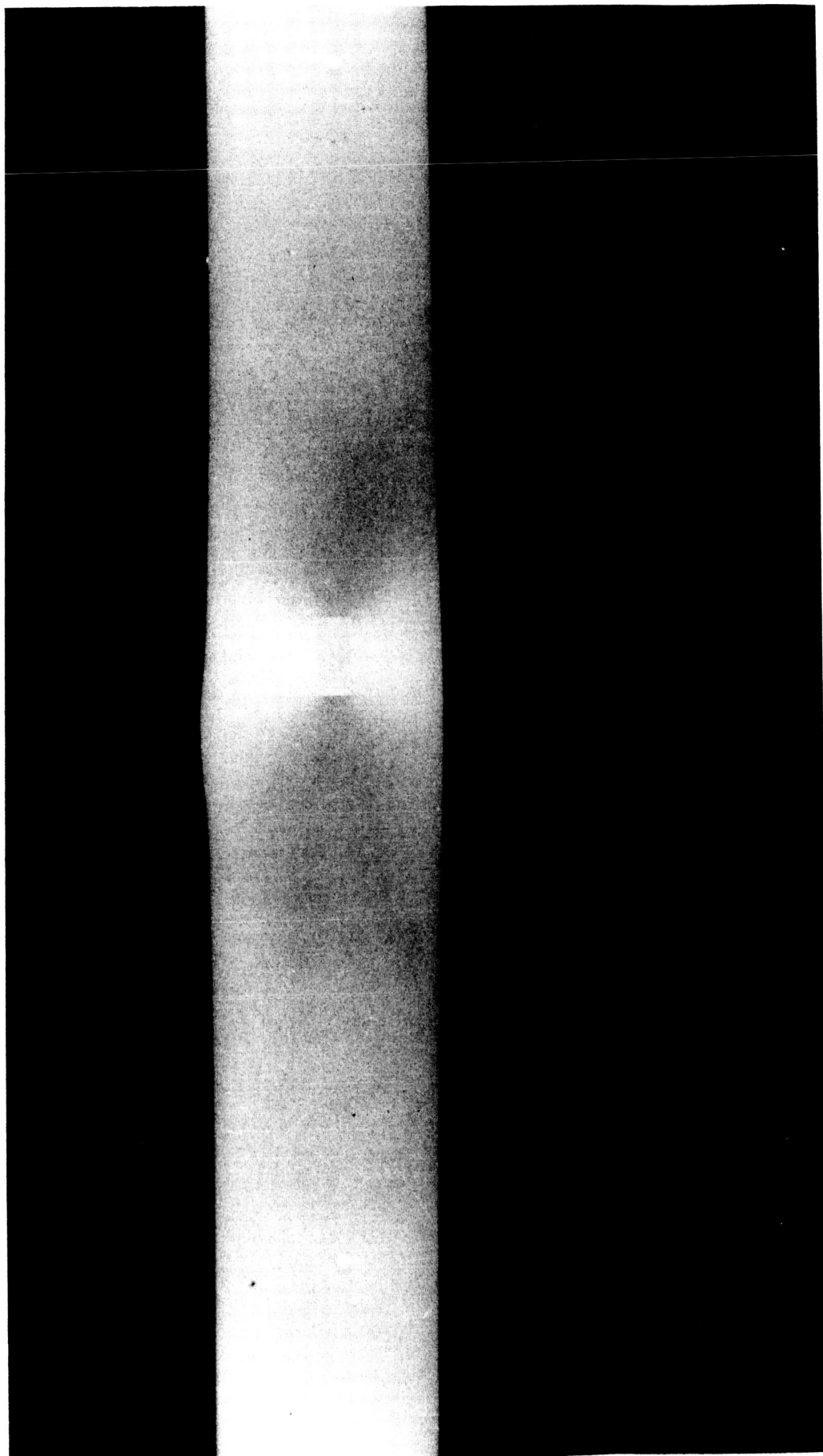


Figure H-2



AISI-310 STAINLESS STEEL TUBE COATED WITH CHROMIUM BLACK



Figure H-3

INTENSITY MAP IN VICINITY OF .035 X .070 BLACK BODY HOLE OF CHROMIUM BLACKENED 310 SS TUBE WITH .005" WALL AT 1445°F AND 2.45U

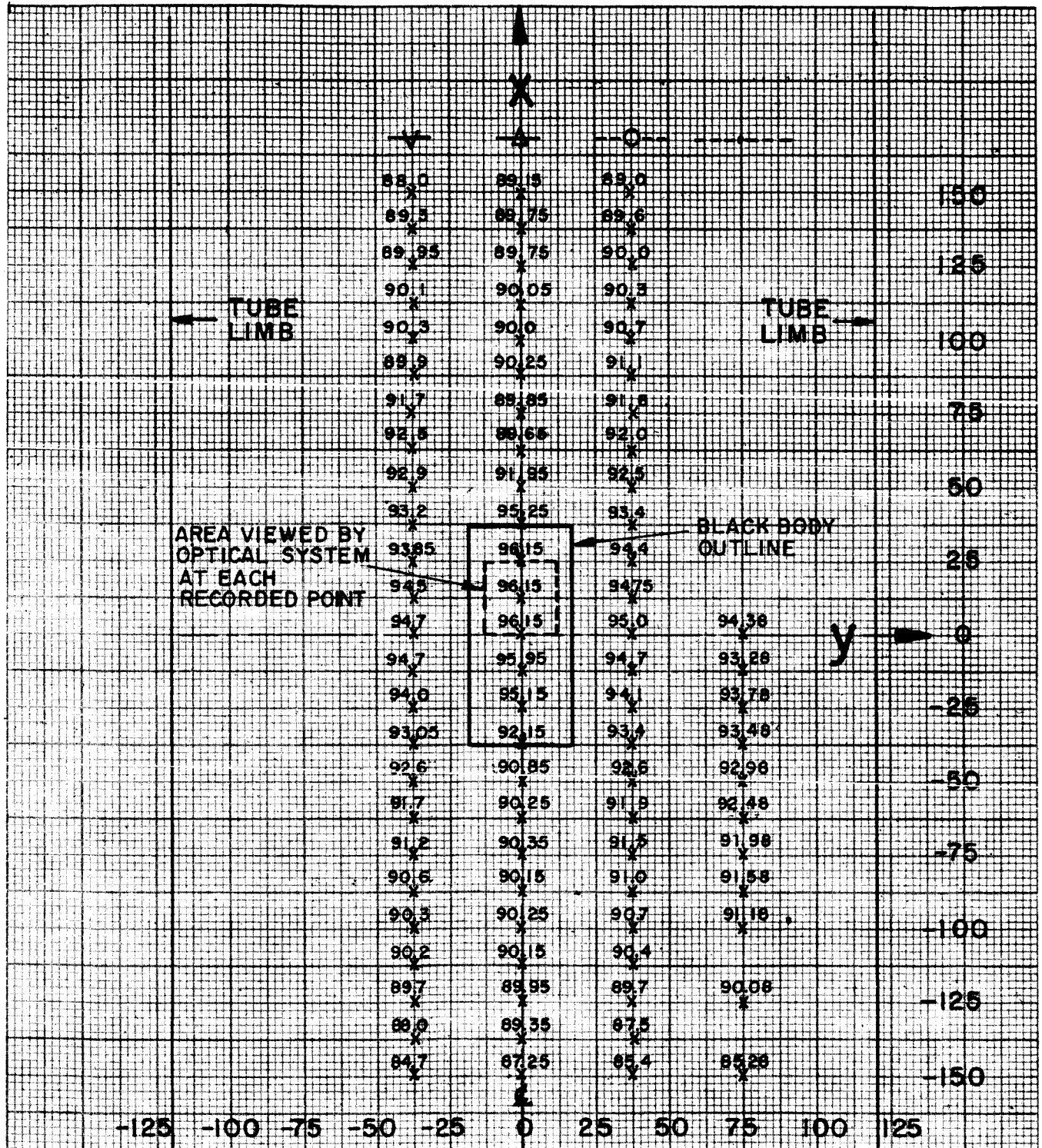


Figure H-4

INTENSITY CONTOURS IN VICINITY OF 0.035 x 0.070
 BLACKBODY HOLE OF CHROMIUM BLACKENED
 310 SS TUBE WITH 0.005 IN. WALL AT 1445 °F
 TOTAL & SPECTRAL $\epsilon = 0.9$
 DATA TAKEN AT 2.45 μ

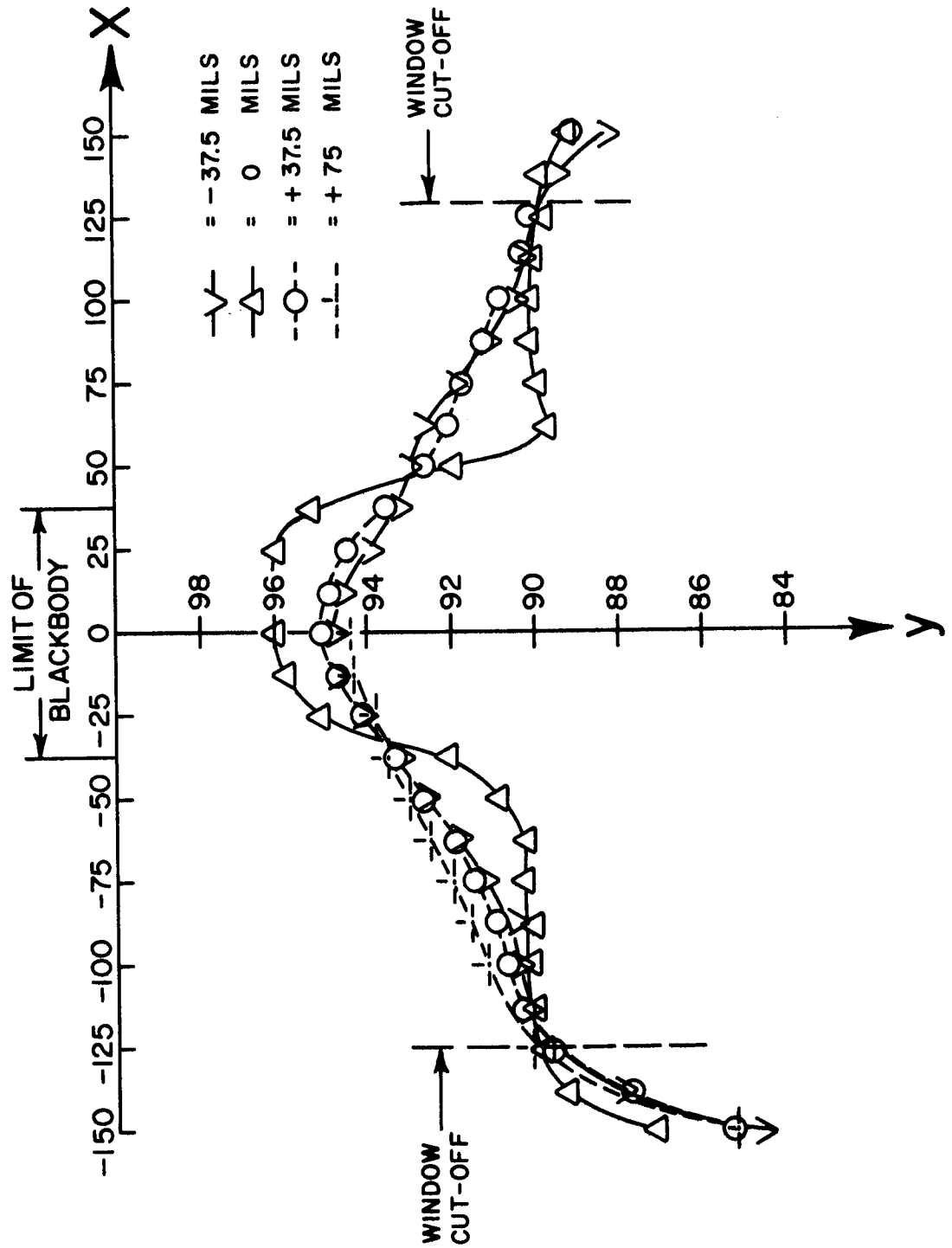
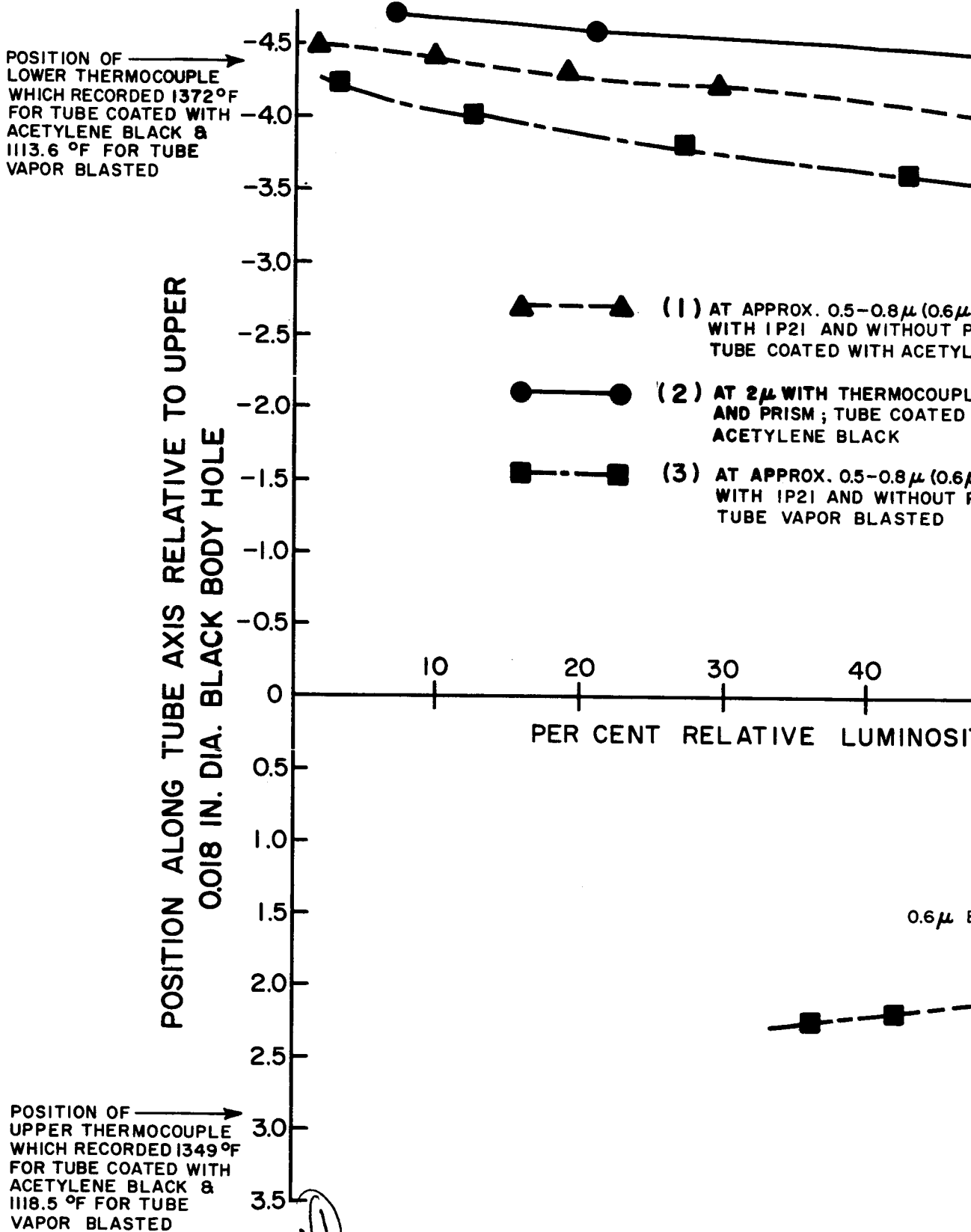


Figure H-5

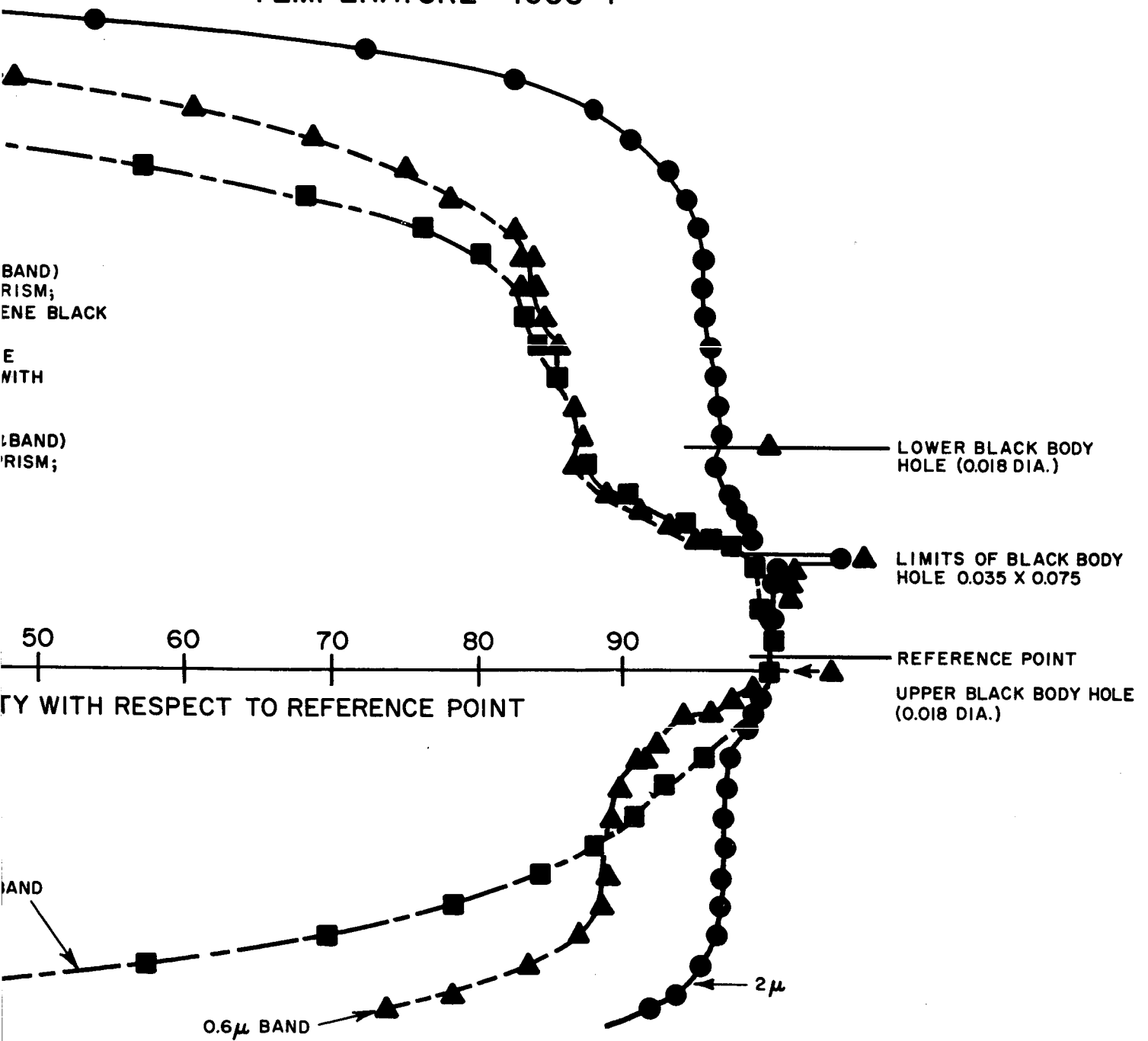
MEASUREMENTS OF R ALONG AXIS OF 1/4 IN 0.0



H-60

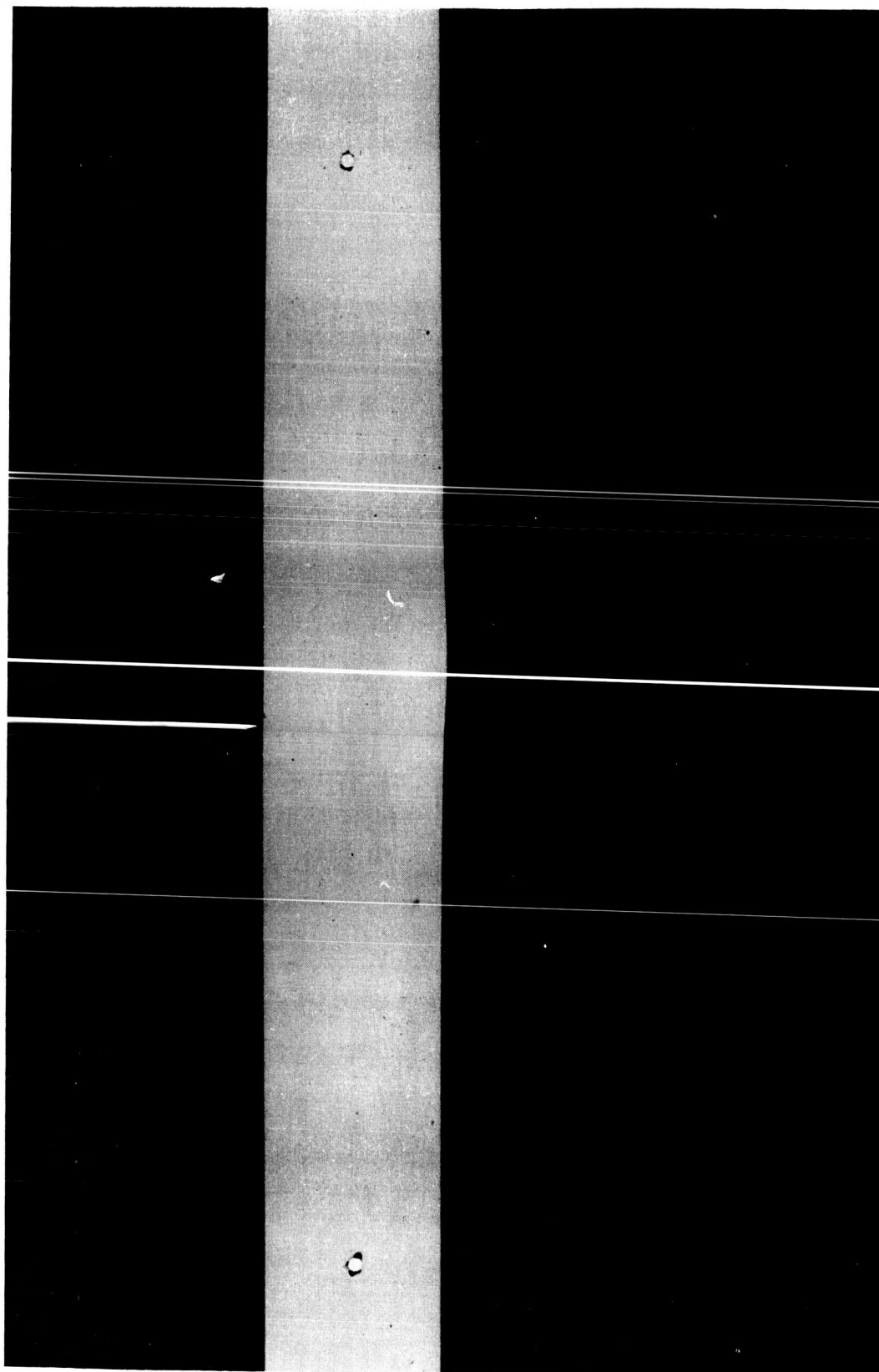
RELATIVE RADIATION INTENSITY 1/8 DIA. COLUMBIUM TUBE WITH 0.05 IN. WALL

CURRENT = 93.11 A REGULATED
TEMPERATURE = 1605 °F



2

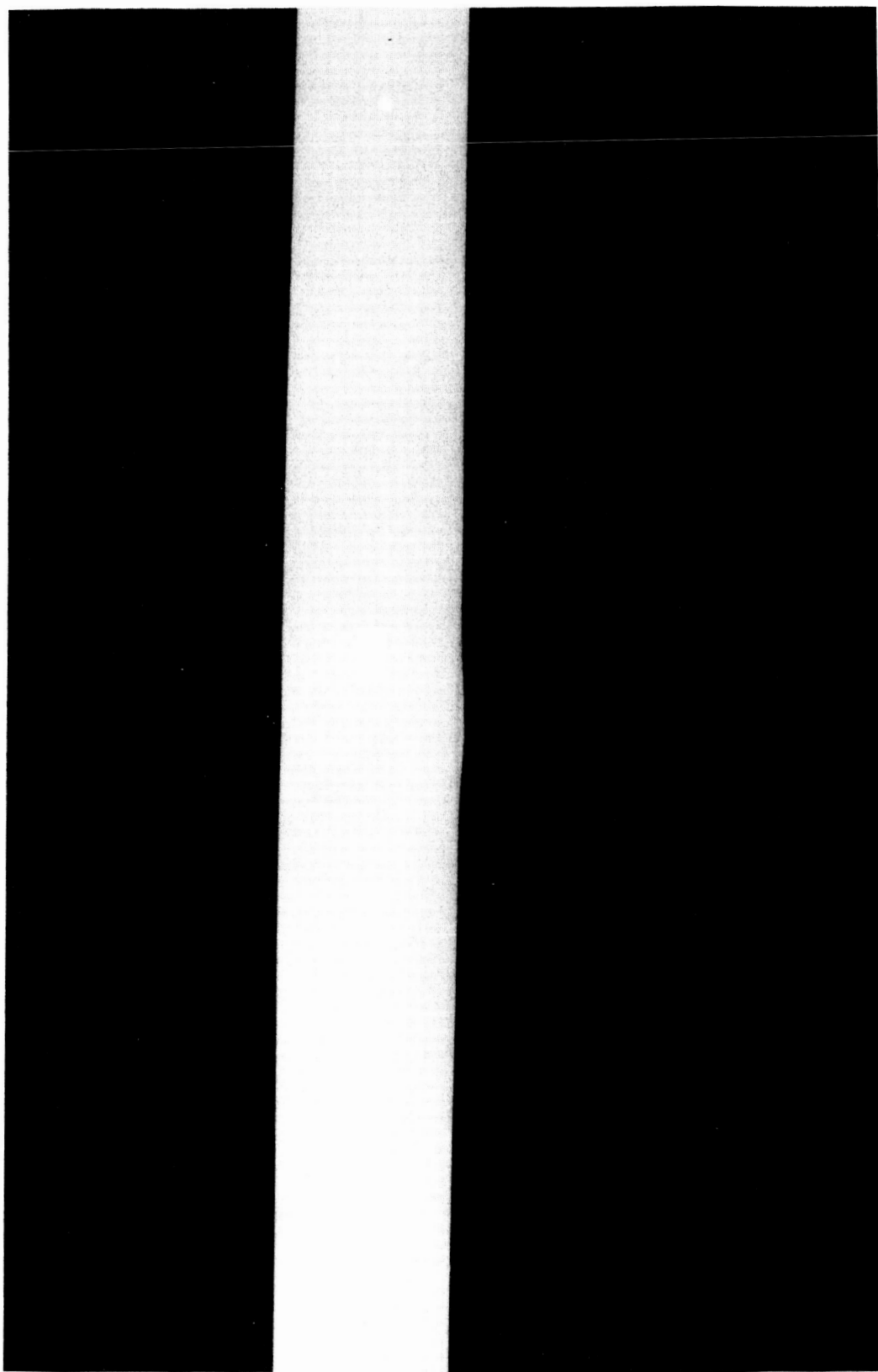
Figure H-6



COLUMBIUM TUBE COATED WITH ACETYLENE BLACK



Figure H-7



VAPOR-BLASTED COLUMBIUM TUBE



Figure H-8

APPENDIX I

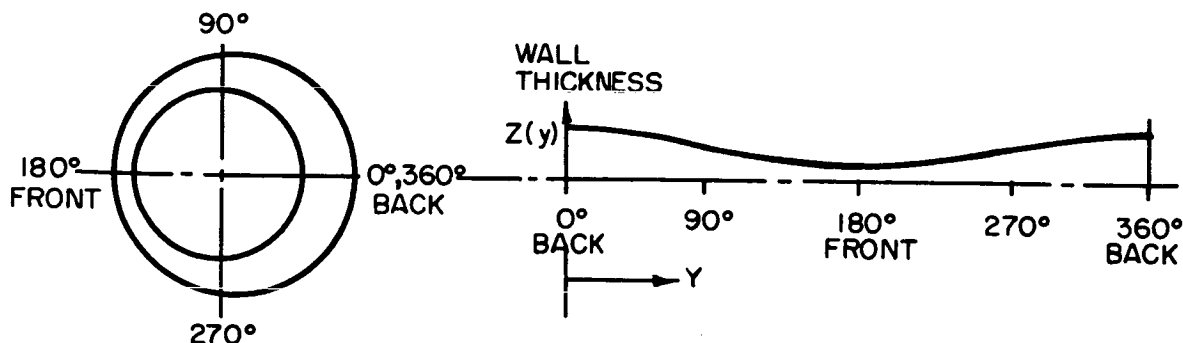
Effect of Nonuniform Wall Thickness
on Temperature Distribution

APPENDIX I

EFFECT OF NONUNIFORM WALL THICKNESS
ON TEMPERATURE DISTRIBUTION

A resistance-heated specimen with a nonuniform wall thickness will have a nonuniform surface temperature. For example, if a cylindrical tubular specimen had a front wall which was thinner than the back wall, the front wall would be cooler than the back wall. The measured emittance of such a specimen would be lower than the true value since the surface radiant intensity of the cooler-than-average front wall would be compared to a black-body hole intensity primarily dependant on the hotter-than-average back wall.

Although the example cited above is a special case, it was felt that this type of nonuniformity merited analysis since drawn tubes were extensively used for spectral emittance measurements. In particular, it will be assumed that the wall thickness nonuniformity is such that the inner cylindrical surface centerline is displaced from the outer cylindrical surface centerline. The wall thickness will then vary as shown in the sketch below.



For determining the approximate peripheral temperature variation, the following assumptions are made:

- 1) Heat is generated throughout the tube wall at the uniform rate per unit volume g_0 ,
- 2) The wall temperature is only a function of peripheral location,

- 3) The heat transferred by radiation on the inside of the tube is negligible compared to the heat transferred by conduction, and
- 4) The thickness of the heat-flow path for conducted heat in the peripheral direction may be approximated as the mean wall thickness.

The wall thickness $z(\gamma)$ may be expressed quite accurately as a mean thickness z_m plus a sinusoidal variation of half amplitude z_1 and period equal to the periphery, that is

$$z(\gamma) = z_m + z_1 \cos(2\pi\gamma/\gamma_0) \quad (I-1)$$

where γ_0 is the periphery of the tube, and γ is the peripheral distance from the thickest point of the wall.

To find the temperature variation around the periphery, consider the heat balance of an element of volume between γ and $\gamma + d\gamma$, where the wall thickness is $z(\gamma)$. The rate of heat generation in the volume element $g_o \times z(\gamma) d\gamma$ is equated to the rate of heat dissipation by radiation from the outer tube surface $[T(\gamma)^4 - T_w^4] \times d\gamma$, plus the rate of conduction out of the element $dy [d/dy] [-kz(\gamma) \times T'(\gamma)]$, yielding the differential equation

$$[d/dy][z(\gamma)T'(\gamma)] - [\epsilon\sigma/k][T(\gamma)^4 - T_w^4] = -(g_o/k)z(\gamma) \quad (I-2)$$

By symmetry, the temperature profile must have a zero slope at $\gamma = 0$ and at $\gamma = (1/2)\gamma_0$, that is, $T'(\gamma=0) = T'(\gamma=1/2\gamma_0) = 0$, and, furthermore, $T(\gamma)$ must be a periodic function of γ of period γ_0 .

Due to the symmetry of the temperature profile, it is also possible to construct the heat balance over the entire periphery, since no conduction heat enters or leaves the region $\gamma=0$ to $\gamma=\gamma_0$. Thus

$$g_o \times z_m \gamma_0 = \epsilon \sigma \times \int_{\gamma=0}^{\gamma_0} (T(\gamma)^4 - T_w^4) d\gamma \quad (I-3)$$

$$\text{Let } \phi(\gamma) = \frac{T(\gamma) - T_{av}}{T_{av}} \quad (I-4)$$

where $T_{av} = (1/\gamma_0) \int_{\gamma=0}^{\gamma_0} T(\gamma) d\gamma$ is the average wall temperature.

For the case where the temperature variation is small compared to the temperature level, that is, where $0 < |\phi(y)| \ll 1$, then

$$T(y)^4 = T_{av}^4 [1 + 4\phi(y)] \quad (I-5)$$

and
$$\int_{y=0}^{y_0} \phi(y) dy = 0 \quad (I-6)$$

Substituting equation (I-5) into equation (I-3) and applying equation (I-6), yields from the overall heat balance

$$q_o = \frac{\epsilon \sigma (T_{av}^4 - T_w^4)}{z_m} \quad (I-7)$$

Substituting equations (I-4), (I-5), and (I-7) into equation (I-2) and applying the approximation that z_m may be substituted for $z(y)$ in the heat conduction term of equation (I-2) yields the differential power balance

$$\phi''(y) - 4B\phi(y) = -B(z_1/z_m) \cos(2\pi y/y_0) \quad (I-8)$$

where

$$B = \frac{\epsilon \sigma T_{av}^3}{k z_m} \quad (I-9)$$

and boundary conditions

$$\phi'(y=0) = \phi'[y=(1/2)y_0] = 0 \quad (I-10)$$

The solution of equation (I-8) which satisfies the boundary conditions of equation (I-10) is

$$\phi(y) = \frac{B y_0^2 z_1 / z_m}{(4\pi^2 + 4B y_0^2) \cos(2\pi y / y_0)} \quad (I-11)$$

The ratio of the maximum per cent deviation of temperature to the maximum per cent deviation of thickness is thus

$$\frac{\phi(y=0)}{z_1 / z_m} = \frac{1}{[4\pi^2 / B y_0^2] + 4} \quad (I-12)$$

It is seen that as $B y_0^2$ approaches infinity, the per cent deviation in temperature increases to one-fourth of the per cent deviation in thickness. For finite $B y_0^2$, the per cent deviation in temperature will be less than one-quarter of the per cent deviation of thickness. As an example, the maximum value of $B y_0^2$ for 1/4-inch diameter tubing such as used for spectral emittance measurements corresponds to maximum emittance 0.9, maximum temperature level

2500°R (2140°F), minimum conductivity 10 BTU/hr-ft-°F., and minimum tube wall thickness 0.005 inch. For these quantities, $B \gamma_o^2 = 26$ (dimensionless), and $\phi(\gamma=0)/(z/z_m) = 0.18$. Specifications for the tubing used required a maximum thickness deviation of less than 1 per cent. For the maximum thickness deviation of 1 per cent the corresponding maximum $\phi(\gamma=0)$ equals 0.0018. If it is further assumed that the orientation of the specimen is such that the surface from which the measuring beam is emitted is at the lowest temperature, and that the black-body radiation is emitted entirely from an area at the highest temperature, then the fractional temperature difference would be 0.0036 and the error in the calculated emittance for this extreme case would be less than 1.5 per cent. Actually, it is believed unlikely that the error in emittance measurements resulting from nonuniform wall thickness ever approached the value calculated for the extreme example cited above.

APPENDIX J

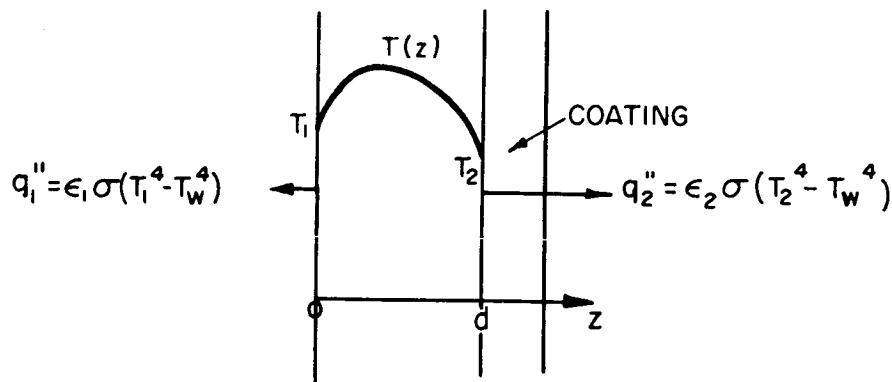
Temperature Difference Between Two
Surfaces of a Thin Strip Radiating
at Two Emittances

APPENDIX J

TEMPERATURE DIFFERENCE BETWEEN TWO SURFACES
OF A THIN STRIP RADIATING AT TWO EMITTANCES

A temperature difference exists between the two surfaces of a specimen strip if these surfaces have different emittances. Specimens coated on only one side were used early in the program and thermocouples were installed only on the uncoated side. Installation of thermocouples on the uncoated side of the specimen precluded possible thermocouple contamination by the coating material and also eliminated the necessity of scratching away the coating at the point of thermocouple attachment. However, it was necessary to determine the temperature differences between the coated and uncoated surfaces of the specimen. This difference is calculated below.

Consider the situation shown in the sketch below:



Assuming that heat is generated only in the base metal strip with a rate per unit volume of g , the one-dimensional differential heat balance for an element within the base metal having a volume thickness dZ is

$$T''(z) = -g/k \quad (J-1)$$

The boundary conditions at $z = 0$ are

$$kT'(z=0) = q_1'', \quad T(z=0) = T_1 \quad (J-2)$$

The rate of heat radiation from the uncoated surface $q_1'' = \epsilon_1 \sigma (T_1^4 - T_w^4)$ plus the rate of heat radiation from the coated surface $q_2'' = \epsilon_2 \sigma (T_2^4 - T_w^4)$ equals the rate of heat generation gd . Thus

$$q_1'' + q_2'' = gd \quad (J-3)$$

Solving equation (J-3) for q_2'' , substituting into equation (J-1) and integrating once with respect to Z yields

$$T'(z) = - (q_1'' + q_2'') z / kd + C_1 \quad (J-4)$$

Combining the first of equations (J-2) with equation (J-4) yields

$$T'(z) = - (q_1'' + q_2'') z / kd + q_1'' / k \quad (J-5)$$

Integrating equation (J-5) once with respect to Z yields

$$T(z) = - (q_1'' + q_2'') z^2 / 2kd + q_1'' z / k + C_2 \quad (J-6)$$

Combining the second of equations (J-2) with equation (J-6) yields

$$T(z) = - (q_1'' + q_2'') z^2 / 2kd + q_1'' z / k + T_1 \quad (J-7)$$

Letting $T(z=d) = T_2$, equation (J-7) yields

$$(T_2 - T_1) / T_1 = (q_1'' - q_2'') d / 2kT_1 \quad (J-8)$$

Now, the Stefan-Boltzmann law gives for the i^{th} surface

$$q_i'' = \epsilon_i \sigma (T_i^4 - T_w^4) \quad (J-9)$$

Let
$$\phi_i = (T_i - T_1) / T_1 \quad (J-10)$$

Then
$$T_i^4 \approx T_1^4 (1 + 4\phi_i) \quad (J-11)$$

for $0 < |\phi_i| < 1$. Substituting equations (J-9), (J-10), and (J-11) into (J-8) and solving for ϕ_2

$$\phi_2 = \frac{\beta [1 - (\epsilon_2 / \epsilon_1)] [1 - (T_w / T_1)^4]}{1 + 4\beta (\epsilon_2 / \epsilon_1)} \quad (\text{J-12})$$

where
$$\beta = \frac{\epsilon_1 \sigma T_1^3 d}{2k}$$

Figure J-1 is a curve of equation (J-12) with T_1 as the variable for a molybdenum strip coated with boron by the Plasmarc process. Figure J-2 contains curves of equation (J-12) for various other strip materials with strip thickness as the variable. It is seen that the effect of temperature drop across the specimen thickness may be neglected.

TEMPERATURE DIFFERENCE BETWEEN TWO SURFACES OF THIN STRIP RADIATING AT DIFFERENT EMISSIVITIES

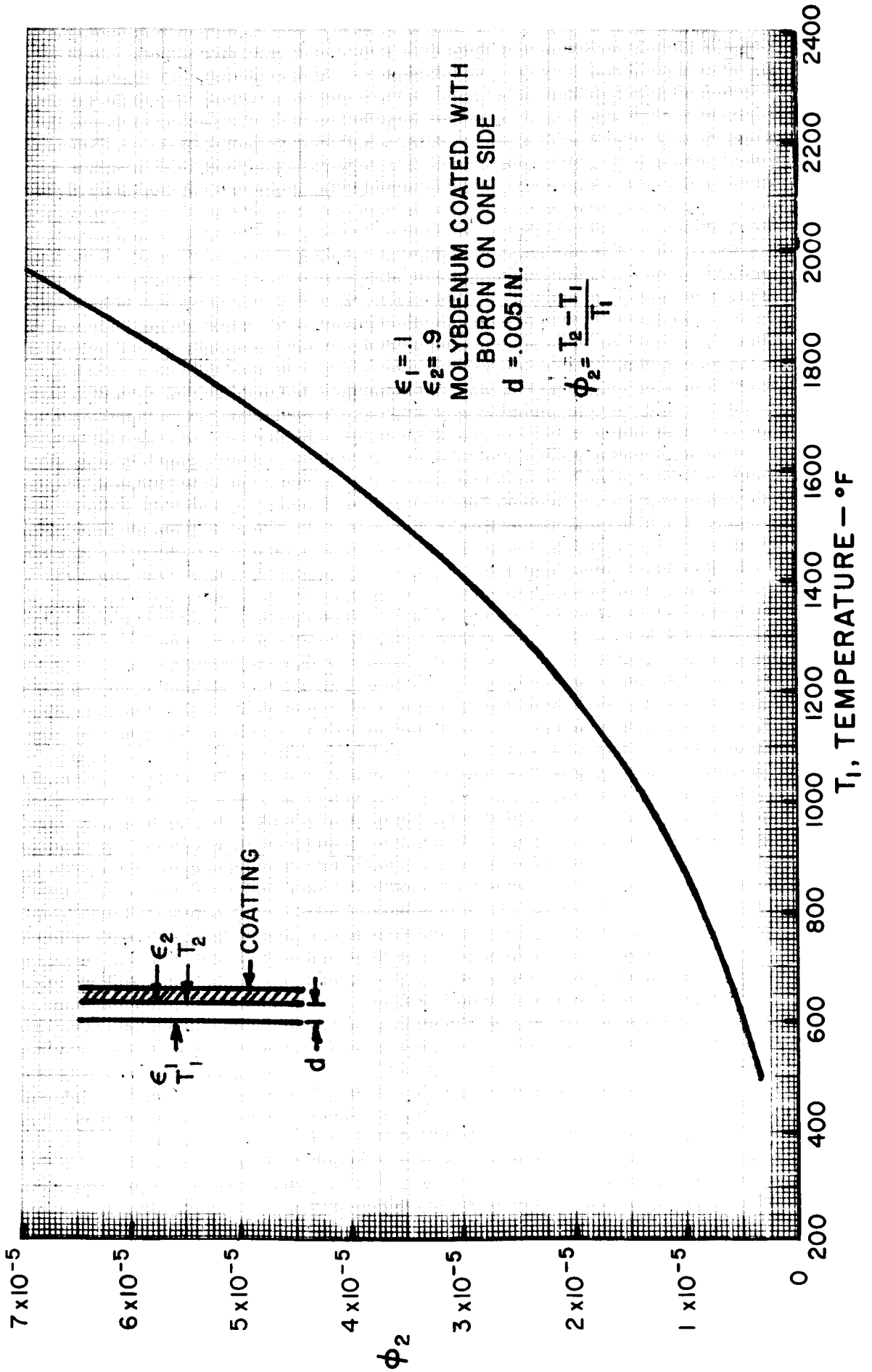


Figure J-1

TEMPERATURE DIFFERENCE BETWEEN TWO SURFACES OF THIN STRIP RADIATING AT DIFFERENT EMITTANCES

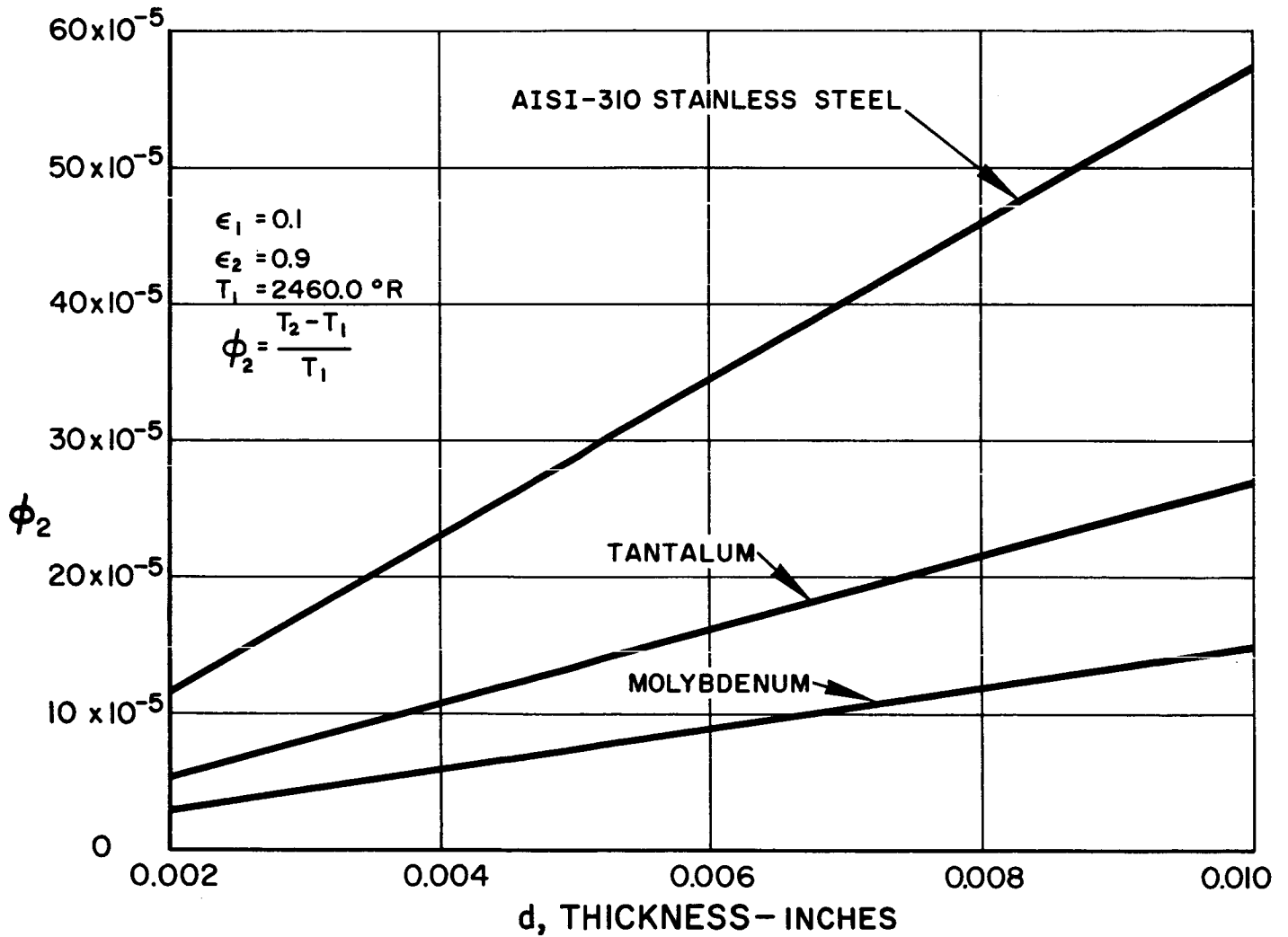


Figure J-2

APPENDIX K

Errors in Total Hemispherical Emittance
Measurements Resulting From the Use
of Alternating Heating Currents

APPENDIX K

ERRORS IN TOTAL HEMISPHERICAL EMITTANCE
MEASUREMENTS RESULTING FROM THE USE
OF ALTERNATING HEATING CURRENTS

Alternating current is used for direct resistance heating of specimens tested in the total hemispherical emittance rig. One of the advantages of using alternating current is that possible errors in thermocouple temperature measurements resulting from the IR voltage drop between the attachment points of two thermocouple leads tend to average out to zero over a cycle. However, since the power generation rate per unit volume varies with time from zero to double the time-average rate twice for each current cycle, it is necessary to estimate how much error in the calculation of emittance results from the corresponding fluctuations in the specimen temperature.

It may be readily seen that the time-average specimen temperature, as indicated by a slow response thermocouple indicator, would not necessarily be equal to the effective mean temperature for thermal radiation from the specimen. Assuming that the thermocouple indicates the time-average temperature, then

$$T_{av} = \frac{1}{\tau} \int_{t=0}^{\tau} T(t) dt \quad (K-1)$$

where τ is the cycle period for the heat generation rate and the specimen temperature, and T_{av} is the average temperature indicated by the thermocouple. In the calculation of total hemispherical emittance as determined in these tests, the basic equation may be written

$$\epsilon_c = \frac{g_o A_{cs}}{\sigma \rho (T_{av}^4 - T_w^4)} \quad (K-2)$$

where g_o is the time-average power generation rate per unit volume, A_{cs} is the test section surface area, σ is the Stefan-Boltzmann constant, ρ is the specimen perimeter, and T_w is the sink temperature. The true emittance is defined by the equation

$$g_o A_{cs} = \epsilon \sigma \rho \frac{1}{\tau} \int_{t=0}^{\tau} [T(t)^4 - T_w^4] dt \quad (K-3)$$

where ϵ is true emittance. Thus ϵ and ϵ_c are equal only if

$$\left[\frac{1}{\tau} \int_{t=0}^{\tau} T(t) dt \right]^4 = \frac{1}{\tau} \int_{t=0}^{\tau} T(t)^4 dt$$

If $T(t)$ varies sinusoidally with time about some mean value T_{av} , the above equation is not true, and ϵ_c is, therefore, not equal to ϵ . To estimate the fractional deviation of ϵ from ϵ_c , the temperature fluctuations of the specimen are estimated analytically and the fractional deviation of ϵ from ϵ_c is determined from equations (K-2) and (K-3) to give

$$\frac{\epsilon_c - \epsilon}{\epsilon} = \frac{\frac{1}{\tau} \int_{t=0}^{\tau} T(t)^4 dt - T_{av}^4}{T_{av}^4 - T_w^4} \quad (K-4)$$

The relation of $T(t)$ to the frequency of power generation and to the temperature level, density, heat capacity, and geometry of the specimen is estimated by consideration of the transient power balance on a portion of the specimen. Temperature is assumed to vary only with time and not with location in the test section. At any particular time the rate of storing heat in the specimen $\chi A_{cs} \rho C_p (dT(t)/dt)$, is equated to the rate of generating heat $\chi A_{cs} g(t)$, minus the rate of radiating heat $\chi p \epsilon \sigma [T(t)^4 - T_w^4]$, where χ is the specimen thickness and C_p is the heat capacity of the material. Thus

$$T'(t) + \frac{p \epsilon \sigma}{A_{cs} \rho C_p} [T(t)^4 - T_w^4] = \frac{g(t)}{\rho C_p} \quad (K-5)$$

where the power generation rate per unit volume is taken to vary as for a sinusoidal current variation with time

$$g(t) = g_o [1 + \cos(\omega t)] \quad (K-6)$$

Here g_o is the mean heat generation rate per unit volume and $\omega = 4\pi f$ where f is the frequency of current oscillation.

Combining equations (K-5) and (K-6) yields a nonlinear differential equation for which the desired periodic solution would be an infinite Fourier series. For the purposes of this analysis it is considered reasonable to approximate $T(t)^4$ with an appropriate linear function of $T(t)$ as indicated below. Combining equations (K-5) and (K-6) and letting $\phi(t) = (T(t) - T_{av}) / T_{av}$, the differential equation (K-5) becomes

$$\phi'(t) = G [1 + \cos(\omega t)] - k \left\{ [1 + \phi(t)]^4 - [T_w / T_{av}]^4 \right\}$$

where $G = g_0 / \rho C_p T$ and $K = \epsilon \rho \sigma T_{av}^3 / A_{cs} \rho C_p$. Restricting consideration to the region $0 < |\phi(t)| \ll 1$

$$[1 + \phi(t)]^4 \approx 1 + 4\phi(t) \quad (K-8)$$

In order to substitute (K-8) into (K-7), K is replaced by K_e where $K_e = \epsilon_e \rho \sigma T_{av}^3 / A_{cs} \rho C_p$ and ϵ_e is a quantity that will be determined to satisfy equation (K-1). Providing that equation (K-1) is valid for the resulting $\phi(t)$, the differential equation (K-7) becomes

$$\phi'(t) + 4K_e \phi(t) = \chi + G \cos(\omega t) \quad (K-9)$$

where $\chi = G - K_e [1 - (T_w/T_e)^4]$. The solution of interest in this analysis is the periodic solution valid after starting transients have died out. This solution may be written in the complex Fourier series from

$$\phi(t) = \sum_{n=-\infty}^{\infty} C_n e^{in\omega t} \quad (K-10)$$

where $i = (-1)^{1/2}$

$$\text{Now } \cos(\omega t) = \frac{e^{i\omega t} + e^{-i\omega t}}{2} \quad (K-11)$$

Substituting (K-10) and (K-11) into (K-9), and equating coefficients of like powers of e

$$C_0 = \frac{\chi}{4K_e} \quad (K-12)$$

$$C_1 = \frac{G [1 - i(\omega/4K_e)]}{8K_e [1 + (\omega/4K_e)^2]} \quad (K-13)$$

$$C_{-1} = \frac{G [1 + i(\omega/4K_e)]}{8K_e [1 + (\omega/4K_e)^2]} \quad (K-14)$$

$$C_{n \geq 2} = C_{n \leq -2} = 0$$

the solution of (K-9) is $\phi(t) = C_0 + C_1 e^{i\omega t} + C_{-1} e^{-i\omega t}$ (K-15)

C_1 and C_{-1} are seen to be complex conjugate constants, and C_0 may be shown to be the mean value of $\phi(t)$ over one cycle of power generation. It is readily seen that for equation (K-15) to satisfy (K-1), C_0 must equal zero. Thus by equation (K-12) $0 = \mathcal{N}/4k_e$ which, upon substitution of the definitions of \mathcal{N} and k_e , gives the relation

$$g_0 A_{cs} = p \epsilon_e \sigma (T_{av}^4 - T_w^4) \quad (K-16)$$

Comparison of equations (K-16) and (K-2) yields the result that $\epsilon_e = \epsilon_c$. Thus, finally, the desired solution is

$$\phi(t) = C_1 e^{i\omega t} + C_{-1} e^{-i\omega t} \quad (K-17)$$

where

$$C_1 = \frac{G [1 - i(\omega/4k_c)]}{8k_c [1 + (\omega/4k_c)^2]} \quad (K-18)$$

$$C_{-1} = \bar{C}_1 \quad (\text{bar denotes "complex conjugate of"}) \quad (K-19)$$

and

$$k_c = \frac{\epsilon_c \rho \sigma T_{av}^3}{A_{cs} \rho C_p} \quad (K-20)$$

Now that the temperature variation with time is established as

$$T(t) = T_{av} [1 + \phi(t)] \quad (K-21)$$

the fractional deviation of ϵ_c from ϵ may be evaluated using equation (K-4). Substitution of equation (K-21) into equation (K-4) yields

$$\frac{\epsilon_c - \epsilon}{\epsilon} = \frac{(1/\bar{T}) \int_{t=0}^{\tau} [4\phi(t) + 6\phi(t)^2 + 4\phi(t)^3 + \phi(t)^4] dt}{1 - (T_w/T_{av})^4} \quad (K-22)$$

where $\gamma = \frac{2\pi}{\omega}$

Substituting equation (K-17) into equation (K-22) and integrating yields

$$\begin{aligned} \frac{\epsilon_c - \epsilon}{\epsilon} &= \frac{12(C_1 \bar{C}_1) + 6(C_1 \bar{C}_1)^2}{1 - (T_w/T_{av})^4} \\ &= \frac{[\frac{3}{16}] [1 - (\frac{T_w}{T_{av}})^4]}{1 + \gamma^2} + \frac{[\frac{3}{32}] [1 - (\frac{T_w}{T_{av}})^4]^3}{(1 + \gamma^2)^2} \end{aligned} \quad (K-23)$$

where
$$\Gamma = \frac{w \rho C_p A_{cs}}{4 \epsilon_c \sigma_p T_{av}^3}$$

As an estimate of the upper limit of fractional deviation due to AC flickering between true emittance ϵ and the calculated value ϵ_c , based on a time average specimen temperature indication, the minimum value of Γ is estimated for the subject tests, taking

$$\begin{aligned} f &= 60 \text{ cycles/second} \\ w &= 4\pi f = 216,000 \text{ per hour} \\ \rho &= 500 \text{ pounds/ft}^3 \\ C_p &= .10 \text{ BTU/pound} - ^\circ\text{R} \\ A_{cs}/\rho &\equiv d_{sa}/2 \text{ for strip sample} = .001 \text{ in.} \\ \epsilon_c &= 0.9 \\ T_{av} &= 2200^\circ\text{F} + 460 = 2660^\circ\text{R} \end{aligned}$$

in this case $\Gamma = 10^2$
and $(\epsilon_c - \epsilon)/\epsilon = 1.9 \times 10^{-5}$

The error in emittance measurements resulting from AC flickering is therefore negligible.

APPENDIX L

Thermocouple Lead Conduction Error

APPENDIX L

THERMOCOUPLE LEAD CONDUCTION ERROR

In a scientific paper entitled "Temperature Error Associated With Embedded Thermocouples," Thomas, Schurin, and Morris¹⁶ account for experimentally determined errors associated with thermocouples used to measure the surface temperature of a thin-walled, electrically-heated platinum tube radiating to cold surroundings in an evacuated chamber. The thermocouple bead was spread by peening into a hole drilled in the tube wall and the lead wires were perpendicular to the tube surface. For the analysis it was assumed that the error resulted from cooling at the surface-thermocouple junction caused by the conduction of heat by the thermocouple lead wires. Although the authors adequately account for the variation in the error with changes in the tube wall temperature, no attempt was made to determine the effects of changes in geometry, emittance, or thermal conductivity of the tube wall or thermocouple wires. In fact, the theoretical equation included an unknown "geometry effect" factor which the authors evaluated from experimental data. They then showed that for the geometry for which the geometry factor had been evaluated, the theory adequately predicted the error over the temperature range tested. The theoretical equation was:

$$\frac{T_{\infty} - T_j}{T_{\infty}} = C T_{\infty}^{3/2}$$

where

T_{∞} represented the wall temperature in the region away from the thermocouple,

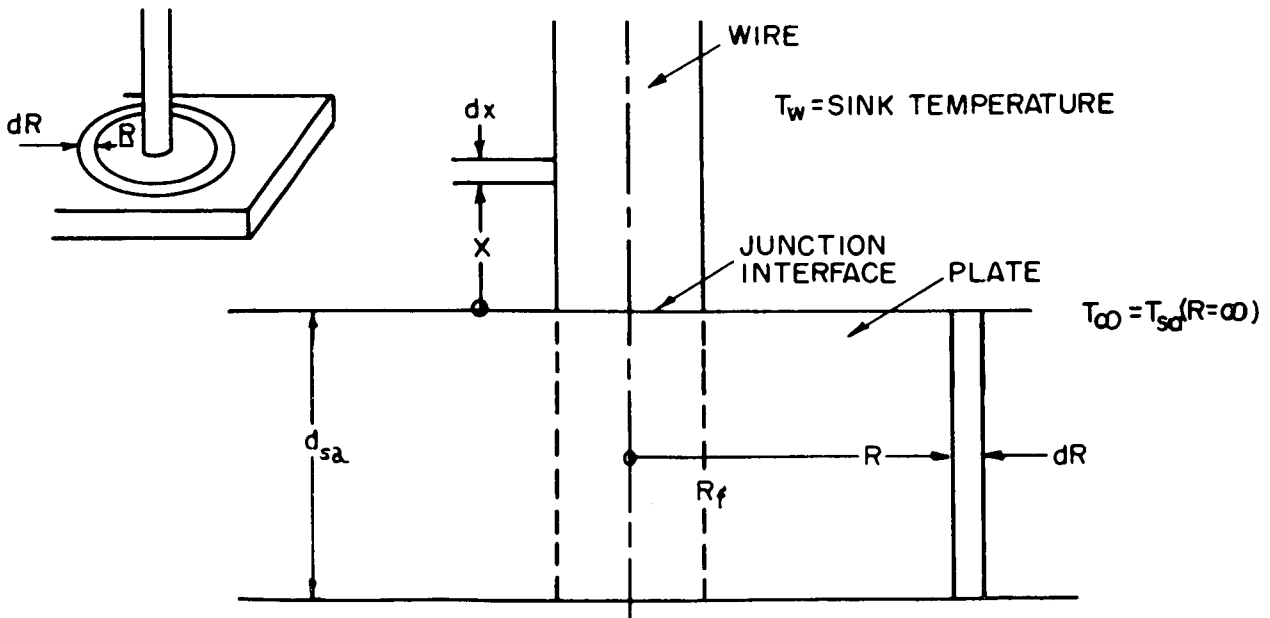
T_j represented the temperature of the thermocouple junction, and

C represented the geometry factor.

Another analysis was conducted by P. J. Schneider in "Conduction Heat Transfer"¹⁵. Commencing on page 172, he analyzes the problem of thermocouple error resulting from the thermocouple wires being subjected to a cooling stream at a temperature different from that of the heated plate to which the thermocouple is attached.

Of primary interest here are errors introduced into thermocouple temperature measurements of strip specimens such as those used in the total hemispherical emittance measurements. An analysis of these errors which borrows freely from both of the references cited above is presented in this appendix.

Consider as a model an infinite plate of thickness d_{sa} to which is attached a single thermocouple of radius R_f . The thermocouple wire is normal to the plate and extends outward from one surface. Heat is generated in the plate at a uniform rate q per unit volume. No heat is generated in the wire. The wire receives heat from the plate by conduction across the boundary between the wire and the plate and dissipates heat by radiation. Heat is conducted in the plate radially toward the thermocouple junction and the boundary between the thermocouple and the plate is at a lower temperature than the remainder of the plate. Since the temperature at the boundary is the temperature measured by the thermocouple, the measured temperature is lower than that of the unperturbed plate.



For this analysis the following assumptions are made:

- 1) Both temperature and temperature gradient in the wire are assumed to be a function only of X , the distance from the common boundary.
- 2) Both temperature and temperature gradient in the plate are assumed to be a function only of R , the distance from the centerline of the wire.
- 3) In the region of the plate where R is less than R_f , the radius of the thermocouple wire, the temperature is assumed to be constant and equal to the temperature of the junction interface.
- 4) No energy is interchanged between the thermocouple wire and the plate by radiation.

Consider an element of volume in the wire of length dx . Heat is radiated from the free surface at a rate per unit surface area of $\epsilon_f \sigma [T_f(x)^4 - T_w^4]$ where ϵ_f is the emittance of the wire, σ is the Stefan-Boltzmann constant, $T_f(x)$ is the wire temperature at X , and T_w is the sink temperature. Heat is conducted away from the volume element at a rate per unit volume of $[d/dx][k_f T_f(x)']$. A power balance for the volume element yields

$$T_f(x)'' = \left[\frac{\epsilon_f \sigma 2 \pi R_f}{k_f \pi R_f^2} \right] [T_f(x)^4 - T_w^4] \quad (L-1)$$

Boundary conditions are: $T_f'(x=\infty) = 0$ (since for large X the wire temperature approximates the sink temperature, i. e., $T_f(x=\infty) = T_w$, and therefore no longer varies with X), and $T_f'(x=0) = -q_f(x=0)/k_f A_{csf}$ where q_f is the rate of heat flow across the junction interface and A_{csf} is the cross-section area of the interface. If $\bar{m} = T_f(x)'$ then $T_f(x)'' = \bar{m} (d\bar{m}/dT)$ and the equation separates and may be integrated with the limits $\bar{m} = 0$ at $T_f(x=\infty) = T_w$, and $\bar{m} = -q_f(x=0)/k_f A_{csf}$ at $T_f(x=0)$. Thus

$$q_f(x=0) = \left\{ 4 \pi^2 \epsilon_f \sigma k_f R_f^3 \left[\frac{T_f(0)^5 - T_w^5}{5} - T_w^4 (T_f(0) - T_w) \right] \right\}^{1/2} \quad (L-2)$$

In the plate, for $R \geq R_f$, consider an element of volume between R and $R + dR$. Heat is radiated from the top and bottom surfaces at the combined rate of $2 \cdot 2 \pi R (dR) \epsilon_{sa} \sigma [T_{sa}(R)^4 - T_w^4]$ where ϵ_{sa} is the emissivity of the plate surface and $T_{sa}(R)$ is the plate surface temperature at R . Heat is conducted away from the element at the rate of $-2 \pi k_{sa} d_{sa} dR [d/dR][R T_{sa}(R)']$. Heat generation in the element is at the rate of $2 \pi R d_{sa} q (dR)$. Equating the heat generation to the losses by conduction and radiation gives

$$\frac{1}{R} \frac{d}{dR} \left[R \frac{dT_{sa}(R)}{dR} \right] = -\frac{q}{k_{sa}} + \frac{2 \epsilon_{sa} \sigma}{k_{sa} d_{sa}} (T_{sa}(R)^4 - T_w^4) \quad (L-3)$$

By applying the boundary condition that far away from the wire the temperature reaches a uniform level corresponding to no heat conduction, equation (L-3) becomes

$$q = \left[\frac{2 \epsilon_{sa} \sigma}{d_{sa}} \right] (T_{sa}(\infty)^4 - T_w^4) \quad (L-4)$$

Substituting equation (L-4) into equation (L-3), letting

$\phi_{sa}(R) = [T_{sa}(R) - T_{sa}(\infty)] / T_{sa}(\infty)$ and applying the approximation that $[1 + \phi_{sa}(R)]^4 \approx 1 + 4\phi_{sa}(R)$, the differential equation (L-3) becomes

$$\phi_{sa}(R)'' + (1/R) \phi_{sa}(R)' - \bar{b}^2 \phi_{sa}(R) = 0 \quad (L-5)$$

where
$$\bar{b}^2 = \frac{8 \epsilon_{sa} \sigma [T_{sa}(\infty)]^3}{k_{sa} d_{sa}}$$

The general solution of this Bessel equation is

$$\phi_{sa}(R) = C_3 I_0(\bar{b}R) + C_4 K_0(\bar{b}R) \quad (L-6)$$

Since $\phi_{sa}(R=\infty) = 0$ while $I_0(\infty) = \infty$, it follows that $C_3 = 0$. Thus, equation (L-6) reduces to

$$\phi_{sa}(R) = C_4 K_0(\bar{b}R) \quad (L-7)$$

from which

$$\phi_{sa}(R)' = -\bar{b} C_4 K_1(\bar{b}R) \quad (L-8)$$

The equation for one-dimensional cylindrically symmetric heat flow in the plate therefore may be determined from equation (L-8) and from the definitions of $\phi_{sa}(R)$ and \bar{b} , thus

$$\begin{aligned} q_{sa}(R) &= -k_{sa} 2\pi R d_{sa} T_{sa}(R)' \\ &= -k_{sa} 2\pi R d_{sa} T_{sa}(\infty) \phi(R)' \quad (L-9) \\ &= +k_{sa} 2\pi R d_{sa} T_{sa}(\infty)^3 \bar{b} C_4 K_1(\bar{b}R) \end{aligned}$$

C_4 may be expressed in terms of $\phi_{sa}(R = R_f)$, using equation (L-7), to give

$$C_4 = \frac{\phi_{sa}(R_f)}{K_0(\bar{b}R_f)} \quad (L-10)$$

and the conduction heat flow in the positive R direction at $R = R_f$ from equations (L-9) and (L-10) is

$$q_{sa}(R_f) = \frac{2\pi R_f [8\epsilon_{sa} \sigma k_{sa} d_{sa} T_{sa}(\infty)^5]^{1/2} \phi_{sa}(R_f) K_1(\bar{b}R_f)}{K_0(\bar{b}R_f)} \quad (L-11)$$

In the plate, the temperature within the cylinder bounded by the surface $R = R_f$ is assumed to be constant and equal to the temperature at the junction of the wire and the plate T_j , that is, $T_j = T_{sa}(R_f) = T_f(0)$ = the temperature at the bottom surface of the plate for $R = R_f$. Heat is generated in the cylinder at the rate of $g\pi R_f^2 d_{sa}$. Heat is conducted out along the wire at the rate $q_f(x=0)$ and is conducted out into the plate at the rate $q_{sa}(R_f)$. Heat is radiated from the bottom surface of the cylinder at the rate $\pi R_f^2 \epsilon_{sa} \sigma (T_j^4 - T_w^4)$. Therefore, by using equation (L-4), the balance-of-power equation for the cylinder may be written as

$$2\pi R_f^2 \epsilon_{sa} \sigma (T_{sa}(\infty)^4 - T_w^4) = q_f(0) + q_{sa}(R_f) + \pi R_f^2 \epsilon_{sa} \sigma [T_j^4 - T_w^4] \quad (L-12)$$

Substitution of the expressions for $q_f(0)$ and $q_{sa}(R_f)$, equations (L-2) and (L-11) respectively, into equation (L-12) would give the general solution for T_j , the temperature measured by the thermocouple, in terms of the unperturbed temperature of the plate, the conductivity and emittance of the plate and wire, and the wire diameter and plate thickness. However, a much simpler expression may be obtained for the special case where $T_w \ll T_{sa}(\infty)$ and where the heat generated in and radiated from the cylinder in the plate bounded by $R = R_f$ may be neglected. In application to thermocouple errors encountered with

emittance measurements, these additional assumptions are valid. Equation (L-12) therefore becomes

$$0 = q_f(0) + q_{sa}(R_f) \quad (L-13)$$

Since it was assumed that $T_j = T_f(0) = T_{sa}(R_f)$ and since $T_f(x=0)^5 = T_{sa}(R=\infty)^5 [1 + \phi_j]^5 \approx T_{sa}(\infty)^5 [1 + 5\phi_j]$ where

$\phi_j = [T_j - T_{sa}(\infty)] / T_{sa}(\infty)$, by using equation (L-2) the conduction heat flow out into the wire may be written as

$$q_f(0) = \left[(4/5) \pi^2 \epsilon_f \sigma k_f R_f^3 T_{sa}(\infty)^5 (1 + 5\phi_j) \right]^{1/2} \quad (L-14)$$

By substituting equations (L-14) and (L-11) into equation (L-13), the result may be solved for the fractional difference in temperature between the junction and the unperturbed portion of the plate to give

$$\phi_j = - \left[\left(\frac{\gamma}{16} \right)^2 + \frac{\gamma}{40} \right]^{1/2} + \frac{\gamma}{16} \quad (L-15)$$

where $\gamma = \left[\frac{k_f \epsilon_f R_f}{k_{sa} \epsilon_{sa} d_{sa}} \right] \left[\frac{k_o(\bar{b} R_f)}{k_i(\bar{b} R_f)} \right]^2$, $\bar{b}^2 = \frac{8 \epsilon_{sa} \sigma T_{sa}(\infty)^3}{k_{sa} d_{sa}}$.

For $\bar{b} R_f < 0.05$

$$\frac{k_o(\bar{b} R_f)}{k_i(\bar{b} R_f)} \approx \bar{b} R_f \left[\log\left(\frac{2}{\bar{b} R_f}\right) - .577 \right]$$

and γ may be approximated as

$$\gamma \approx \frac{8 k_f \epsilon_f R_f^3 \sigma T_{sa}(\infty)^3}{k_{sa}^2 d_{sa}^2} \left[\log\left(\frac{2}{\bar{b} R_f}\right) - .577 \right] \quad (L-16)$$

A further approximation is possible where $0 < |5\phi_j| \ll 1$. In this case, equation (L-15) may be approximated as

$$\phi_j \approx - \left(\frac{\gamma}{40} \right)^{1/2} \quad (L-17)$$

If both the approximations for equations (L-15) and (L-16) are valid, then

$$\phi_j \approx - \left\{ \frac{k_f \epsilon_f R_f^3 \sigma [T_{sa}(\infty)]^3}{5 k_{sa}^2 d_{sa}^2} \right\}^{1/2} \left[\log\left(\frac{2}{\bar{b} R_f}\right) - .577 \right] \quad (L-18)$$

It is noted that in equation (L-18) the fractional error in temperature with a particular configuration is proportional to $T_{sa}(\infty)^{3/2}$, the result derived by Thomas, Schurin, and Morris, and that the additional logarithm term varies only slowly for $\bar{b}R_f < 0.05$.

The theoretical fractional deviation in junction temperatures for the cases of a 1-mil diameter platinum wire attached to a 2-mil and a 5-mil thick molybdenum foil are presented below. Since the model on which the above analysis is based is by no means perfect for application to the temperature measurements made in the total hemispherical emittance rig, the tabulated values should be treated only as order-of-magnitude estimates. It may be seen, however, that the effects of heat conduction by the thermocouple leads on measured temperature values are negligible.

$$\phi_j = [T_j - T_{sa}(\infty)] / T_{sa}(\infty)$$

$T_{sa}(\infty)$ (°F)	$d_{sa} = 2$ mils	$d_{sa} = 2$ mils	$d_{sa} = 5$ mils	$d_{sa} = 5$ mils
	$\epsilon_{sa} = 0.5$	$\epsilon_{sa} = 0.7$	$\epsilon_{sa} = 0.5$	$\epsilon_{sa} = 0.7$
1000	-.000318	-.000309	-.000135	-.000132
1200	-.000380	-.000370	-.000163	-.000159
1400	-.000446	-.000434	-.000189	-.000186
1600	-.000515	-.000500	-.000221	-.000215
1800	-.000590	-.000570	-.000254	-.000248

APPENDIX M

Temperature Perturbation at Scratch in
Specimen Surface Coating

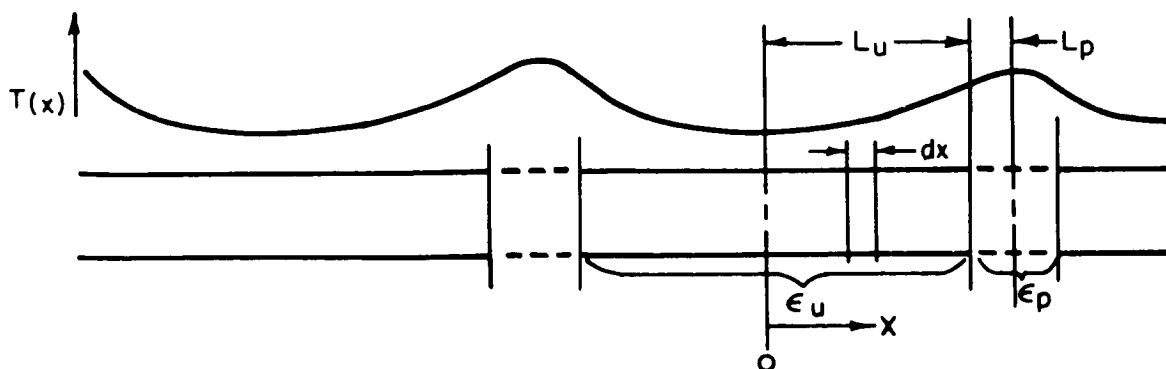
APPENDIX M

TEMPERATURE PERTURBATION AT SCRATCH IN
SPECIMEN SURFACE COATING

In order to measure the temperature of a metal strip specimen with a coating on both sides, it was generally necessary to make a small scratch in the coating to permit the thermocouple wires to be welded directly to the substrate material. Since the area exposed by the scratch might have an emittance appreciably different from that of the surrounding coated area, some perturbation of the sample temperature at the thermocouple junction could be anticipated. If the thermocouple measured a temperature which was 1 per cent higher than the unperturbed specimen temperature, a direct 4 per cent underestimate of the emittance would result since the calculated emittance varies approximately inversely as the fourth power of the specimen temperature.

The magnitude of the emittance error resulting from the temperature perturbation in the region of the scratch has been estimated by a simplified one-dimensional analysis relating the correction to be made on the uncorrected emittance value ϵ_c , to the emittances of the region exposed by the scratch and of the unblemished surface, and to the specimen thermal conductivity, temperature level, and dimensions.

Consider a long strip specimen with equidistant scratches perpendicular to the longitudinal axis of the strip. It will be shown that if the material exposed by the scratch has an emittance lower than that of the surrounding area, then the temperature profile along the strip has a wave form with sharp crests at the scratches and broad valleys between, as shown in the sketch below.



For this analysis it is assumed that the temperature is only a function of x . The region u is the unblemished region and has an emittance of ϵ_u . The region p is the scratch region and has an effective average emittance of ϵ_p . In the u region, heat is generated in a volume element by direct resistance heating at a rate of q per unit volume of specimen material. Heat is radiated from the surface at the rate per unit surface area of $\epsilon_u \sigma [T_u(x)^4 - T_w^4]$, where $T_u(x)$ is the temperature at x and T_w is the sink temperature. Heat is conducted out of the volume element at the rate of $[d/dx] [-k T_u'(x)]$. As in Appendix F, the balance-of-power equation may be obtained by substituting the following

$$\frac{\epsilon_c \sigma P (T_m^4 - T_w^4)}{A_{cs}} = q$$

$$\phi_u(x) = \frac{T_u(x) - T_m}{T_m}$$

$$a_u = \left[1 - \left(\frac{T_w}{T_m} \right)^4 \right] \left[\frac{\epsilon_c - \epsilon_u}{\epsilon_u} \right]$$

$$b_u = \frac{\epsilon_u \sigma T_m^3 P}{k A_{cs}}$$

This results in

$$\phi_u''(x) = b_u \{ [1 + \phi_u(x)]^4 - 1 - a_u \} \quad (M-1)$$

with the boundary condition

$$\phi_u'(x=0) = 0 \quad (M-2)$$

to require symmetry about $x=0$ in region u .

Using the approximation that $[1 + \phi_u(x)]^4 \approx 1 + 4\phi_u(x)$, since $0 < \phi_u(x) \ll 1$ in cases of interest, equation (M-1) becomes

$$\phi_u''(x) - 4b_u \phi_u(x) \approx -a_u b_u \quad (M-3)$$

With constant a_u and b_u , the general solution of (M-3) is

$$\phi_u(x) = C_{1u} \cosh(2b_u^{1/2} x) + C_{2u} \sinh(2b_u^{1/2} x) + a_u/4 \quad (M-4)$$

The symmetry of $\phi_u(x)$ about $x=0$ requires that $C_{2u} = 0$ so that

$$\phi_u(x) = C_{1u} \cosh(2b_u^{1/2} x) + a_u/4 \quad (M-5)$$

Differentiation of (M-5) yields

$$\phi_u'(x) = 2b_u^{1/2} C_{1u} \sinh(2b_u^{1/2} x) \quad (M-6)$$

and

$$C_{1u} = \frac{\phi_u'(x=L_u)}{2b_u^{1/2} \sinh(2b_u^{1/2} L_u)} \quad (M-7)$$

Substituting (M-7) into (M-5) yields

$$\phi_u(x) = \frac{\phi_u'(x=L_u) \cosh(2b_u^{1/2} x)}{2b_u^{1/2} \sinh(2b_u^{1/2} L_u)} + \frac{a_u}{4} \quad (M-8)$$

which becomes a solution for region u .

For cases of interest, region p , the scratch region, is considered isothermal in the sense that the temperature measured in this region by a thermocouple with no lead conduction error is assumed to be equal to the temperature at the boundary between regions u and p . This assumption permits T_m to be identified not only as the temperature from which ϵ_c is calculated, but also as the boundary temperature between regions u and p . Therefore

$$\phi_u(x=L_u) = 0 = \frac{\phi_u'(x=L_u) \cosh(2b_u^{1/2} L_u)}{2b_u^{1/2} \sinh(2b_u^{1/2} L_u)} + \frac{a_u}{4} \quad (M-9)$$

where

$$\phi_u'(x=L_u) = -(1/2) a_u b_u^{1/2} \tanh(2b_u^{1/2} L_u) \quad (M-10)$$

Also, the heat balance for the left hand side of region p may be written in integrated form with the heat conduction rate across the boundary at $x=L_u$ denoted in terms of $\phi_p'(x=L_u)$. Thus, the heat generation rate between $x=L_u$ and $x=L_u+L_p$, which is $(g A_{cs} L_p)$, is equated to the heat radiation rate from the corresponding surface, which is $(p L_p \epsilon_p \sigma) (T_p^4 - T_w^4)$, plus the heat conduction rate across the $x=L_u$ plane, which is $A_{cs} k T_p'(x=L_u)$.

Letting $\phi_p(x=L_u) = T_p'(x=L_u) / T_m$,

$$a_p = \left[1 - \left(\frac{T_w}{T_p} \right)^4 \right] \left[\frac{\epsilon_c - \epsilon_p}{\epsilon_p} \right], \quad b_p = \frac{\epsilon_p \sigma T_m^3 p}{k A_{cs}}$$

and recalling that

$$\epsilon_c = \frac{g A_{cs}}{\sigma_p (T_m^4 - T_w^4)}$$

the heat balance for region p becomes

$$L_p b_p \partial_p = \phi_p'(x=L_u) \quad (M-11)$$

Equating $\phi_p'(x=L_u)$ and $\phi_u(x=L_u)$ as the condition that the conduction heat flow rate be continuous at the boundary gives

$$L_p b_p \partial_p = - (1/2) a_u b_u'^{1/2} \tanh(2 b_u'^{1/2} L_u) \quad (M-12)$$

Equation (M-12) may now be solved for the fractional difference between the emittance as estimated most simply by the temperature in the scratch region ϵ_c , and the true emittance of the unscratched region ϵ_u , yielding

$$\frac{\epsilon_c - \epsilon_u}{\epsilon_u} = \frac{\Delta \epsilon_u}{\epsilon_u} = \frac{1 - (\epsilon_p / \epsilon_u)}{1 + [\tanh(2 b_u'^{1/2} L_u)] / [2 b_u'^{1/2} L_p]} \quad (M-13)$$

The results of applying equation (M-13) to typical materials with high emittance coatings in the extreme situation where the effective emittance over the scratch region is assumed to be $\epsilon_u/2$ (a mean of ϵ_u on one side and zero on the other), where the assumed full scratch width is three times the 0.001-inch diameter of the thermocouple wire, and where the specimen strip thickness is the minimum tested of 0.002 inch, are indicated in Figure M-1. Molybdenum and tantalum were chosen for calculations as being representative of most of the strip samples tested during Phase I. However, a low conductivity metal would show more deviation than estimated for molybdenum and tantalum. Figure M-2 shows results for tantalum as a function of scratch width and temperature level.

For the molybdenum strips coated on both sides it is estimated that the error in measured emittance due to the mounting of the thermocouples in scratches in the coatings did not exceed 1 per cent and was less than 1/2 per cent in most cases.

EMITTANCE ERROR DUE TO TEMPERATURE PERTURBATION AT THERMOCOUPLE SCRATCH

PWA-2206

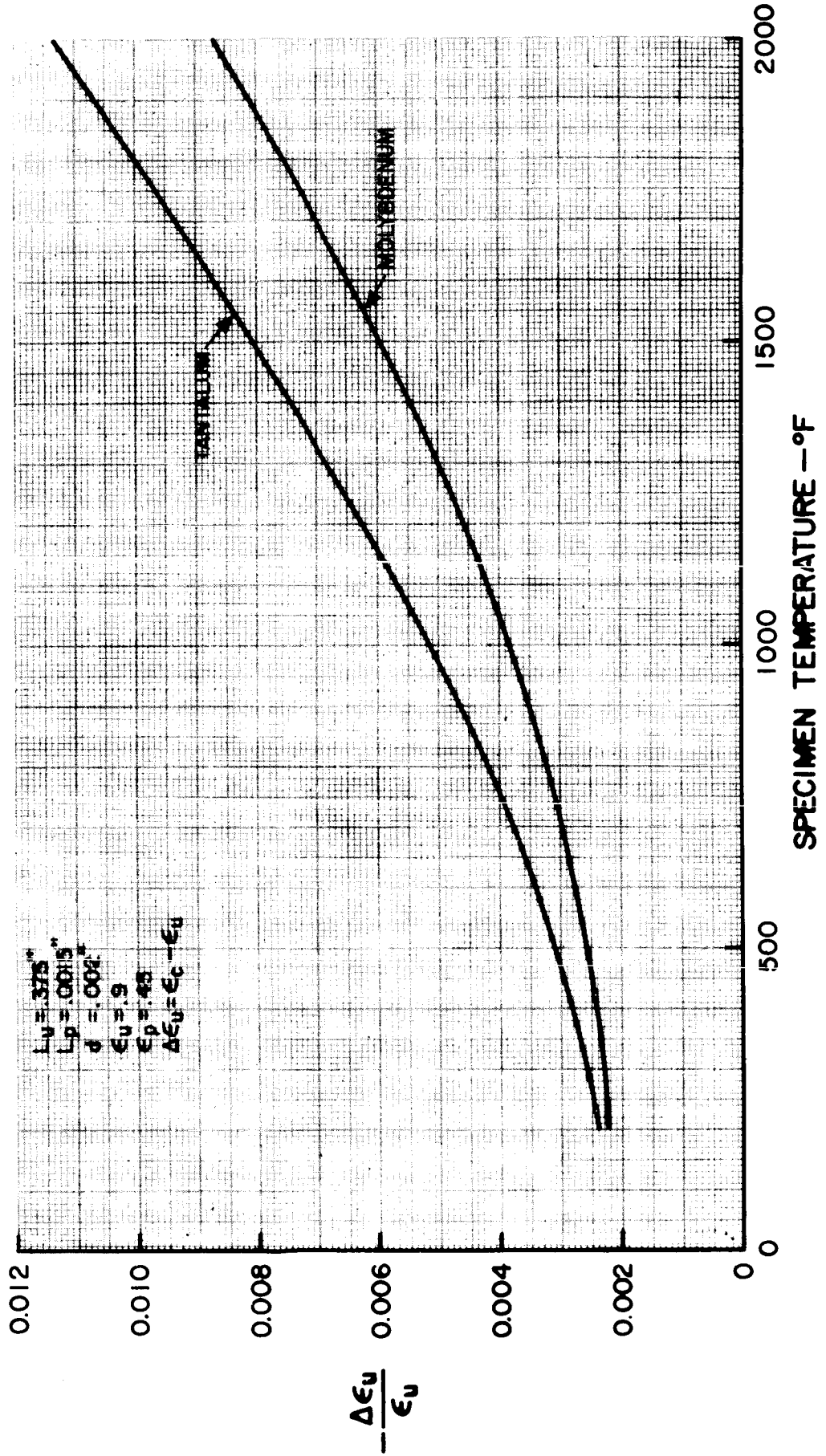


Figure M-1

EMITTANCE ERROR DUE TO TEMPERATURE PERTURBATION AT THERMOCOUPLE SCRATCH (TANTALUM)

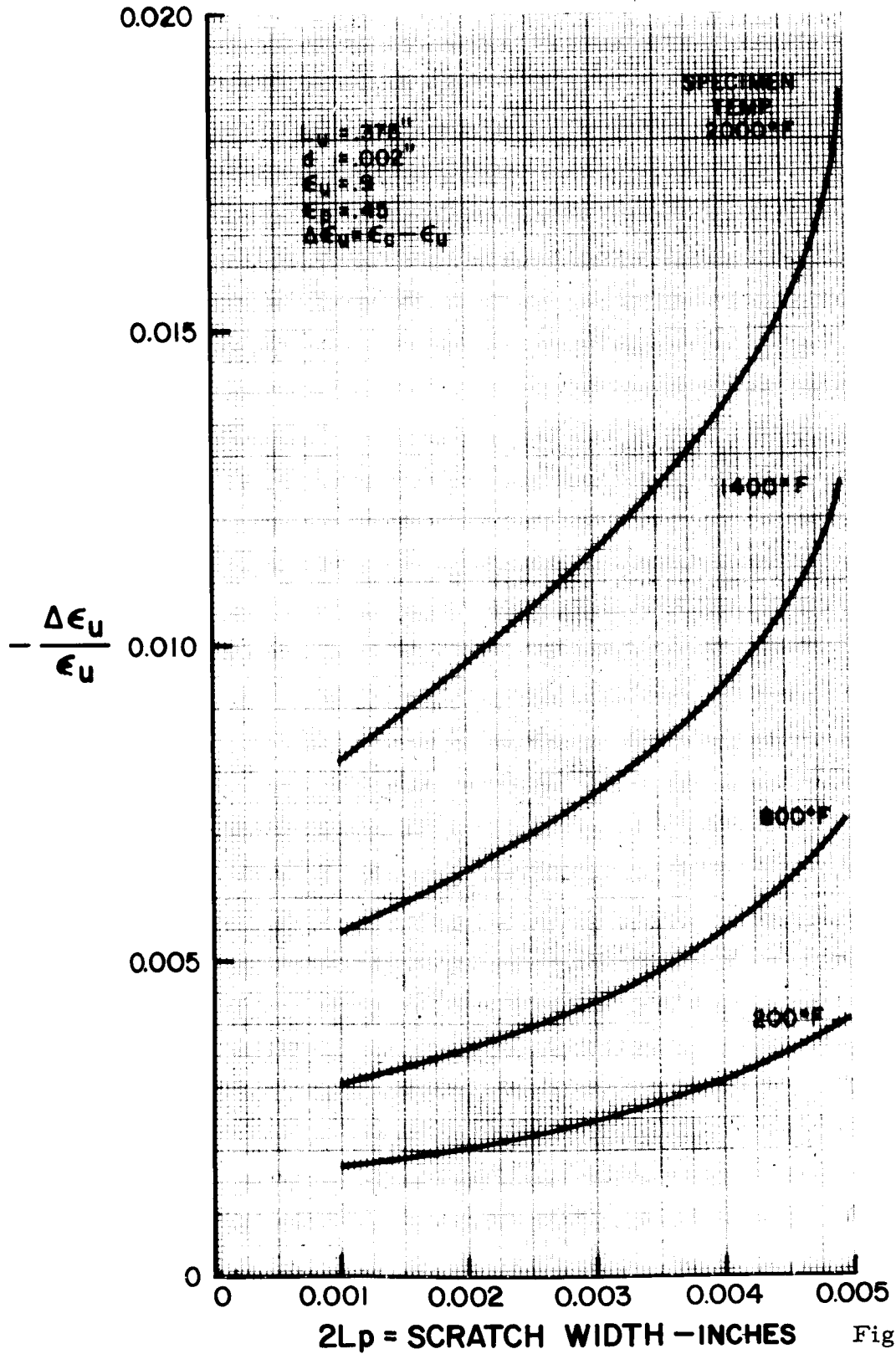


Figure M-2

APPENDIX N

Comparison of Thermocouple and
Optical Pyrometer Temperature Measurements

APPENDIX N

COMPARISON OF THERMOCOUPLE AND OPTICAL
PYROMETER TEMPERATURE MEASUREMENTS

Thermocouple temperature measurements were one source of error in the determination of total hemispherical emittance values. Experiments were therefore conducted to determine the accuracy of the chromel-alumel and of the platinum-platinum 10 per cent rhodium thermocouples. All tests were conducted at 10^{-6} mm Hg or lower.

Early measurements in the program had indicated a lack of agreement between temperatures measured by the two types of thermocouples. In one case, measurements were made on a strip of molybdenum in the as-received condition. During the first heating cycle, the emittance values based on data from each of the thermocouples agreed to within 1 per cent in the temperature range of 1420 to 2060°F. The second heating cycle, however, included several minutes of testing above 1800°F and during the third cycle it was found that the voltage output from the chromel-alumel thermocouple had increased by as much as 2 per cent relative to the output of the platinum-platinum 10 per cent rhodium thermocouple over the entire range of temperatures. As a result, total hemispherical emittance values calculated from the two sets of data differed by 4 to 8 per cent for the third heating cycle. (See Figure N-1).

A second series of tests was conducted on a vapor-blasted molybdenum specimen. Again, after about ten minutes of operation above 1800°F, the chromel-alumel thermocouple indicated higher temperatures than the platinum-platinum 10 per cent rhodium thermocouple. The effect on the total hemispherical emittance values is shown in Figure N-2.

To determine which, if either, type of thermocouple was indicating correctly, tests were conducted in the spectral emittance rig using a molybdenum wedge-shaped specimen. The temperatures indicated by both types of thermocouples could then be compared with optical pyrometer measurements. Total hemispherical emittance measurements based on all three types of measurements are compared in Figure N-3. As can be seen, the values obtained using optical pyrometer and platinum-platinum 10 per cent rhodium thermocouple data agree to within 1 per cent throughout the test. Since the optical pyrometer is regarded as a standard for the range in which it can be used, the validity of platinum-platinum 10 per cent rhodium thermocouple

data was confirmed. However, as may be seen in Figure N-3, above 1800°F emittance values based on chromel-alumel thermocouple data are in considerable disagreement with values based on optical pyrometer data. The data taken at temperatures below those where the optical pyrometer is usable disagree with data obtained by the platinum-platinum 10 per cent rhodium thermocouple. It therefore appears that the calibration shift covers the entire temperature range.

These tests indicate that the output from chromel-alumel thermocouples permanently shifts upwards after exposure to 1800°F and high vacuum for a brief period of time. It is believed that this shift in calibration is related either to the small size (1 mil) of the thermocouple wire or to the steep temperature gradient in the wires near the junctions on the specimen surface, or possibly to both of these factors. It is also possible that the high vacuum may influence the performance of these thermocouples. Since the high temperature and vacuum conditions did not appreciably change the response of the platinum-platinum 10 per cent rhodium thermocouples, thermocouples of this type have been preferred for emittance measurements.

TOTAL HEMISPHERICAL EMITTANCE OF MOLYBDENUM STRIP (COLD-ROLLED CHEMICALLY CLEANED)

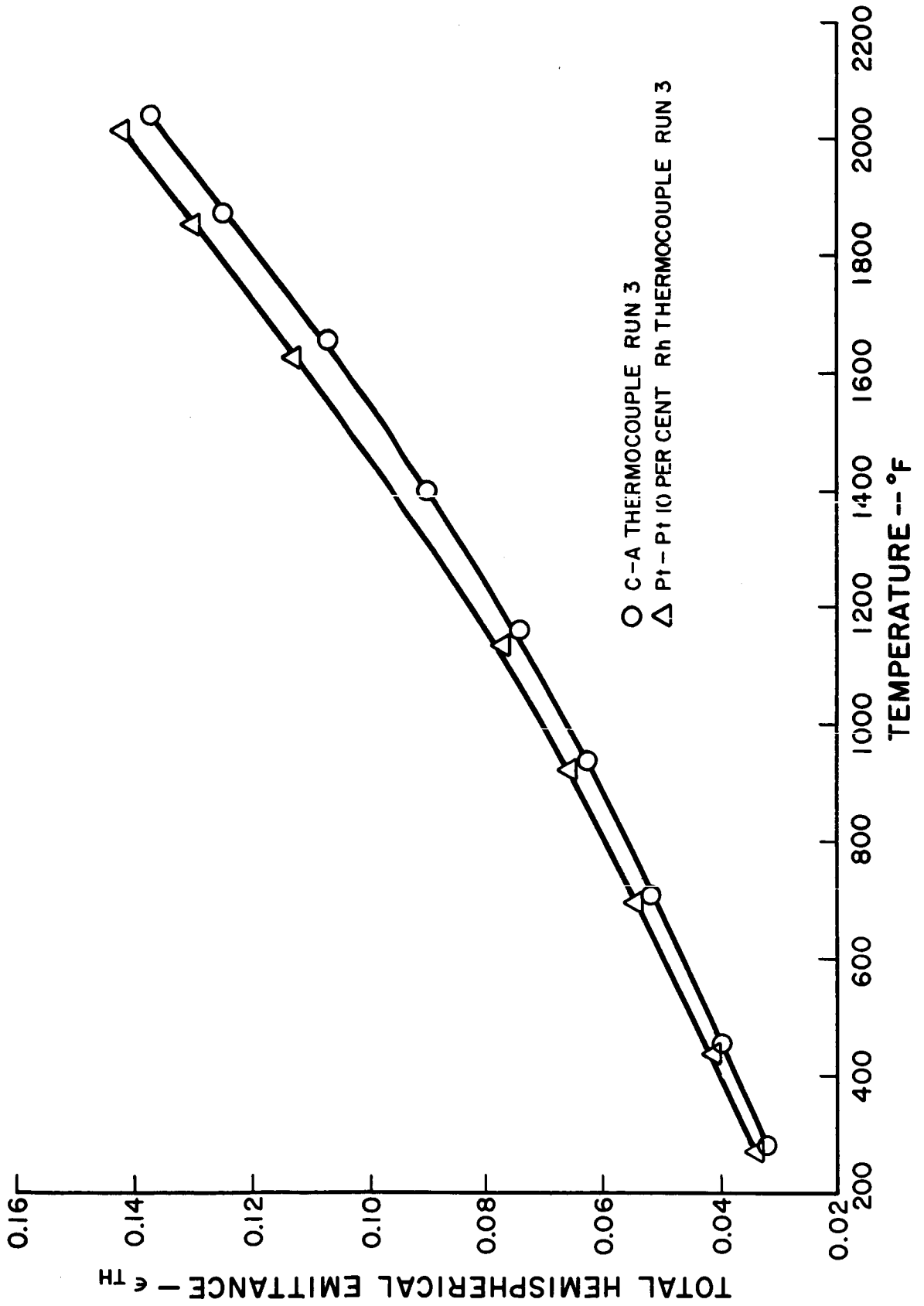


Figure N-1

TOTAL HEMISPHERICAL EMITTANCE OF VAPOR-BLASTED MOLYBDENUM STRIP

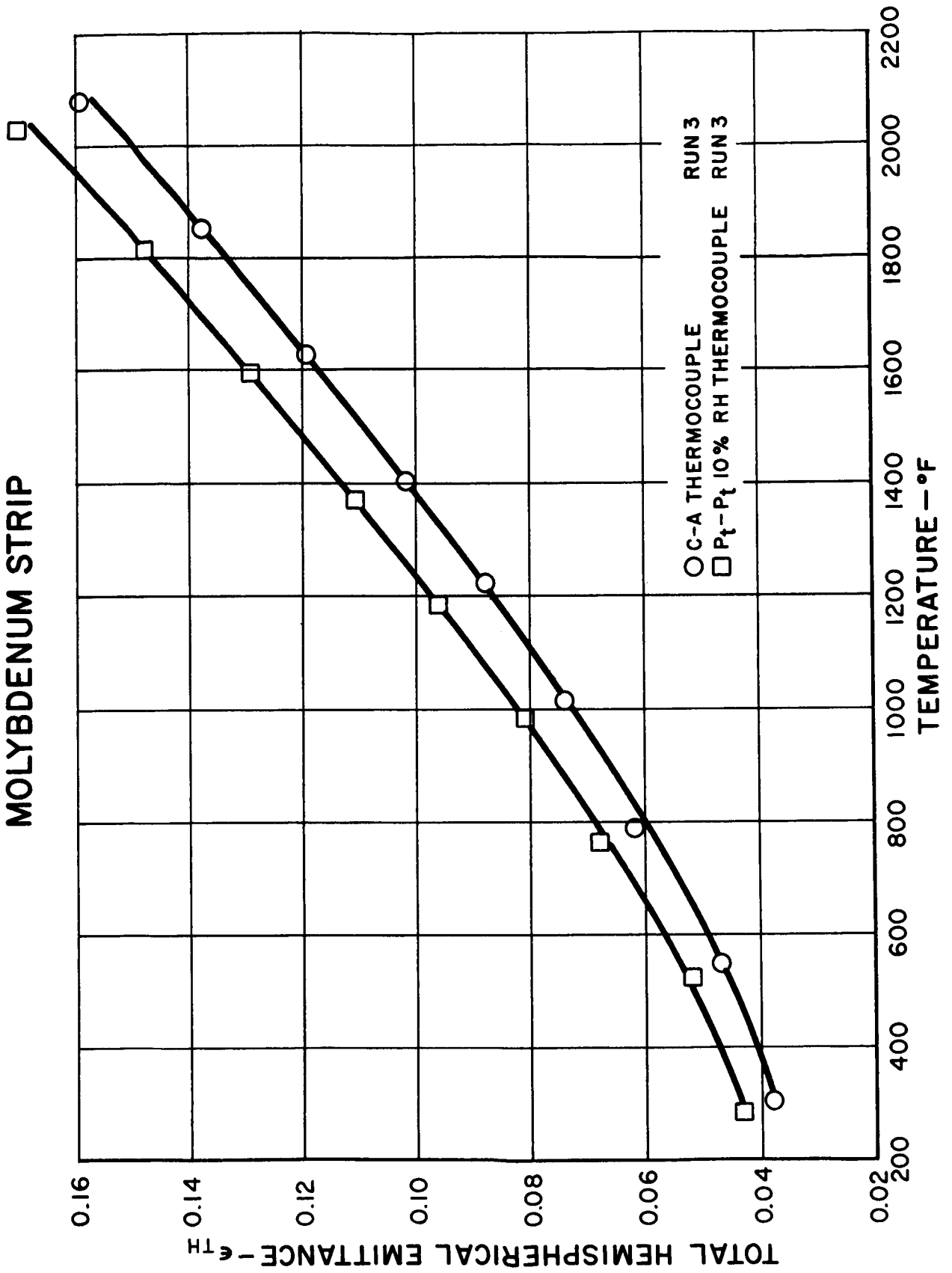


Figure N-2

TOTAL HEMISPHERICAL EMITTANCE OF MOLYBDENUM TRIANGULAR SPECIMAN

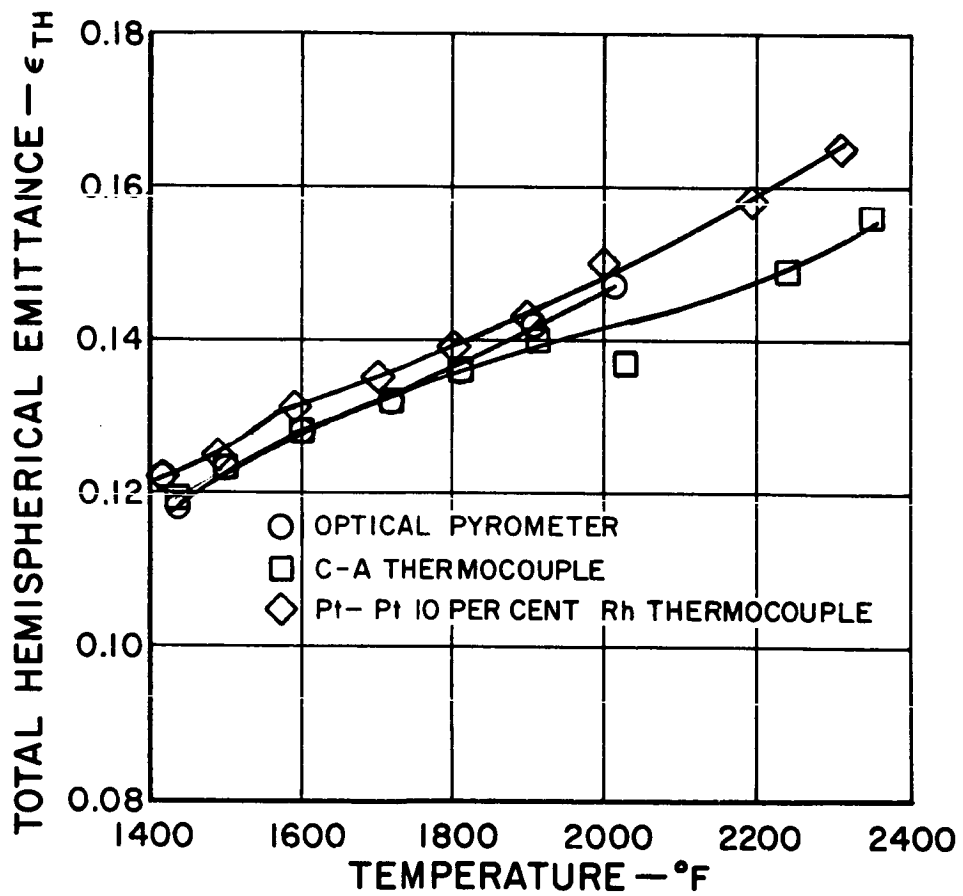


Figure N-3

APPENDIX O

References

APPENDIX O

REFERENCES

1. Larrabee, R. D. The Spectral Emissivity and Optical Properties of Tungsten, Technical Report 328, Massachusetts Institute of Technology Research Laboratory of Electronics, Cambridge, Massachusetts, May 21, 1957
2. De Vos, J. C. "A New Determination of the Emissivity of Tungsten Ribbon," Physica, XX, 1954, Research Department of the M. V. Kema, Arnhem, Nederland
3. Langmuir, I., and Jones, H. A., "The Characteristics of Tungsten Filaments as Functions of Temperature," General Electric Review, Vol. XXX (1927), June, pp. 310-319 and July, pp. 354-361. General Electric Company, Schenectady 5, New York
4. Electrodeposition of Black Chromium Coatings, Allied Chemical Corporation, New York 6, New York
5. De Vos, J. C., "Evaluation of the Quality of a Blackbody," Physica, XX, 1954, Research Department of the M. V. Kema, Arnhem, Nederland
6. N. B. Hanney, Semiconductors, Reinhold Publishing Corporation, New York 22, New York, 1959
7. Forsythe, W. E., and Watson, E. M., "Resistance and Radiation of Tungsten as a Function of Temperature," Journal of the Optical Society of America, Volume XXIV (1934), April, pp. 114-118, American Institute of Physics, New York 17, New York
8. Hodgman, Charles D. (ed.), Handbook of Chemistry and Physics, 40th Edition, Table of Properties of Tungsten (Roeser and Wenzel, National Bureau of Standards), Chemical Rubber Publishing Company, Cleveland, Ohio
9. Campbell, I. E., High Temperature Technology, John Wiley & Sons, Incorporated, New York, 1956, P. 82

10. Ryshkewitch, E., Oxide Ceramics, Physical Chemistry and Technology, Academy Press, New York, 1960, P. 399
11. Wade, W. R., and Casey, F. W., Jr., Measurements of Total Hemispherical Emissivity of Several Stably Oxidized Nickel - Titanium Carbide Cemented Hard Metals from 600° to 1600°F, NASA Memorandum, 5-13-59L, National Aeronautics and Space Administration, Langley Field, Virginia, June 1959
12. Dunkle, R. V., Transactions of the American Society of Metallurgical Engineers, American Society of Metallurgical Engineers, Easton, Pennsylvania, 1954
13. Jakob, M., Heat Transfer, Volume II, John Wiley & Sons, Incorporated, New York, 1949
14. Milne-Thompson, Theoretical Hydrodynamics, Third Edition, Macmillan Company, New York, 1950
15. Schneider, P. J., Conduction Heat Transfer, Addison-Wesley Publishing Company, Cambridge, Massachusetts, 1955
16. Thomas, A. R., Shurin, B., and Morris, J. C., "Temperature Error Associated with Embedded Thermocouples," Review of Scientific Instruments, American Institute of Physics, New York 17, New York

APPENDIX P

Nomenclature

APPENDIX P

NOMENCLATURE

A = Area

A_s^*, A_b^* = Area of spot on specimen or black-body hole surface upon which measuring or reference beam is focused

A_s^+, A_b^+ = Auxiliary area around A_s^* or A_b^* which contributes power to measuring or reference beam

$$a = [(\epsilon_c - \epsilon)/\epsilon][1 - (T_w/T_o)^4]$$

$$a_p = [(\epsilon_c - \epsilon)/\epsilon_p][1 - (T_w/T_p)^4]$$

$$a_u = [(\epsilon_c - \epsilon)/\epsilon_u][1 - (T_w/T_u)^4]$$

$$B = \epsilon \sigma T_{av}^3 / k z m$$

$$b = \epsilon \sigma T_o^3 p / k A_{cs}$$

$$b_p = \epsilon_p \sigma T_p^3 p / k A_{cs}$$

$$b_u = \epsilon_u \sigma T_m^3 p / k A_{cs}$$

$$\bar{b} = [8 \epsilon_{sa} \sigma T_{sa}(\infty)^3 / k_{sa} d_{sa}]^{1/2}$$

C_1, C_2 = Planck's first and second radiation constants

C_n = n^{th} integration constant or Fourier series constants

C_p = Heat capacity

c = Velocity of light

d_{sa} = Specimen wall thickness

E = Total emissive power of a surface

E_{λ} = Spectral emissive power of a surface

\vec{E} = Vector electric field

$F(\eta) = I_{\lambda_b}(T) / E_{\lambda_b}(T)$

F_r = Fraction of radiation emitted by specimen which is incident on it via chamber wall reflection(s)

f = Frequency of current oscillation

\underline{f} = Frequency of electromagnetic radiation (in Planck law)

$G = g_o / \rho C_p T_n$

g = Heat generation rate per unit volume in specimen wall

g_o = Mean heat generation rate per unit volume in specimen wall

H = Increment of length along x or y coordinate

h = Planck constant

I = Intensity of total emitted radiation

I_{λ} = Intensity of spectral emitted radiation

$I_o(V)$ = Zeroth order modified Bessel function of the first kind of argument "V"

I_{ts} = Heating current through test section

$i = (-1)^{1/2}$

\vec{j} = Current density

$k = \epsilon \sigma \rho T_m^3 / A_{cs} \rho C_p$

$k_e = \epsilon_e \sigma \rho T_m^3 / A_{cs} \rho C_p$

$$k_c = \epsilon_c \sigma_p T_m^3 / A_{cs} \rho C_p$$

$k_0(v), k_1(v)$ = Zeroth or first order modified Bessel function of the second kind of argument "V"

k = Thermal conductivity

\underline{k} = Boltzmann constant (in Planck equation)

L_u = Half length of undisturbed coating along specimen

L_p = Half width of scratch in coating for thermocouple attachment

m = Strength of line source in two-dimensional flow

\bar{m} = $dT_f(x)/dx$

n = Fourier series term number

P_0 = Total radiation power emitted by specimen

P_1, P_2 = Portions of P_0 surviving first and second wall reflections

$P_{b\lambda}^*$ = Spectral reference beam power

P_{bs}^* = Scattered reference beam power

$P_{s\lambda}^*$ = Spectral measuring beam power

P_{ss}^* = Scattered measuring beam power

P_e = Electrical power input to specimen

p = Specimen outside perimeter

q = Heat flow rate

q'' = Net heat radiated or conducted per unit time and per unit area

R = Radius from centerline of thermocouple wire to point in specimen wall

- R_f = Radius of thermocouple wire
 r = Reflectance
 $S_{s\lambda}, S_{b\lambda}$ = Spectral intensity of the auxiliary area around surface of black body sampling region
 T = Temperature
 T_m = Temperature measured at thermocouple scratch in specimen coating (for zero lead conduction effect)
 T_o = Maximum temperature along specimen
 T_∞ = Specimen temperature away from perturbation
 t = Time
 U = Uniform velocity at $X = +\infty$ and $-\infty$
 u = x component of velocity
 v = y component of velocity
 V = Electrical potential
 V_{ts} = Voltage drop across test section of specimen
 $V_{\lambda 1b}, V_{\lambda 2b}$ = Spectrophotometer output voltage for No. 1 or 2 beam viewing black body hole in the wavelength range λ to $\lambda + \Delta\lambda$
 $V_{\lambda 1s}$ = Spectrophotometer output voltage for No. 1 beam viewing specimen surface in the wavelength range λ to $\lambda + \Delta\lambda$
 ω = Angular frequency of power oscillation, radians per unit time
 w = $\phi + i\gamma$ = fluid flow complex potential
 X = $\pi x / 2 y_w$
 x = Coordinate along specimen axis or along thermocouple lead wire

$$Y = \pi y / 2 y_w$$

Y = Coordinate in peripheral direction around specimen tube

Y_w = Half of perimeter of tube specimen

Z = $x + iy$, denoting location in complex plane

\bar{Z} = Coordinate in direction normal to specimen surface

Z_1 = Half amplitude of wall thickness deviation from the mean

$$\alpha = \epsilon \sigma T_\infty^3 H^2 / kd$$

$$\beta = \epsilon, \sigma T_1^3 d / 2k$$

$$\Gamma = \omega \rho C_p A_{cs} / 4 \epsilon_c \sigma_p T_m^3$$

$$\gamma = \frac{k_f \epsilon_f R_f}{k_{s2} \epsilon_{s2} d_{s2}} \frac{k_0(\bar{b} R_f)}{k_1(\bar{b} R_f)}$$

ϵ = Emittance

$$\xi = \phi'(\xi)$$

$$\eta = \lambda T$$

θ = Angle between direction of interest and surface normal

λ = Wavelength of electromagnetic radiation

$$\mu = (-\phi)^{1/2}$$

ν = $u - i\nu$, complex velocity

$$\xi = b^{1/2} x$$

ρ = Reflectance or resistivity

σ = Stefan-Boltzmann constant

τ = AC heating cycle period

$\tau_{\lambda 1}, \tau_{\lambda 2}$ = Wavelength-dependent combined transmission and reflection coefficient for No. 1 or 2 beam

- Φ = Potential function (two-dimensional potential flow)
 $\phi_i(v) = \frac{[T(v) - T_i]}{T_i}$ deviation of specimen temperature from T_i as function of coordinate
 $\phi_{m,n} = \frac{(T_{m,n} - T_\infty)}{T_\infty}$ deviation of specimen temperature from $T(x = \infty, y)$ at x_m, y_n
 φ = Radiant flux density
 ψ = Stream function (two-dimensional potential flow)
 ω = Solid angle subtended from point on surface
 $\chi = G - K_e \left[1 - \left(\frac{T_w}{T_e} \right)^4 \right]$

Subscripts

- a = Refers to absorbed portion
 A_p = Apparent value of
 av = Average value of
 b = Of a black surface, or of the specimen black body hole
 c = As calculated from data without corrections
 cs = Of specimen cross-section
 e = Effective value of
 f = Of thermocouple wire (filament)
 j = At thermocouple junction to specimen surface
 m = Measured value of
 m, n = At X_m, Y_n
 n = Normal
 p = Of scratch in coating for thermocouple mount
 s = Of specimen surface

- s_d = Of the specimen
- t_h = Total hemispherical value of
- t_n = Total normal value of
- τ_s = Refers to test section of specimen
- u = Of unperturbed portion of specimen
- w = Of the chamber wall
- θ = In a direction θ from the normal, or per unit solid angle in direction θ
- λ = At wavelength λ , or per unit wavelength at wavelength λ
- λ_n = Spectral normal value of

Distribution List
NASW-104

<u>To</u>	<u>Number of Copies</u>	<u>To</u>	<u>Number of Copies</u>
National Aeronautics and Space Administration Washington, D.C. 20546 Attention: F. Schulman	1	Aeronautical Systems Division Non-metallic Materials Laboratory Directorate of Materials and Processes Wright-Patterson Air Force Base, Ohio Attention: James Mattice	1
James J. Lynch	1		
Conrad Mook	1		
James J. Gangler	1		
National Aeronautics and Space Administration Lewis Research Center 21000 Brookpark Road Cleveland, Ohio, 44135 Attention: Bernard Lubarsky - 86-1	1	Aeronautical Systems Division Applications Laboratory Directorate of Materials and Processes Wright-Patterson Air Force Base, Ohio Attention: M. L. Minges	1
Roger Mather - 86-5	1	Information Processing Section	1
Herman Schwartz - 86-5	18		
Tom Moss - 86-5	1	Aeronautical Systems Division Flight Accessories Laboratory Wright-Patterson Air Force Base, Ohio Attention: George E. Thompson	1
Martin Gutstein - 86-5	1	Charles Armbruster	1
James H. Diedrich - 7-1	1		
Henry Curtis - 77-1	1	Commanding Officer U.S. Army Signal Research and Development Lab Fort Monmouth, New Jersey Attention: Stuart J. Shapiro	1
Sal Grisaffe - 49-1	1		
Charles Walker - 86-1	1		
Norman Musial - 77-1	1		
Library - 3-7	2		
Report Control Office - 5-5	1		
National Aeronautics and Space Administration Ames Research Center Moffett Field, California, 94035 Attention: Library	2	U.S. Atomic Energy Commission Technical Reports Library Washington 25, D.C. Attention: J. M. O'Leary	3
Carr Neel	1		
National Aeronautics and Space Administration Langley Research Center Hampton, Virginia, 23365 Attention: Library	2	U.S. Atomic Energy Commission Technical Information Service Extension P.O. Box 62 Oak Ridge, Tennessee	3
Samuel Katzoff	1		
William Wade	1	Argonne National Laboratory 9700 South Cass Avenue Argonne, Illinois Attention: Library	1
National Aeronautics and Space Administration Goddard Space Flight Center Greenbelt, Maryland, 20771 Attention: Library	1	Oak Ridge National Laboratory Oak Ridge, Tennessee Attention: Library	1
Milton Schach	1	D. L. McElroy	1
National Aeronautics and Space Administration Manned Spacecraft Center Houston, Texas, 77001 Attention: Library	2	University of California Berkeley, California Attention: R. A. Seban	1
Jess Goree	1		
National Aeronautics and Space Administration Marshall Space Flight Center Huntsville, Alabama, 35812 Attention: Library	1	Purdue University Lafayette, Indiana Attention: Claire Chapin	1
Gearhardt Heller	1		
Daniel Gates	1	IIT Research Institute Chicago 16, Illinois Attention: Library	1
National Aeronautics and Space Administration Scientific and Technical Information Facility P.O. Box 5700 Bethesda 14, Maryland	2 + 1 repro	Gene A. Zerlaut	1
National Aeronautics and Space Administration Jet Propulsion Laboratory 4800 Oak Grove Drive Pasadena, California, 91103 Attention: Library	1	Battelle Memorial Institute Columbus 1, Ohio Attention: DMIC	1
William F. Carroll	1	Webster Wood	1
National Aeronautics and Space Administration Western Operations Office 150 Pico Boulevard Santa Monica, California, 90406 Attention: John Keeler	1	Southern Research Institute 2000 Ninth Avenue South Birmingham 5, Alabama Attention: Library	1
National Bureau of Standards Washington 25, D.C. Attention: Joseph C. Richmond	1	C.D. Pears	1
Dwight Moore	1	Southwest Research Institute San Antonio, Texas Attention: W. Weatherford	1
		Aerojet-General Corporation Power and Equipment Division Azusa, California Attention: Ernest Perez	1

<u>To</u>	<u>Number of Copies</u>	<u>To</u>	<u>Number of Copies</u>
Aerona Manufacturing Corporation Middletown, Ohio Attention: James Krissos	1	Atomics International Canoga Park, California Attention: J.R. Crosby	1
Aerospace Corporation El Segundo, California Attention: Seymour Konopken Robert J. Champetier	1 1	Convair Division General Dynamics Corporation Fort Worth, Texas Attention: Library T.R. deTonnacour R.N. Oliver	1 1 1
Lockheed Missiles and Space Company Palo Alto, California Attention: Roger Ganner Loa McKellar	1 1	Electro-Optical Systems 125 North Vinado Avenue Pasadena, California Attention: Donald H. McClelland	1 1
Space Technology Laboratories Los Angeles 45, California Attention: Jerry T. Bevans	1	Ferro Corporation Cleveland, Ohio Attention: R.W. Pelz	1
Hughes Aircraft Company Culver City, California Attention: Library	1	General Electric Company Missile and Space Division Space Power Propulsion Section Cincinnati, Ohio Attention: Morris Zipkin	1
General Dynamics/Astronautics San Diego, California Attention: Library W. M. Brandenberg	1 1	Thompson-Ramo-Wooldridge, Inc. 2355 Euclid Avenue Cleveland, Ohio, 44116 Attention: Library	1
Boeing Airplane Company Seattle, Washington Attention: Library Wilson A. Clayton	1 1	North American Aviation Inc. International Airport Los Angeles 45, California Attention: Robert Klemm	1
The Martin Company Baltimore 20, Maryland Attention: N. J. Brown	1	Thompson-Cotton Santa Anna, California Attention: Library	1
ITT Industries Dallas, Texas Attention: R. L. Cox	1	Speedring Corporation 7111 East 14 Mile Road Warren, Michigan Attention: J. R. Sander	1
Oklahoma State University School of Mechanical Engineering Stillwater, Oklahoma Attention: J.B. Wiseloft	1	Continental Coatings Corporation 1776 Miles Cleveland, Ohio Attention: Ben Jones	1
Arthur D. Little, Incorporated Cambridge, Massachusetts Attention: A. G. Emslie	1	General Atomic P.O. Box 608 San Diego 12, California Attention: R.W. Pridg	1
McDonnell Aircraft Corporation St. Louis, Missouri Attention: Library	1	General Electric Company Missile and Space Division Valley Forge, Pennsylvania Attention: Library F. J. Schmidt	1 1
U.S. Naval Radiological Defense Laboratory San Francisco, California Attention: William J. Parker	1	General Electric Company SPNSO - Valleritos Atomic Lab P.O. Box 846 Pleasanton, California Attention: Burt C. Voorhees	1
AiResearch Manufacturing Company Phoenix, Arizona Attention: John Danner	1	Republic Aviation Corporation Farmingdale, New York Attention: Robert E. Bastian	1
AiResearch Manufacturing Company 1851-1951 Sepulveda Boulevard Los Angeles 45, California Attention: James J. Killackey	1	State University of New York College of Ceramics Alfred University Alfred, New York Attention: Milton Tuttle	1
Allison Division General Motors Corporation Indianapolis 6, Indiana Attention: Library	1		
American Machine and Foundry Alexandria Division 1125 North Royal Street Alexandria, Virginia Attention: Elliot Serrata	1		

<u>To</u>	<u>Number of Copies</u>	<u>To</u>	<u>Number of Copies</u>
Westinghouse Electric Corporation Aerospace Electrical Division Lima, Ohio Attention: P. E. Kueser	1	Marquardt Corporation Van Nuys, California Attention: S. Sklarew	1
SNAP-50/SPUR Program Office Atomic Energy Commission Washington 25, D.C. Attention: Herbert D. Rothen	1	Grumman Aircraft Bethpage, New York Attention: Library	1
U.S. Atomic Energy Commission Washington 25, D.C. Attention: M.J. Whitman	1	Ball Brothers Research Boulder, Colorado Attention: J. H. vonDalebor	1
Kennametal, Incorporated Latrobe, Pennsylvania Attention: Library	1	Solar Aircraft Company San Diego, California Attention: Alvin R. Stetson	1
Sandstrand Denver 2480 West 70th Avenue Denver 21, Colorado Attention: Robert Boyer	1	AVCO Wilmington, Massachusetts Attention: Library	1
North American Aviation Information and Space Division Downey, California Attention: Library	1	Bell Aerosystems Company Buffalo, New York Attention: Library	1